NASA Contract Report 191014

Advanced Small Rocket Chambers Option 1 – 14 Lbf Ir-Re Rocket

Final Report

Donald M. Jassowski and Mark L. Gage
GenCorp Aerojet
Propulsion Division
Sacramento, California

August 1992

Prepared for
Lewis Research Center
Under Contract NAS3-25646

NASA
National Aeronautics and
Space Administration

NASA
National Aeronautics and Space Administration

Report Documentation Page

1. Report No.	2. Government Accession No.	3. Recipient's Catalog No.
NASA-CR-191014		

4. Title and Subtitle

Advanced Small Rocket Chambers
Option 1, 14 lbf Ir-Re Rocket
Final Report

5. Report Date

August 1992

6. Performing Organization Code

7. Author(s)

D.M. Jassowski
M.L. Gage

8. Performing Organization Report No.

10. Work Unit No.

506-42-31

9. Performing Organization Name and Address

GenCorp Aerojet
Propulsion Division
Sacramento, CA 95813

11. Contract or Grant No.

NAS3-25646

12. Sponsoring Agency Name and Address

National Aeronautics and Space Administration
Lewis Research Centre
Cleveland, OH 44135-3191

13. Type of Report and Period Covered

Contractor Report
Option 1, Final

14. Sponsoring Agency Code

15. Supplementary Notes

Project Manager - Dr. Steven J. Schneider
Space Propulsion Technology Division
NASA Lewis Research Center

16. Abstract

A high performance Ir-Re 14 lbf (62 N) chamber and nozzle which can be a direct replacement for a production engine was designed, built, hot fired and vibration acceptance tested. It passed all acceptance tests satisfactorily and demonstrated a 20 sec increase in Is over the conventional 14 lbf silicide coated Cb chamber. The high performance engine uses the production valve and injector without modification. Incorporation of a secondary mixing device or Boundary Layer Trip within the combustion chamber results in elimination of the fuel film coolant, improvement in flow uniformity, the 20 sec performance increase, and reduction of a potential source of spacecraft contamination. Measured specific impulse (Is) was 305 sec at 75:1 area ratio, with monomethylhydrazine and nitrogen tetroxide propellants. Qualification tests remain to be done.

17. Key Words (Suggested by Author(s))

Rockets; Satellite Propulsion; Rhenium Thrusters; Iridium Coatings; Chemical Vapor Deposition; Bipropellants; Radiation Cooling; High Performance; High Temperature; Long Life

18. Distribution Statement

Unclassified, Unlimited
Subject Category 20

19. Security Classif. (of this report)	20. Security Classif. (of this page)	21. No of pages	22. Price*
Unclassified	Unclassified	227	A05

NASA FORM 1626 OCT 86

*For sale by the National Technical Information Service, Springfield, Virginia 22161

Contract NAS 3-25646

ADVANCED SMALL ROCKET CHAMBERS

Phase II, Option 1

14 lbf Ir-Re Rocket Final Report
August 1992

Aerojet Propulsion Division
P.O. Box 13222
Sacramento, CA 95813-6000

Prepared By:

D. M. Jassowski
Project Engineer

M.L. Gage
Project Engineer

Approved By:

B. Reimer
Program Manager

Prepared For:

NASA-Lewis Research Center
Cleveland, OH 44135

TABLE OF CONTENTS

	Page
1.0 Summary	1
2.0 Introduction	3
2.1 Program Approach	3
2.2 Design	6
3.0 Technical Discussion	10
3.1 Thruster Design	10
3.1.1 Preliminary Thruster Design	10
3.1.2 Thermal and Performance Analysis	13
3.1.3 Vibration Analysis	19
3.1.4 Optimization Tests	21
3.1.5 Assembly Design	42
3.2 Thruster Fabrication	47
3.2.1 Chamber Fabrication	47
3.2.2 Chamber Assembly	53
3.3 Thruster Hot Fire Testing	56
3.3.1 Test	69
3.3.2 Test Results	69
3.4 Vibration Acceptance Test	98
4.0 Conclusions and Recommendations	113

APPENDICES

Appendix		Page
A	14 lbf Re Nozzle Vibration Analysis	A-1
B	Thermal Analysis of 14 lbf Ir-Re Chambers	B-1
C	14 lbf Vibration Test Readiness Review	C-1
D	Vibration Test Data Analysis	D-1

FIGURE LIST

Figure		Page
2-1	Program Logic	4
2-2	Phase II, Option I Schedule	5
2-3	Characteristics of Production 14 lbf Engine (Si/Cb)	7
3.0-1	Program Logic for Option 1, Design, Fabrication and Test of an Advanced 14 lbf Ir-Re Reaction Control Thruster	11
3.1-1	The Advanced Ir-Re 14 lbf RCT was Similar to an Existing C-103 RCT	12
3.1-2	Ranges of Critical Chamber Dimensions Were Established During Preliminary Design	14
3.1-3	Current RCT Nozzle Contour	15
3.1-4	Front End Geometry for Thermal and Vibration Analysis	16
3.1-5	The Production 14-lbf Chamber Successfully Restarts at Temperatures Up to 600°F	18
3.1-6	Induced Stresses Equivalent to Von Mises Yield Criterion for 14-lb Nozzle	20
3.1-7	Optimization Hardware Assembly Drawings	22
3.1-8	Assembled 14-lbf Optimization Thruster	23
3.1-9	Optimization Trip Rings	24
3.1-10	14-lbf Optimization Hardware Instrumentation Locations	25
3.1-11	14-lbf Optimization Test Summary	27
3.1-12	Rhenium Foil Loss Rates Were Calculated Based on Exposed Surface Area	28
3.1-13	Performance Measurements of Optimization Test	29
3.1-14	Rhenium Rates, Calculated From Weight Loss, as a Function of Chamber Length	30
3.1-15	Rhenium Erosion Rates, Calculated From Weight Loss as a Function of Trip Height	31
3.1-16	An Expanded Scale is Required to Show all Erosion Rates as a Function of Trip Height	32
3.1-17	Rhenium Erosion Rates in Chamber Barrel	34
3.1-18	Rhenium Erosion Rates in Nozzle	35
3.1-19	Post Test Appearance of Chamber Barrel Foils	36
3.1-20	Posttest Appearance of Nozzle Foils	37
3.1-21	Radiometer Signals Provided an Independent Measure of Rhenium Loss	38
3.1-22	C* Performance of Optimization Hardware	39
3.1-23	Ipsv Performance of Optimization Hardware	40
3.1-24	Ir-Re 14-lbf Chamber	43

FIGURE LIST (CONT)

Figure		Page
3.1-25	Final Flight-Type Trip Ring Design	44
3.1-26	Optimization Hardware Ready for Test	45
3.1-27	Advanced 14-lbf RCT Assembly Drawing	46
3.2-1	Chamber S/N 1 Had a Very Thick Layer of Rhenium After the CVD Operation	48
3.2-2	Chamber S/N-1 Wall Thickness After Grinding	50
3.2-3	Ir-Re Chamber S/N-2 Demonstrated Good Control of the CVD Wall Thickness. Subsequent Grinding Operation Further Shaped Wall Thickness	51
3.2-4	S/N-2 As Received From Ultramet	52
3.2-5	Wall Thickness Measurements on Ir-Re 14-lbf Chamber S/N-2	54
3.2-6	Optical Microscope (50X) Shows the Sample Braze Joints Formed Without Cracks or Voids. SEM Examination Showed that the Apparent Crack in Specimen B is Only an Artifact of Polishing During Sample Preparation	55
3.2-7	14 lbf Ir-Re Chamber S/N-2 Weld With Brazed Tip Ring and Flange	57
3.2-8	Fully Assembled Ir-Re 14 lbf Engine	58
3.2-9	14 lbf Engines – Left: Ir-Re S/N-2, Right: C103 Engineering Development Unit	59
3.3-1	14# Ir-Re S/N-2 Nozzle Exit, Prior to Test	61
3.3-2	Post-Test Nozzle Exit Patterns	62
3.3-3	Chamber Dimensions	63
3.3-3A	14# Ir-Re Nozzle Throat OD and ID vs Firing Time	64
3.3-3B	14# Ir-Re Chamber Dimensions vs Time	65
3.3-4	Plumbing Schematic for 14 Pound Acceptance and Qualification Test in Test Bay A-1	66
3.3-5	Overall View of 14# Ir-Re Altitude Facility	67
3.3-6	Summary of Planned ARCT Test Program	68
3.3-7	Chamber Thermocouple Locations	70
3.3-8	Exhaust Plume Optical Measurement System	71
3.3-9	14# Ir-Re Thruster S/N-2 Showing Plume Monitor	72
3.3-10	Hydrogen Shroud System	73
3.3-11	Operating Pressure Envelope – Standard Thruster	74
3.3-12	Data Measurements List	75
3,3-13	High Performance 14-lbf Thrust Engine Test Data Summary	76
3.3-14	Acceptance Test Matrix	78
3.3-15	14 lbf Ir-Re Operating Map	79

FIGURE LIST (CONT)

Figure		Page
3.3-16	14 lbf Ir-Re Is vs MR, Tests -101 Through -134	80
3.3-17	14 lbf Ir-Re Is vs MR, Performance Tests at Nominal	82
3.3-18	14 lbf Ir-Re Is vs MR, Pulse Performance	83
3.3-18A	Pulse Train Used in 14# Tests -135 and -136	84
3.3-18B	14# Ir-Re S/N-2 I Bit Versus Pulse Number	85
3.3-19	14 lbf Ir-Re Is vs Pc	86
3.3-20	14 lbf Ir-Re T_{ech} W_{all} vs MR	87
3.3-21	14# Ir-Re: T_{wall} vs Time	88
3.3-21A	14# Ir-Re Thruster Temperature vs Time, Test -112	89
3.3-22	14# Ir-Re Temperature vs Time, Test -121	90
3.3-23	Thermal Comparison of RCT and Modified RCT Thrust Chamber	92
3.3-24	lbf Ir-Re Thruster Washer Stacks After Testing	93
3.3-25	14-lbf Ir-Re S/N-2 Plume Optical Data	95
3.3-26	14-lbf Plume Optical Measurement – Run 106	96
3.3-27	Total Emission at 350 nm vs Time	97
3.3-28	Calculated Temperature for 350 nm Emission	99
3.4-1	14# Ir-Re Engine Prior to Post Test Inspection	100
3.4-2	14# Ir-Re Engine Post Test Chamber	101
3.4-3	14 lbf Ir-Re Thruster Being Assembled Into RCTM for Vibration Acceptance Test	102
3.4-4	Vibration Power Levels	104
3.4-5	Z-Axis Random Vibration Acceptance Test – 14# Ir-Re Thruster	105
3.4-6	RCTM With 14# Ir-Re Thruster in Z-Axis Vibration Set-Up	106
3.4-7	Accelerometers Mounted on Thruster Valve	107
3.4-8	Strain Gages on Ir-Re Chamber Throat	108
3.4-9	Power Ratio Gain and Loss vs db	109
3.4-10	Advanced 14 lb X-Axis SG 1 (Micro Strain)	110
3.4-11	Advanced 14 lb X Axis Acceleration-Control	111
3.4-12	Advanced 14 lb X Axis Acceleration-Nozzle Y	112

1.0 SUMMARY

This report describes the activities of Option 1 of NASA LeRC Contract NAS 3-25646, Advanced Small Rocket Chambers program. In this phase of the program, a high performance Ir-Re 14 lbf (62 N) chamber and nozzle which can be a direct replacement for a production engine was designed, built, hot fired and vibration acceptance tested. It passed all acceptance tests satisfactorily and demonstrated a 20 sec increase in I_s over the conventional 14 lbf silicide coated Cb chamber. The high performance engine uses the production valve and injector without modification. Qualification tests remain to be done.

The overall objectives of the Advanced Small Rocket Chambers Program are to advance the state-of-the-art of small chemical rocket chambers significantly by 1) examining fundamental combustion processes, 2) evaluating new high temperature materials in relevant environments, and 3) evaluating small rocket concepts by direct hot fire testing.

This activity was conducted under tasks 7, 8, and 9 of the program. The intent of this work was to demonstrate the understanding of the combustion/materials interaction processes studied in the first phase of the program by applying them to a flight-type rocket engine.

The approach used in this portion of the program was to demonstrate the performance improvement that can be made by substitution of a high temperature (4000°F) (2200°C) Ir-Re chamber for a production C-103 Cb silicide coated chamber and nozzle.

After detailed thermal, performance, mechanical, and dynamic design analyses of the full engine, two Ir-Re chambers were built for Aerojet by Ultramet, using the chemical vapor deposition (CVD) process.

The production 14 lbf engine uses ~40% fuel film cooling; this is required to keep the Cb chamber at an acceptable operating temperature of under 2400°F (1300°C). The requirement for a cool boundary layer throughout the chamber and throat implies unmixed, unreacted fuel exiting the nozzle which may produce a performance loss of about 20 sec and a potential source of spacecraft contamination. Use of the production injector forces the Ir-Re engine to operate with the 40% fuel film cooling. Incorporation of a secondary mixing device or Boundary Layer Trip (BLT) within the combustion chamber, (Aerojet Patents 4882904 and 4936091) results in elimination of the fuel film coolant, improvement in flow uniformity, and a significant performance increase.

The geometry and location of the trip (BLT) was optimized for this particular injector/chamber configuration by conducting hot firings in witness foil chambers to measure performance and compatibility.

The Ir-Re chamber assembly is completed by brazing the optimized BLT fabricated from a Pt-10% Rh alloy to the rhenium which in turn was brazed to a stainless steel flange that mates to the production platelet injector and Moog bipropellant valve.

This engine assembly was successfully hot fired using the standard production acceptance testing criteria. This was followed by completing a portion of the qualification testing during which optical measurements were made of the exhaust. Measured specific impulse (I_S) was 304.8 sec at nominal conditions (the production engine I_S is 285 sec for the same conditions) an increase in performance of 20 sec. A total test time of 746 sec were accumulated in 349 steady state and pulsed starts with no hardware damage and satisfactory thermal performance.

The engine was successfully subjected to the production engine random vibration acceptance test following the hot fire testing. Strain measurements made during these tests indicate the engine will survive qualification level vibration tests.

2.0 INTRODUCTION

The Advanced Small Rocket Chambers Program, NASA LeRC Contract NAS 3-25646 has as its goal the understanding of rocket chamber material/combustion interaction mechanisms for high temperature radiation-cooled rocket engines.

Program Logic

The logic to carry out this program is shown in Figure 2-1. The program is a base program plus three options consisting of 15 tasks and reporting in Task 16. The Basic Program, Tasks 1 through 6, included study and selection of materials, propellants and fabrication processes, basic combustion product/material interaction research in collaboration with Sandia/Livermore Combustion Research Facility using their advanced laser diagnostics techniques, and exposure of candidate chamber materials to simulated rocket engine conditions.

These tasks led to the portion of the program covered by this report, Option I, Tasks 7, 8, and 9. In this option, the understanding of the knowledge gained in the Basic Program was demonstrated by designing, building and testing a flight-type thruster which had significantly improved performance relative to engines of conventional design. As part of this program, components were built for two engines; one engine was assembled, and successfully passed hot fire and vibration acceptance tests.

Activity on this program began in November, 1989; technical activity was concluded in March 1991, Figure 2-2. It consisted of design, fabrication, and testing of the flight type advanced 14 lbf Ir-Re engine (AJ10-220 HP). Hot fire testing was interrupted in November 1990 for vibration testing, which was conducted in February of 1991. Resumption of hot fire testing was deferred to focus on Option 3 demonstration of a 100 lbf Ir-Re engine, which is in process.

2.1 PROGRAM APPROACH

The initial program concept was to conduct this option of the program with a generic 5 lbf thruster. However, a more rational approach developed in which a direct comparison could be made between a current engine in production with a state-of-the-art radiation cooled chamber and the improved advanced Ir-Re chamber. For this purpose, the 14 lbf silicide coated columbium thruster in production at Aerojet was chosen as a model. This engine is flight qualified and has rigorous procedures in place for hot fire and vibration acceptance tests which could be adapted directly. It uses a high performance platelet injector and a Moog dual shutoff

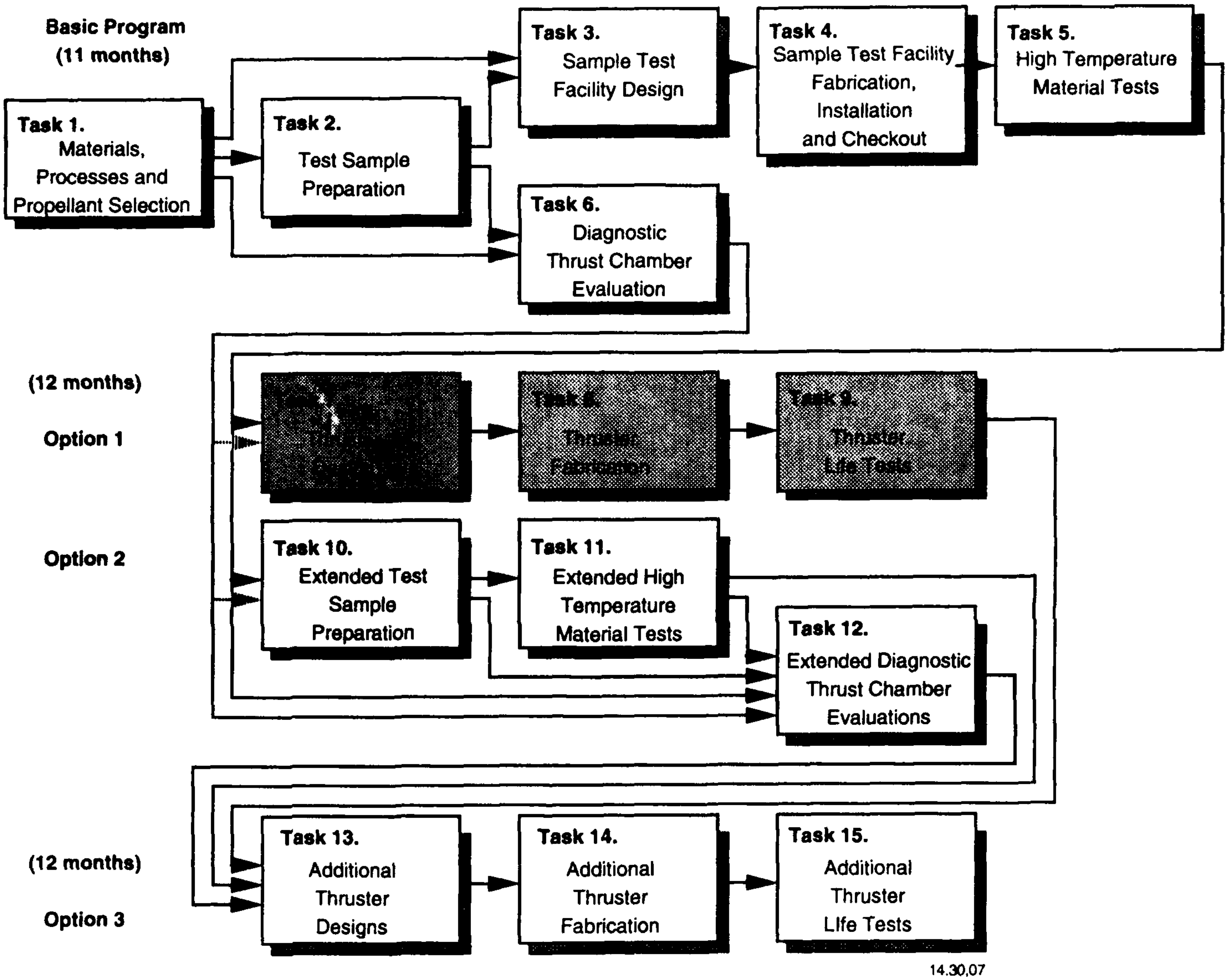


Figure 2-1. Program Logic

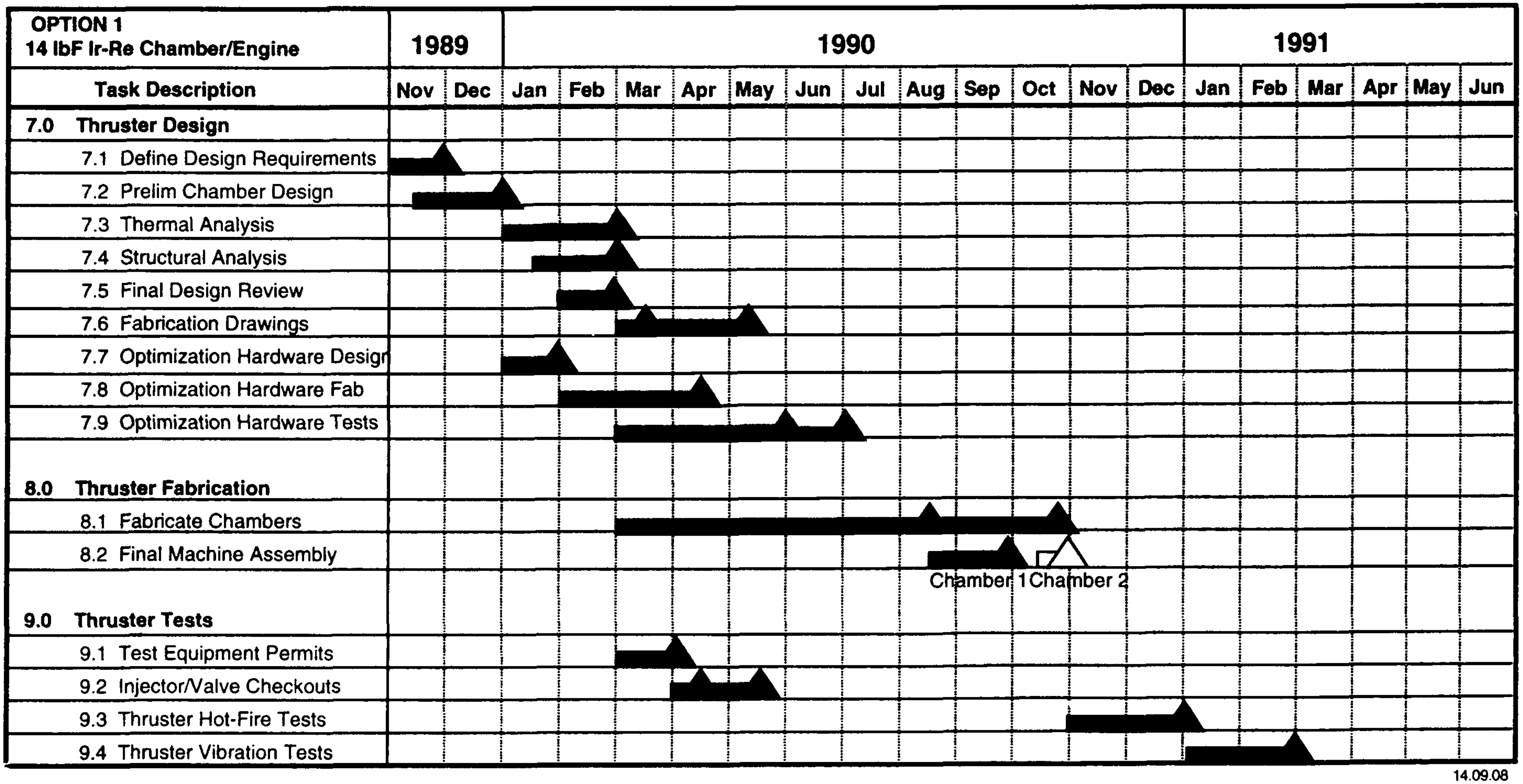


Figure 2-2 Option 1 Schedule

torque motor bipropellant valve. Since the Cb/Si chamber bolts to the valve, it was practical to remove it and replace it with an Ir-Re chamber with no other changes to the engine.

A set of hardware which had been well-characterized in development testing was loaned to the contract for this program. The characteristics of the production 14 lbf engine are summarized in Figure 2-3.

2.2 DESIGN

The task 7 design activities included development of a long life chamber design which would provide a significant improvement in performance over the production unit while still meeting its front end thermal and vibration requirements.

The production engine injector design provides 40% film cooling of the chamber wall to maintain the silicide-coated Cb chamber at a safe operating temperature. Since the Ir-Re chamber does not require film cooling for chamber protection (although it is essential for front-end temperature management) the new chamber design incorporated Aerojet's two stage combustor (Patents 4882904 and 4936091). The invention allows the engine to run at maximum performance by mixing the film cooling with the core flow. In doing so, the chamber wall downstream of the secondary mixing stage reaches temperatures in the 3500°F range, about 1000°F higher than can be tolerated by the Si-Cb.

The significant characteristics of the design are the length and height of the trip which must be optimized for a specific installation (injector/operating point/chamber geometry). To set the trip design hot fire optimization tests were conducted as part of tasks 7.7, 7.8, and 7.9. These permitted choice of a trip geometry which could give long chamber life because of compatible chamber wall and nozzle conditions, while still giving acceptably high performance.

Attachment of the hot Ir-Re chamber to the relatively cold engine front end is a challenging design task. The transition must withstand thousands of thermal cycles and block thermal input from steady state, pulsed, and post fire heat soak. It requires joining three dissimilar metals, the Ir-Re chamber, the Pt-10% Rh trip, and the 304 stainless flange which duplicates the production engine interface and which bolts to the injector. Joining experiments were conducted to determine that satisfactory joints could be made. Thermal and structural dynamic analyses were conducted to assure that the engine could withstand the hot fire thermal environment and the launch vibration environment.

STEADY STATE
ACCEPTANCE TEST DATA
DATA SHEET NO. 2

NOMENCLATURE: 14 LB.F REACTION CONTROL THRUSTER **PAGE** 1 **OF** 2

PART NUMBER: 1197555- **SERIAL NUMBER:** 0000001

ACCEPTANCE TEST SPECIFICATION: -47145

TEST NO.: 2504-148-A1-589 **TEST STAND:** A-1

TEST DATE: 11-20-85 **CONTRACT NO.:** 5804

TEST TIME: 2248 **WORK ORDER NO.:** 2504

COMPUTER PROGRAMS: STEADY STATE PERFORMANCE JOB J0880

ITEM	TEST VALUE	SPECIFIED VALUE	SPECIFICATION AND PARAGRAPH
SUMMARIZED DATA			
..1 DURATION OF STEADY STATE SUMMARY PERIOD. FS1 + 15 TO 20 SECONDS	5.0	5 MIN.	ATS 3.10.2.1
1.2 MIXTURE RATIO AT STANDARD INLET CONDITIONS. MR-SIC	1.65	1.6 - 1.7	ATS 4.2.4.2.2.1
1.3 VACUUM THRUST AT STANDARD INLET CONDITIONS. FVAC-SIC LBS.	14.49	13.3-14.7	ATS 4.2.4.2.2.1
1.4 VACUUM SPECIFIC IMPULSE AT STANDARD INLET CONDITIONS. ISP-SIC SECS.	287.9	270. MIN.	ATS 4.2.4.2.2.1
1.5 PROPELLANT INLET PRESSURE. PSIA			ATS 4.2.4.2.1
OXIDIZER POLT	220	215 - 225	
FUEL PFLT	223	215 - 225	
1.6 PROPELLANT INLET TEMPERATURE. DEG.F			ATS 4.2.4.2.1
OXIDIZER TPO	71	65 - 75	
FUEL TPF	70	65 - 75	

NOTE: * SIGNIFIES OUT OF SPEC. CONDITION

CERTIFICATION

ENGINEERING ANALYST: H C Howard **DATE:** 23 November 1985

46 **LOG PAGE**

Figure 2-3. Characteristics of Production 14 lbf Engine (Si/Cb), Page 1 of 2

STEADY STATE
ACCEPTANCE TEST DATA
DATA SHEET NO. 2

NOMENCLATURE: 14 LB.F REACTION CONTROL THRUSTER **PAGE** 2 **OF** 2

PART NUMBER: 1197555- **SERIAL NUMBER:** 0000001

TEST NO.: 2504-148-A1-589 **ITEM**	**TEST VALUE**	**SPECIFIED VALUE**	**SPECIFICATION AND PARAGRAPH**
1.7 VALVE COMMAND VOLTAGE. VOLTS	22.9 *	23 - 25	ATS 4.2.4.2.1
1.8 MAXIMUM THRUSTER ROUGHNESS DURING STEADY STATE OPERATION. %	2.5	10 MAX.	ATS 4.2.4.2.2
1.9 STEADY STATE THRUST REPEATABILITY. %	.0	-2.0 TO 2.0	ATS 4.2.4.2.2.1
2. INSTANTANEOUS DATA			
2.1 THRUSTER RESPONSE. MILLISECS			ATS 4.2.4.2.2
START-UP	10	20 MAX.	
SHUTDOWN	11	40 MAX.	
2.2 SIMULATED ALTITUDE AT FS1. FEET	182274	120000 MIN.	ATS 4.2.4
2.3 TEST DURATION. SECS.	100.00	95 - 105	ATS 4.2.4.2.1
2.4 MAXIMUM CHAMBER TEMPERATURE DURING TEST. DEG.F INSTRUMENT CALIBRATION NOT CERTIFIED.	1979	2000 MAX.	ATS 4.2.4.2.2
2.5 MAXIMUM FIRING DETECTION SENSOR DURING TEST. DEG.F	185	150 MIN.	ATS 4.2.4.2.2.1
3. TEST RESULTS VERIFICATION			
VERIFIED BY: QUALITY ASSURANCE			
* NOTE: ACTION TAKEN			

49 LOG PAGE

Figure 2-3. Characteristics of Production 14 lbf Engine (Si/Cb), Page 2 of 2

Fabrication

Two sets of chamber hardware were fabricated, the Ir-Re chambers by Ultramet using the CVD process and the Pt-10% Rh trip rings by Johnson-Mathey by conventional machining. The components were joined by brazing, inspected and assembled in the same facility and by the same personnel who produce the production 14 lbf engine. The unit was assembled with a flight transducer and the forward joint sealing system used on the flight engine.

Testing

The engine assembly was then instrumented with thermocouples to measure temperatures at critical locations and installed in Aerojet's altitude test facility, where it was subjected to acceptance, performance and a portion of a qualification test series. The engine performance and thermal characteristics matched predictions. Performance was 20 sec higher than the production engine. No measurable changes occurred in throat or chamber dimensions in 746 sec of testing and 349 starts.

After hot firing, the engine was disassembled, inspected and then reassembled for vibration acceptance testing and installed in a two-engine flight module. In addition to the normal acceptance test measurements, the engine was instrumented with strain gages at the throat, and accelerometers on the valve body and at the nozzle exit. The engine was subjected to acceptance test levels of random vibration on the X-, Y- and Z- axes. Each test series started -12 db down and progressed in 3 db steps to the -0 db level. After each run, the nozzle exit location was measured to determine if any permanent deflection resulted. None occurred.

The engine passed the acceptance test series without damage. Strain measurements made during these tests were used to predict the engine's response to the +3db qualification random vibration tests. Positive margins on stress are predicted for all critical areas.

The advanced 14 lbf Ir-Re thruster has proven the utility of this material system over conventional silicide coated Cb for small radiation cooled thrusters using storable propellants. A second set of components is available; these can be used to demonstrate the repeatability of these results. With a modest effort the two sets of hardware can be used to demonstrate flight qualification of this concept.

3.0 TECHNICAL DISCUSSION

In Option 1 of the program, an advanced, high-temperature, iridium-rhenium 14 lbF reaction control thruster (RCT) was designed, fabricated, and tested. Aerojet is currently in production with a flight-qualified 14 lbF RCT constructed of columbium alloy C103. The new iridium-rhenium thruster built in this program was designed to provide a substantially higher specific impulse than the current production 14 lbF RCT, without reducing the operational life, thermal, or vibrational requirements of the current engine.

The objectives of this option were accomplished through the conduct of three technical tasks (1) Thruster Design, (2) Thruster Fabrication, and (3) Thruster Hot-Fire and Vibration Tests. The overall organization of the three tasks is shown in Figure 3.0-1. This section of the report details the approach and results of each of these three tasks.

3.1 THRUSTER DESIGN

3.1.1 Preliminary Thruster Design

The preliminary design of the Ir-Re thrust chamber was derived from the current 14 lbF production RCT.

The qualification level hot-fire, life, and vibration requirements of the existing 14 lbf RCT were adopted as the design basis for the Ir-Re thruster. The Ir-Re thruster was designed to use an injector and valve from the current production program. This requirement established the interface of the front-end flange and the inside diameter of the boundary layer trip ring. Other constraints also kept the new design similar to that of the current production engine. The nominal Pc (100 psia) and MR (1.65) were not changed. The chamber throat diameter (.320 ± .004 in.) and nozzle exit expansion area ratio (75:1) were copied from the current production RCT.

These design constraints resulted in a preliminary design of the Ir-Re chamber sketched in Figure 3.1-1. Note that on this figure, there are three dimensions which were not specified at the preliminary design phase, namely:

T_L – Boundary Layer Trip Length

T_H – Boundary Layer Trip Height and

L' – Chamber Length

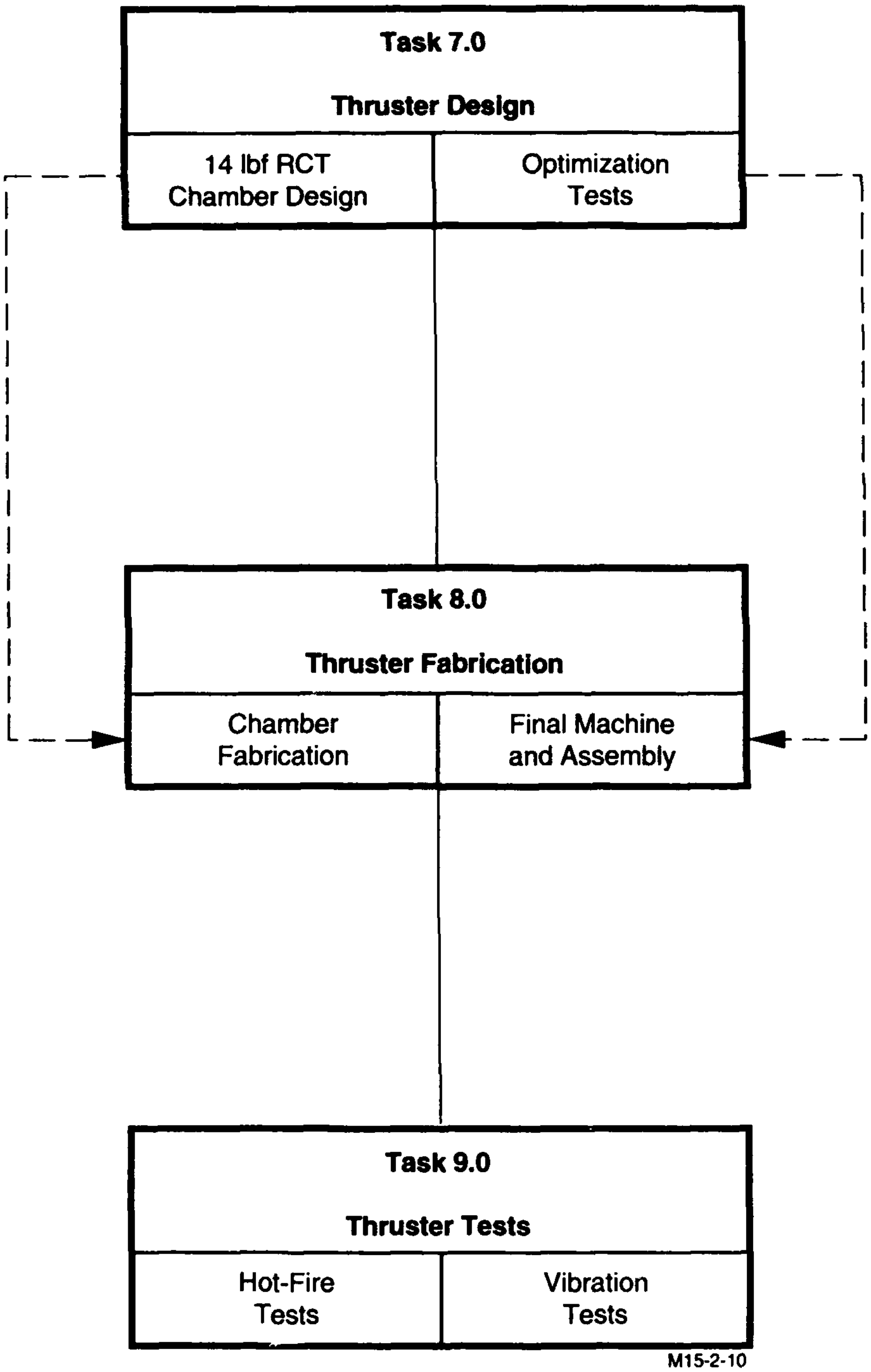


Figure 3.0-1 Program Logic for Option 1. Design, Fabrication, and Test of an Advanced 14 lbf Ir-Re Reaction Control Thruster

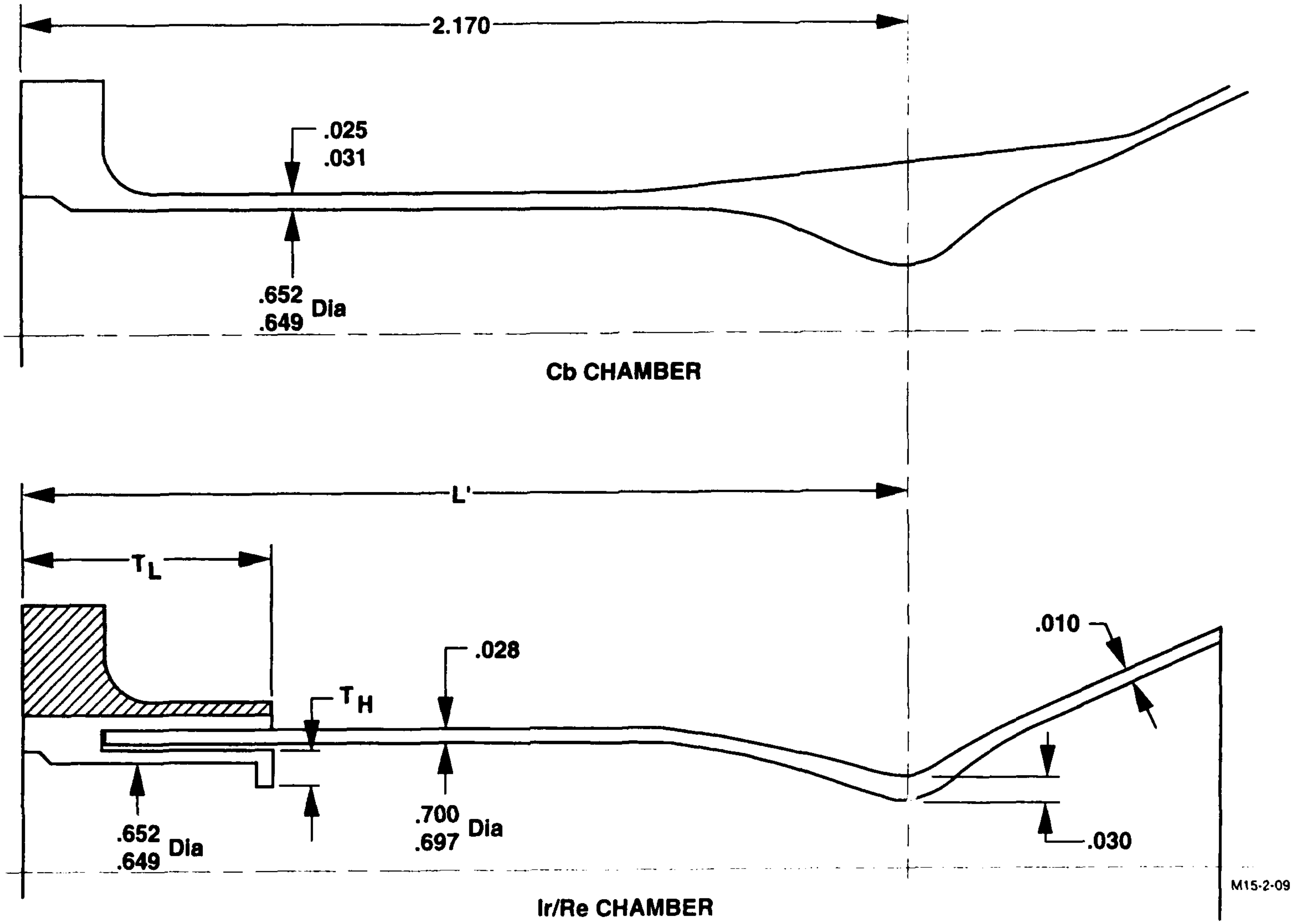


Figure 3.1-1 The Advanced Ir-Re 14 lbf RCT Was Similar to an Existing C-103 RCT

These three items were the subject of parametric thermal and dynamic analysis. Hot-fire optimization tests were also conducted to support selection of these design values. Based on previous experience with Ir-Re chambers at the 5-lbf level a range of possible values was developed for each of these three dimensions. These ranges are shown in Figure 3.1-2.

3.1.2 Thermal and Performance Analysis

A 3-D ANSYS model of the proposed 14 lbf Ir-Re chamber was constructed to support thermal analysis. Figures 3.1-3 and 3.1-4 document the initial model geometry.

Three types of analysis were done: (1) steady state wall temperature profiles, (2) transient wall temperatures during soakback, and (3) thermal stress profiles. Pulse mode operation was not analyzed. A summary of the results is presented in this section, and the memoranda which discuss the thermal analysis results more completely are included as Appendix B of this report. All analyses used the shortest L' chamber (2.1 in.) because it represented the worst case for thermal management.

The steady state thermal analysis predicted that the engine would have adequate thermal margin during steady state operation. The predicted maximum wall temperature in the chamber was 3562°F, just upstream of the throat. Front end thermal profiles were calculated based on an assumed fuel-film cooled temperature of 300°F on the inside surface of the trip ring. This showed that the shortest trip ring length being considered (0.50 in.) would result in unacceptably high front end temperatures at the platinum-rhenium joint and at the front end flange. Increasing the trip ring length to 0.75 in. solved this problem, and lowered the temperatures in the front end by approximately 400°F. Further addition to the trip ring length should continue to ameliorate the front end thermal management issues, assuming the fuel-film cooling layer remains effective to the end of the trip ring. However, examination of hot-fire thermal data from the current 14 lbf production engine indicated that the fuel-film cooling layer is only effective for the first 0.8 in. of length. Thus, there may be little advantage to lengthening the trip ring. This was later verified by testing during the optimization test series.

Transient thermal analysis predicted that the chamber would accommodate thermal soakback from a single steady state burn without overheating the injector, valve, or the trip ring-to-chamber joint. The transient thermal analysis was based on a trip ring length of 0.75 in. and a chamber L' of 2.1 in. The thermal profile predicted for steady state operation was assumed at time zero. The transient analysis predicted temperature rises during thermal

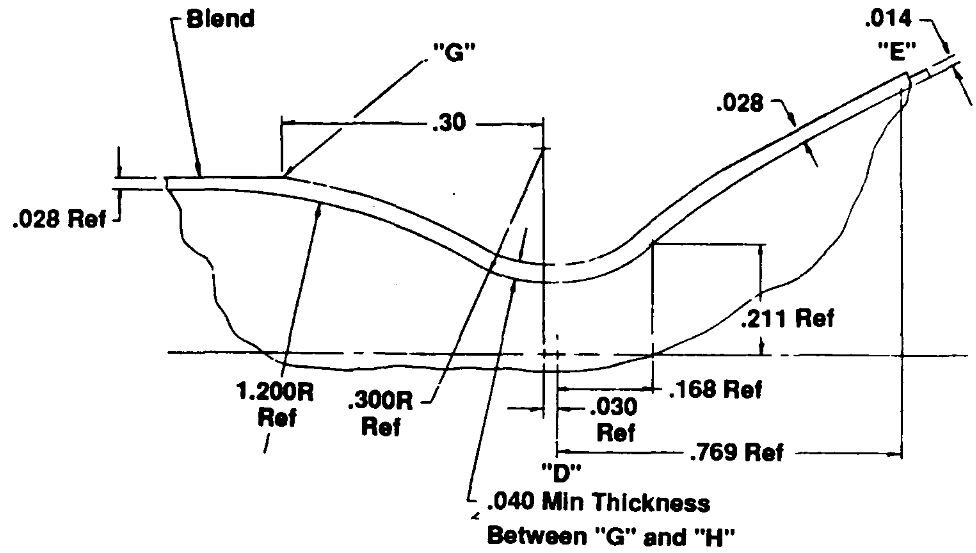
	Min	Max
Trip Height, T_H	0.03	0.07
Trip Length, T_L	0.50	1.00
Chamber Barrel Length, L'	2.17	3.50

Note: All Dimensions in Inches

14.12.32

Figure 3.1-2. Ranges of Critical Chamber Dimensions Were Established During Preliminary Design

X BASIC	R BASIC
.000	.160
.168	.211
.197	.230
.254	.270
.311	.310
.368	.347
.426	.386
.483	.424
.540	.460
.597	.495
.654	.526
.769	.587
.883	.637
1.055	.707
1.227	.772
1.398	.832
1.579	.887
1.742	.939
1.913	.988
2.085	1.035
2.257	1.078
2.428	1.118
2.608	1.157
2.772	1.193
2.943	1.227
3.115	1.258
3.287	1.287
3.458	1.314
3.630	1.340
3.802	1.365
3.974	1.389



View **A** Scale 8/1

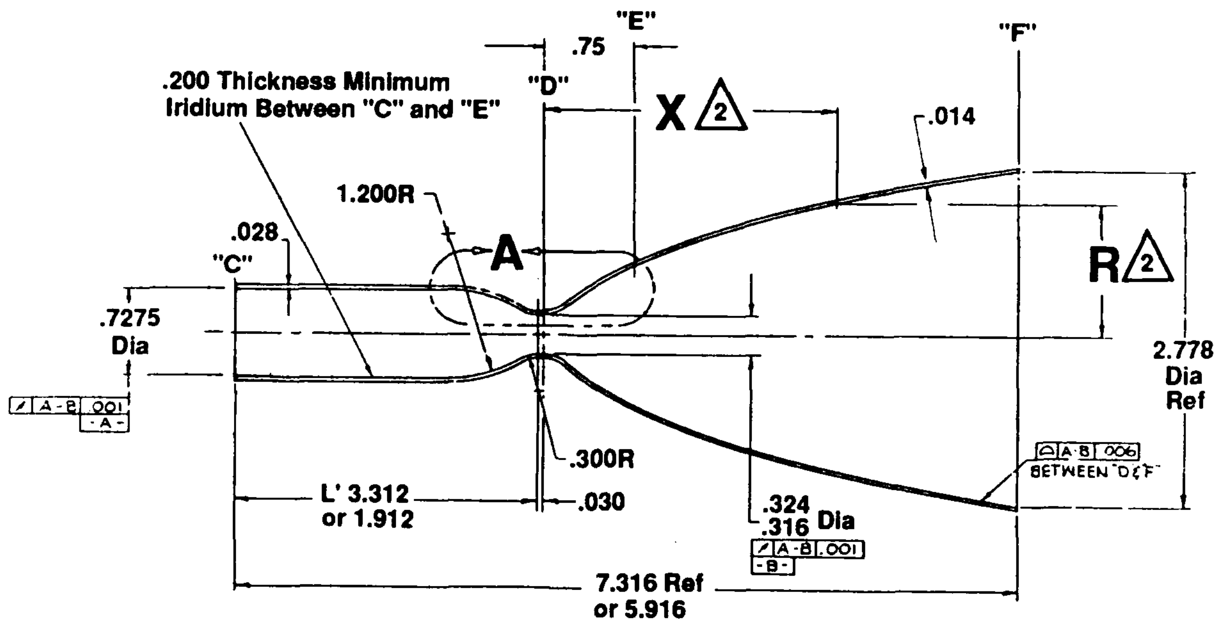


Figure 3.1-3. Initial Geometry for Thermal and Vibration Analyses

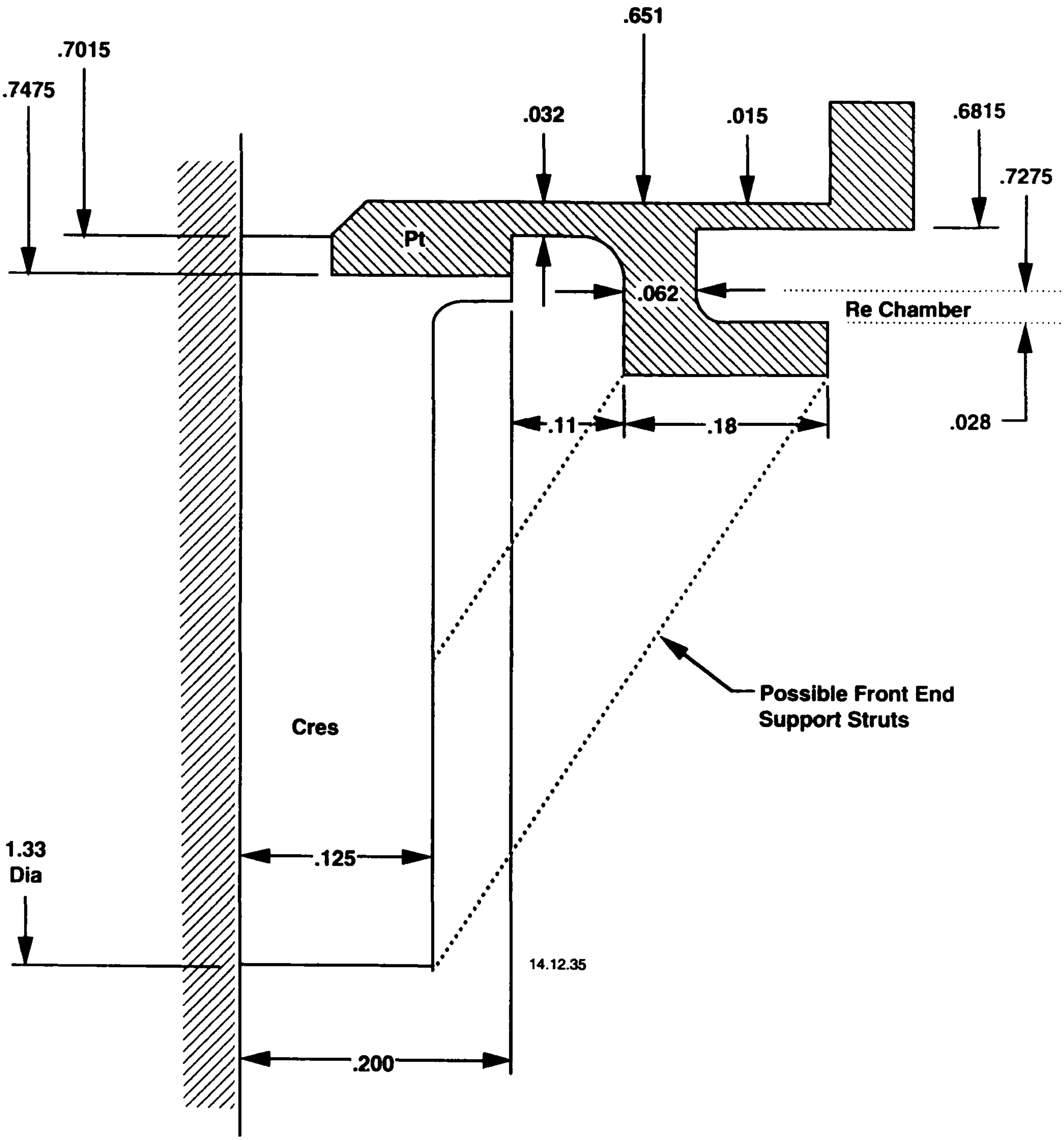
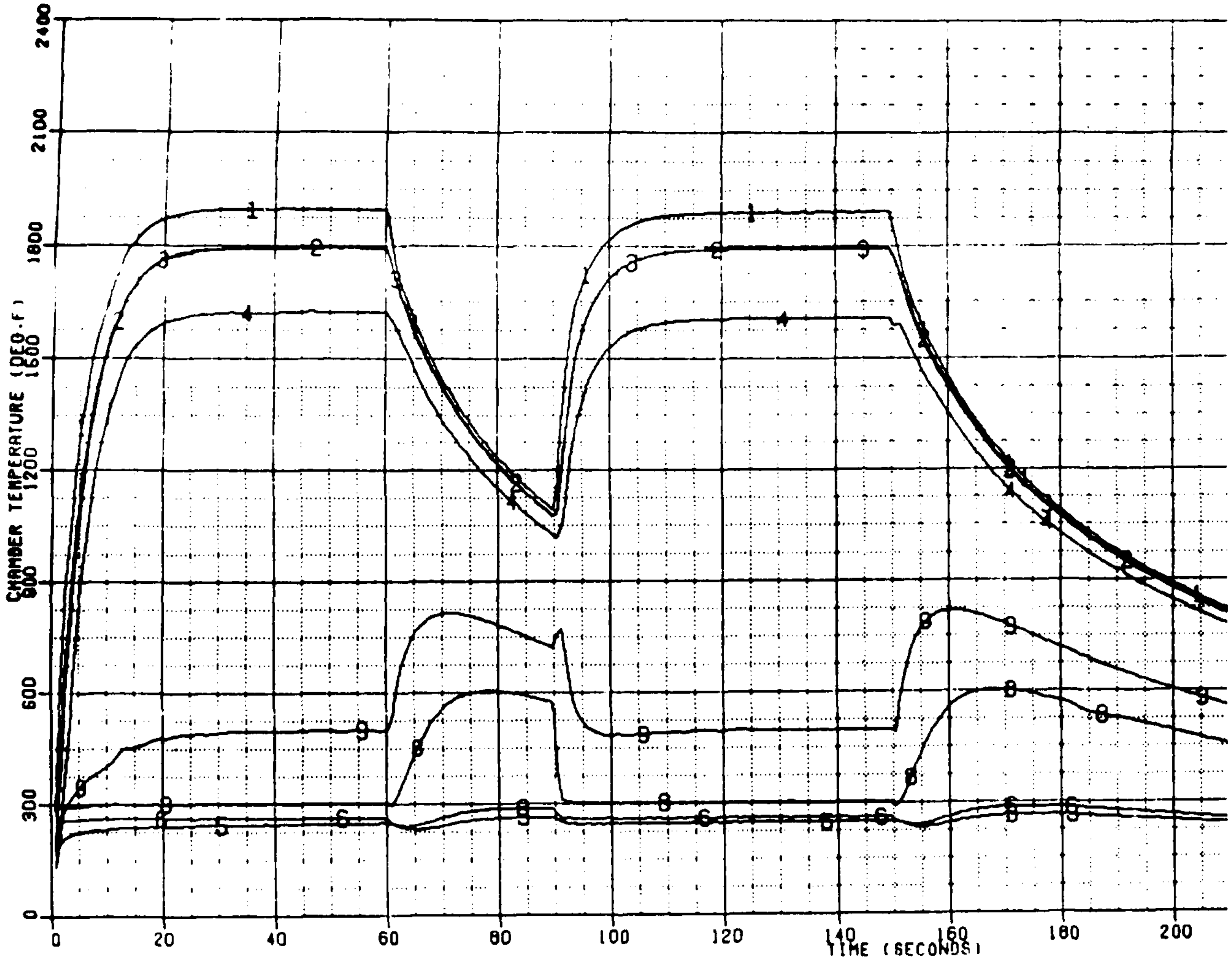


Figure 3.1-4. Front End Geometry for Thermal and Vibration Analysis

soakback of 200°F in the front end stainless steel flange, 275°F in the platinum trip ring, and 715°F at the attachment between the rhenium chamber and the platinum trip ring. These are all acceptable soakback conditions.

However, multiple firings and various duty cycles were not considered as part of the analysis and the ability of the engine to successfully restart during thermal soakback conditions was not analyzed. Analyses indicate that the platinum BLT surface temperature will exceed the MMH autodecomposition temperature (450°F, 230°C) within one second of shutdown and requires at least 30 to 60 seconds cooldown before the temperature is again below decomposition temperature. The effect of MMH decomposition on hot restart remains to be determined, but as shown in Figure 3.1-5, the current 14-lbf engine successfully restarts at front end flange and barrel temperatures approaching 600°F. This is well above the predicted 500°F maximum front end flange temperature for the flight-type Ir-Re chamber. The hot-fire tests demonstrated the ability of the Ir-Re engine to meet the steady state and 10% duty cycles demanded of the current 14-lbf engine.

Performance calculations were conducted to predict the specific impulse of the engine. Of particular interest was the effect of a change in the nozzle contour from the current C103 engine. For maximum performance, the current production engine exits the throat with a short 0.046 in. radius corner. Failure of the iridium coating occurred in this area with a similar small radius exit with a 5 lbf chamber on a previous Aerojet program. The exact cause of this failure is not known with certainty, but the small radius of curvature does increase the stress in this area. It was decided to adopt a larger radius of curvature on the exit of the throat if it could be done without a large performance penalty. The performance of two nozzle contour designs were analyzed. The first was an Ir-Re chamber with the current RCT nozzle contour. The second design increased the radius of curvature on the downstream side of the throat to equal that of the upstream side, i.e., 0.300 inches (as shown in Figure 3.1-3). This contour was then blended into the current nozzle design approximately 0.760 in. downstream of the throat. TDK-BLM performance calculations showed the large radius exit would cost less than one second of specific impulse, and that the predicted performance of this engine with C* efficiency of 98% was approximately 305 seconds at nominal Pc and MR. This is approximately a 22 second improvement over the current 14 lbf C103 RCT. It was decided to sacrifice a little performance and adopt the large exit radius nozzle contour.



1	TC-1	DEG F	9	TC 1.5, 150	DEF F
2	TC-2	DEG F	0	TC 1.5, 330	DEG F
3	TC-3	DEG F			
4	TC-4	DEG F			
5	TC .35, 150	DEG F			
6	TC .35, 330	DEG F			
7	TC .85, 150	DEG F			
8	TC .85, 330	DEG F			

Figure 3.1-5. The Production 14-Lbf Chamber Successfully Restarts at Temperatures Up to 600°F

These thermal and performance calculations establish the inside contour of the Ir-Re chamber. Any additional changes required to accommodate vibrational loads were made through adjustments in the wall thickness and outside dimensions of the RCT.

3.1.3 Vibration Analysis

A finite element ANSYS model of the 14 lbf Ir-Re chamber was constructed to support dynamic structural analysis of the chamber. The stress profile of the chamber was calculated based on the qualification-level random vibration spectrum for the current 14-lbf RCTM. The chamber was modeled as a stand-alone RCT, with a rigid attachment at the injector interface. No modeling was done of the injector, valve, or the module structure, in which each RCT resides. This is a significant factor in the interpretation of the results. In the vibration tests and in the actual operating service, the vibration spectrum is applied to the outside of the RCTM. It has been established that the module assembly attenuates much of the vibration energy. Thus, this analysis in which the full vibration spectrum was applied directly to chamber yielded conservative estimates of the resulting stress profile.

Four cases were analyzed. The dynamic response of the chamber was calculated and the sensitivity of the dynamic response to various design alternatives was estimated using these four cases.

Two areas of the chamber were calculated to have stress above the estimated yield strength of the materials. The first area was at the throat, where the calculated stress on the rhenium exceeded 70,000 psi. The second area was at the BLT, where the stress in the platinum was as high as 23,000 psi. Figure 3.1-6 summarizes the stresses calculated in these two areas for the three cases analyzed. It should be noted that the entries in this table are equal to three times the one sigma stress calculated in these areas. This margin of safety is applied to provide a 99.7% statistical probability that the actual maximum stress encountered in random vibration testing will be less than the values shown in this table.

Based on these preliminary structural analyses, a number of design recommendations were developed:

- The wall around the chamber throat was thickened to approximately 0.040-in. This reduced the stress at the throat by approximately 10%, without a significant increase in stress at the front end of the chamber.

Description	Maximum Stresses Eqivalent to Von Mises Yield Criterion at Throat Section (ksi)	Maximum Stresses Equivalent to Von Mises Yield Criterion at Front End (ksi)
1.9 inch throat length with struts and 0.028 inch throat thickness	76.8 (55.0)*	8.4 (30.0)**
1.9 inch throat length without struts and 0.028 inch throat thickness	72.9 (55.0)	24.6 (30.0)
3.3 inch throat length with struts and 0.028 inch throat thickness	74.4 (55.0)	16.5 (30.0)
3.3 inch throat length with struts and 0.04 inch throat thickness	66.6 (55.0)	16.0 (30.0)

The number in parenthesis is the corresponding yield strength of the material.

*CVD Rhenium, as deposited, based on limited data.
**Pt-10 Rh

Maximum stresses shown in the table are 3-sigma values.

Figure 3.1-6. Induced Stress Equivalent to Von Mises Yield Criterion for 14-lb Nozzle

- A high strength platinum alloy (Pt-10Rh) was used in construction of the BLT. Use of this higher strength material increased the allowable stress in this area by a factor of 2. This enabled design of the chamber without the use of external support struts.

A memorandum discussing the dynamics analysis performed is included in Appendix A of this report.

3.1.4 Optimization Tests

As discussed in Section 3.1, hot-fire optimization tests were conducted to determine the final design of the BLT height (T_H), the BLT length (T_L), and the overall chamber barrel length (L').

The tests used the same injector and valves which were eventually tested with the Ir-Re chambers. All testing was conducted at sea level using a three-piece stainless steel heat sink chamber. The design of the optimization hardware is shown in Figure 3.1-7, and is pictured fully assembled in Figure 3.1-8. As seen in the assembly view of Figure 3.1-7, each test configuration included a front end flange (-1), a cylindrical barrel section -2, -3, or -4), and a throat (-5 or -10). The front end flange was bolted to the injector and valve and was not removed during the test series. The barrel and throat pieces, on the other hand, were changed before each test. The barrel and throat piece was lined with 0.010-in. Grafoil and 0.003-in. rhenium prior to assembly on the test stand in most of the tests.

Figure 3.1-9 shows a drawing of the trip rings used in the optimization tests. Eight trip rings were built, four from stainless steel -2, -3, -5, and -6), and four from Pt-10Rh (-5, -6, -8, and -9). The tip of one stainless steel trip ring was cut off to provide a trip ring of zero trip height. This trip ring had an overall length of 0.43 in.

The location of temperature and pressure measurements for the test chamber are shown in Figure 3.1-10. The engine plume was monitored for the presence of rhenium with a two-channel emission radiometer. Steady state thrust measurements were obtained in every test.

Twelve hot-fire tests were conducted during the optimization test series. The independent test variables were trip height (TH), trip length (TL), and chamber length (L'). The dependent variables were the rhenium foil loss rate and the thrust performance of the engine. The objective was to find the combination of design parameters which would minimize rhenium loss and maximize engine performance. The set of test conditions used to investigate the

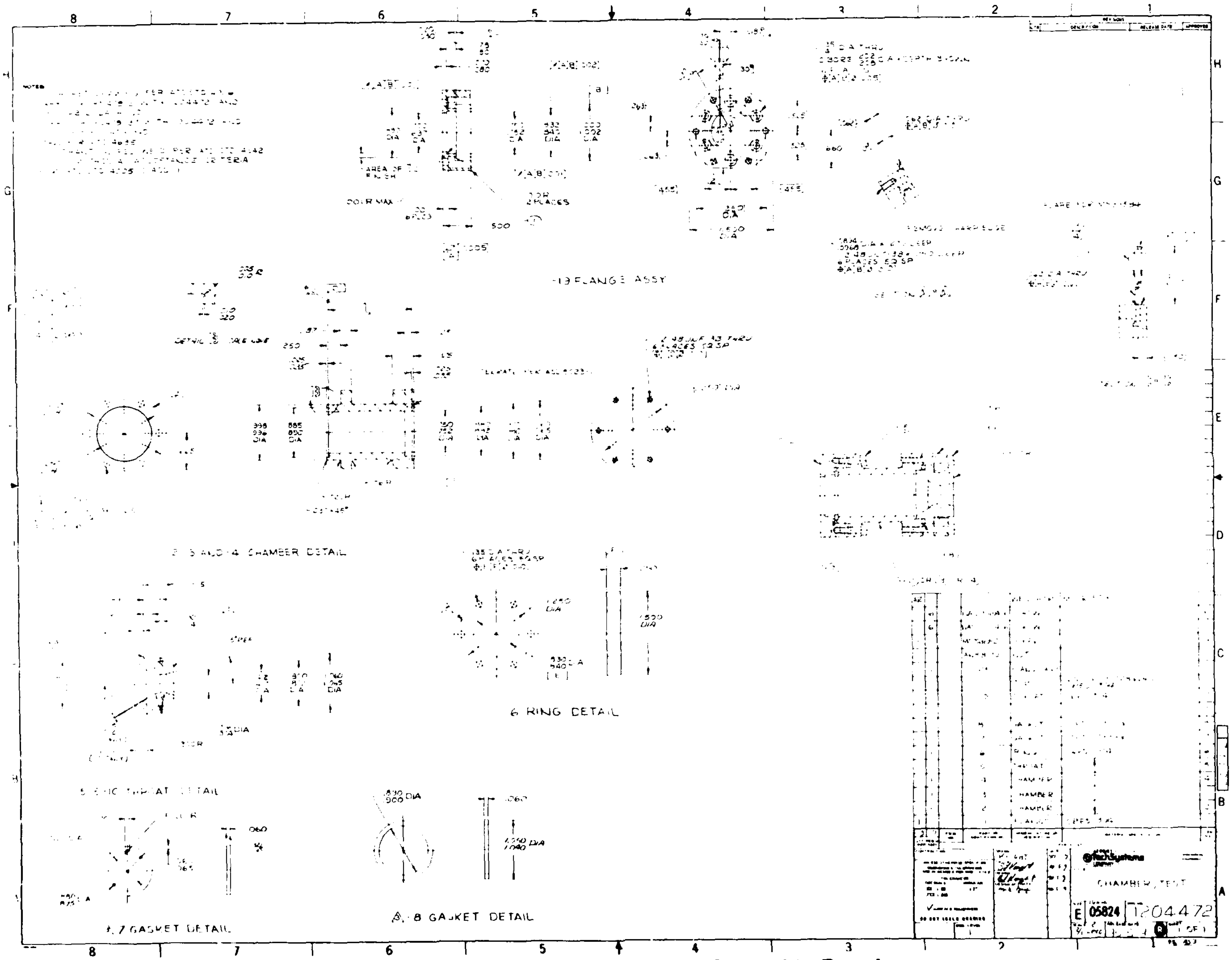
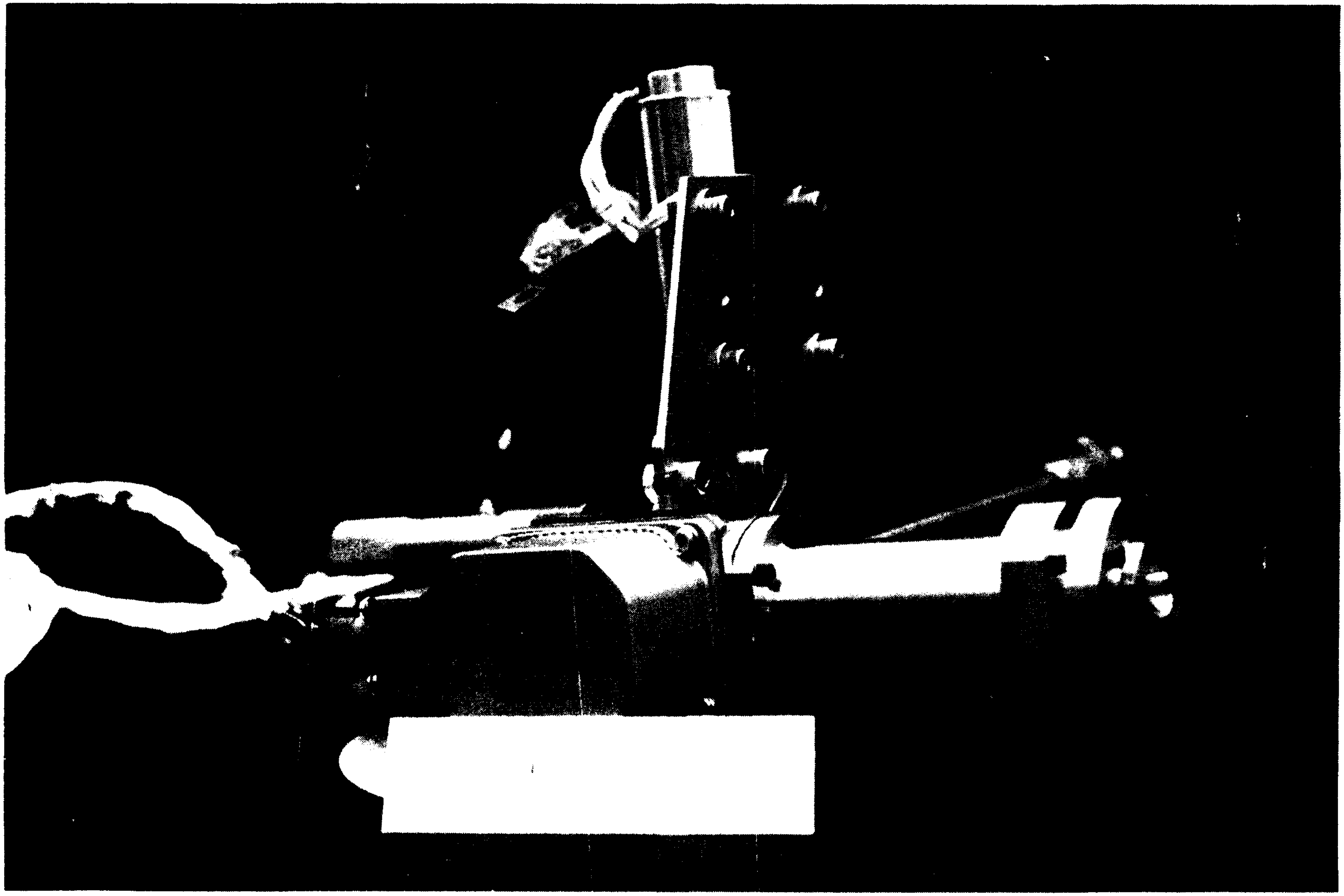


Figure 3.1-7. Optimization Hardware Assembly Drawings



(C0590 2128)

Figure 3.1-8. Assembled 14-Lbf Optimization Thruster

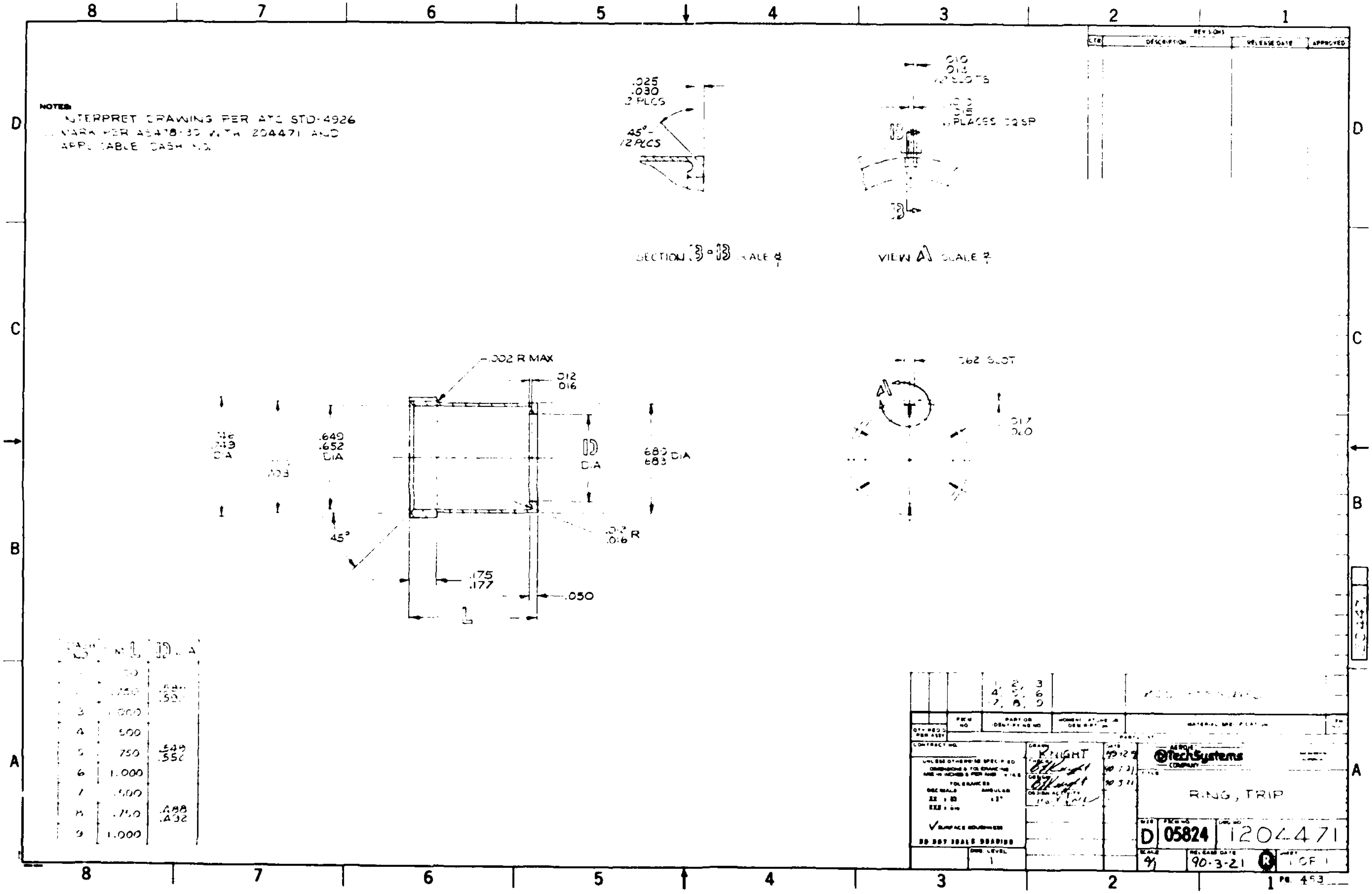


Figure 3.1-9. Optimization Trip Rings

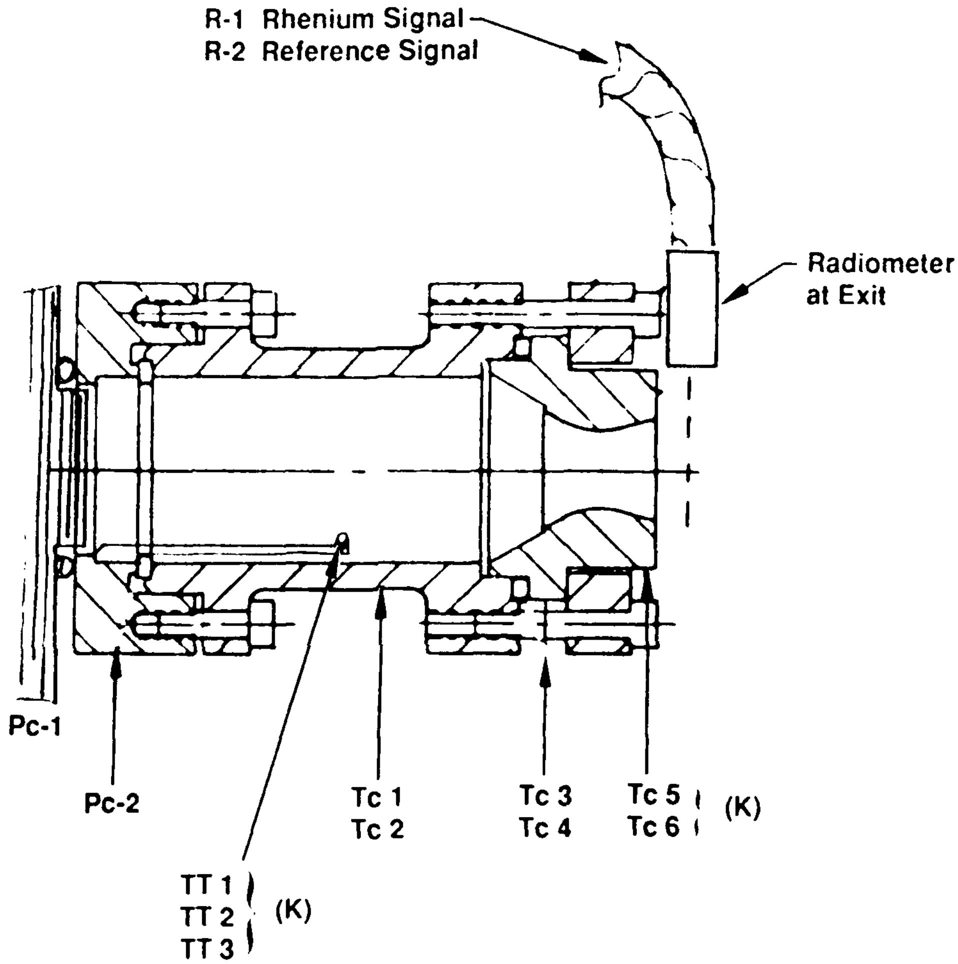


Figure 3.1-10. 14-Lbf Optimization Hardware Instrumentation Locations

relationship of each of these variables was optimized through use of Taguchi analysis. The test conditions and results are summarized in Figure 3.1-11.

Test 101 was the first checkout test (no rhenium foil). It was killed on low chamber pressure after only 0.3 sec. No attempt was made to reduce the performance data after this short, non-steady state firing. The low chamber pressure kill was attributed to the use of a Pc tap with a long response time. On subsequent tests, an alternative Pc tap was used for redline monitoring and data reduction.

Tests 102 and 103 were also checkout tests (no rhenium foil) used to adjust line pressures to obtain the correct Pc (100 psia) and MR (1.65). Performance data were averaged over one second intervals on these two tests and compared with theoretical C* and Isp calculated by TDK-BLM runs for those particular conditions. Energy Release Efficiencies (Measured Isp/Theoretical Isp) of 98.6% and 98.4% were obtained for runs 102 and 103, respectively. Calibration of the thrust stand instrumentation was adequate and a chamber barrel and nozzle lined with rhenium foil were mounted on the test stand prior to the next test.

Test 104 was conducted at nominal MR and Pc conditions. No damage to the chamber and nozzle foils was seen upon visual examination after the test. As a result, the targeted MR was increased to 1.9 for Test 105. Again, post test examination did not show any rhenium erosion, and the targeted MR was increased to 2.0 for Test 106. During this test, marks were observed on the rhenium foil in the nozzle. All subsequent tests were run at a nominal MR of 2.0.

The data were analyzed by several independent methods. The pre- and post test appearance of each piece of hardware was examined, both visually and under an optical microscope. Particular attention was paid to the condition of the rhenium foils and the surfaces of the trip ring. Photographs recorded the post test condition of all of the foils. The weight of each foil was measured, both alone and as part of the assembled hardware, before and after each test. Rhenium loss rates were calculated based on the individual foil weights before and after the tests (See Figure 3.1-12). Theoretical Isp and C* values were calculated by TDK-BLM for each test condition and compared with the measured thrust stand performance. Data from a plume radiometer were analyzed for the presence of rhenium in the engine plume.

Figures 3.1-13 through 3.1-16 present an overall summary of the performance and material compatibility data as a function of the two most critical test parameters

14 lbF OPTIMIZATION TEST SUMMARY

Run	Lc in	Lt in.	Ht in.	Duration, sec.	PC-2 psia	Fcorr lbF	Wp lbm/s	MR O/F	PA psia	Dt in.	Ae/At	Fvac lbF	Isvac sec	C* ft/sec	Theo. Is sec	Theo C* ft/sec	Fract. Theo Is	Fract. Theo C*	Chamber Foil Loss gm	Duration sec.	Gross Chamber Foil Loss, gm/hr	Exposed Chamber Fraction	Corr Chamber Foil Loss, gm/hr	Nozzle Foil Loss, gm	Nozzle Foil Loss, gm/hr	Exposed Chamb Length	Chamber Loss, mils/hr	Nozzle Loss, mils/hr
-102	3.5	1	0.05	4.97	107.5	9.814	0.0501	1.832	14.548	0.315	1.736	11.78	235.2	5380	238.6	5587	0.986	0.963	No Foil	4.97	--	--	--	--	--	--	--	--
-103	3.5	1	0.05	4.99	103.1	9.310	0.0479	1.701	14.548	0.315	1.736	11.28	235.6	5398	239.5	5607	0.984	0.963	No Foil	4.99	--	--	--	--	--	--	--	--
-104	2.1	1	0.05	5.00	100.4	9.041	0.0484	1.616	14.548	0.317	1.714	11.01	227.3	5266	239.7	5613	0.948	0.938	0.01994	5.00	14.36	0.4444	32.31	0.00831	5.98	0.611	29.64	44.20
-105	2.7	1	0.03	5.00	107.0	9.632	0.0509	1.841	14.553	0.318	1.703	11.60	227.7	5370	238.3	5584	0.956	0.962	No Meas	5.00	--	--	--	--	--	--	--	--
-106	2.7	1	0.03	9.13	111.2	10.034	0.0533	2.002	14.553	0.318	1.703	12.00	225.4	5335	236.6	5545	0.953	0.962	0.00682	9.13	2.69	0.6132	4.39	0.05170	20.39	1.211	2.80	150.58
-107	3.5	0.75	0.08	7.01	113.7	10.338	0.0526	2.014	14.553	0.316	1.725	12.31	234.0	5456	236.6	5543	0.989	0.984	0.00650	7.01	3.34	0.8148	4.10	0.00221	1.13	2.261	1.86	8.38
-108	2.1	0.25	0	10.00	108.2	9.626	0.0534	1.950	14.474	0.315	1.736	11.58	217.0	5083	237.2	5558	0.915	0.915	0.01943	10.00	6.99	0.8333	8.39	0.35303	127.09	1.361	6.48	938.78
-109	2.7	1	0.08	6.74	111.9	10.152	0.0525	1.998	14.474	0.318	1.703	12.11	230.6	5448	236.7	5545	0.974	0.982	0.00	6.74	0.00	0.6132	0.00	0.00215	1.15	1.211	0.00	8.48
110	3.5	0.25	0	8.85	110.8	9.914	0.0542	2.001	14.474	0.315	1.736	11.87	219.1	5125	236.7	5544	0.926	0.924	No Foil	8.85	--	--	--	--	--	--	--	--
-111	2.1	0.75	0.05	8.30	110.6	9.896	0.0537	2.015	14.474	0.318	1.703	11.85	220.9	5267	236.6	5543	0.934	0.950	0.00490	8.30	2.13	0.6262	3.40	0.00655	2.84	0.861	3.12	21.00
-112	2.7	0.75	0.08	7.72	113.4	10.133	0.0525	1.985	14.474	0.318	1.703	12.09	230.4	5522	236.8	5549	0.973	0.995	0.00254	7.72	1.18	0.7397	1.60	0.00368	1.72	1.461	1.38	12.67
Calc Mass Loss Data for One "Typical" Spotweld Nugget =																			0.00069	10	0.25	0.7	0.35	0.00069	0.25	1.2	0.37	1.83

Figure 3.1-11. 14-Lbf Optimization Test Summary

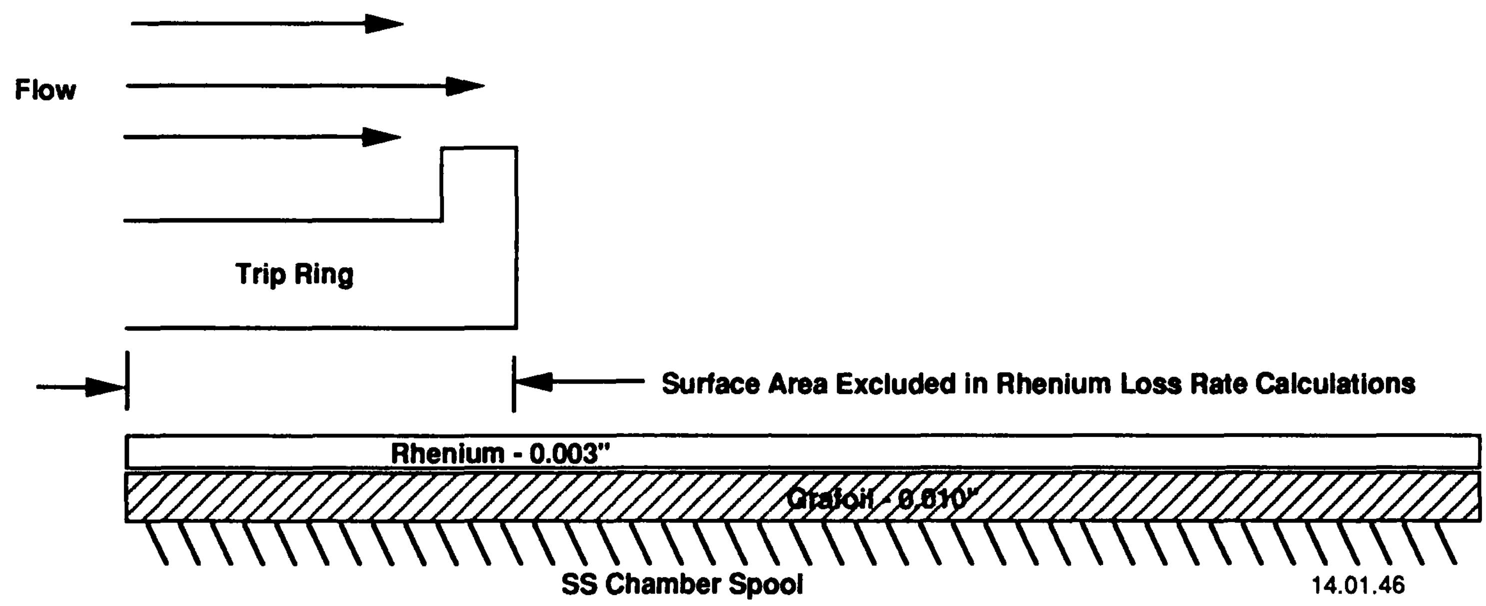


Figure 3.1-12. Rhenium Foil Loss Rates Were Calculated Based on Exposed Surface Area

ASRC 14# Optimization, Is & C* EFFIC.

Test - 102 Thru -112

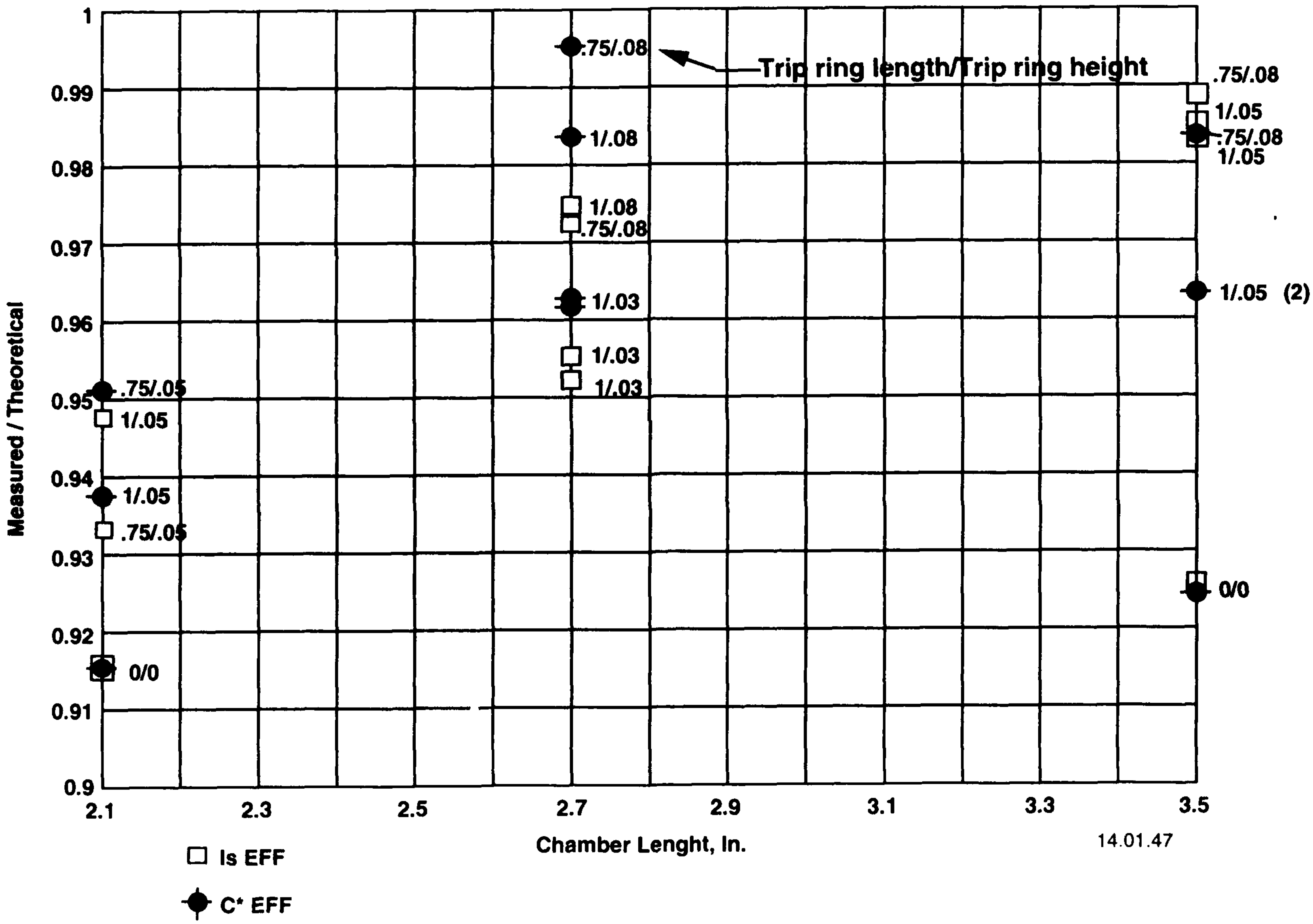


Figure 3.1-13. Performance Measurements of Optimization Test

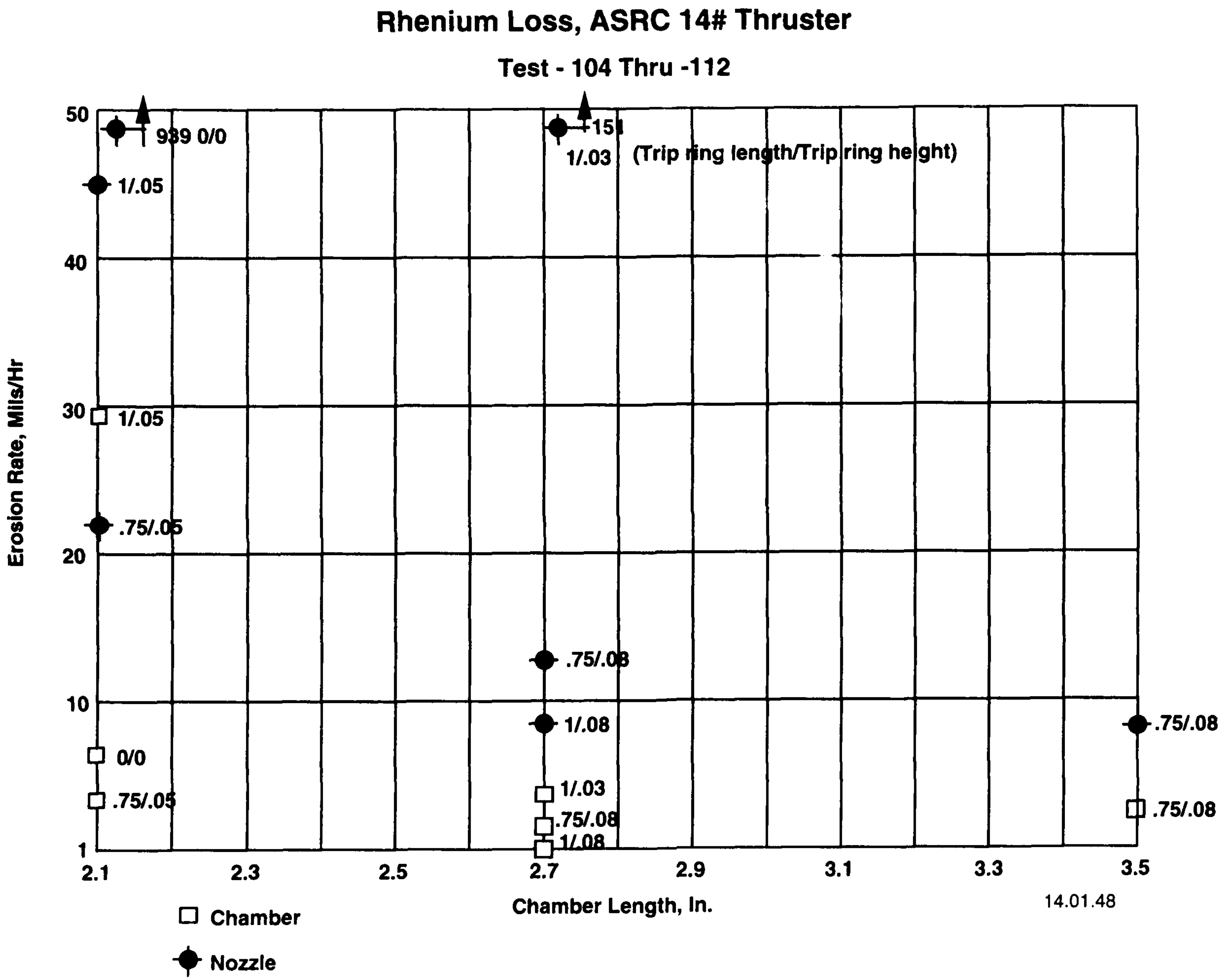


Figure 3.1-14. Rhenium Erosion Rates, Calculated From Weight Loss, as a Function of Chamber Length

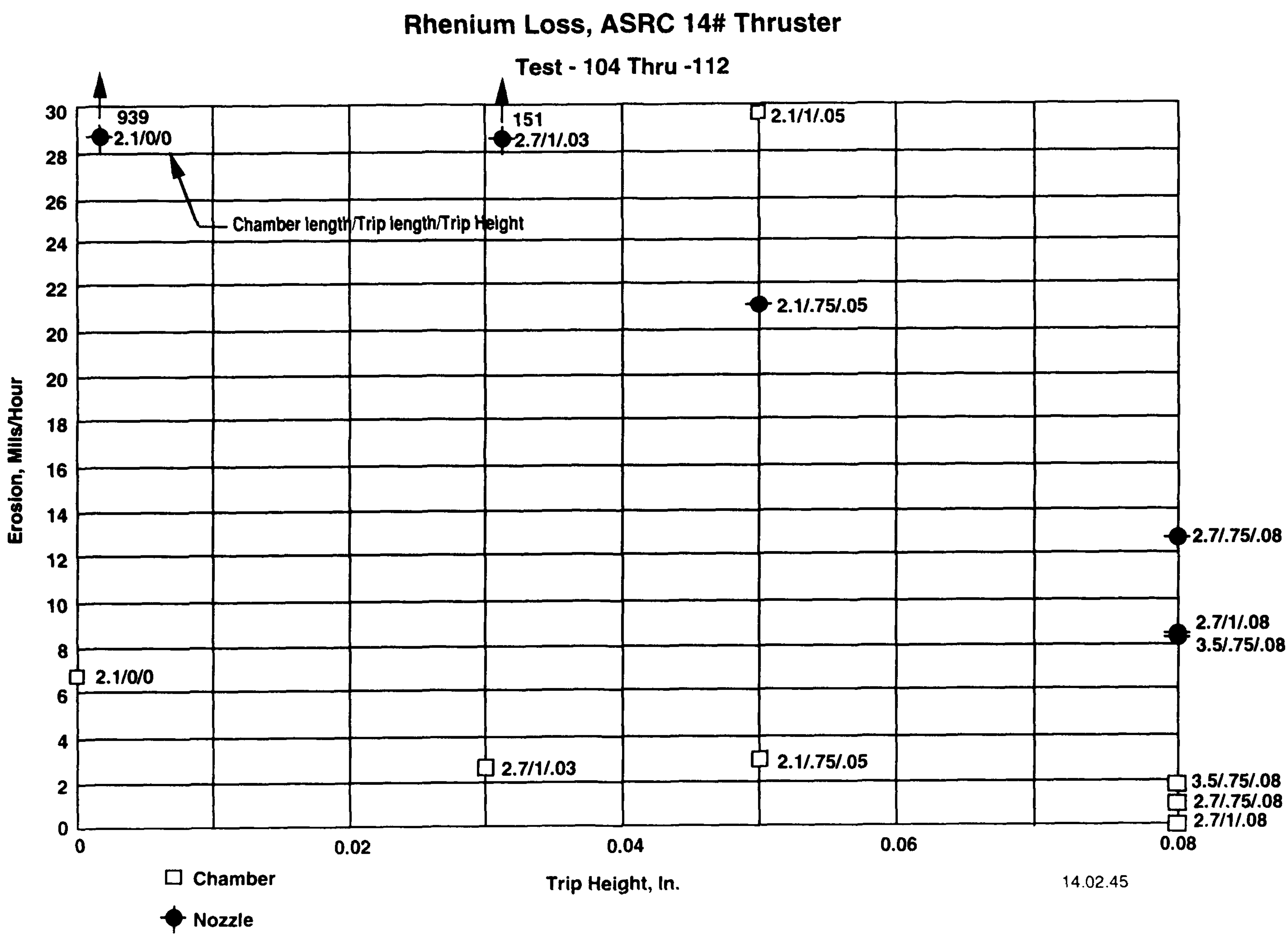


Figure 3.1-15. Rhenium Erosion Rates, Calculated From Weight Loss, as a Function of Trip Height

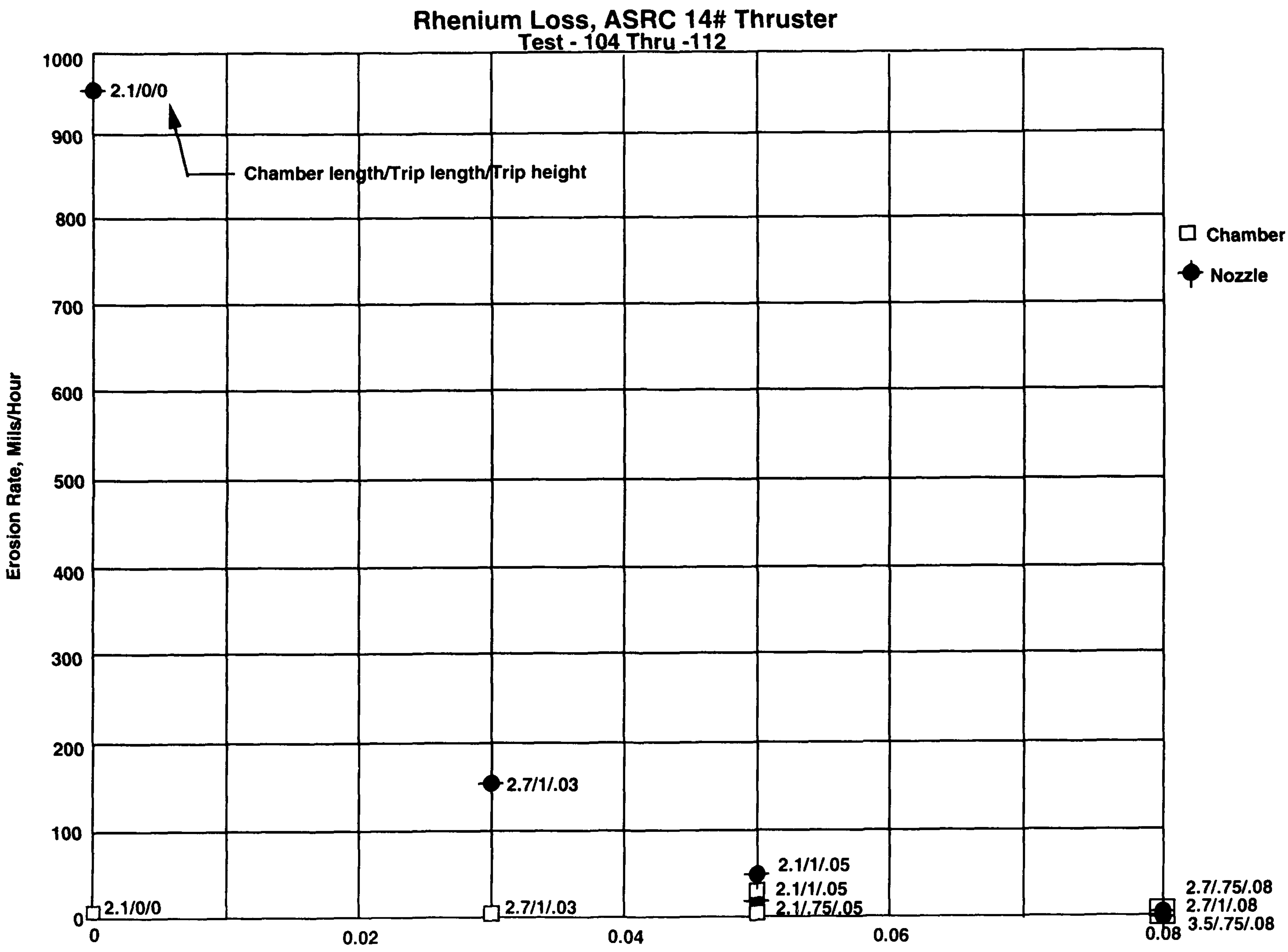


Figure 3.1-16. An Expanded Scale is Required to Show All Erosion Rates as a Function of Trip Height

– chamber length and trip height. The major conclusions reached from the optimization tests follow.

1. An increase in the trip ring height from 0 to 0.080 in. improved both the material compatibility and the delivered performance of the engine.

Figures 3.1-17 and 3.1-18 show the rhenium loss rate in the barrel and the nozzle as a function of trip height. Particularly at the nozzle, the rhenium loss rate is a strong function of trip height. This is confirmed by visual inspection of the rhenium foils. As shown in Figures 3.1-19 and 3.1-20 the foils from the test with a zero height trip ring (Test 108) show major damage. Plume radiometer data also support the conclusions that rhenium loss rates decreased when the trip ring height was increased, as shown in Figure 3.1-21. The radiometer data are plotted as a function of the square root of the rhenium concentration in the plume (calculated by foil weight differences) in this figure.

The performance of the engine was definitely improved by increasing the trip height. Figures 3.1-22 and 3.1-23 show the percentage of theoretical Isp and C* measured in the tests as a function of trip height. The lowest Isp efficiencies were measured in tests with the lowest trip rings. At zero trip height, 91.5% of theoretical Isp was attained. This is within approximately 1% of the nominal performance of the current 14 lbf production engine, and corresponds to an Isp of 282 sec at an area ratio of 75:1. The highest Isp efficiencies were delivered in the three tests with the highest trip ring. The average Isp delivered during these three tests was approximately 97.9% of theoretical, which corresponds to an Isp of 302 sec at an area ratio of 75:1.

2. An increase in the chamber length from 2.1 to 3.5 in. improved both the material compatibility and delivered performance of the engine.

Figures 3.1-17 and 3.1-18 show the rhenium loss rate in the barrel and nozzle as a function of chamber length. Particularly in the nozzle, the rhenium loss rate is a strong function of chamber length. This was confirmed by visual inspection of the rhenium foils, as documented in Figures 3.1-19 and 3.1-20. Plume emission data support the conclusion than rhenium loss rates decreased as the chamber length increased.

The performance of the engine was also improved by an increase in the chamber length. Figures 3.1-22 and 3.1-23 show the percentage of theoretical Isp and C* attained in the tests as a function of chamber length.

Chamber Erosion Versus L_c , L_t , H_t & MR

from Taguchi Matrix

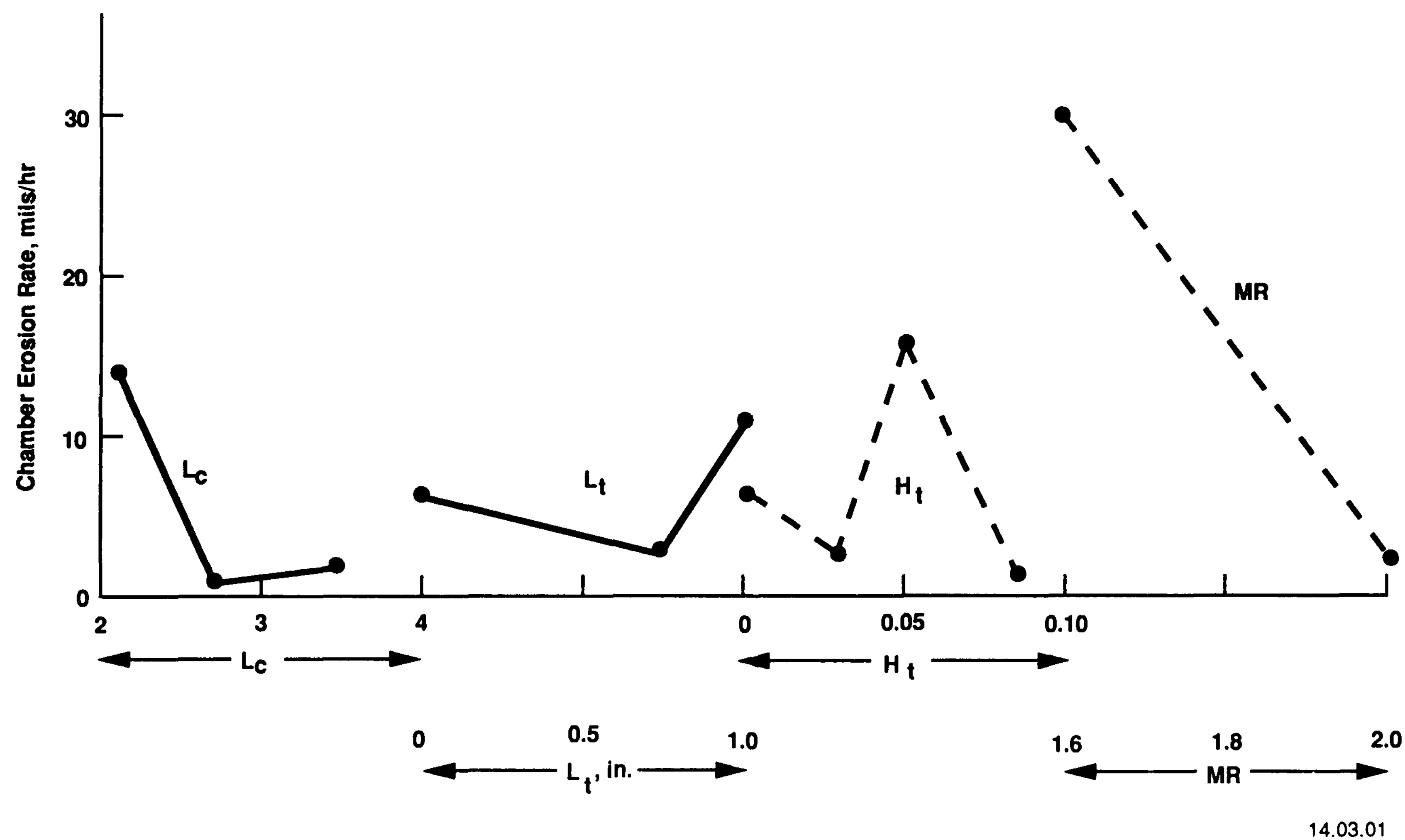


Figure 3.1-17. Rhenium Erosion Rates in Chamber Barrel

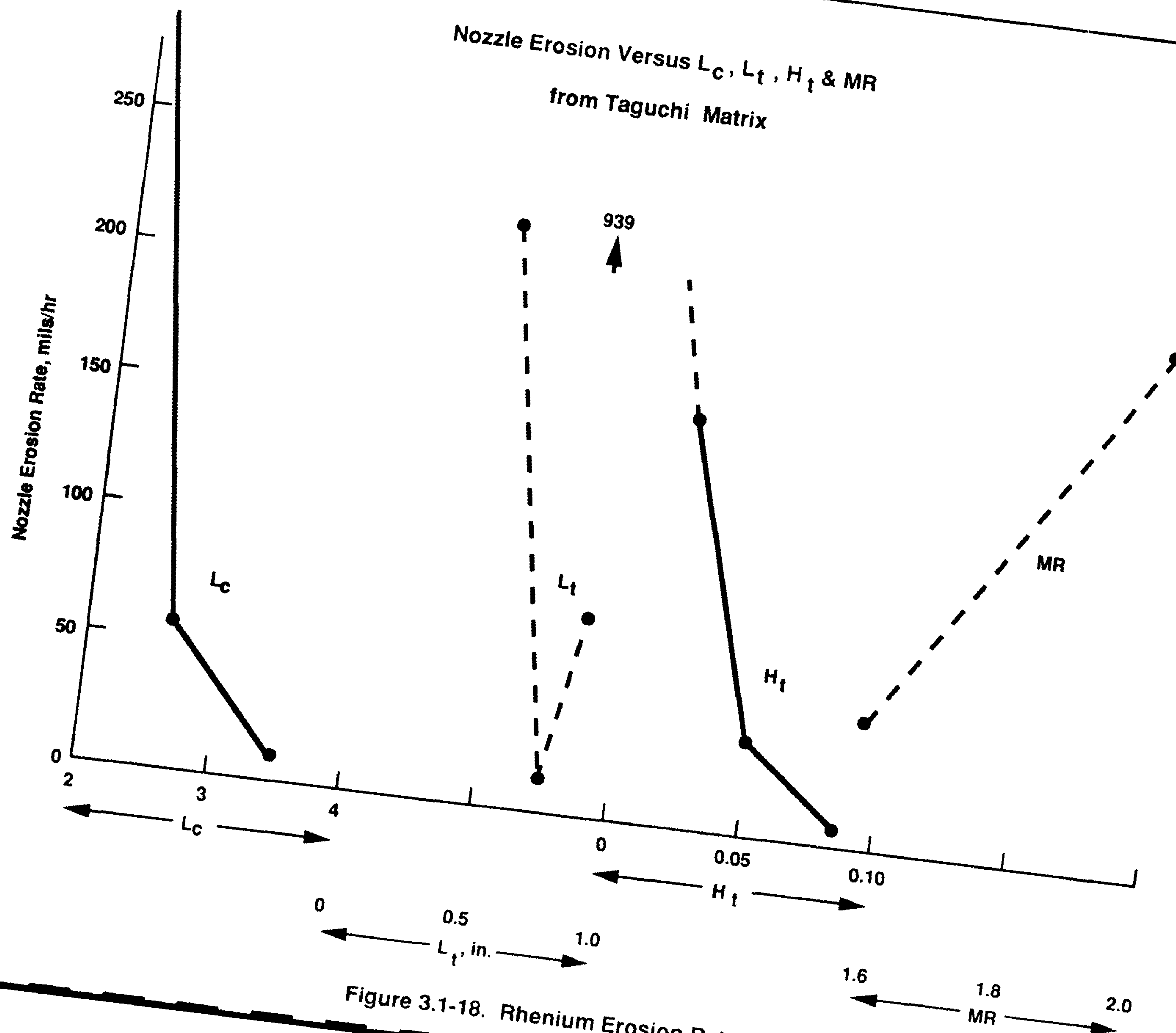


Figure 3.1-18. Rhenium Erosion Rates in Nozzle

14.03.02

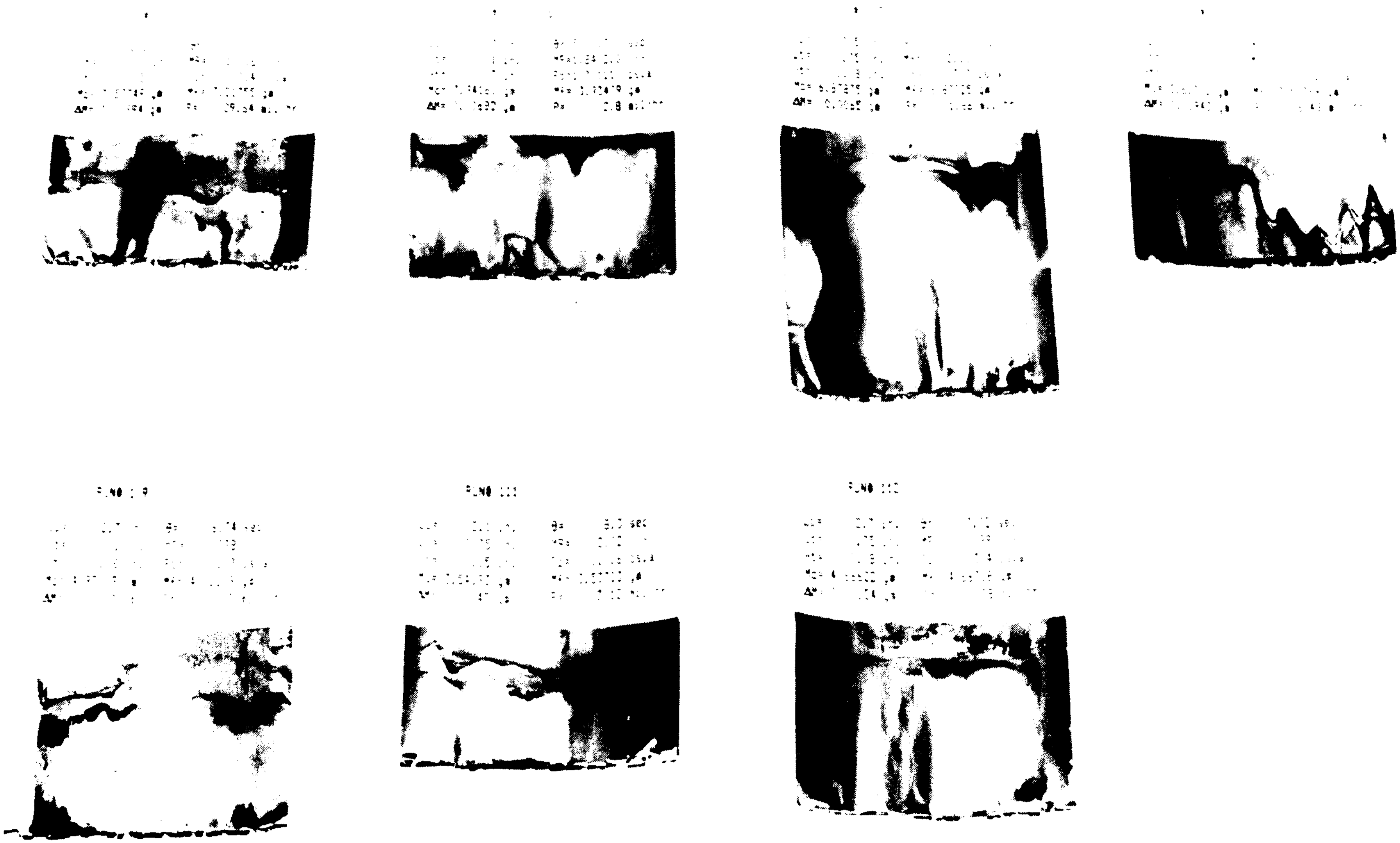


Figure 3.1-19. Post Test Appearance of Chamber Barrel Foils

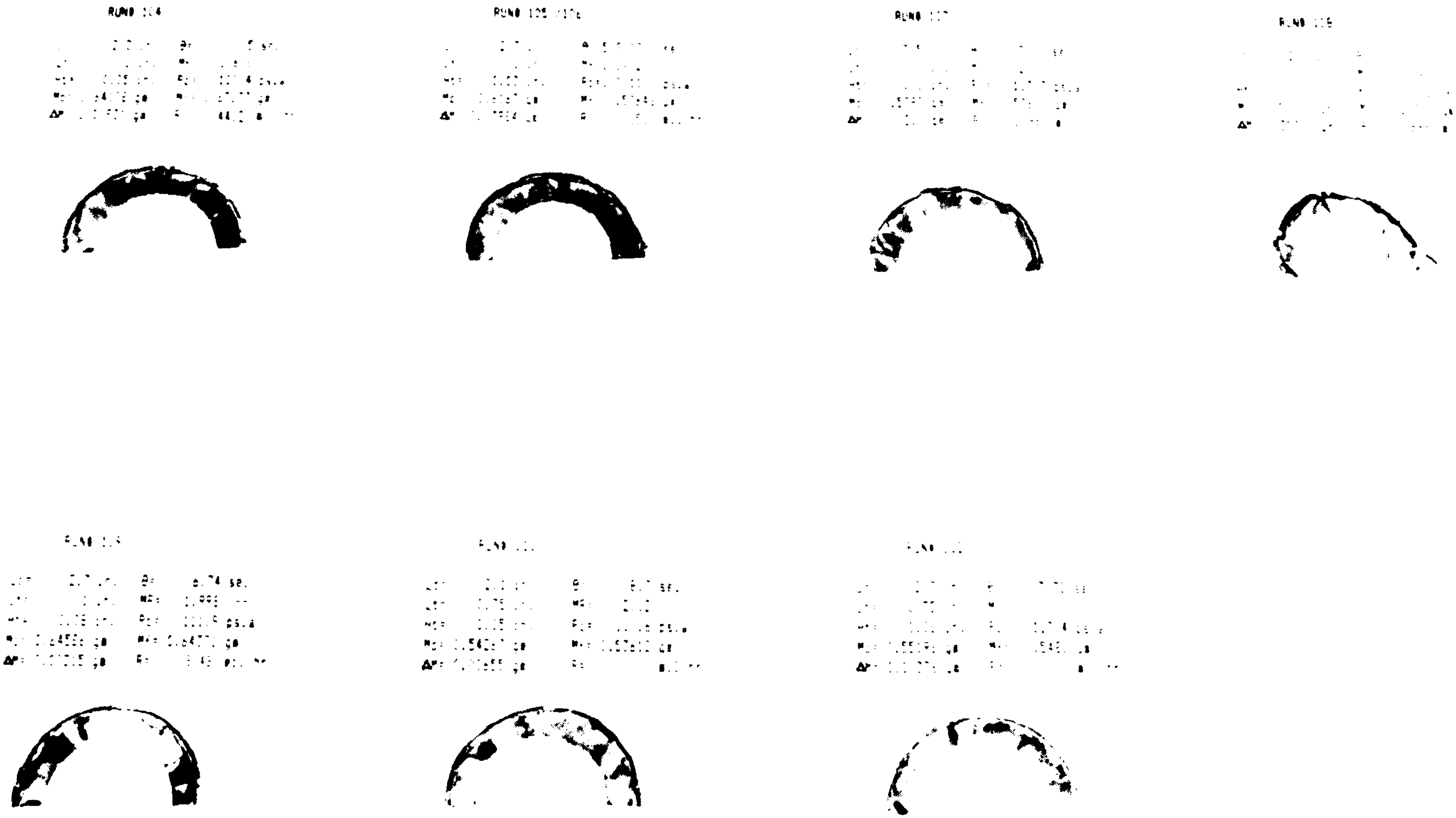


Figure 3.1-20. Post Test Appearance of Nozzle Foils

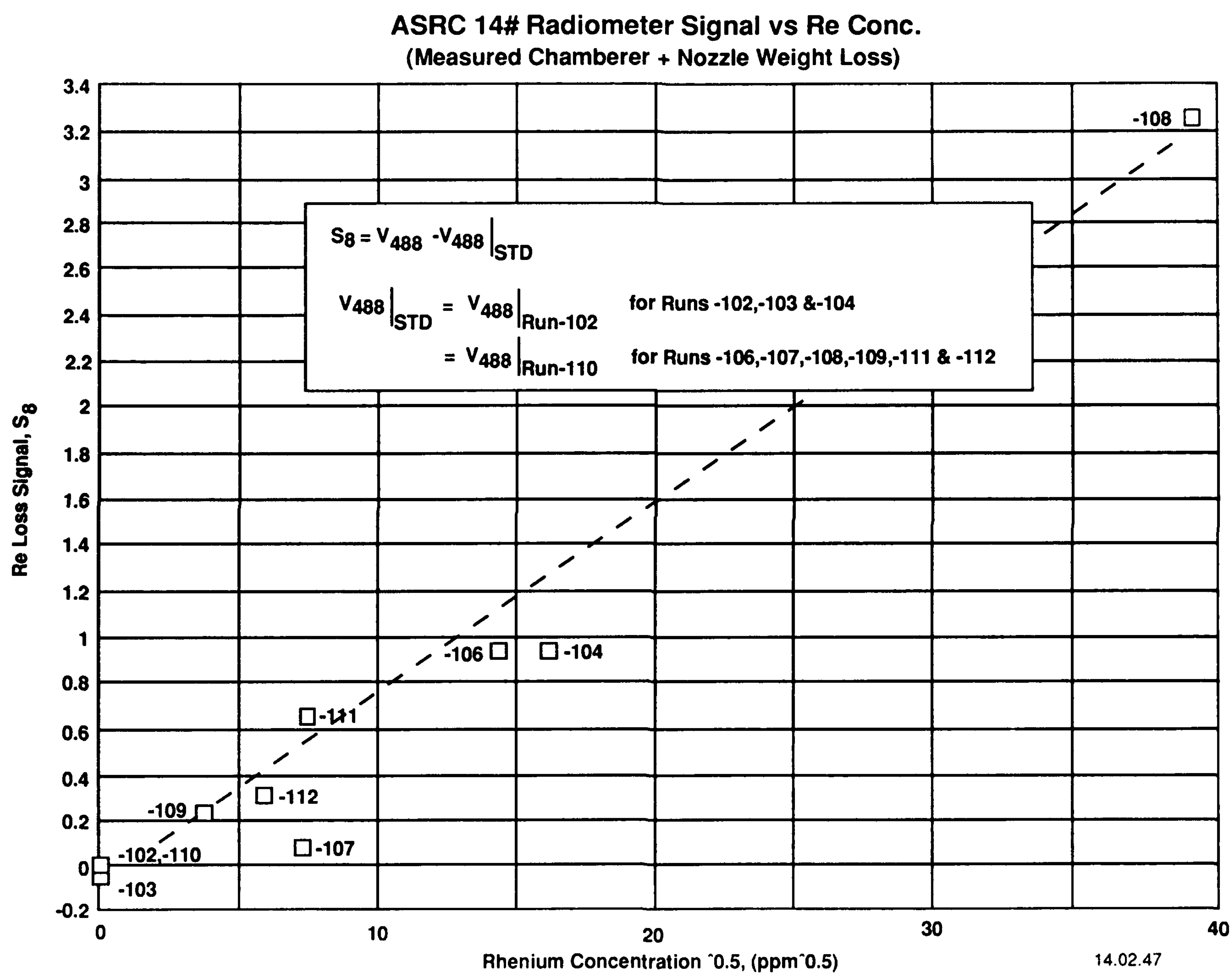


Figure 3.1-21. Radiometer Signals Provided an Independent Measure of Rhenium Loss

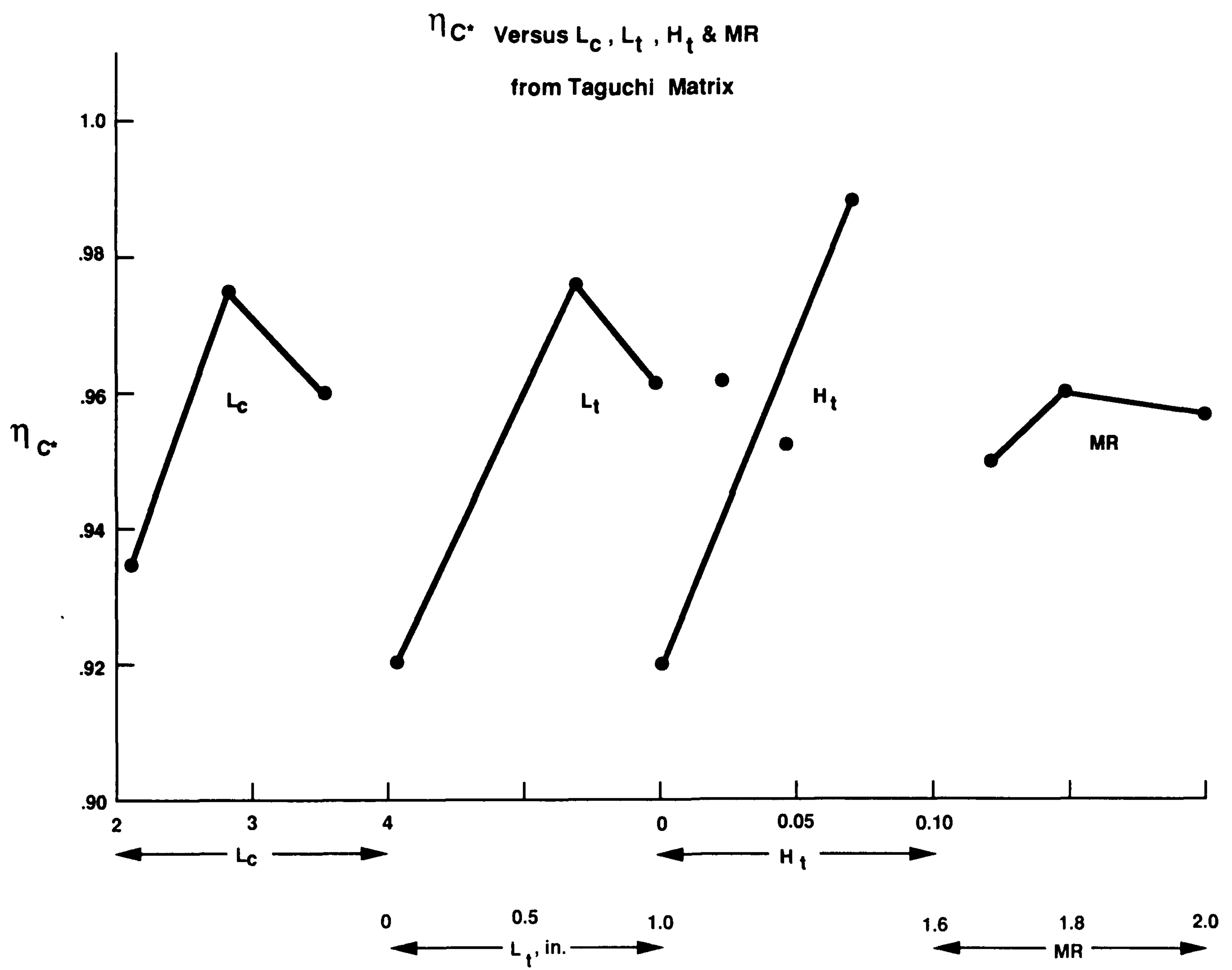


Figure 3.1-22. C* Performance of Optimization Hardware

14.03.03

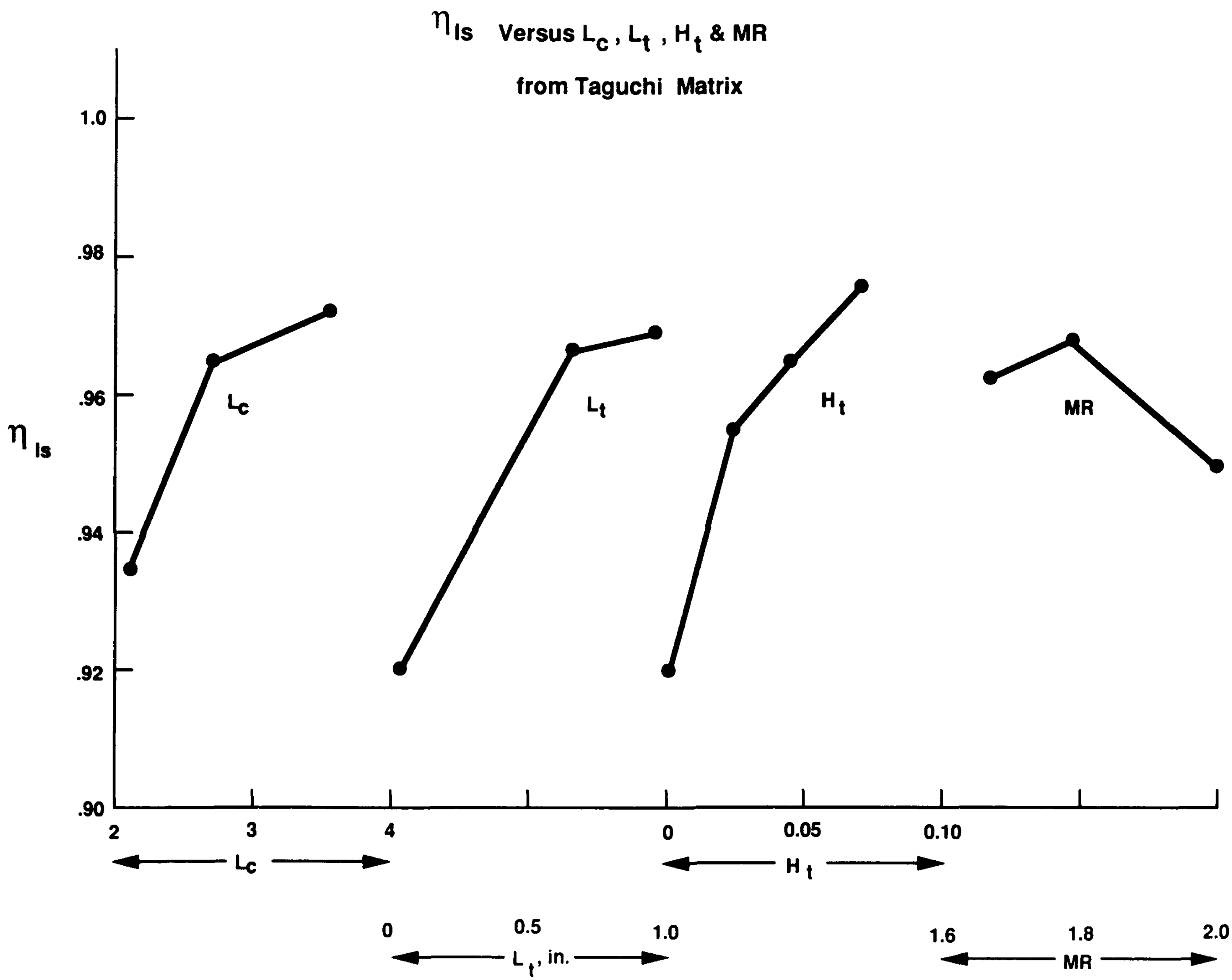


Figure 3.1-23. Ispv Performance of Optimization Hardware

3. Increasing the trip length from 0.75 to 1.00 inches had only a small impact on either the material compatibility or the delivered performance of the engine.

Figures 3.1-17 and 3.1-18 show the material loss rate in the barrel and nozzle as a function of trip ring length. It appears that there is a minimum in the rhenium loss rate curve at a trip ring length of 0.75 in. Examination of matched parts of tests, where the trip length is the only differing parameter (109, 112) and (104, 111) supports this conclusion. However, the loss rate of iridium is still anticipated to be very low, at a trip length of either 0.75 or 1.00 in.

An increase in trip length does not have a clear effect on the delivered performance of the engine. As seen in Figures 3.1-22 and 3.1-23, an increase in trip length from 0.75 to 1.00 in. increased the Isp efficiency, but decreased the C* efficiency.

4. The interchangeable nozzle section provided a more sensitive test section for measuring material compatibility than the chamber barrel.

As seen in the material loss data, there was much more difference in the rhenium loss rates from test to test in the nozzle than there was in the barrel. Photographs of the foils from the nozzle and the chamber confirm that there was much more visible damage to the nozzle foils than to the barrel foils. This is consistent with the results from long duration firings of 5 lbf Ir-Re chambers.

5. Increasing the MR from 1.65 to 2.00 had an uncertain effect on material compatibility and a minimal impact on delivered performance.

As shown in Figures 3.1-17 and 3.1-18, the material loss rates in the chamber appear to go down in the chamber and up in the nozzle with increasing MR. However, it should be noted that these curves are based on only one low MR test (Test 104). Still, concern was raised by the fact that the only test near the nominal 1.65 MR produced a high material recession rate in the chamber. However, post test weight of the chamber and foil assembly was higher than the pretest assembly weight, which indicated no material loss. As well, visual examination of the chamber and nozzle foils from Test 104 did not indicate heavy damage, as shown in Figures 3.1-19 and 3.1-20. It may be that the pretest foil weight was in error, though it is impossible to confirm this now.

An increase in MR did not have a major impact on the performance of the engine, as documented in Figures 3.1-17 and 3.1-18.

6. No trip rings were damaged during the tests.

A major concern prior to the optimization tests was loss of the trip ring tip, either through rapid oxidation or melting. This was not observed in any tests. Stainless steel tip rings of 0.030-in. trip height were not damaged, nor were the 0.050 or 0.080 in. high Pt-10Rh trips. No weight loss was measured on any trip rings, and SEM examination of the tip surface did not show significant material loss.

As a result of the optimization tests, design decisions were made about the flight-type Ir-Re hardware. The trip ring was made to a length of 1.00 in. and a height of 0.08 in. The height of the trip ring was chosen because of its advantageous effect on chamber compatibility and performance. The 1.00 in. long trip ring was chosen because it offers improved thermal management of the front end.

A chamber length of 2.7 in. was selected because it represented a compromise between good combustion performance (the longer the better) and good vibration performance (the shorter the better). The chambers were fabricated to provide an L' of 2.9 in. to reduce fabrication risk. If the first braze run of the platinum trip ring onto the chamber were unsatisfactory, the chamber could be cut again, eliminating the unsatisfactory braze joint. The trip ring could then be reattached and still maintain an overall L' of 2.7 in. In fact, this proved to be unnecessary, as all braze operations were successful the first time. Decisions on these design parameters allowed the release of the final drawings of the chamber and trip ring. The released drawings for these components are shown in Figure 3.1-24 and 3.1-25, respectively. Figure 3.1-26 shows the set of optimization test components.

3.1.5 Assembly Design

Concurrent with the conduct of the optimization tests, assembly drawings of the Ir-Re chamber, trip ring, and front-end flange were prepared. Various concepts and materials for the metallurgical joints at the front end were proposed. For each of the concepts, the assembly procedures were thoroughly discussed, and had considerable impact on the final design of the front end pieces.

Final selection was an assembly with two braze joints formed simultaneously. Drawing 1204490 (Figure 3.1-27) is the final assembly drawing which was released for assembly of the Ir-Re 14-lbf RCT design.

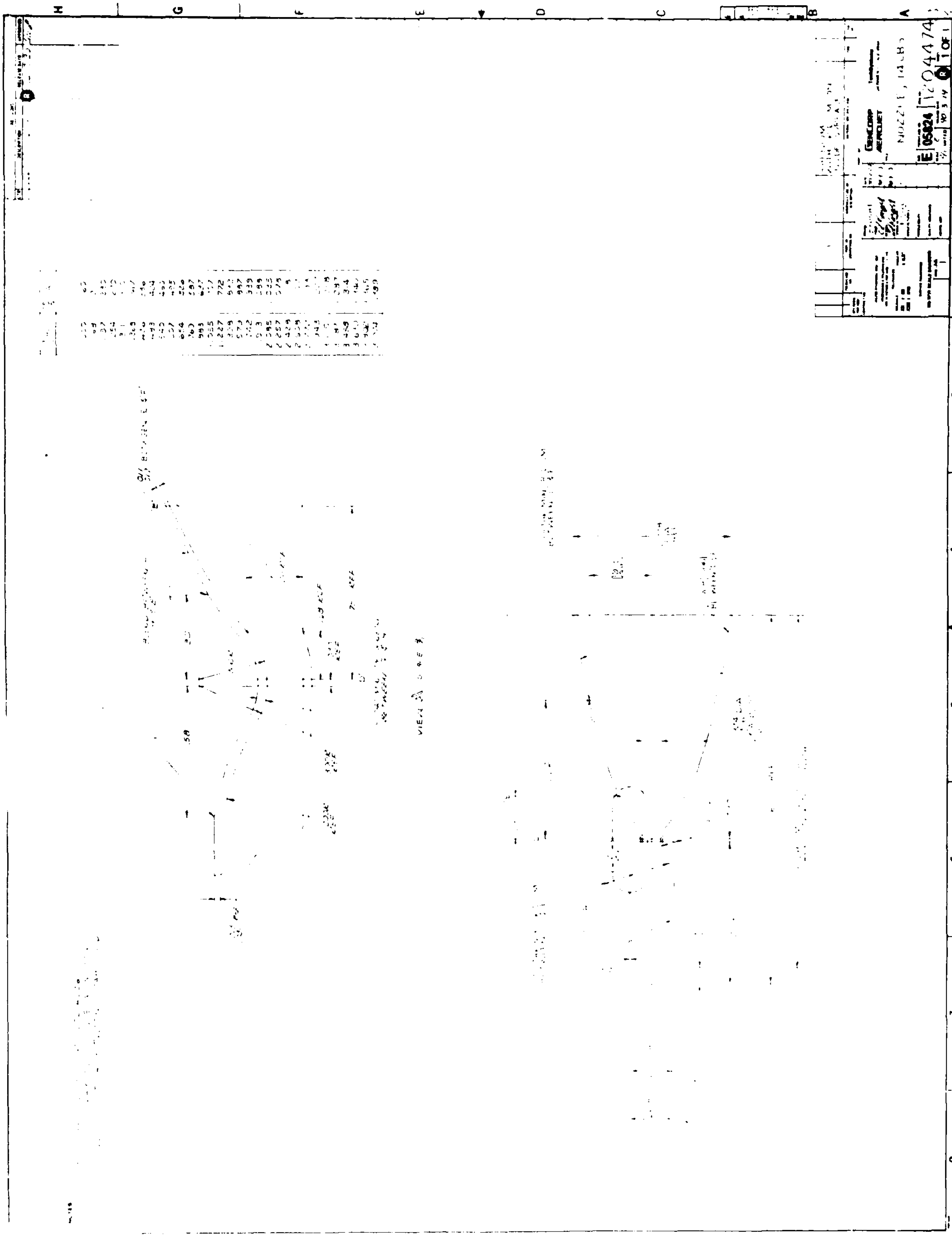


Figure 3.1-24. Ir-Re 14-Lbf Chamber

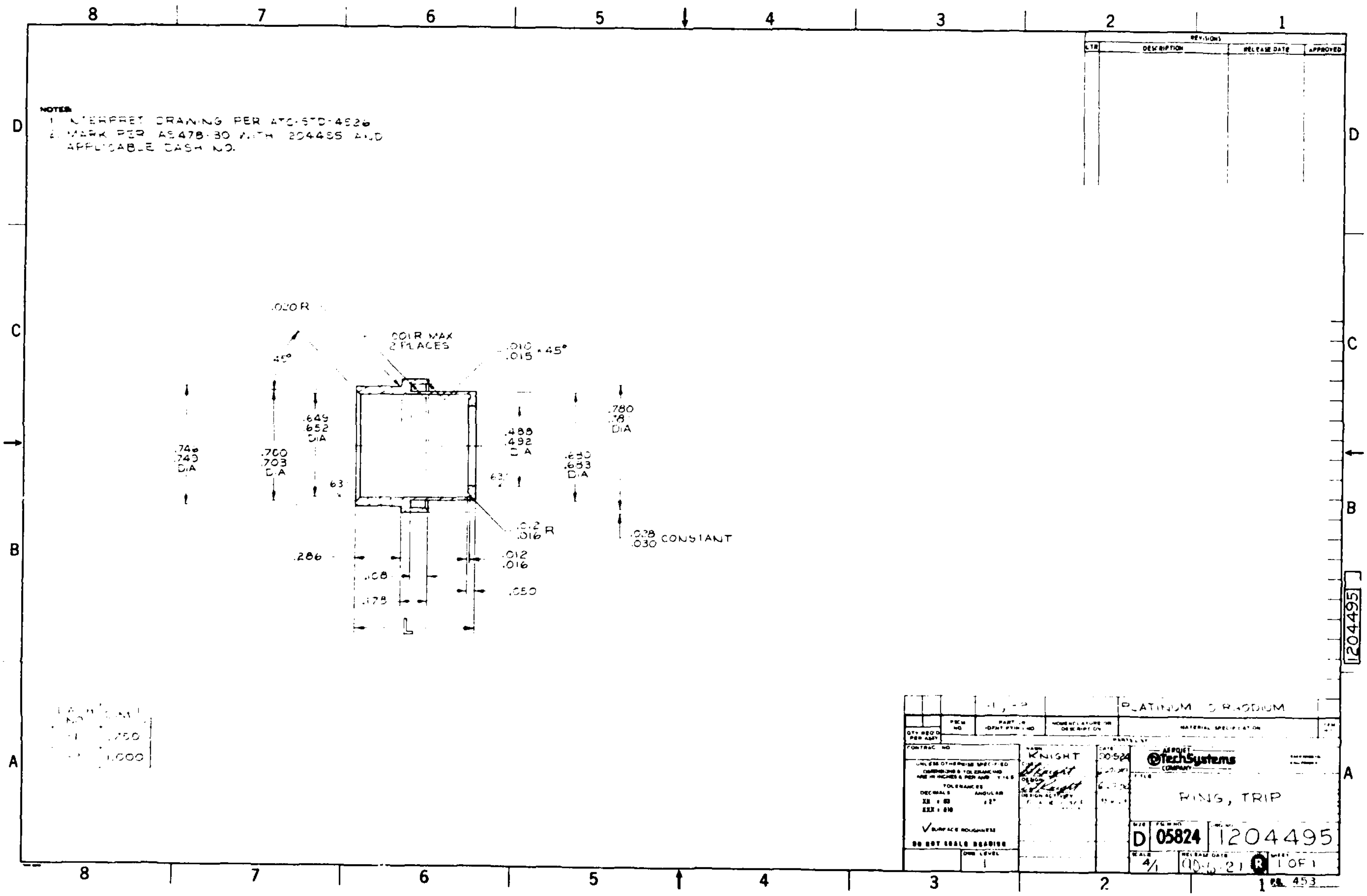
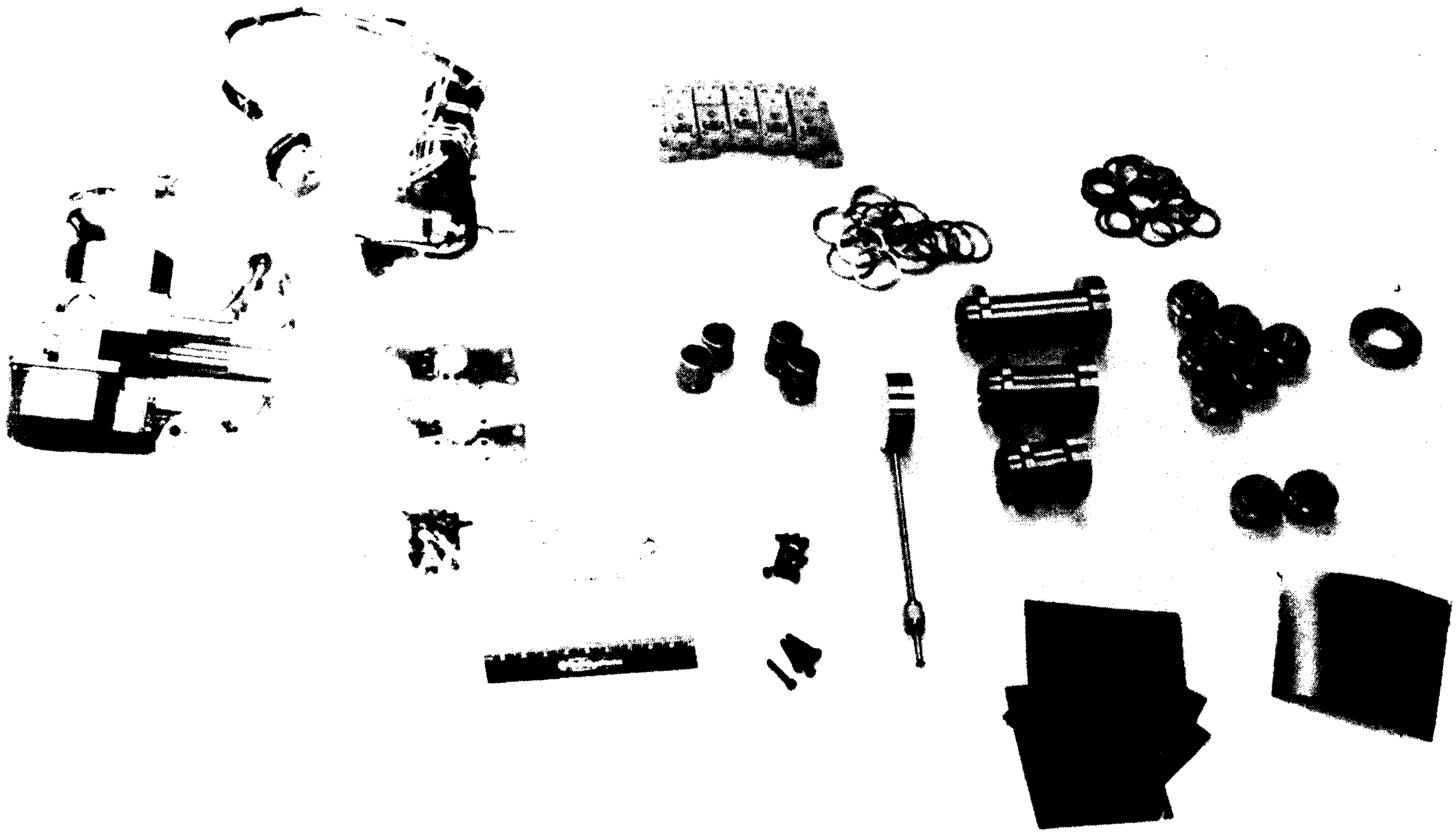


Figure 3.1-25. Final Flight-Type Trip Ring Design



(C0590 1857)

Figure 3.1-26. Optimization Hardware Ready for Test

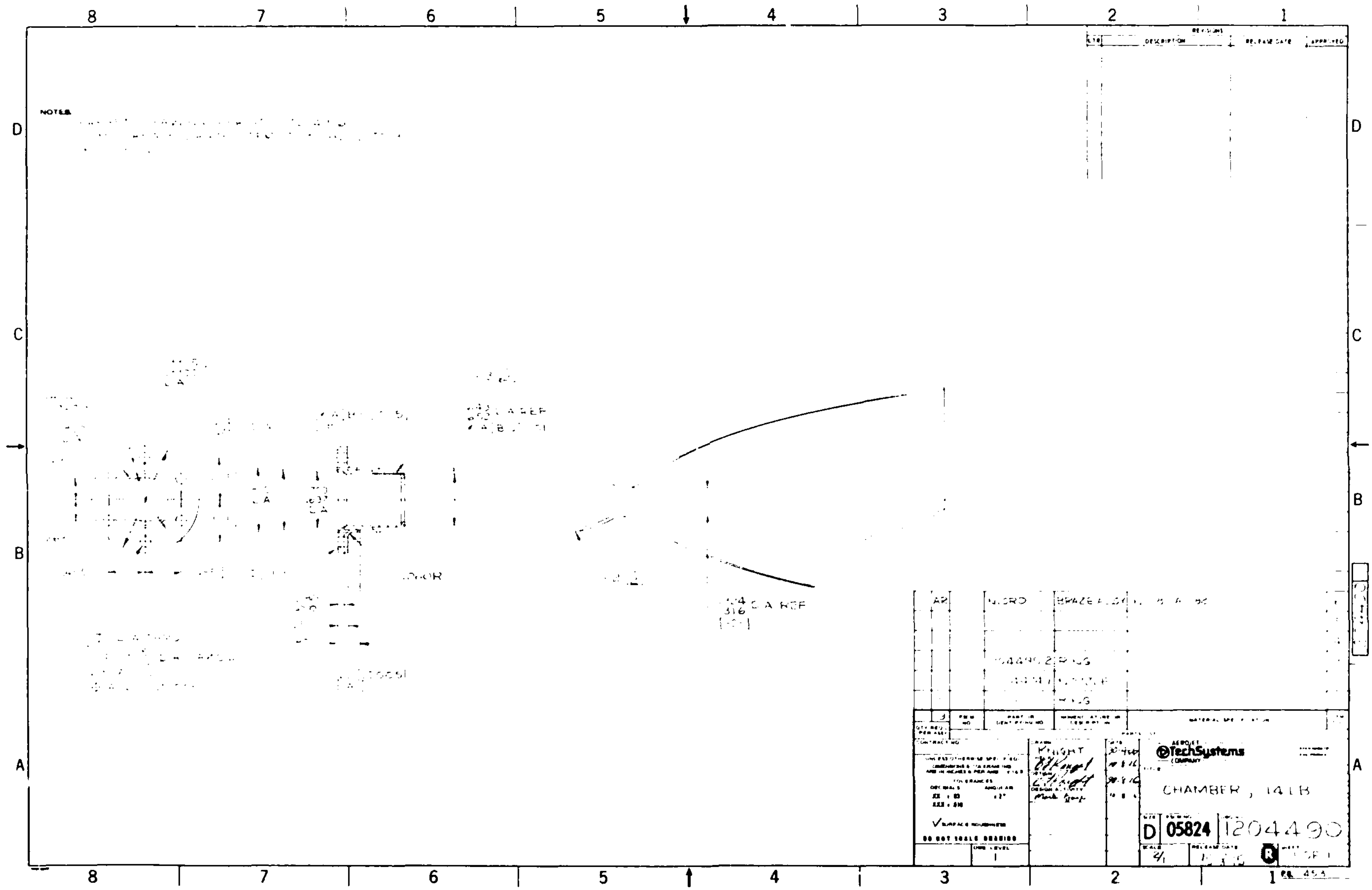


Figure 3.1-27. Advanced 14-lbf RCT Assembly Drawing

3.2 THRUSTER FABRICATION

Fabrication of the 14 lbf Ir-Re RCT's was accomplished in two subtasks: (1) Chamber Fabrication and (2) Chamber Assembly. In the first of these subtasks, 2 Ir-Re chambers, 2 Pt-10 Rh boundary layer trip rings, and 4 stainless steel flanges were fabricated and delivered to Aerojet. Two injectors and one bipropellant valve were furnished by the current C103 RCTM production program. In the second of the subtasks, the chamber, trip ring, and flange were brazed together, and then bolted onto an injector and valve for hot-fire testing. This section of the report documents the events of each of these subtasks.

3.2.1 Chamber Fabrication

Two 14 lbf Ir-Re chambers were built and delivered to Aerojet by Ultramet. Ultramet fabricated the chambers in six distinct steps: (1) fabricate molybdenum male mandrel, (2) apply by CVD .001-.002 in. Ir coating, followed by the structural rhenium layer, (3) grind the rhenium layer to reduce the wall thickness and weight of chamber, (4) cut the chamber to specified length, (5) etch the molybdenum mandrel from the inside and (6) apply a thin dentoid (tooth like), high emissivity black coating of rhenium to the chamber O.D. Ultramet considers some details of these steps proprietary, and was not forthcoming with procedures or status either during or after completion of the chambers. In fact, as documented in this section, the chambers did not go through identical fabrication processes. Fabrication of the chambers required five months.

Ultramet forwarded diameter measurements of chamber S/N 1 at the completion of the rhenium CVD run. A summary of the measurements is shown in Figure 3.2-1. The iridium layer was successfully applied to a nominal thickness of 2.8 mils in the throat. The rhenium layer was then applied in one CVD run, without masking the nozzle or barrel sections of the chamber. As a result, a wall thickness of 0.047-in. was obtained in the throat, but only after a large amount of excess rhenium had been deposited on the chamber barrel and nozzle. Excess rhenium in the chamber barrel would adversely affect thermal management of the front end by reducing the efficiency of the thermal dam. Excess rhenium in the skirt would adversely effect the ability of the chamber to withstand the vibration test environment. Assuming a simple cantilevered beam analogy, the moment provided by this as-fabricated design was calculated and compared to the analyzed geometry. These calculations showed the moment of the as-fabricated skirt was approximately 2.5 times more than the analyzed geometry.

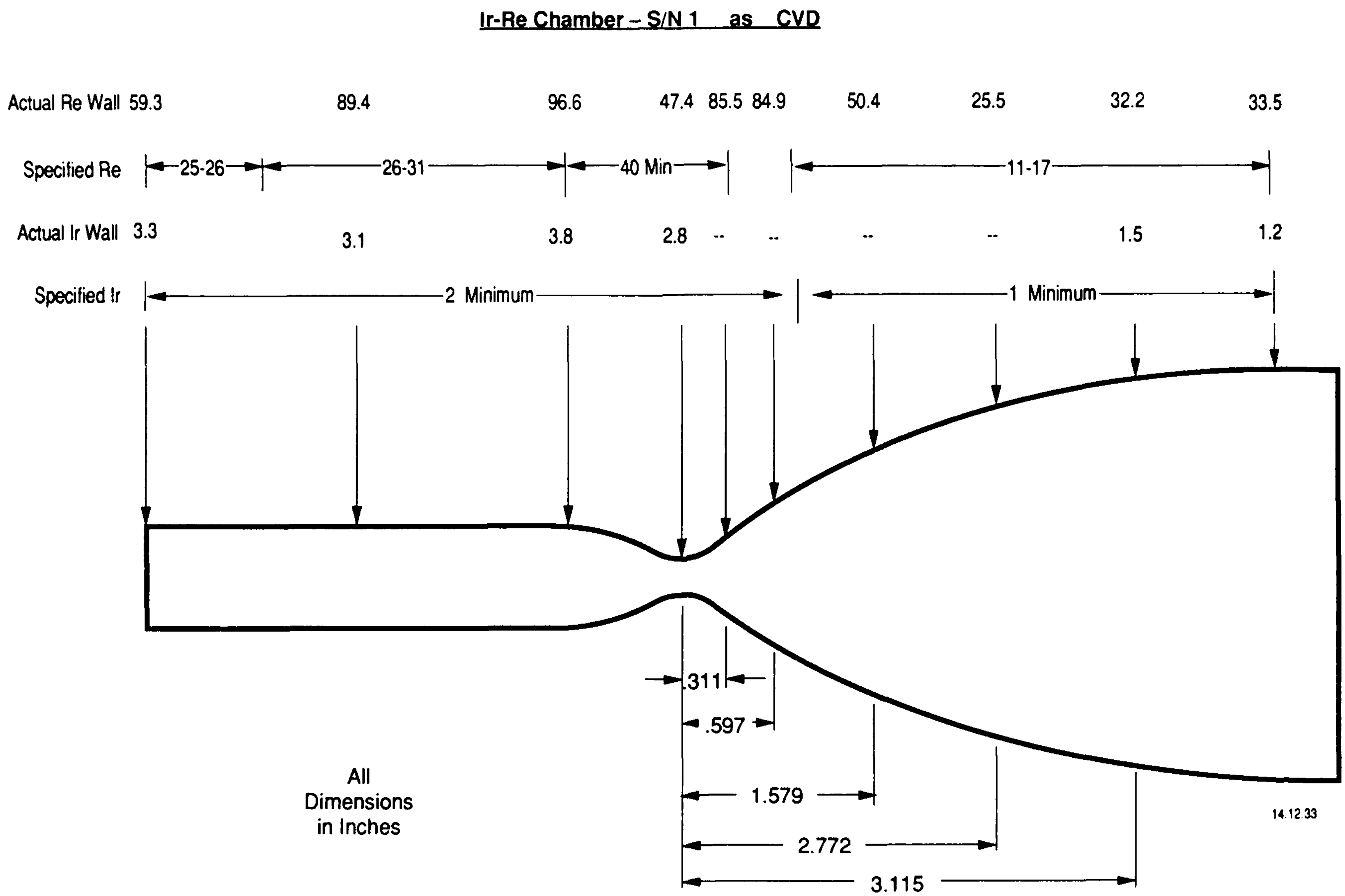


Figure 3.2-1. Chamber S/N 1 Had a Very Thick Layer of Rhenium After the CVD Operation

Ultramet etched the molybdenum mandrel from the inside, constructed tooling to locate and hold the true center of the CVD structure, and ground the rhenium layer of chamber S/N 1 to near-point dimensions. Measurements of the chamber wall thickness provided by Ultramet after the grinding operation are shown in Figure 3.2-2. As a final step, the high emissivity black coating was applied to the outside of the chamber, and the chamber front end was ground to accommodate the front-end trip ring and flange assembly.

The rhenium chamber S/N 2 was applied in two layers. The first layer applied Re to a maximum thickness of .016 in. in the nozzle skirt. The nozzle was then masked off and rhenium was applied until the throat was clearly above the minimum required .040 in. thickness.

Excess rhenium was ground from this part with the mandrel still in place. Figure 3.2-3 shows the thickness of the Ir and Re layers of chamber S/N 2 before and after the grinding operation.

In spite of the improved control of the deposition process, the wall thickness of chamber S/N 2 was still not in conformance with the original drawings of the chamber. However, Ultramet stated that there was a significant risk of breaking the part at the throat with continued grinding. Estimates of the total moment of the as-fabricated skirt were made. The fabricated nozzle developed approximately 30% more moment than the nozzle which was designed and analyzed. Partially offsetting this, the most sensitive structural portion of the chamber, the throat, was also approximately 20% thicker than the analyzed design, and thus could accommodate a higher skirt mass. Given the potential consequences of failing the part because of further grinding, and the resulting delay in the program, it was decided to accept delivery of the chamber.

Chamber S/N 2 was cut to length, and the final coating was applied. The molybdenum mandrel was then etched away. After the mandrel was removed, Ultramet performed a final dye penetrant inspection of the iridium coating. They concluded from this inspection that there was a crack around the entire circumference of the throat. They shipped the part to Aerojet with this caveat.

Upon arrival at Aerojet, the chamber was photographed (Figure 3.2-4) and carefully inspected. Visual examination showed a slight anomaly at the chamber throat. The inside of the chamber was examined with a borescope. No cracks could be found in the coating, though an irregularity in the contour and a flaky appearance on the inside surface near the throat

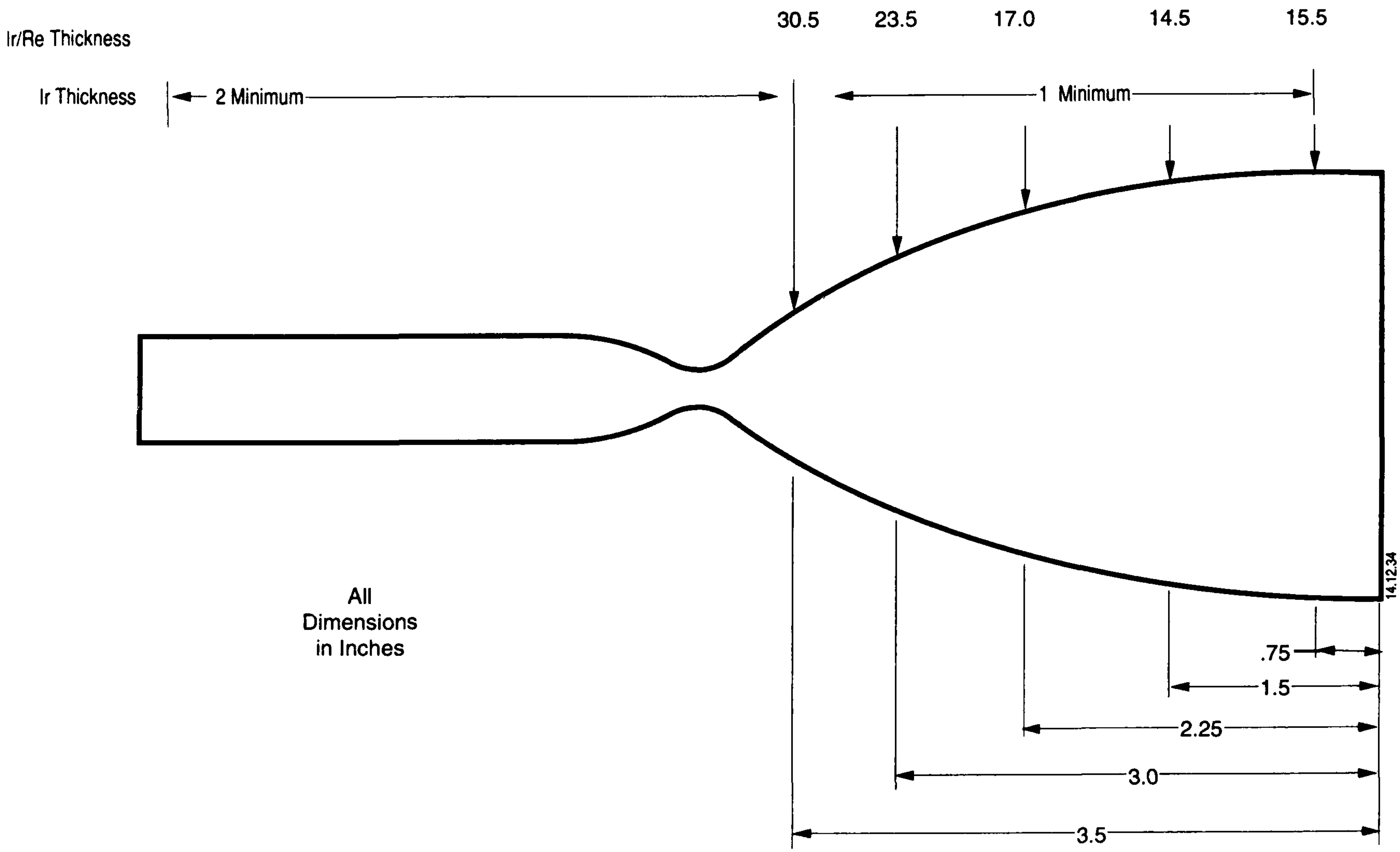


Figure 3.2-2. Chamber S/N 1 Wall Thickness After Grinding

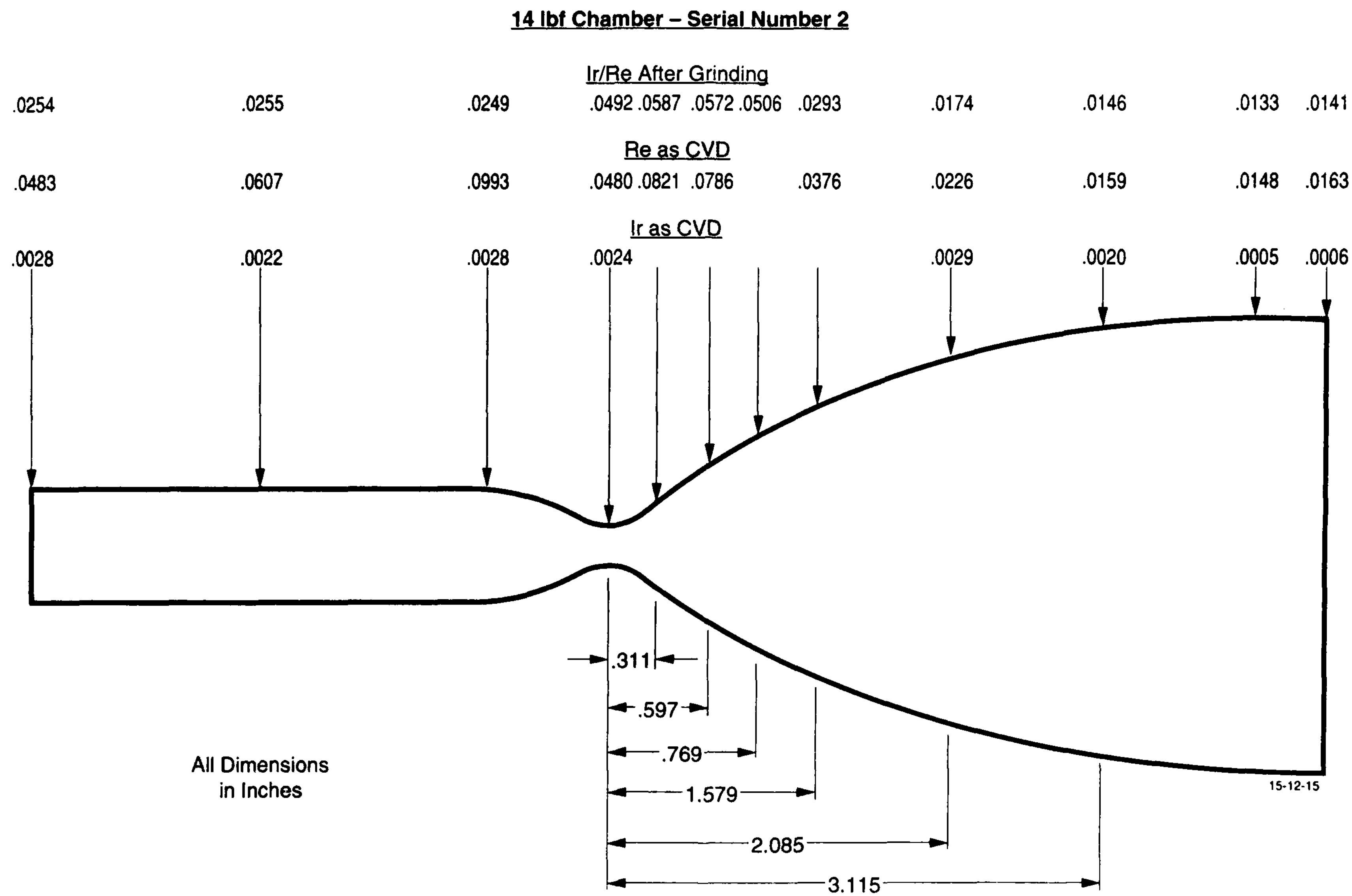
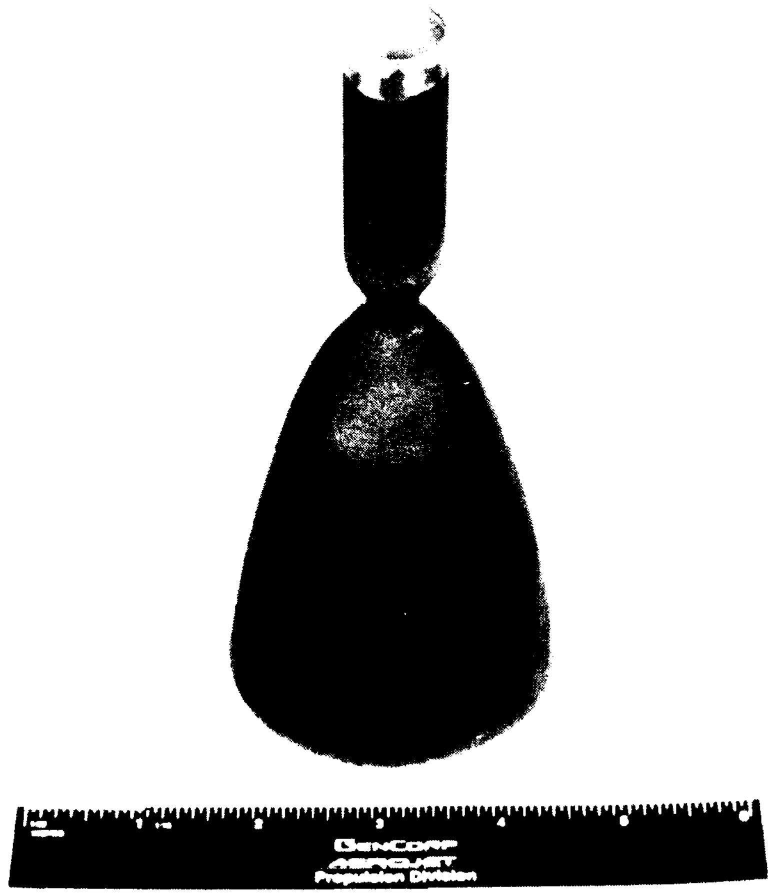


Figure 3.2-3 Ir-Re Chamber S/N 2 Demonstrated Good Control of the CVD Wall Thickness. Subsequent Grinding Operation Futher Shaped Wall Thickness.



14 LBF IR-RE CHAMBER S/N 2

Figure 3.2-4. S/N2 As Received From Ultramet (C0990 4339)

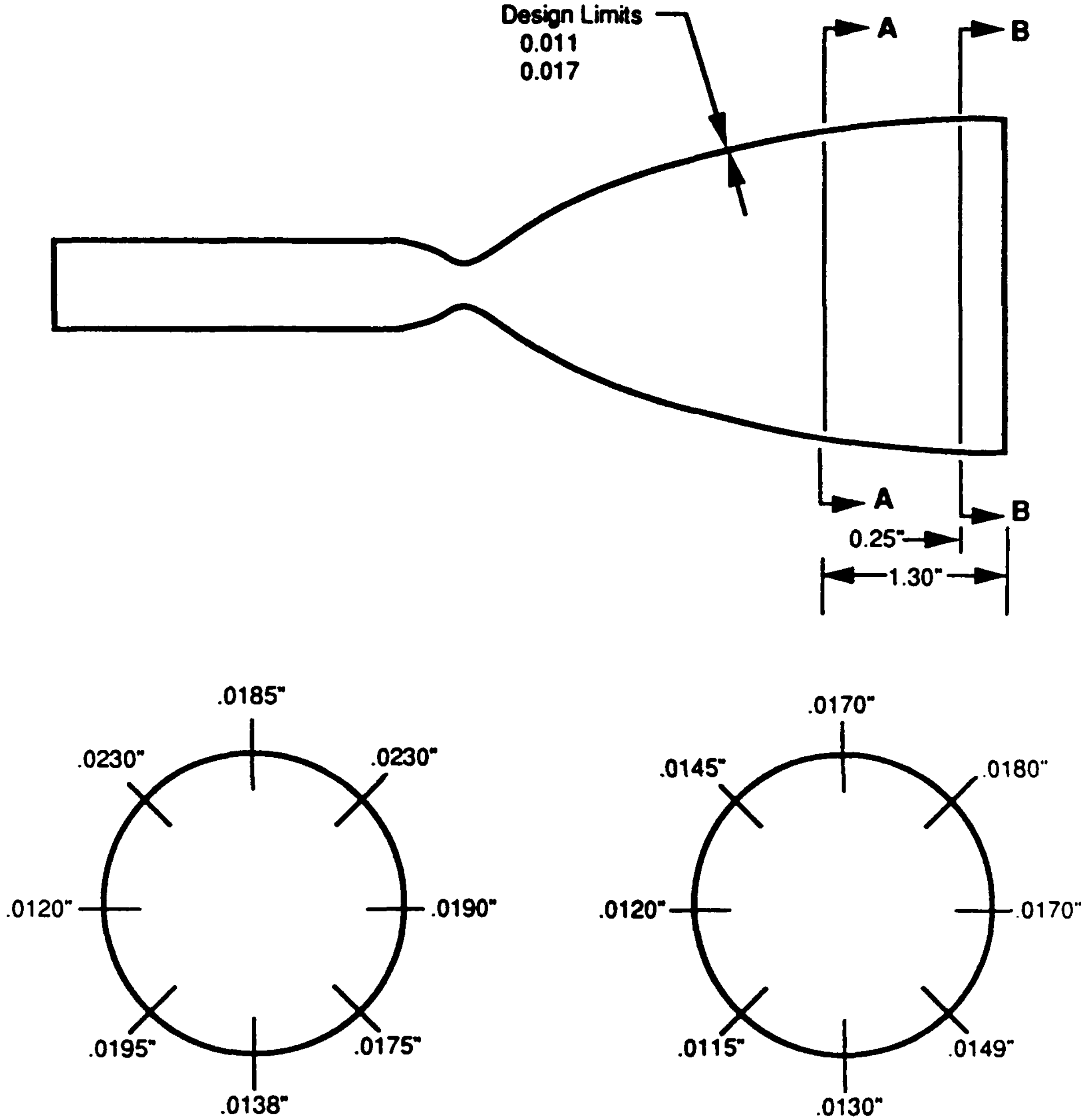
was observed. The chamber was flushed with alcohol to remove any loose material from the inside surface. A second borescope inspection indicated that the loose flakes of material had been removed by the alcohol rinse, though a slight bump or depression (it was impossible to tell which) could still be observed through the borescope. No cracks or discontinuity of the coating could be seen.

It was concluded from these examinations and further telephone conversations with Ultramet that there was no crack in the coating, and that the small anomaly of the contour, along with the loose material in the throat, was responsible for an incorrect interpretation of the dye-penetrant test.

Detailed dimensional inspections of chamber S/N 2 were conducted by the Aerojet Q/A staff. All diameter and wall thickness dimensions upstream of the throat were to print. Two slight problems were discovered during this inspection. First, the front end of the chamber was not cut perpendicularly to the barrel and throat. The maximum error in the cut was approximately 0.005-in. This may introduce a very slight cant (0.3°) of the front end trip ring and injector relative to the centerline of the barrel. This was not expected to be a problem in hot-fire test. Second, the wall thickness varied substantially around the circumference of the skirt. The wall thickness was measured every 45 degrees with a tube micrometer at two axial locations, as shown in Figure 3.2-5. These variations in the wall thickness were because the grinding of the skirt was done by axial movement of the tool. Again, these variations were not considered to compromise the integrity of the chamber. Two Pt-10 Rh trip rings were machined per drawing 1204495 by Johnson-Mattley. Four stainless steel flanges were machined per drawing 1204490 by Harris Precision Machine.

3.2.2 Chamber Assembly

Experiments were conducted to support the final assembly and joining of the Ir-Re chamber. These experiments established that the two joints (the chamber-to-trip ring and the trip ring-to-flange) could be made without voids or diffusion of the filler metal into the machined parts. The experiments were conducted with small specimens which duplicated the joint configuration and materials of the flight-type chambers. The experimental pieces were assembled and stacked in the same furnace used in the joining of the final chamber. Furnace conditions duplicated those used in the final production run. Visual inspection of the specimen did not reveal any flaws or voids in the joint. The specimens were sectioned and examined under Optical and Scanning Electron Microscopes (SEM). Figure 3.2-6 shows micrographs taken during inspection of the samples under an optical microscope. These examinations established



Section A

Max	Min	Δ
.0230	.0120	.0110

Section B

Max	Min	Δ
.0180	.0115	.0065

M10.001

Figure 3.2-5. Wall Thickness Measurements on Ir-Re 14-Lbf Chamber S/N 2

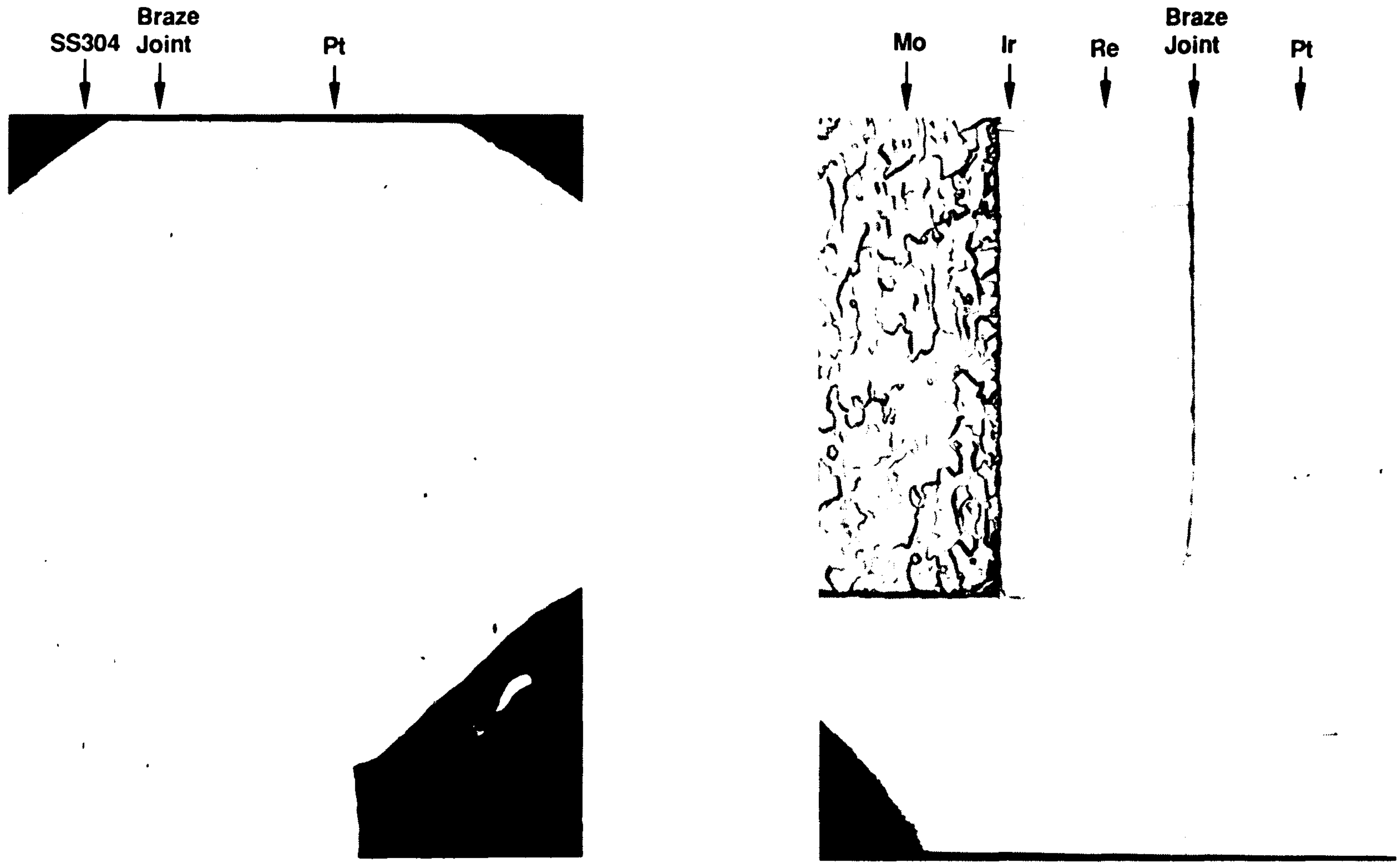


Figure 3.2-6. Optical Microscope (50x) Shows the Sample Braze Joints Formed without Cracks or Voids. SEM Examination Showed that in Specimen B Which Appears to be a Crack is Only an Artifact of Polishing During Sample Preparation.

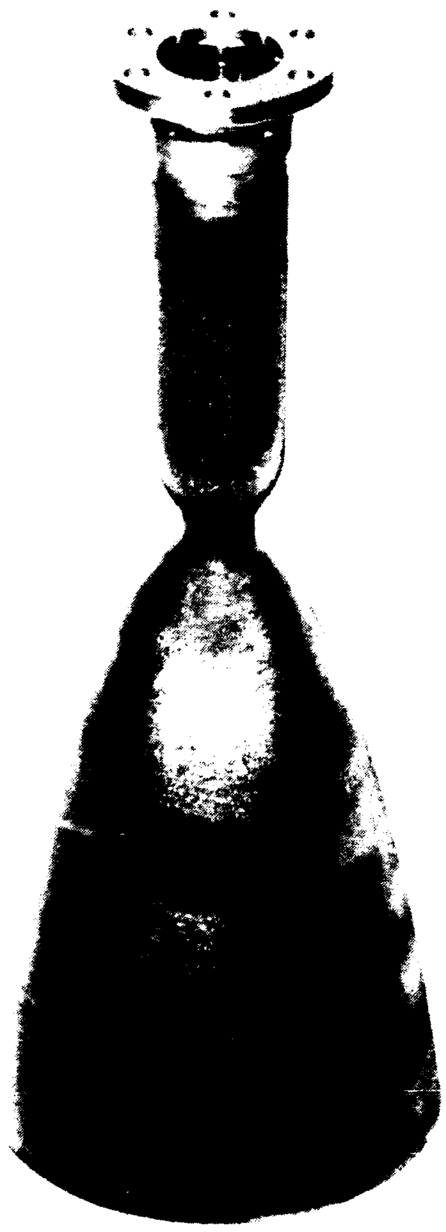
that the joints were continuous and free of voids or cracks, and that diffusion of the alloy into the base metals was not significant.

Upon successful completion of the joining experiments, Ir-Re chamber S/N 2 was fabricated. Assembly, stacking and furnace operations established by the experiments were repeated. The fabrication of the chamber appeared to be a complete success. Figure 3.2-7 shows the chamber S/N 2 after joining and polishing.

The chamber was submitted for final inspection and assembly to the valve/injector. Dimensional inspection confirmed that the flange and trip ring were concentric and square with the throat to within 0.024 in., and to the exit dia. by 0.048 in. No discrepancies were noted by a dye penetrant inspection of the inside surface of the nozzle, indicating the iridium coating was free of cracks or voids downstream of the throat. Final assembly of the chamber with the valve/injector went smoothly. The helium leak sensor employed for acceptance of production engines was used to checkout the first engine assembly. No leakage from the joints was detected. A very small leak (4.2×10^{-6} SCCS of Helium) was noted around the gold seal and flange bolts. This small leak was not anticipated to be a problem, and could be remedied if necessary with further polishing and flattening of the flange face. Figure 3.2-8 shows chamber S/N 2 after assembly with the injector and bipropellant valve. Figure 3.2-9 shows the fully assembled engine S/N 2 next to the C103 engineering development unit. Note that C103 thrust chamber has an overall expansion ratio of 47:1, while the Ir-Re unit has an area ratio of 75:1.

3.3 THRUSTER HOT FIRE TESTING

A total of 746 sec of firing was accomplished in tests up to 100 sec long, with a total of 339 starts. Specific impulse at nominal conditions (220 psia inlet pressure) was 304.8 sec for steady state operation and 282.6 for pulsed operation (0.1 sec on, 1.0 sec off). Replacing the production Cb-silicide coated chamber with the Ir-Re chamber and BLT, with no other changes has resulted in an increase of 20 sec. Chamber temperature at the nominal operating point was 3430°F; maximum chamber temperature for the test series was 3580°F (at MR = 1.89), giving a margin of over 400°F on the demonstrated long life temperature for Ir-Re chambers of 4000°F. Steady state thermal performance was satisfactory and agreed with the results of the thermal analysis used in the design. The hardware performed satisfactorily, without damage or throat erosion.



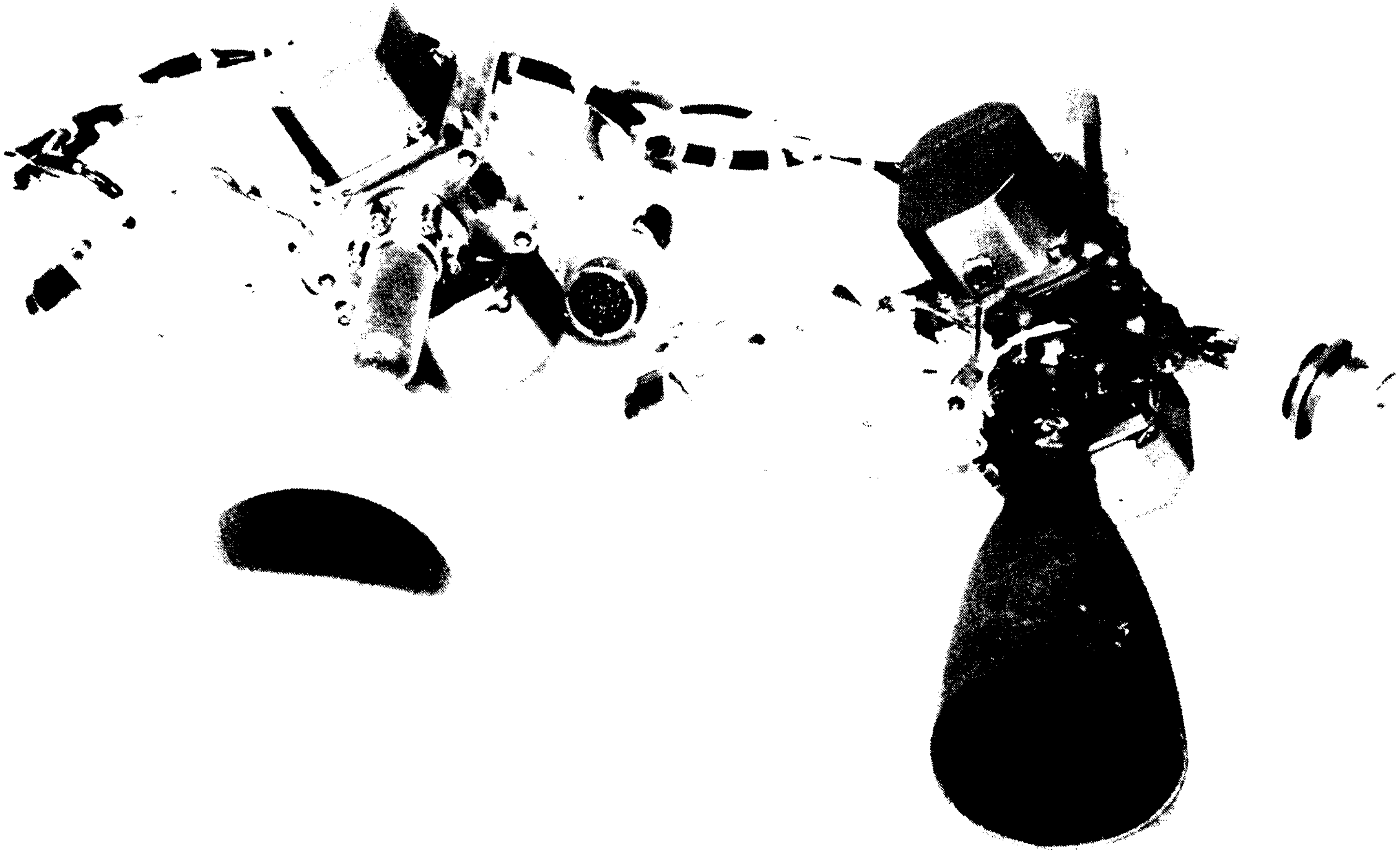
(C1090 5135)

Figure 3.2-7. 14 lbf Ir-Re Chamber S/N 2 With Brazed Trip Ring and Flange



(C1090 5131)

Figure 3.2-8. Fully Assembled Ir-Re 14 lbf Engine.



(C1090 5130)

Figure 3.2-9. 14 lbf Engines. Left: Ir-Re S/N2.
Right: C103 Engineering Development Unit.

The physical appearance of the hardware is shown in Figure 3.3-1 prior to test and in Figure 3.3-2 after test where the posttest interior surface of the nozzle is compared to that of the standard 14-lbf columbium unit. Although both units use precisely the same injector, the eight-streak pattern typical of the production RCT does not occur on the Ir-Re thruster, presumably because of the flow uniformity produced by the trip ring (BLT). The uniform, light circumferential pattern on the Ir-Re nozzle appears to be related to the thermal gradients which exist between the throat and the exit.

Thruster dimensions, taken at several times throughout the program, are listed in Figure 3.3-3. External dimensions are monitored primarily to determine if reaction is occurring with the ambient test cell gases. There is no evidence of systematic change in external chamber dimensions. The variations seen are due to the difficulty of making repeatable measurements of the contoured surfaces of the thruster while it is mounted on the test stand. The internal measurement of the nozzle throat shows a slight increase (less than 0.001 in.). The 0.324 in. gage which partially inserted pretest could be inserted completely after Test-128. This could be the result of removal of small asperities on the surface.

The results of throat I.D. and O.D. measurements taken throughout the testing are shown in Figure 3.3-3A; chamber external dimensions taken during the testing are plotted in Figure 3.3-3B. The changes in dimensions noted are within the accuracy of the measuring techniques.

After assembly and leak test the S/N 2 engine was installed in the Bay A-1 altitude test facility. Figure 3.3-4 is a schematic of the facility propellant system. Figure 3.3-5 shows the 14 lbf Ir-Re thruster installed in the test facility. The planned test program is shown in Figure 3.3-6. The intent of the test program was to run the standard acceptance test series required of the production 14 lbf engine, followed by performance, thermal stability, and a portion of the qualification test series as conducted for the production 14 lbf engine. This was to be followed by a repeat acceptance test to demonstrate that no degradation of the engine had occurred. However, actual testing was reduced significantly to assure that funds were available for vibration acceptance testing of the engine assembly (Section 3.4).

A total of 36 firings were made with an accumulated firing time of 746 sec in a total of 349 starts, comprising checkout, acceptance testing and a portion of the performance mapping and qualification series.

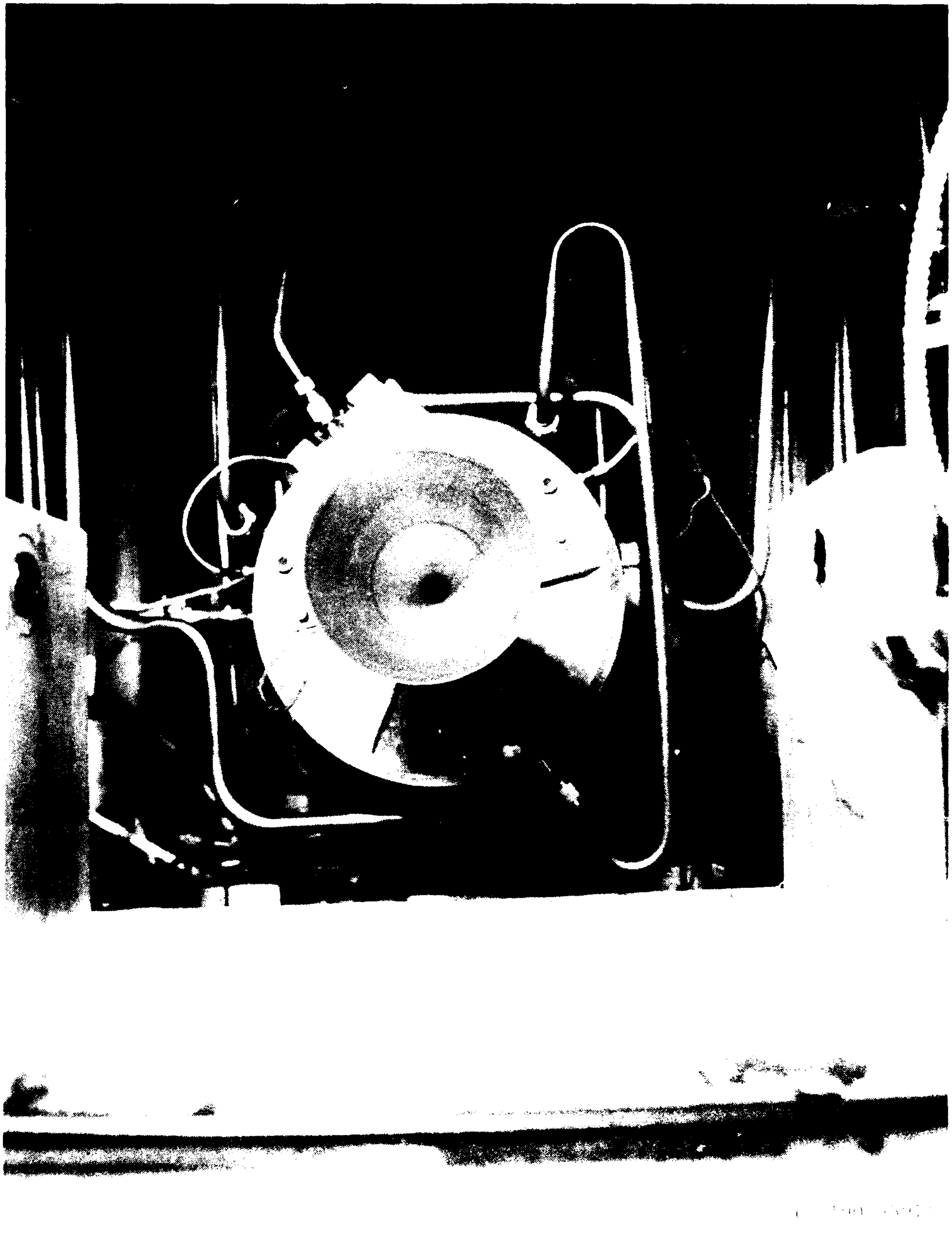
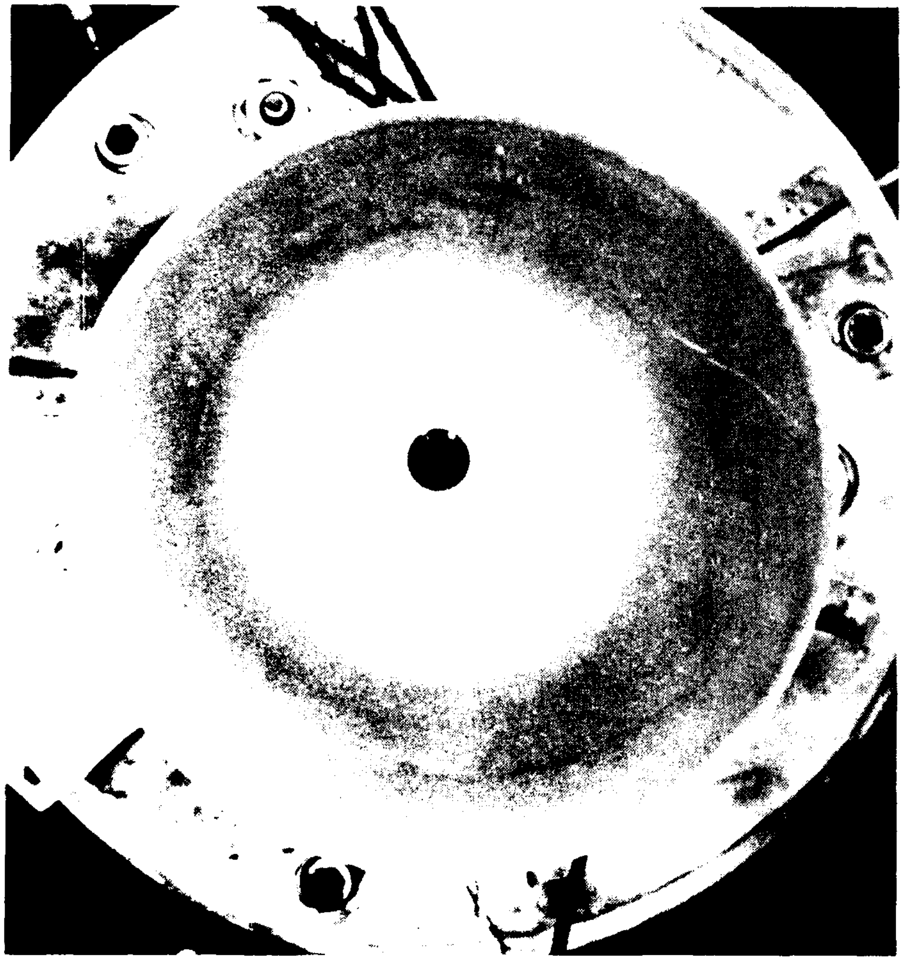


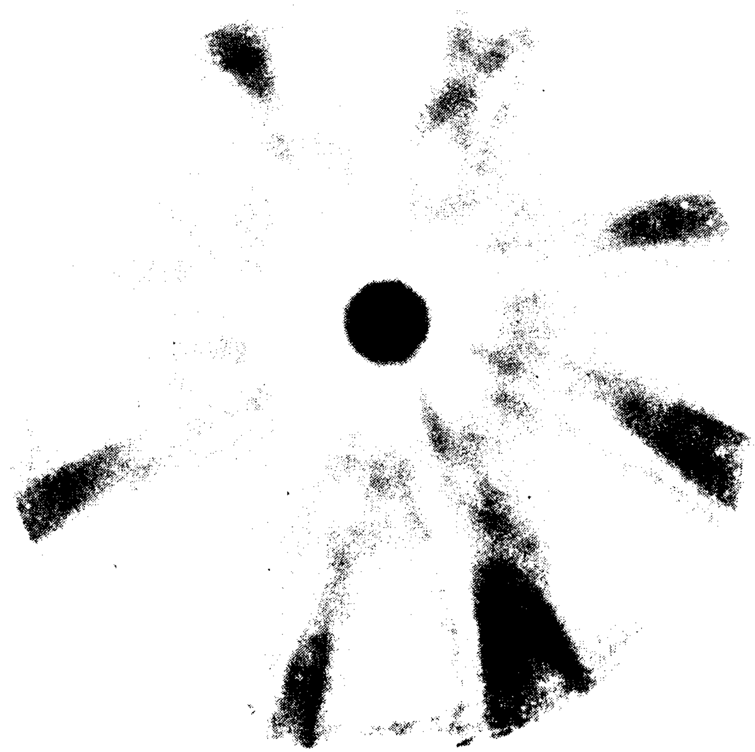
Figure 3.3-1. 14# Ir-Re S N 2 Nozzle Exit, Prior to Test



C1290 5823

Advanced 14-lbF Ir-Re Chamber

Shows Uniform Circumferential Flow Produced by Trip



C1186 3614

Standard 14-lbF RCT Columbium Chamber

Shows Pattern From Injector Elements

Both Thrusters Use The Same Injector Design

Figure 3.3-2. Post-Test Nozzle Exit Patterns

TIME	TOTAL FIRING TIME	Dch1		Dch2		ODth		IDth		ODnoz ex		IDnoz ex	
		VERT	HORIZ	VERT	HORIZ	VERT	HORIZ	GO	NO-GO	VERT	HORIZ	VERT	HORIZ
PRETEST	0	0.7925	0.7885	0.7905	0.7900	0.4225	0.4235	0.323	0.324	2.8180	2.8070		
POST 103	26		0.7890	0.7905	0.7880			0.323	0.324	2.8168	2.8077	2.762	2.776
POST 117	200.6	0.7885	0.7875	0.7942	0.7875			0.323	0.324				
POST 128	603.6	0.7900	0.7882	0.7925	0.7890	0.4240	0.4255	0.324	0.325	2.8177	2.8143		
POST 136	723.6	0.7893	0.7887	0.7915	0.7880	0.4242	0.4255	0.324	0.325	2.8180	2.8119		
AVG.		0.7901	0.7884	0.7918	0.7885	0.4236	0.4248	0.3234	0.3244	2.8176	2.8102	2.762	2.776

Figure 3.3-3. Chamber Dimensions

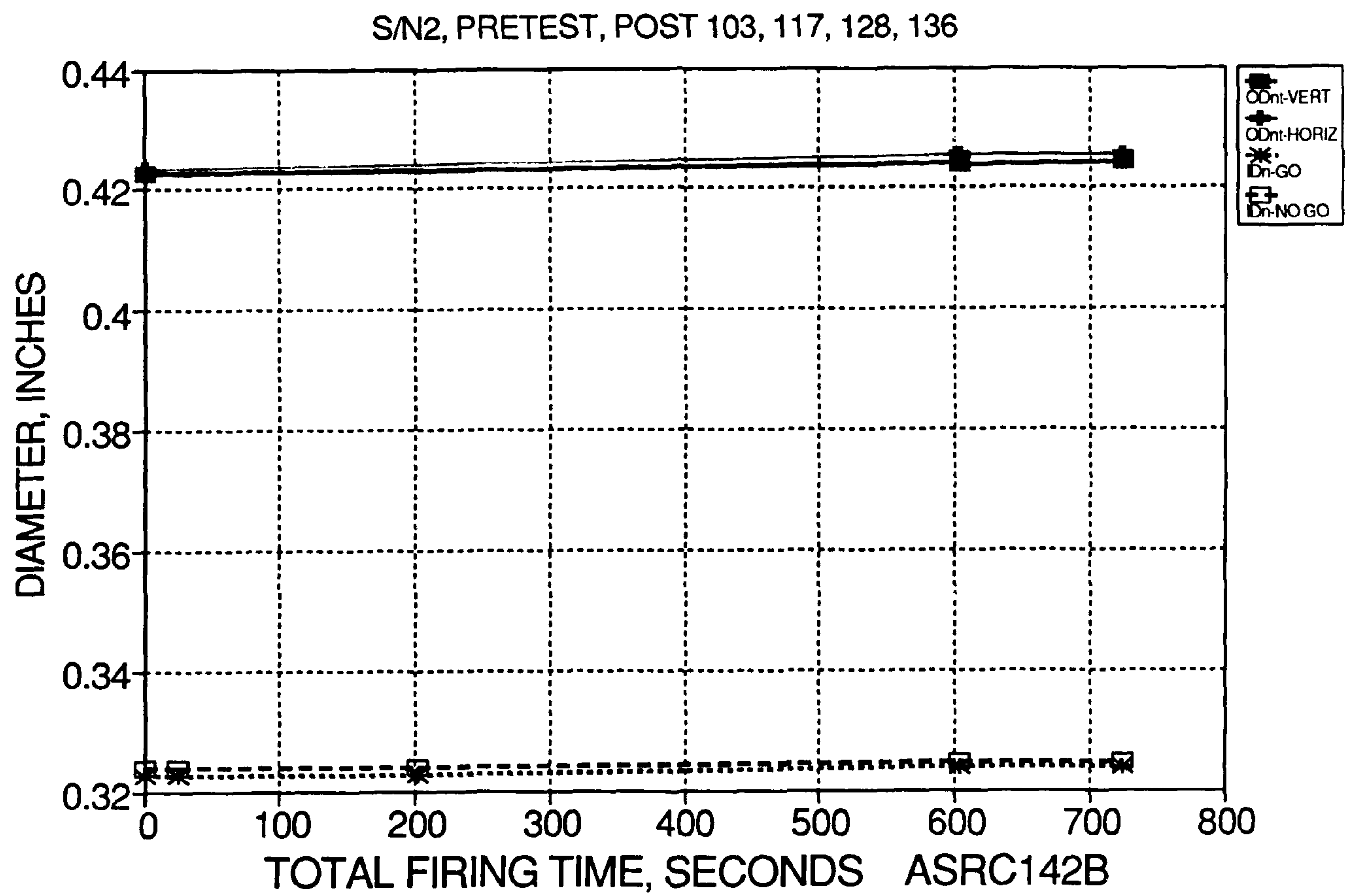


Figure 3.3-3A. 14# Ir-Re Nozzle Throat OD and ID vs Firing Time

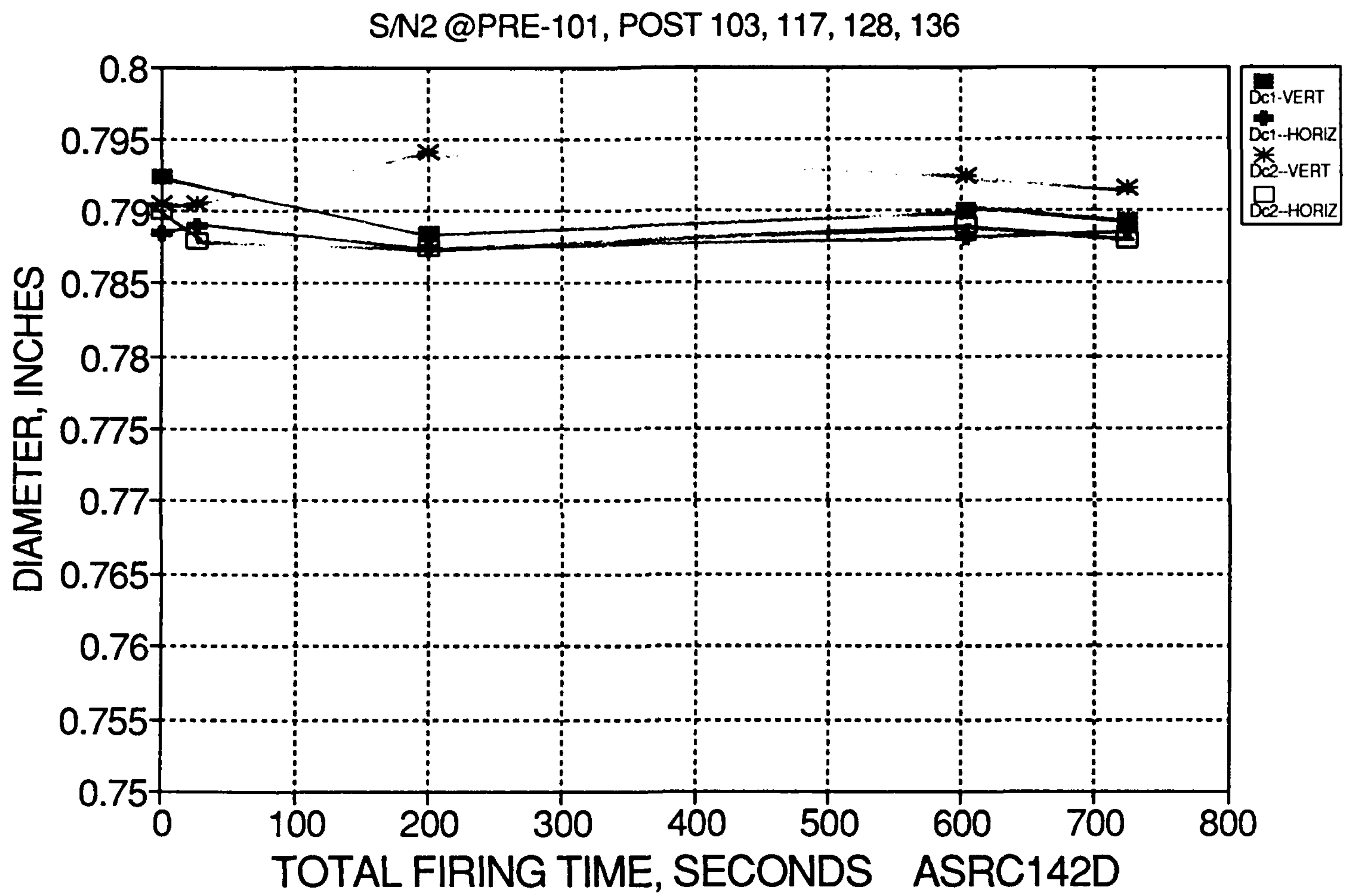


Figure 3.3-3B. 14# Ir-Re Chamber Dimensions vs Time

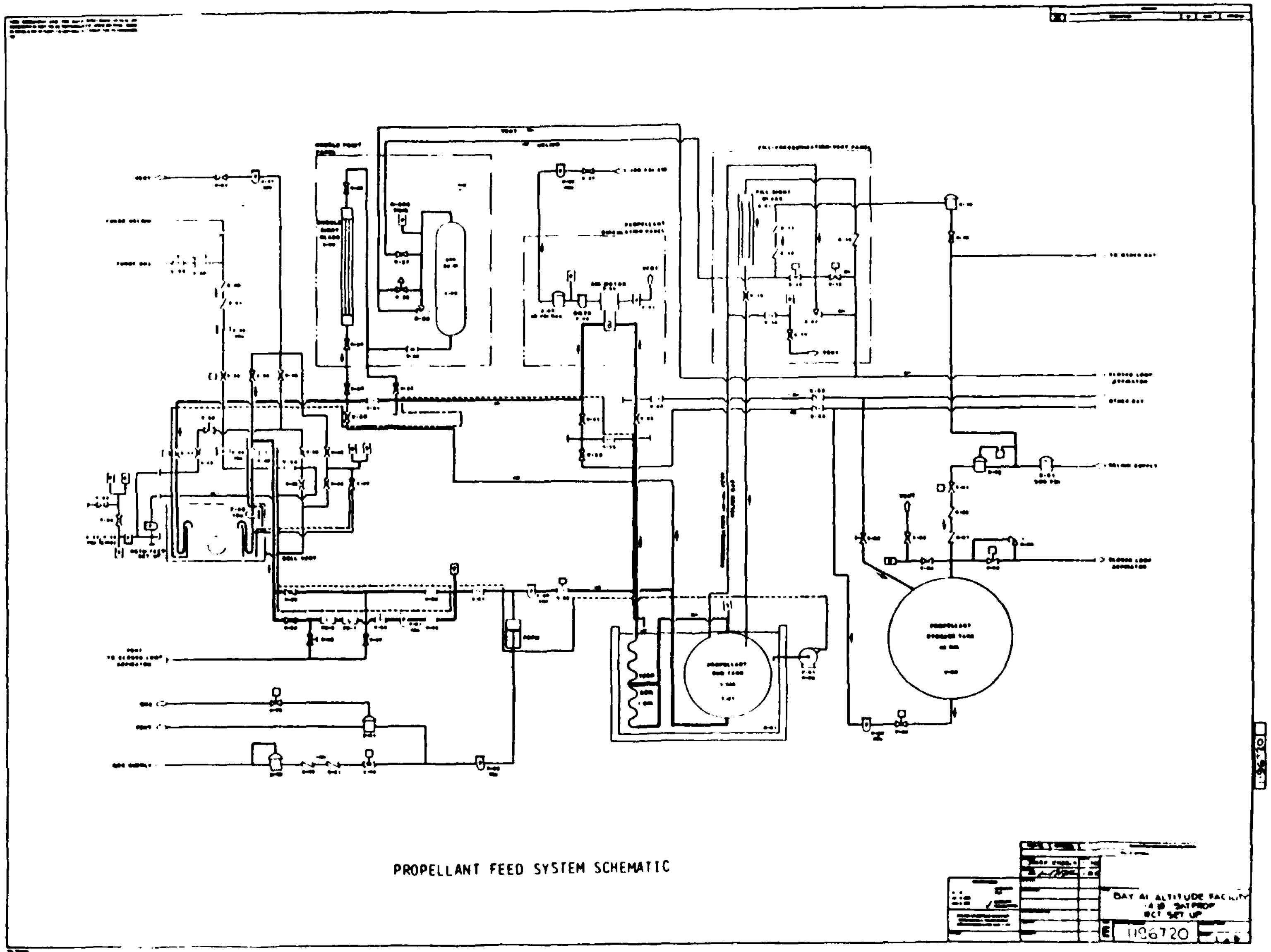


Figure 3.3-4. Plumbing Schematic for 14 Pound Acceptance and Qualification Test in Test Bay A-1

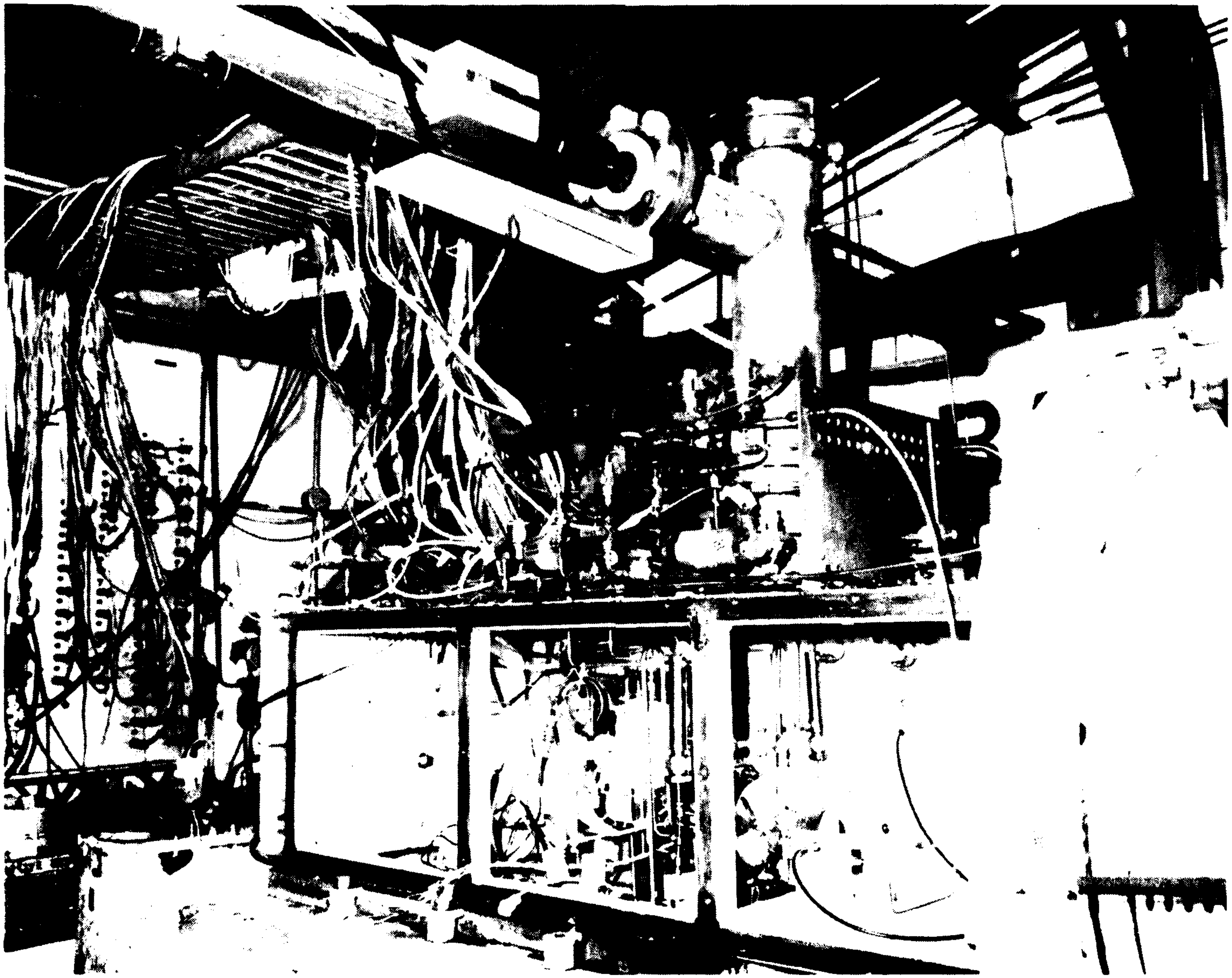

(C1190 5598)

Figure 3.3-5. Overall View of 14# Ir-Re Altitude Facility

		Each Thruster		
Test Type	Thruster S/N	Total No. Burns	Total Firing Time,	Longest Burn, sec
Acceptance	#2, #1	244	329	100
Performance Map	#2	1,713	240	20
Thermal Stability	#2	8,948	5,060	60
Qualification	#2	8,226	2,804	5
Re-acceptance	#2	81	108	100
Totals, S/N #2		19,212	8,541	
Totals, S/N #1		244	329	
Program Total		19,456	8,870	

Figure 3.3-6. Summary of Planned ARCT Test Program

3.3.1 Test Installation and Instrumentation

Installation of the engine was accomplished in the same facility as used for acceptance testing of the production 14 lbf Cb thruster with modifications special to the Ir-Re program. The chamber was instrumented with type K thermocouples as shown in Figure 3.3-7. In addition, chamber temperature was monitored with a Ircon two-color pyrometer, and a Thermovision IR thermal mapping system.

Plume optical absorption and emission measurements were made using the ESMS system shown schematically in Figure 3.3-8. The water-cooled detector head at the engine exhaust is shown in Figure 3.3-9.

To protect the exterior of the Ir-Re chamber from oxidation by the residual gas in the test cell, a shroud directs a small flow of hydrogen over the chamber. The details of this shroud are shown in Figure 3.3-10.

The engine was operated without a diffuser to eliminate the influence that this would have on pulse performance measurements during start up and unload.

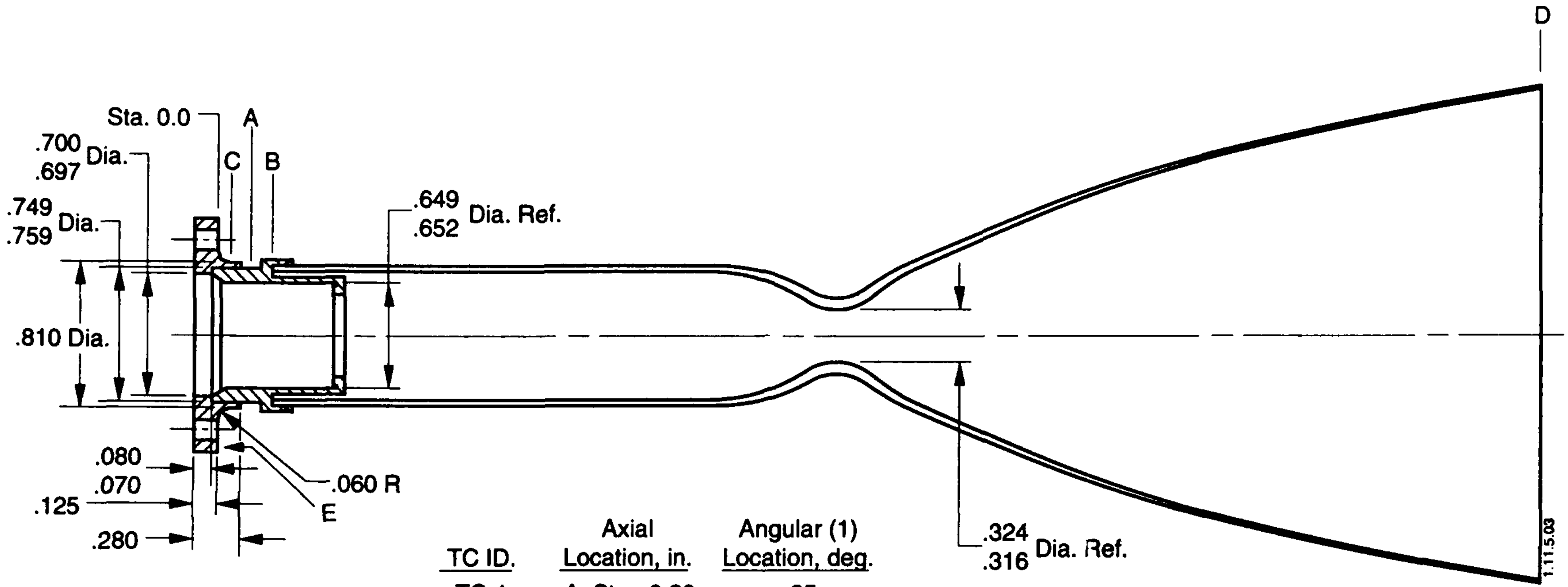
The inlet operating pressure map for the engine is shown in Figure 3.3-11. The data measurements made during the testing are identified in Figure 3.3-12. The test data tapes are identified as 5804-A01-0A-[Run Number] and are archived.

3.3.2 Test Results

The engine operating conditions and measured performance are shown in Figure 3.3-13. The initial range of test conditions were those required by the acceptance test matrix, Figure 3.3-14. These tests covered the inlet pressure range from 145 psia to 370 psia for steady state durations of 5 and 100 sec. Pulse trains of 80 each 0.1 sec on 1.0 sec off were also run over the inlet pressure range. Additional tests of 10, 15, and 20 sec duration were conducted over a wider inlet pressure range, approx 150 psia to 400 psia. The full map of operating conditions is shown in Figure 3.3-15. The map covers the test range of MR from 1.4 to 1.89 and the vacuum thrust range from 11.3 to 22.0 lbf.

Performance Data

Measured vacuum specific impulse for the engine in steady state operation is shown in Figure 3.3-16 as a function of mixture ratio over the full test range. The cluster of data



TC ID.	Axial Location, in.	Angular (1) Location, deg.
TC-1	A, Sta. 0.20	85
TC-2	√ √	150
TC-3	√ √	330
TC-4	B, Sta. 0.30	85
TC-5	√ √	150
TC-6	√ √	330
TCF-1	C, Sta. 0.10	85
TCF-2	√ √	150
TCF-3	√ √	330
TN-1	D 0.10 from Exit	85
TF-1	E, Sta. 0.0	85
TF-2	√ √	150
TF-3	√ √	330

(1) PcPort=150°

Figure 3.3-7. Chamber Thermocouple Locations

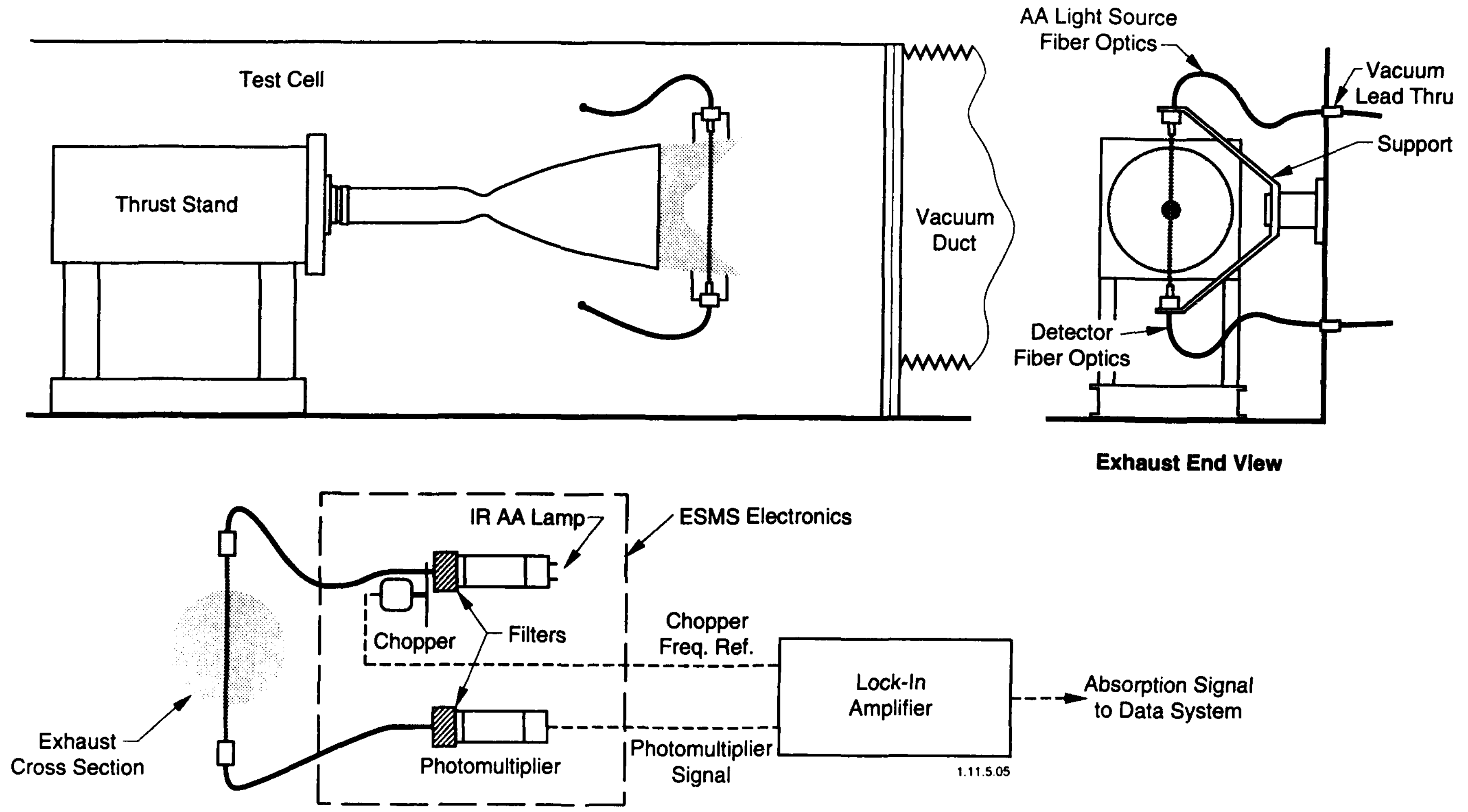


Figure 3.3-8. Exhaust Plume Optical Measurement System

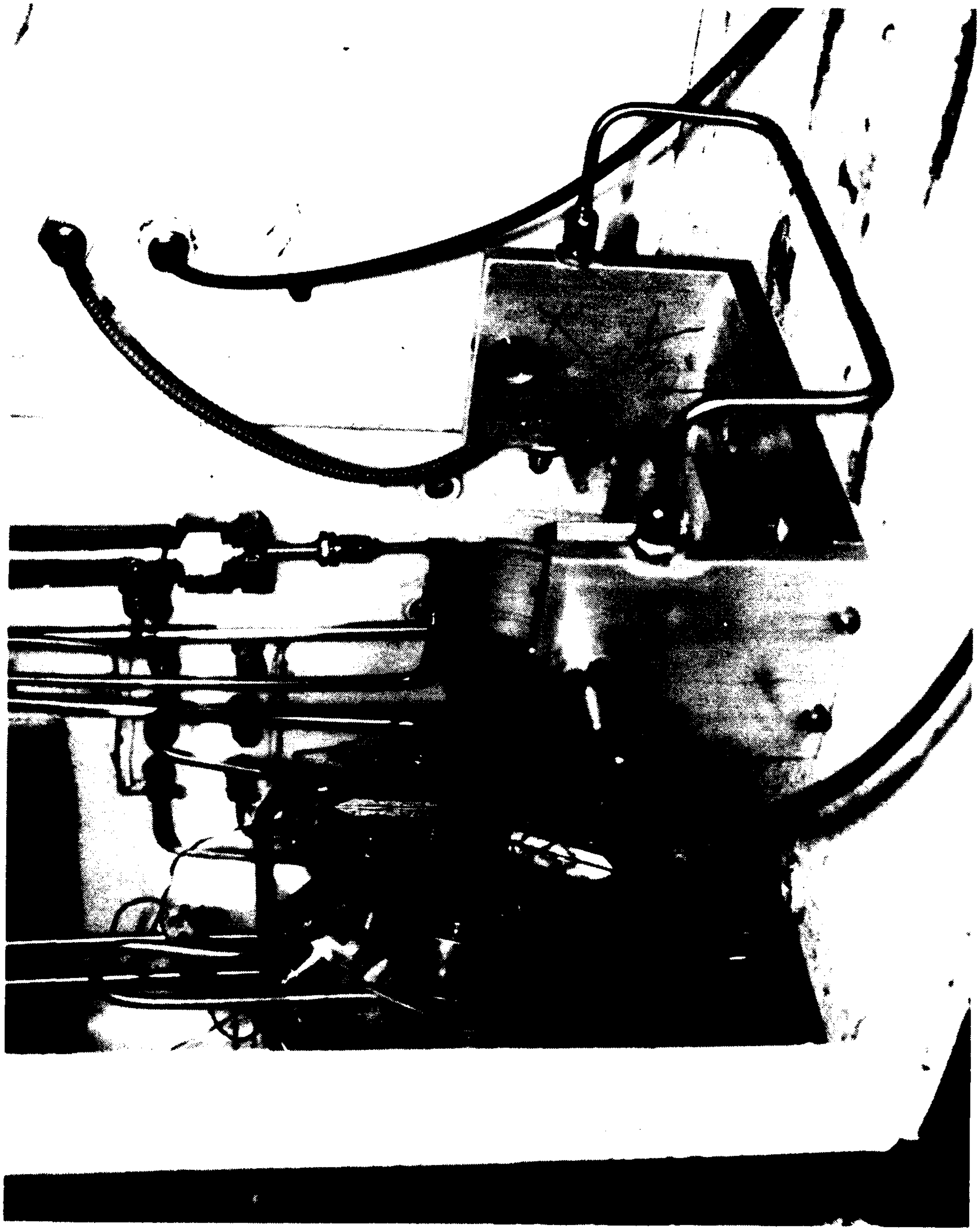


Figure 3.3-9. 14# Ir-Re Thruster S/N2 Showing Plume Monitor

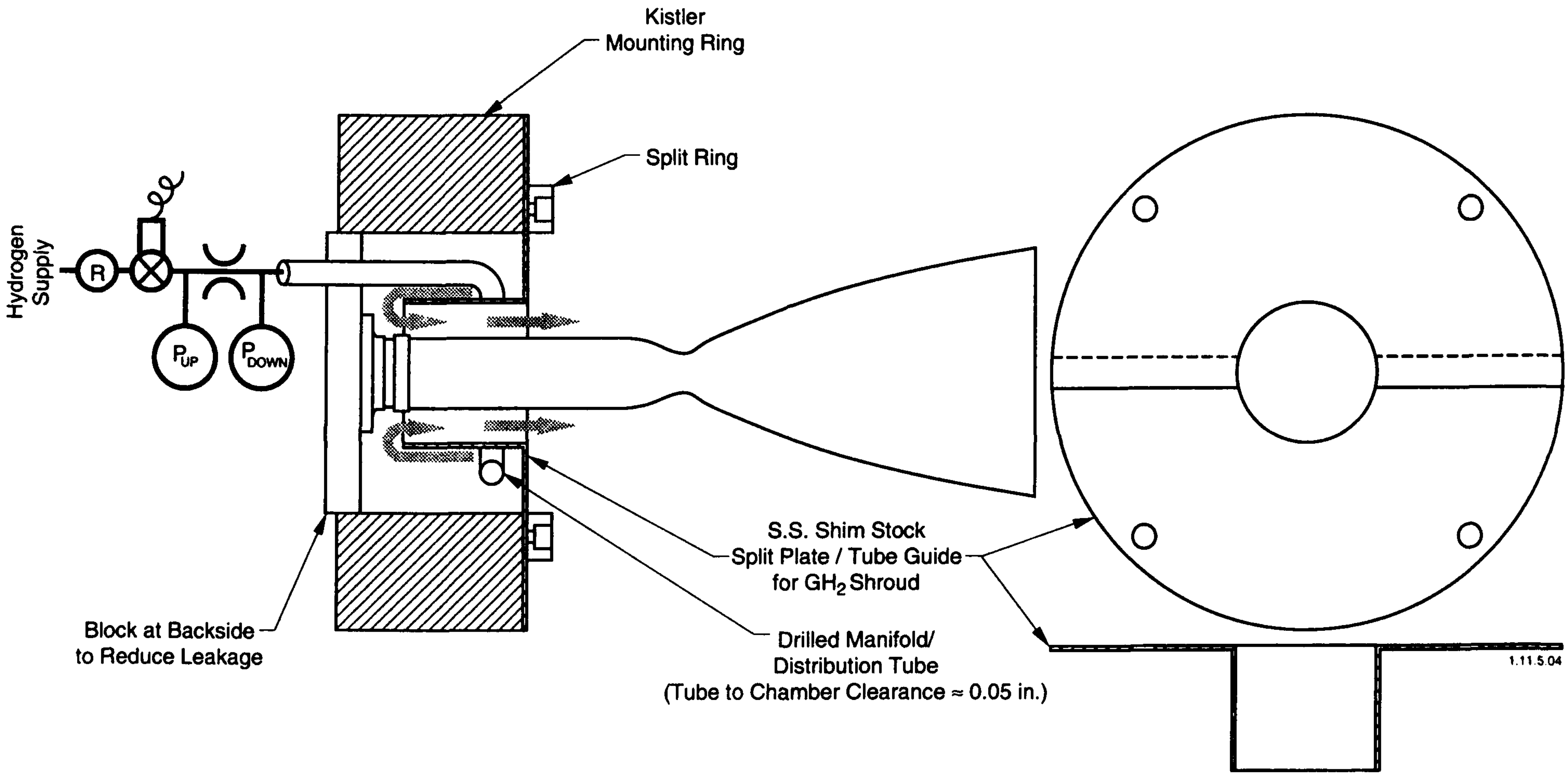
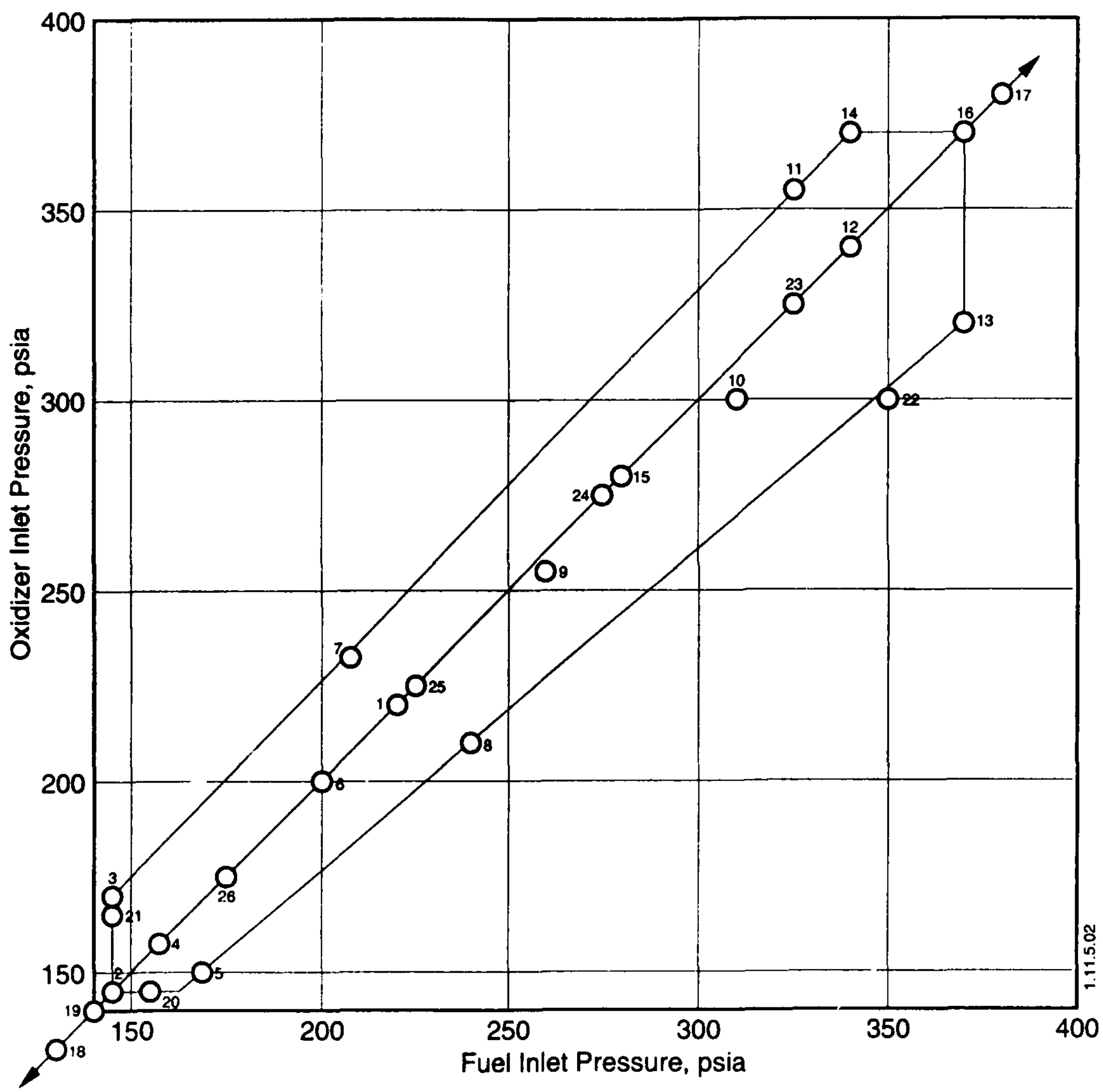


Figure 3.3-10. Hydrogen Shroud System



Inlet Condition	P_{OL} (psia)	P_{FL} (psia)	F (lbf)
1	220	220	14.0
2	145	145	10.6
3	170	145	11.2
4	157	157	11.2
5	150	168	11.2
6	200	200	13.2
7	233	207	14.0
8	210	240	14.2
9	255	260	15.6
10	300	310	17.4
11	355	325	18.7
12	340	340	18.7
13	320	370	18.8
14	370	340	19.9
15	280	280	16.5
16	370	370	19.7
17	400	400	20.7
18	125	125	9.5
19	140	140	10.3
20	145	155	10.8
21	165	145	11.1
22	300	350	18.1
23	325	325	18.2
24	275	275	16.3
25	225	225	14.2
26	175	175	12.0

Figure 3.3-11. Operating Pressure Envelope – Standard Thruster

[illegible] CALIBRATION PROGRAM

TEST [illegible] 114 [illegible] Date-11-[illegible]-90 Time-[illegible]

[illegible]

NEFF No.- 1 [illegible] Part. Name-FI814 [illegible] 747 1- Data Edit-Hi= 1 Mode 20 to- 75

CHANNEL LOCATION ENTRIES

0	73	72	1	2	3	4	19	20	11	12	13	14	10	7	42
43	40	41	0	0	0	0	0	0	0	0	0	0	0	0	-1

L+ 1	14.59[illegible]	0.000000	0.000000	0.000000	0.000000	.3197000	[illegible]0000	1.027160
L+ 9	1.000000	1.000000	1.000000	1.000000	2.000000	.1595000	.1695000	.8513981
L+17	0.000000	1.000000	0.000000	0.000000	0.000000	0.000000	0.000000	0.000000
L+41	0.000000	0.000000	0.000000	0.000000	8.000000	0.000000	0.000000	240.0000
L+49	.5000000	3.000000	0.000000	6.000000	12.00000	16.00000	20.00000	0.000000
L+57	76.00000	76.00000	9.000000	7.000000	10.00000	10.00000	9.000000	9.000000

SEQ	NEFF	PARAMETER	RANGE	CONV.	WD	GAIN	FACTOR	OFFSET	VARIABLE	E.U.	D/UNITS	FIL	DISP	S/N	MFR	DUE DATE	INDX
57	9	FCAL	19.5560	400	0	1	.00000	.00000	.00000	1		10.	26	8546	BAB	11/09/91	0
2	80	VTCV	99.6532	8004800		1	.00000	.00000	.00000	1		1200.	8	263	AEJ	01/21/90	10
3	76	FD[illegible]	30.0000	94014000		4	.00000	.00000	.00000	1		1200.	12		KIB	11/15/89	20
64	10	F-STATIC	19.4400	400	0	1	.00000	.00000	.00000	1		10.	27	6848	BAB	11/09/91	23
49	7	PC	250.0000	92014801		2	.00000	.00000	.00000	1		10.	28			/ /	25
4	72	WOFDFM	.5593	94053000		2	.00000	.00000	.00000	1		600.	1	001	AEJ	11/25/89	30
5	73	WFFDFM	.5530	94053000		2	.00000	.00000	.00000	1		600.	2	002	AEJ	11/25/89	40
25	1	FMO-1	21381.73	1019600		2	.00000	.00000	.13659E-02	1		10.	15	557	FOG	11/23/90	50
32	2	FMO-2	23013.02	1019600		2	.00000	.00000	.11512E-02	1		10.	16	559	FOG	11/15/89	60
40	4	FMF-2	21492.03	1019600		2	.00000	.00000	.16656E-02	1		10.	17	679	FOG	11/23/90	70
33	3	FMF-1	21412.64	1019600		2	.00000	.00000	.16339E-02	1		10.	19	556	FOG	11/23/90	80
41	5	THVB	9757.100	98042600		4	.00000	.00000	242.90	1		10.	0			/ /	90
48	6	THFD	5000.000	98042600		4	.00000	.00000	5000.0	1		10.	0			/ /	90
56	8	ITCV	4.0145	8004801		1	.00000	.00000	.00000	1		10.	9	225	SIA	12/05/89	100
65	11	FOLI-1	500.0000	202	2	1	.00000	.00000	.00000	1		10.	21	840508	TAI	11/23/90	150
72	12	FOLI-2	500.0000	202	2	1	.00000	.00000	.00000	1		10.	22	741800	TAI	03/02/91	160
73	13	FFLI-1	500.0000	202	2	1	.00000	.00000	.00000	1		10.	24	820513	TAI	02/23/91	170
80	14	FFLI-2	500.0000	202	2	1	.00000	.00000	.00000	1		10.	25	820519	TAI	02/23/91	180
81	15	FOTR	750.0000	202	2	1	.00000	.00000	.00000	1		10.	31	611911	TAI	03/02/91	190
88	16	FFTR	750.0000	202	2	1	.00000	.00000	.00000	1		10.	32	611921	TAI	03/02/91	200
97	19	PVAC-1	1.5100	202	701	1	.00000	.00000	.00000	1		10.	38	5365	BEY	03/09/91	230
104	20	PVAC-2	1.5410	202	701	1	.00000	.00000	.00000	1		10.	39	5380	BEY	03/09/91	240
105	21	PDIFF	100.0000	202	2	1	.00000	.00000	.00000	1		10.	18	651246	TAI	11/23/90	250
184	40	TOFM	20.0000	3004005		4	.00000	.00000	.00000	5		10.	4			/ /	300
185	41	TFFM	20.0000	3004005		10	.00000	.00000	.00000	5		10.	5			/ /	310
192	42	TO	20.0000	3004805		10	.00000	.00000	.00000	5		10.	36			/ /	320
193	43	TF	20.0000	3004005		10	.00000	.00000	.00000	5		10.	37			/ /	330
200	44	TTR	20.0000	3004005		10	.00000	.00000	.00000	5		10.	7			/ /	340
201	45	TENC	20.0000	3004005		10	.00000	.00000	.00000	5		10.	23			/ /	350
16	74	PK-HI	6.0000	94015000		10	.00000	.00000	.00000	1		4800.	0			/ /	370
17	75	PK-LO	6.0000	94015000		10	.00000	.00000	.00000	1		4800.	0			/ /	390
69	17	FOT[illegible]	1000.000	202	2	1	.00000	.00000	.00000	1		10.	13	611061	TAI	11/15/89	900
96	18	FFT[illegible]	1000.000	202	2	1	.00000	.00000	.00000	1		10.	14	651301	TAI	11/15/89	910
241	55	[illegible]	100.0000	8004800		1	.00000	.00000	.00000	1		10.	3			/ /	0
112	22	PGH1	100.0000	202	2	1	.00000	.00000	.00000	1		10.	34	651230	040	04/08/91	0
113	23	PGH[illegible]	30.0000	202	2	1	.00000	.00000	.00000	1		10.	35	801223	TAI	02/09/91	0
120	24	T[illegible]	100.0000	3004005		1	.00000	.00000	.00000	5		10.	0			/ /	0
161	25	TC2	100.0000	3004005		1	.00000	.00000	.00000	5		10.	0			/ /	0
160	34	TC3	100.0000	3004005		1	.00000	.00000	.00000	5		10.	0			/ /	0
129	27	TC4	100.0000	3004005		1	.00000	.00000	.00000	5		10.	33			/ /	0
176	28	TC5	100.0000	3004005		1	.00000	.00000	.00000	5		10.	29			/ /	0
[illegible]	29	TC6	100.0000	3004005		1	.00000	.00000	.00000	5		10.	0			/ /	0
144	30	TCF1	100.0000	3004005		1	.00000	.00000	.00000	5		10.	0			/ /	0
[illegible]	31	TCF2	100.0000	3004805		1	.00000	.00000	.00000	5		10.	0			/ /	0
152	32	TCF3	100.0000	3004005		2	.00000	.00000	.00000	5		10.	0			/ /	0
[illegible]	33	TN1	100.0000	3004005		2	.00000	.00000	.00000	5		10.	0			/ /	0
[illegible]	36	[illegible]	1600.000	9004702		1	.00000	.00000	2722.0	1	DEG F	10.	11			/ /	0
[illegible]	37	[illegible]	1000.000	8004900		1	.00000	.00000	.00000	1		10.	0			/ /	0
[illegible]	38	[illegible]	100.0000	3004005		1	.00000	.00000	[illegible]	[illegible]		10.	0			/ /	0
177	39	T[illegible]	100.0000	3004005		1	.00000	.00000	.00000	5		10.	0			/ /	0

Figure 3.3-12. Data Measurements Identification

DATE	TEST No.	DURATION, (SEC)	OXID. PRESSURE (PSIA)	FUEL PRESSURE (PSIA)	MIXTURE RATIO O/F	CHAMBER PRESSURE (PSIA)	CHAMBER WALL TEMP. (Tmax,oF)	MEASURED THRUST, LBF	DELIVERED Ispv, (SEC)
11-16-90	101	1	209	237	1.57	--	--	14.68	
	102	5	212	237	1.63	100.0	3025	14.99	
	103	20	154	199	1.41	86.8	2979	12.32	300.4
11-19-90	104	5							
	105	20	219	214	1.57	102.9	--		303.8
11-20-90	106	20	361	352	1.60	141.7	3350	20.69	304.9
	107	0.6					--		--
	108 a	8	150	153	1.44	--	2580		277.9
	109 a	8	230	228	1.59	--	2590		282.6
11-26-90	110	15	147	148	1.54	79.2	3241	11.42	299.7
	111	15	234	222	1.64	106.2	3388	15.48	304.7
	112	15	236	222	1.65	106.6	3406	15.57	305.0
	113	15	234	222	1.64	105.9	3475	15.47	304.9
11-29-90	114	15	225	237	1.64	106.9	3434	15.59	304.9
	115	20	155	150	1.59	81.0	3344	11.70	302.7
	116	10	343	317	1.65	133.9	3419	19.90	304.6
	117	10	401	363	1.68	140.9	3427	21.70	305.0

(a)Pulse test, 80 pulses, 0.1 sec on/1.0 sec off

Figure 3.3-13. High Performance 14-lbf Thrust Engine Test Data Summary 75:1 Area Ratio Iridium-Coated Rhenium Chamber, Page 1 of 2

DATE	TEST	DURATION, (SEC)	OXID. PRESSURE (PSIA)	FUEL PRESSURE (PSIA)	MIXTURE RATIO O/F	CHAMBER PRESSURE (PSIA)	CHAMBER WALL TEMP. (Tmax,oF)	MEASURED THRUST, LBF	DELIVERED Ispv, (SEC)
1130-90	118	15	231	218	1.66	104.7	3468	15.20	304.7
	119	5	232	228	1.59	96.6	3341	15.40	303.3
	120	5	227	218	1.62	93.7	3368	15.08	303.8
	121	100	238	217	1.66	105.1	3434	15.30	305.0
	122	10	152	147	1.63	77.7	3370	11.57	301.2
12-03-90	123	20	151	146	1.64	79.1	3296	11.30	299.6
	124	100	154	149	1.64	80.4	3284	11.50	302.1
	125	20	381	370	1.57	134.3	3348	21.20	306.0
	126	100	391	364	1.64	140.2	3419	21.38	305.0
	127 a	8	408	386	1.63		2600		288.4
	128	20	174	147	1.82	83.3	3492	12.05	299.9
12-04-90	129	20	152	168	1.38	84.3	3280	11.70	299.8
	130	20	259	209	1.89	104.6	3578	15.50	298.7
	131	20	213	237	1.41	103.3	3316	14.80	301.4
	132	20	292	304	1.50	122.0		18.00	301.6
	133	20	321	361	1.40	130.5	3321	19.40	300.6
	134	20	417	392	1.63	146.3	3494	22.00	301.8
	135 b	10.3	235	224			3268		
	136 b	10.7	236	224	1.62		3262	15.1	286.1
		746.6	sec in 339 starts						
								STD DEV @	0.15
								AVG @ NOM	304.9

(a)Pulse test, 80 pulses, 0.1 sec on/1.0 sec off

(b) Pulse trains, 32 and 36 pulses, respectively of varying pulse width as defined in Figure 3.3-18A

Figure 3.3-13. High Performance 14-lbf Thrust Engine Test Data Summary 75:1 Area Ratio Iridium-Coated Rhenium Chamber, Page 2 of 2

Test Type	Inlet Condition I.D. No.	Inlet Pressures, psia		Cycle I.D.	S.S. Burn, sec	Number of Pulses	Pulse 'On" Time, sec	Pulse 'OFF' Time, sec	Thrust, lbf
		P_{ox}	P_{fu}						
Checkout	#1	220	220	--	5	0	0	0	14
Steady State	#1	220	220	--	100	0	0	0	14
Pulse	#1	220	220	--	0	80	0.1	1	14
Steady State	#2	145	145	--	100	0	0	0	10.6
Pulse	#2	145	145	--	0	80	0.1	1	10.6
Steady State	#16	370	370	--	100	0	0	0	19.7
Pulse	#16	370	370	--	0	80	0.1	1	19.7

Figure 3.3-14. Acceptance Test Matrix

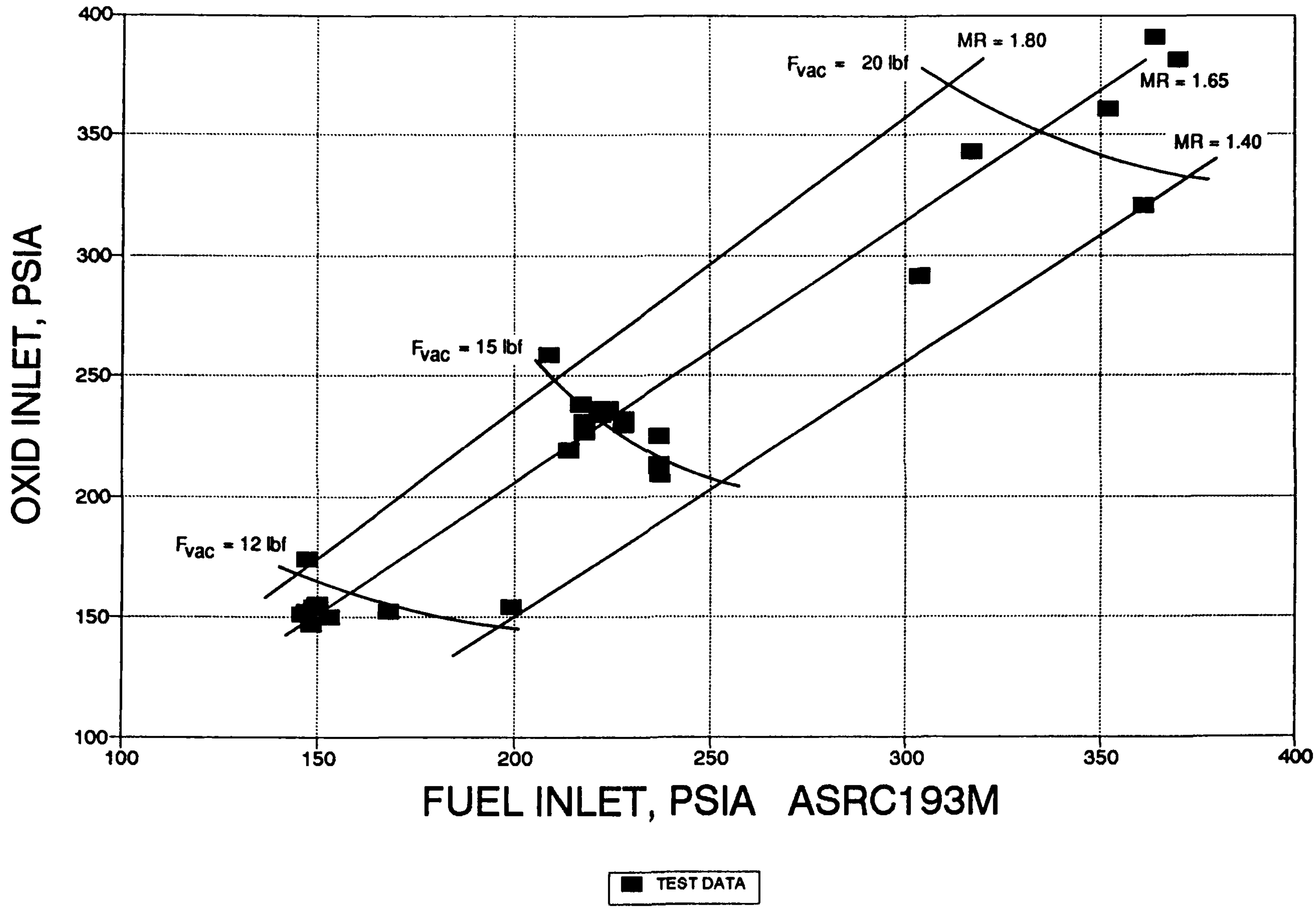


Figure 3.3-15. 14 lbf Ir-Re Operating Map Oxid Inlet vs Fuel Inlet

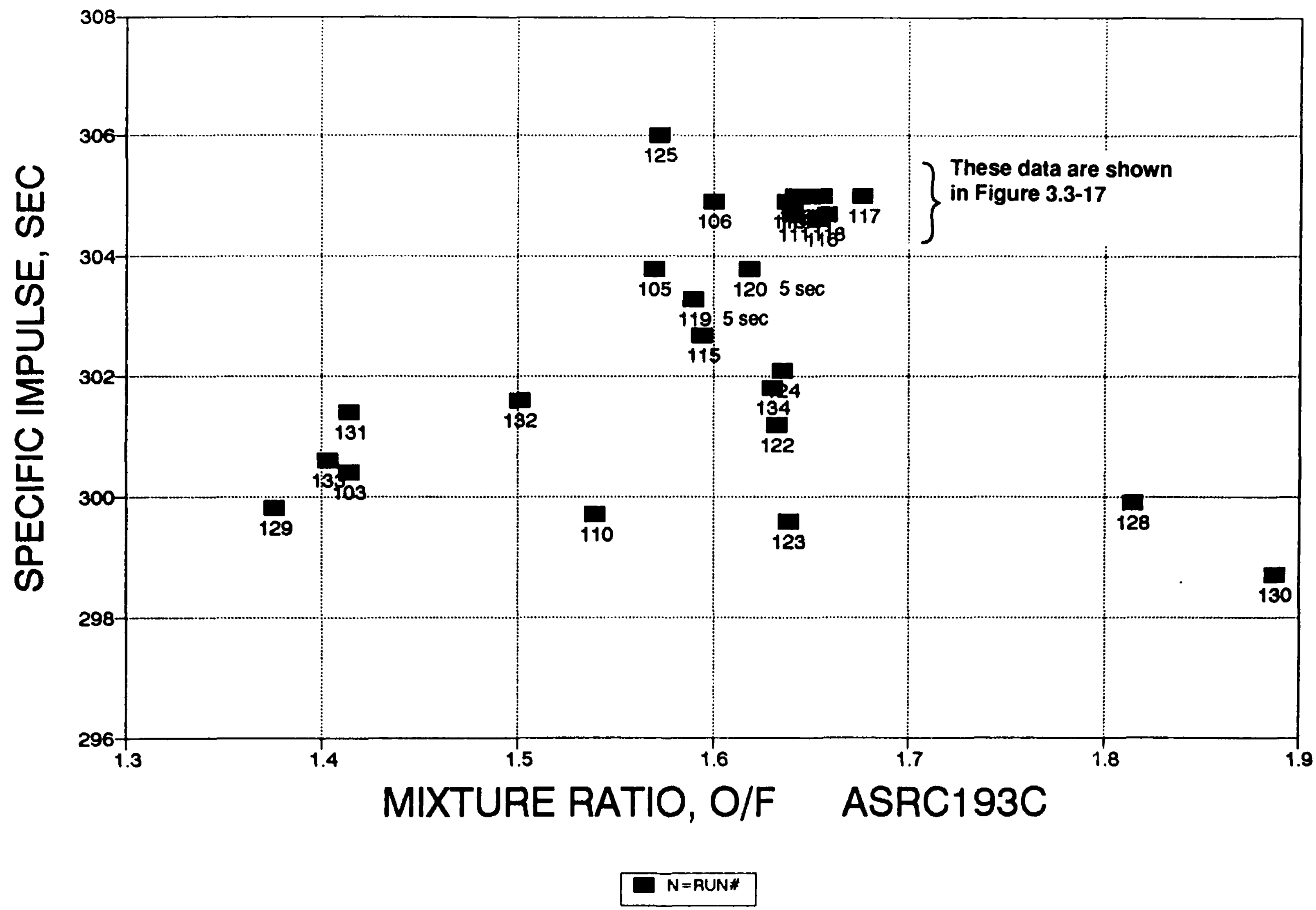


Figure 3.3-16. 14 lbf Ir-Re Is vs MR Performance, Tests -101 Through -134

points at nominal inlet conditions is shown again on a highly expanded scale in Figure 3.3-17. The average specific impulse at nominal conditions is 304.9 sec with a 3σ deviation of ±0.45 sec.

Pulse performance for the engine is shown in Figure 3.3-18 as a function of mixture ratio for tests -108, -109, and -127, which were 80-pulse trains, 0.1 sec on/1.0 sec off. The I_s for pulse test -136, 36 pulses of from 0.1 to 1.0 sec width is also shown. The pulse trains used in these tests is shown in Figure 3.3-18A. The I_s delivered for pulsed operation is above that required for the production engine in steady state firing. Impulse bit (I bit) delivered for the 100 ms electrical pulse widths of test-108 is shown in Figure 3.3-18B. The average I-bit is 1.18 lbf-sec ± 0.15 lbf sec over the 80 pulse train.

Specific impulse is shown as a function of chamber pressure in Figure 3.3-19 for the steady-state tests. It should be noted that the small diameter line which connected the pressure transducer to the engine was eventually partially blocked, possible from excess braze at a coupling in the line. It therefore gave slow response with delays of seconds before finally reaching steady state. At test-126 the line plugged completely. For the remainder of the tests chamber pressure is calculated from the measured propellant flows, the inlet pressures, and the previously measured engine Kw,. The independent Pc values provided from the oxidizer and fuel flows provided a check of consistency.

Thermal Data

Chamber external wall temperature at a point in the contraction region upstream of the throat measured with a two-color radiation pyrometer set for grey-body emission is shown in Figure 3.3-20 as a function of mixture ratio. There is an increase of 300°F in wall temperature over the full MR range, from 3280°F at MR = 1.38 to 3580°F at MR = 1.89. Note that there is no clear correlation of wall temperature with chamber pressure for this engine. Data for tests through -105 are not included since the pyrometer was aimed at a cooler location, downstream of the throat region. Short duration tests (< 5 sec) have been removed from the data set because the chamber has not reached steady state temperature. This occurs at about 10 sec, as shown in Figure 3.3-21, where temperature is plotted as a function of time for test -121.

Temperature data for test -112, a 15 sec firing, are shown in Figure 3.3-21A. The temperatures reach maximum values at about 5 seconds after shutdown, due to heat soakback, and then fall off to less than 300°F at the end of the 100 sec coast. Temperature data for five locations on the engine, as defined in Figure 3.3-7, are plotted in Figure 3.3-22 for Test -121, a 100 sec firing at nominal conditions. TF-2 located at the flange reaches a high of 160°F

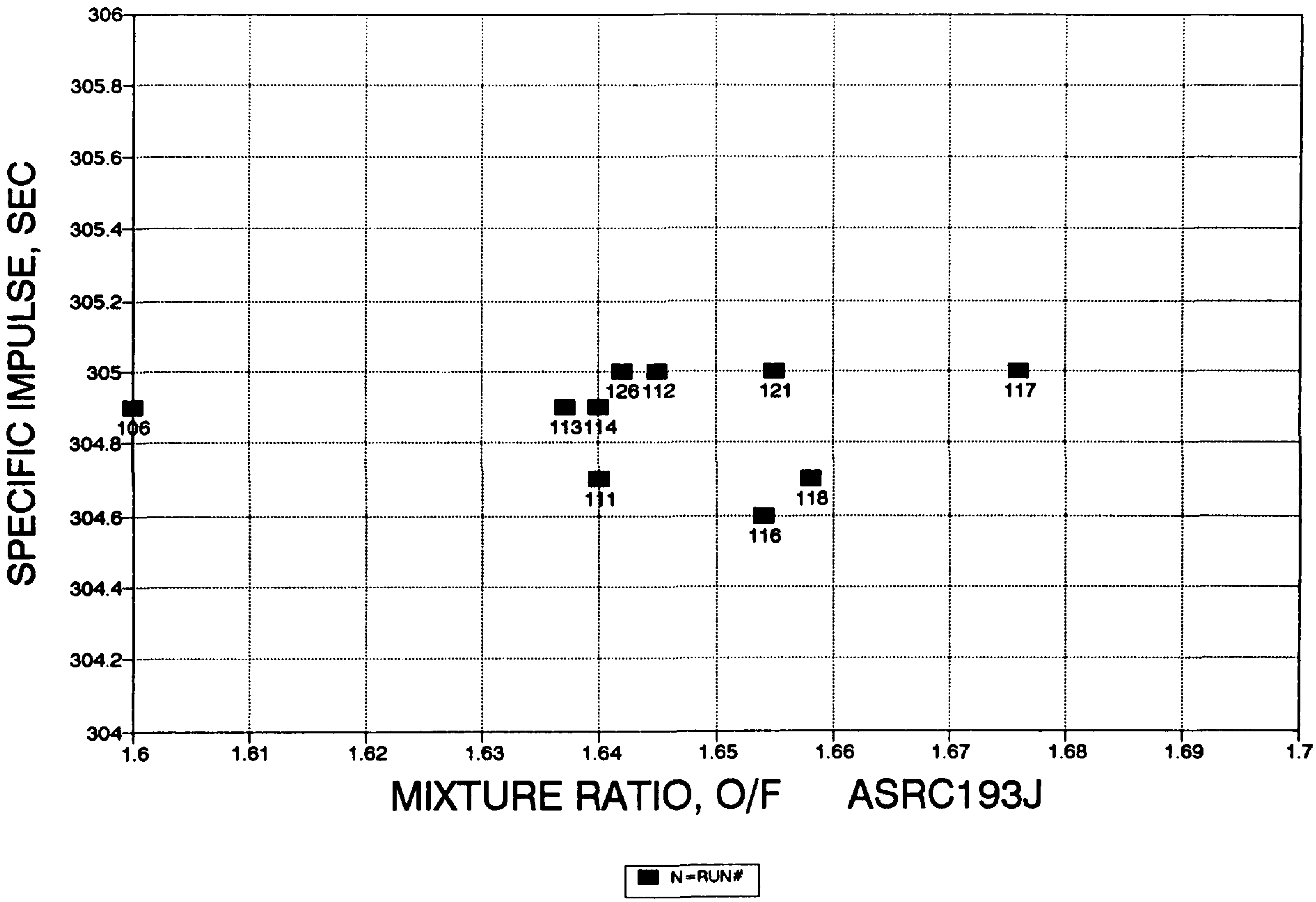


Figure 3.3-17. 14 lbf Ir-Re Is Vs MR Performance Tests at Nominal

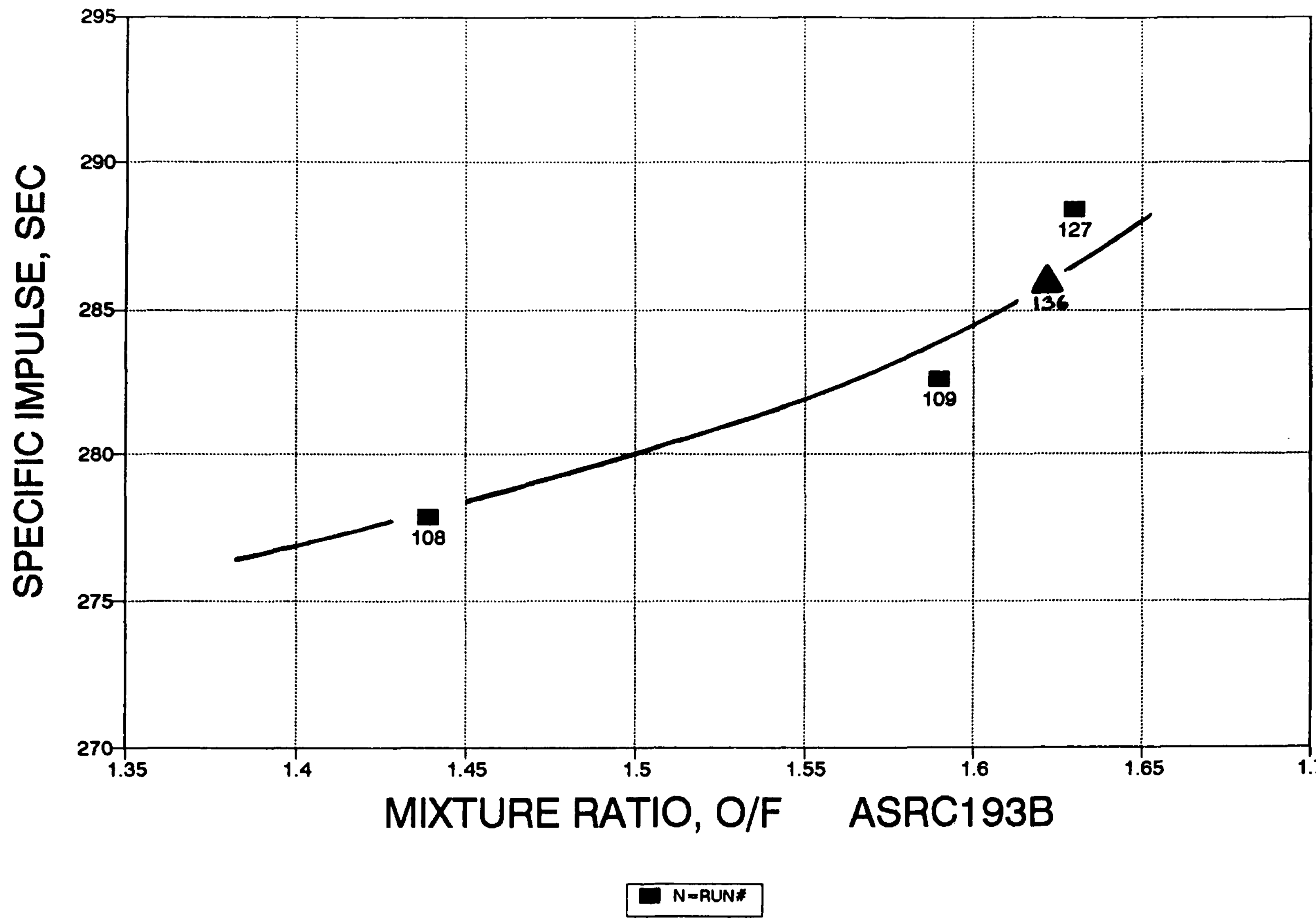


Figure 3.3-18. 14 lbf Ir-Re Is vs MR Pulse Performance (0.1 Sec On, 1.0 Off)

IDENT.	ON SEC	OFF SEC	REPEAT CYCLE	CUM. PULSES	CUM FIRING SEC	CUM TOTAL SEC
I6	1	0.5	4	4	4	6
I6	0.5	0.5	5	9	6.5	11
I6	0.25	0.5	10	19	9	18.5
I6	0.1	0.5	25	44	11.5	33.5

-135 STOPPED AT PULSE #32; -136 AT PULSE #36.

Figure 3.3-18A. Pulse Train Used in 14# Tests -135 and -136

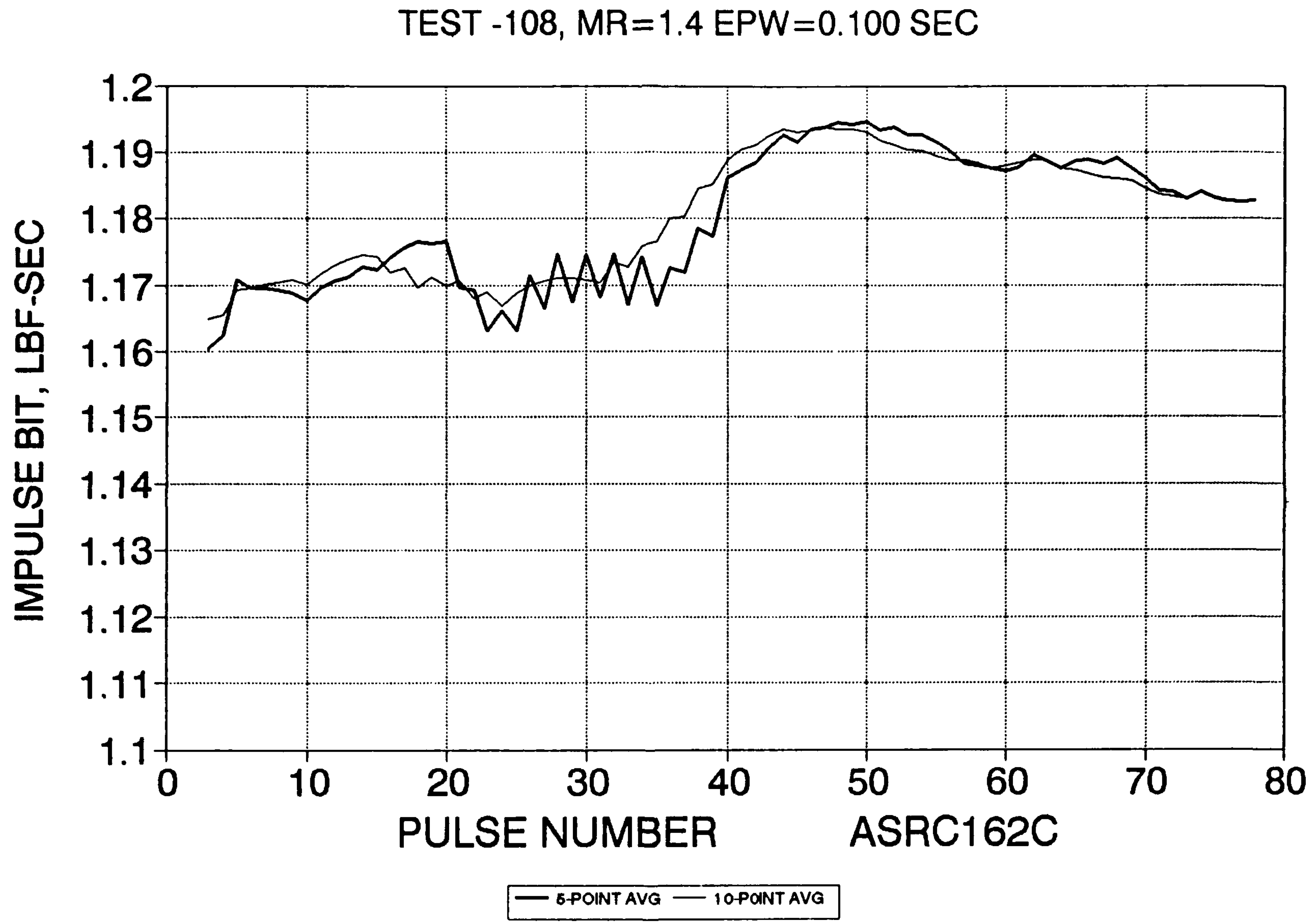


Figure 3.3-18B. 14# Ir-Re S/N2 I-Bit Versus Pulse Number

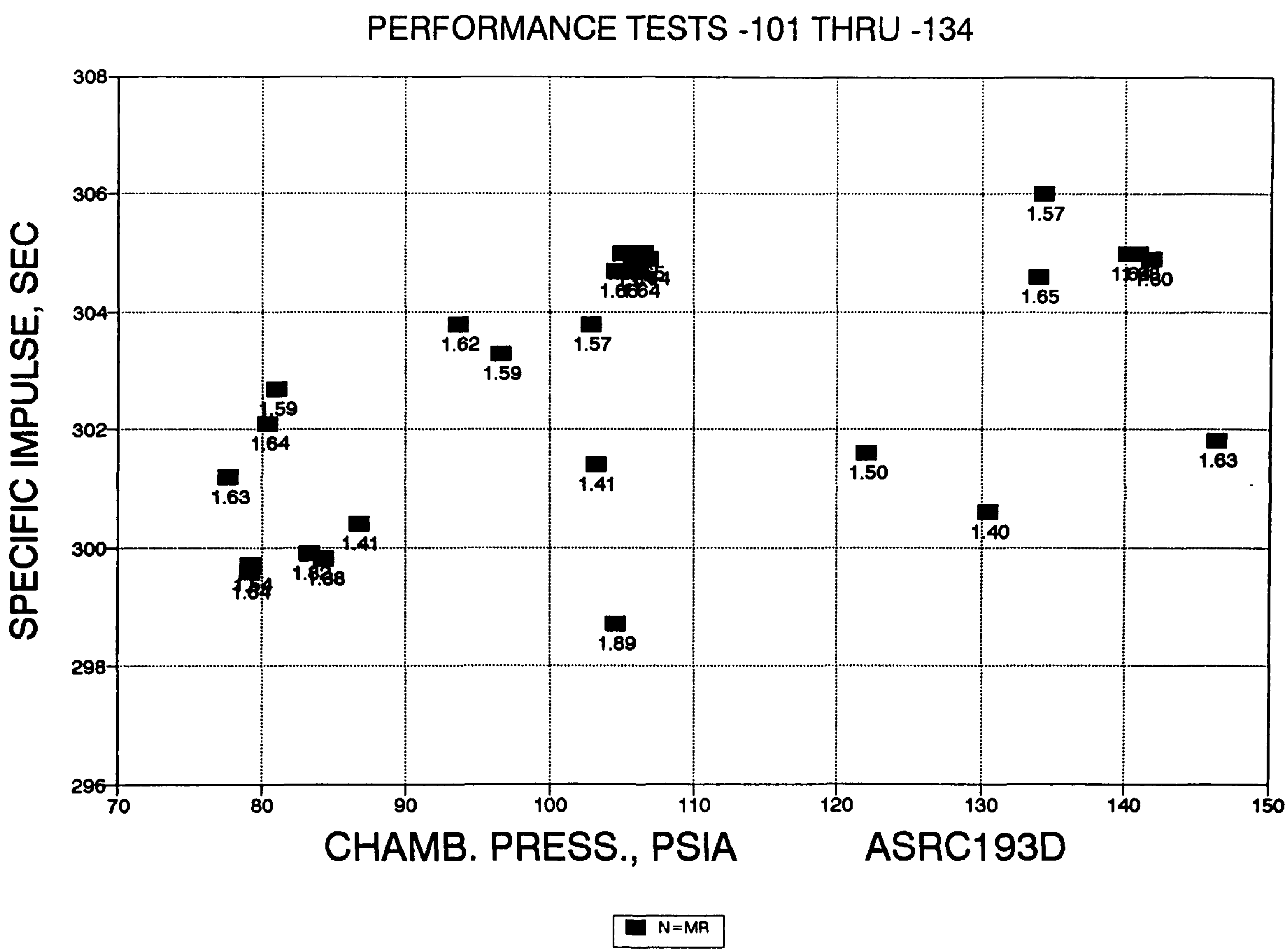


Figure 3.3-19. 14 lbf Ir-Re Is vs Pc

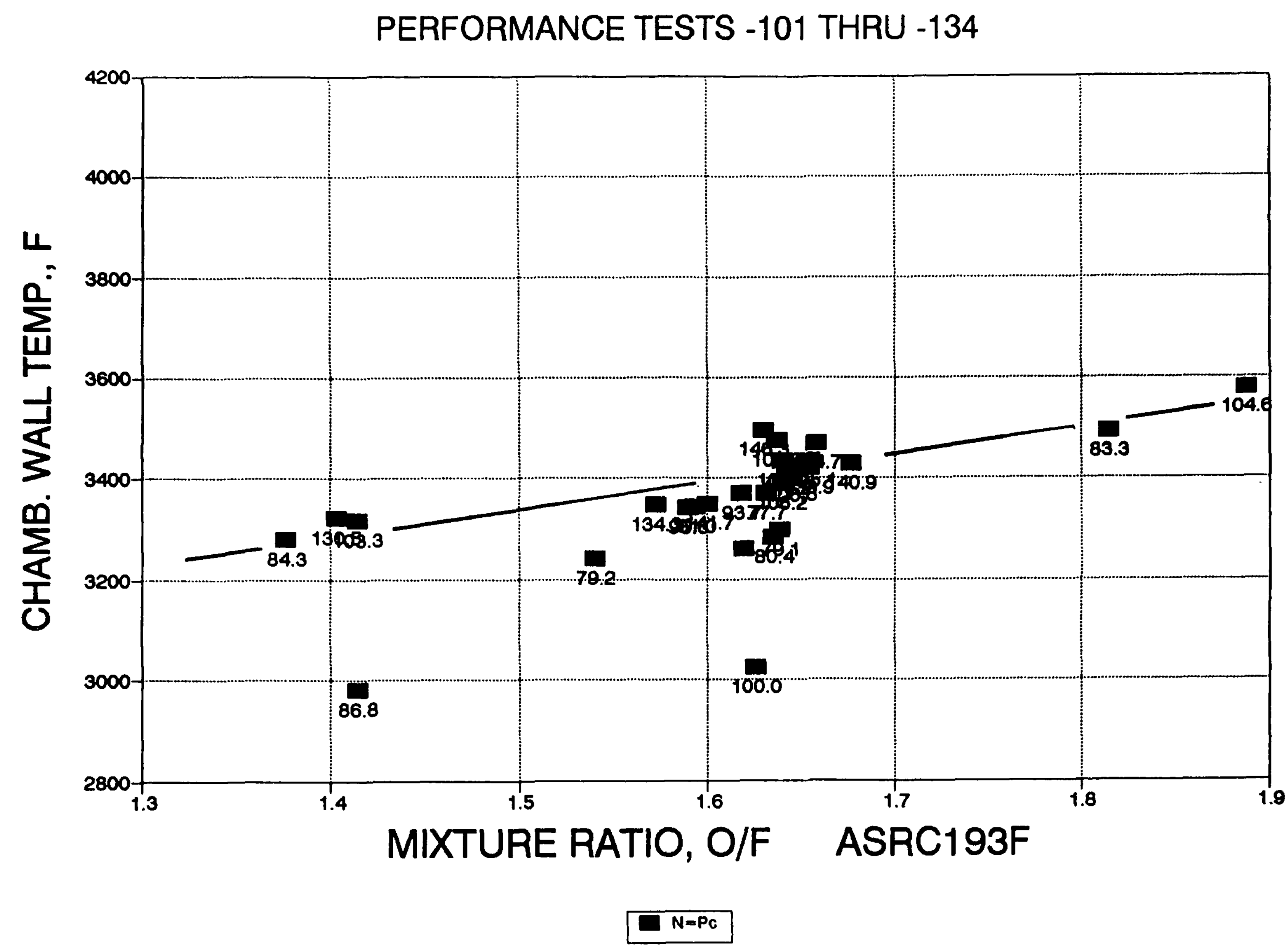


Figure 3.3-20. 14 lbf Ir-Re Tch. Wall vs MR

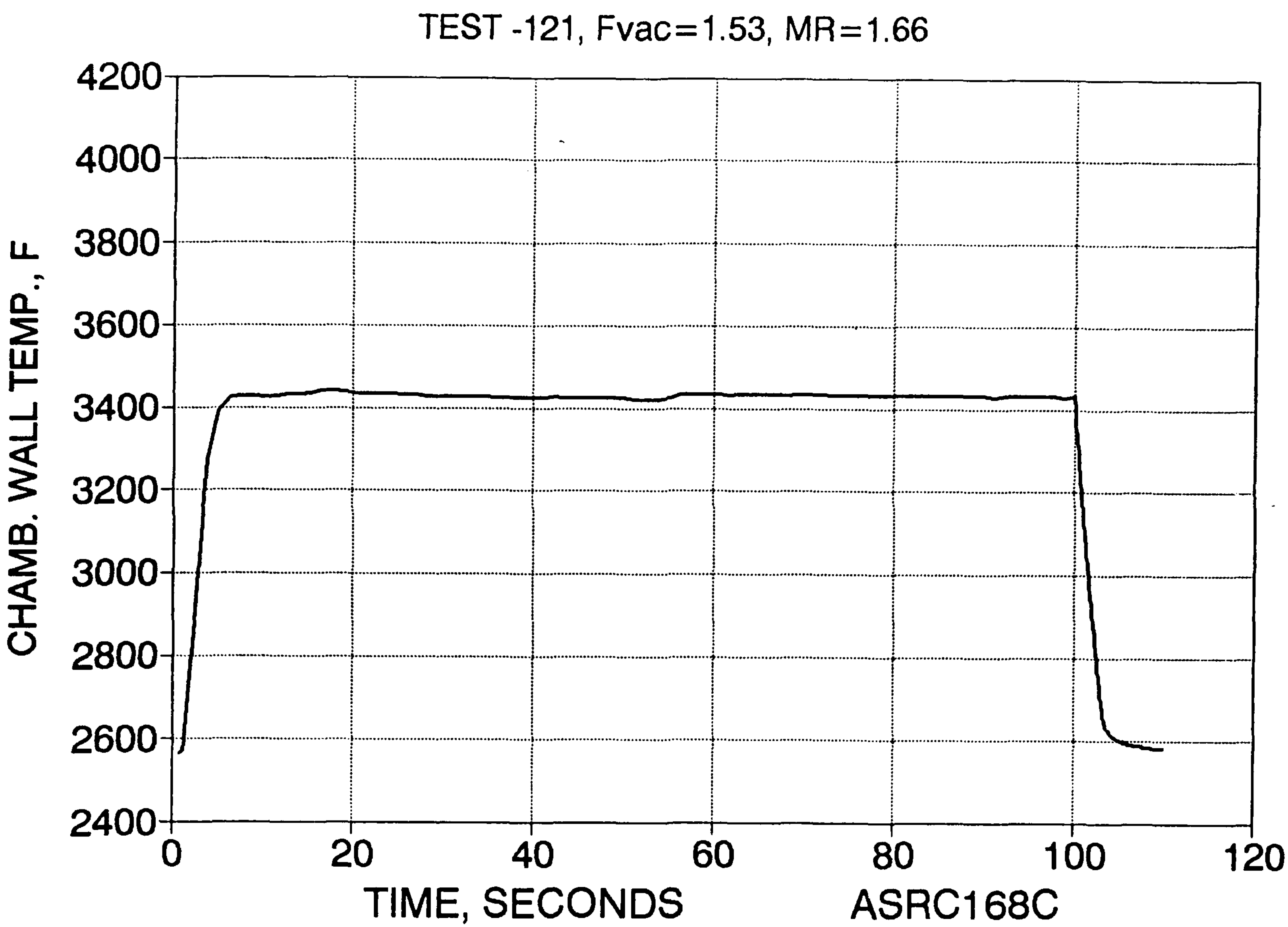
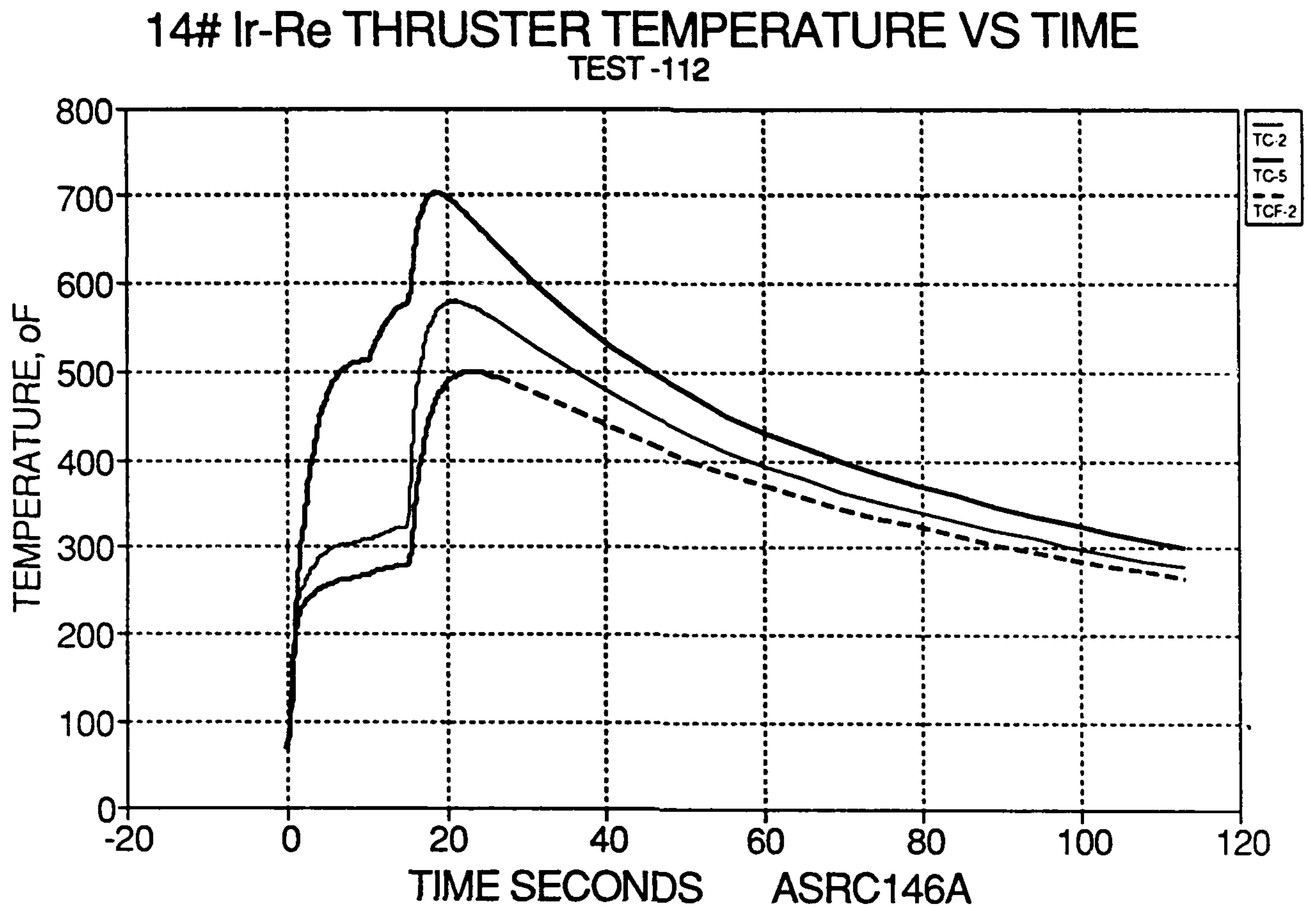
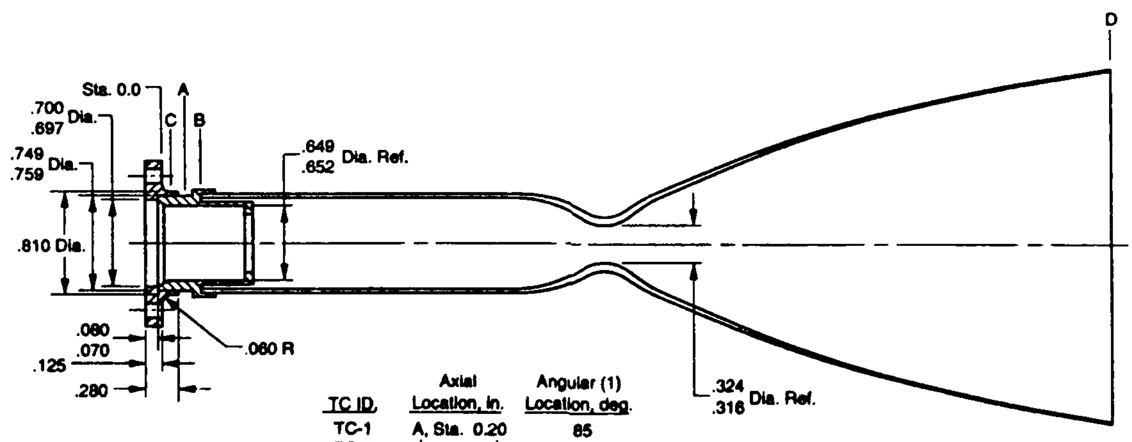


Figure 3.3-21. 14# Ir-Re: T_{wall} vs Time





TC ID.	Axial Location, in.	Angular (1) Location, deg.
TC-1	A, Sta. 0.20	85
TC-2	√ √	150
TC-3	√ √	330
TC-4	B, Sta. .03	85
TC-5	√ √	150
TC-6	√ √	330
TCF-1	C, Sta. 0.10	85
TCF-2	√ √	150
TCF-3	√ √	330
TN-1	D 0.10 from Exit	85

(1) P_C Port = 150°

Chamber Thermocouple Locations

Figure 3.3-21A. 14# Ir-Re Thruster Temperature vs Time

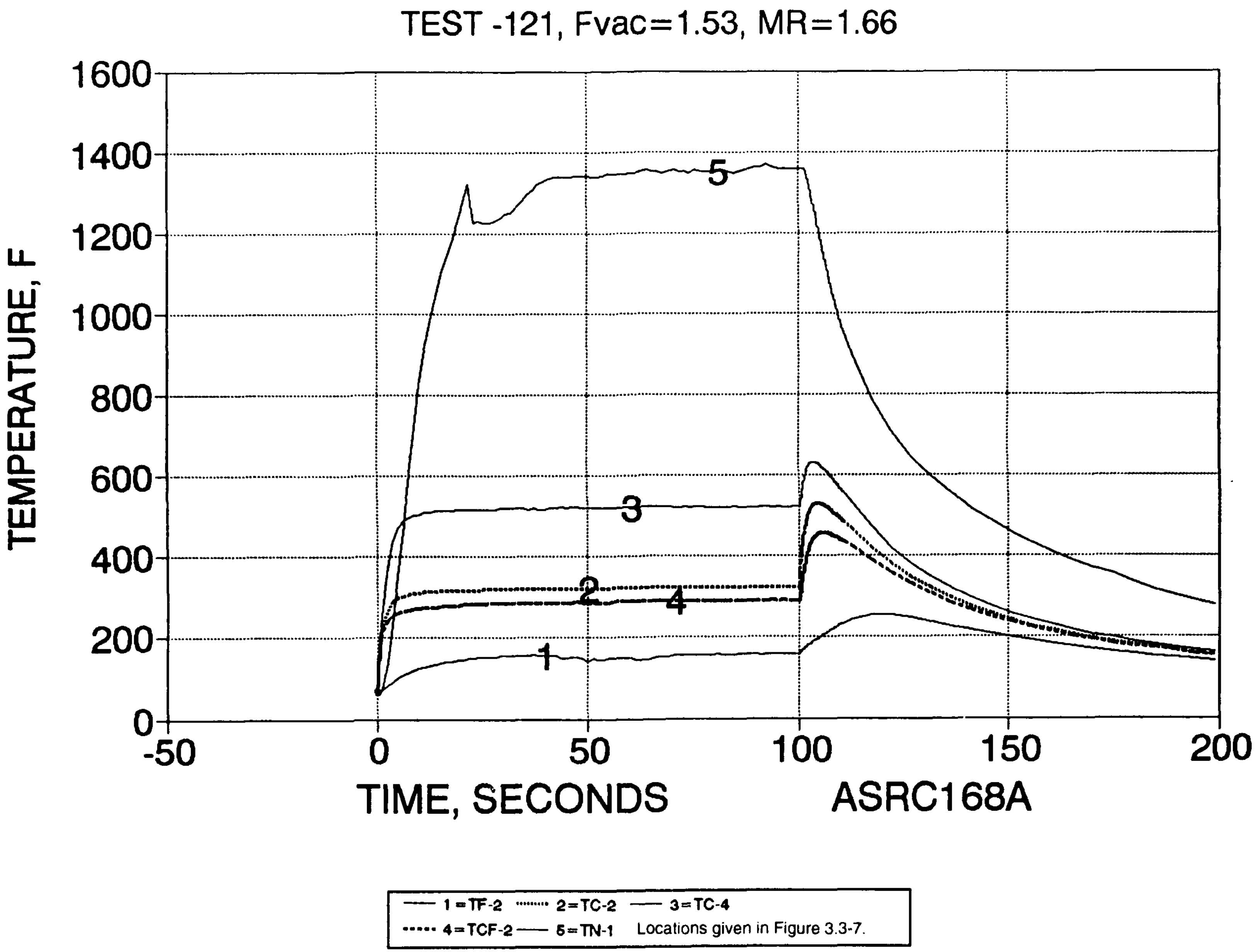


Figure 3.3-22. 14# Ir-Re: Temperatures vs Time

at 95 sec, then climbs to a maximum of 255°F at 17 sec of coast, and cools to 142°F) in 100 sec of coast. TC2, located on the exterior of the trip ring, halfway between the forward flange and the Pt-to-Retjoint, reaches a maximum of 323°F at 62 sec into the firing. It peaks at 530° after 4 sec of soakback during coast, and then falls to 155 °F in 100 sec of coast. The temperature of the Pt-to-Re joint, TC-4, reaches its maximum steady state temperature of 522°F 46 sec into the firing. At shutdown, this temperature rises to 632°F in 3.5 sec of coast, and then falls to 162°F in 100 sec of coast.

The temperature of the stainless flange-to-Pt joint, TCF-2, reaches a maximum valve of 290°F at 68 sec into the firing. It climbs to a post firing maximum of 457°F in 5.6 sec and then falls to 156°F in 100 sec. The temperature of the Ir-Re nozzle at the exit, TN-1 rises to a maximum of 1357°F at 70 sec into the firing. After shutdown, the nozzle exit temperature falls to 277°F in 100 sec. The steady state firing measured temperatures are compared to the results of the design thermal analysis (Appendix B) in Figure 3.3-23. the agreement with the analysis in good; all temperatures are well below the long life allowable temperature for the engine.

The measured performance at nominal operating conditions of the S/N 2 thruster is 304 ± 1 sec. This agrees well with the predicted value at a C* efficiency of 98% and represents a 20 sec improvement over the production design. However, in the last group of steady state tests, repeat points fall about 2-3 sec below this value. Posttest leak check of the chamber showed leakage past the gold seal between the chamber flange and the injector. In the standard 14 lbf thrust columbium chamber thruster, this seal is made using 6 bolts with stacks of belleville spring washers. These accommodate the difference in thermal expansion between the stainless bolts and the columbium chamber flange. They are not needed in the Ir-Re design because the flange and bolts are stainless. However, they were retained to provide maximum similarity between the two thrusters. Posttest examination shows that the spring washers interfered slightly with the chamber assembly. It is postulated that this resulted in design torque being achieved without obtaining full compression in the washer stack. It is postulated that the marginal preload was relieved during thermal cycle testing. Figure 3.3-24 shows the washer stacks after testing.

The last two tests were pulse series, as defined in Figure 3.3-18A, which were part of the qualification test series. The first test, -135 was terminated at 32 pulses when TCF-2 reached its preset kill temperature of 500°F. Since this is the stainless-to-Pt joint, temperatures of more than twice this value could be tolerated, although with some concern for the subsequent overheating of the injector which could occur. The temperature limit was

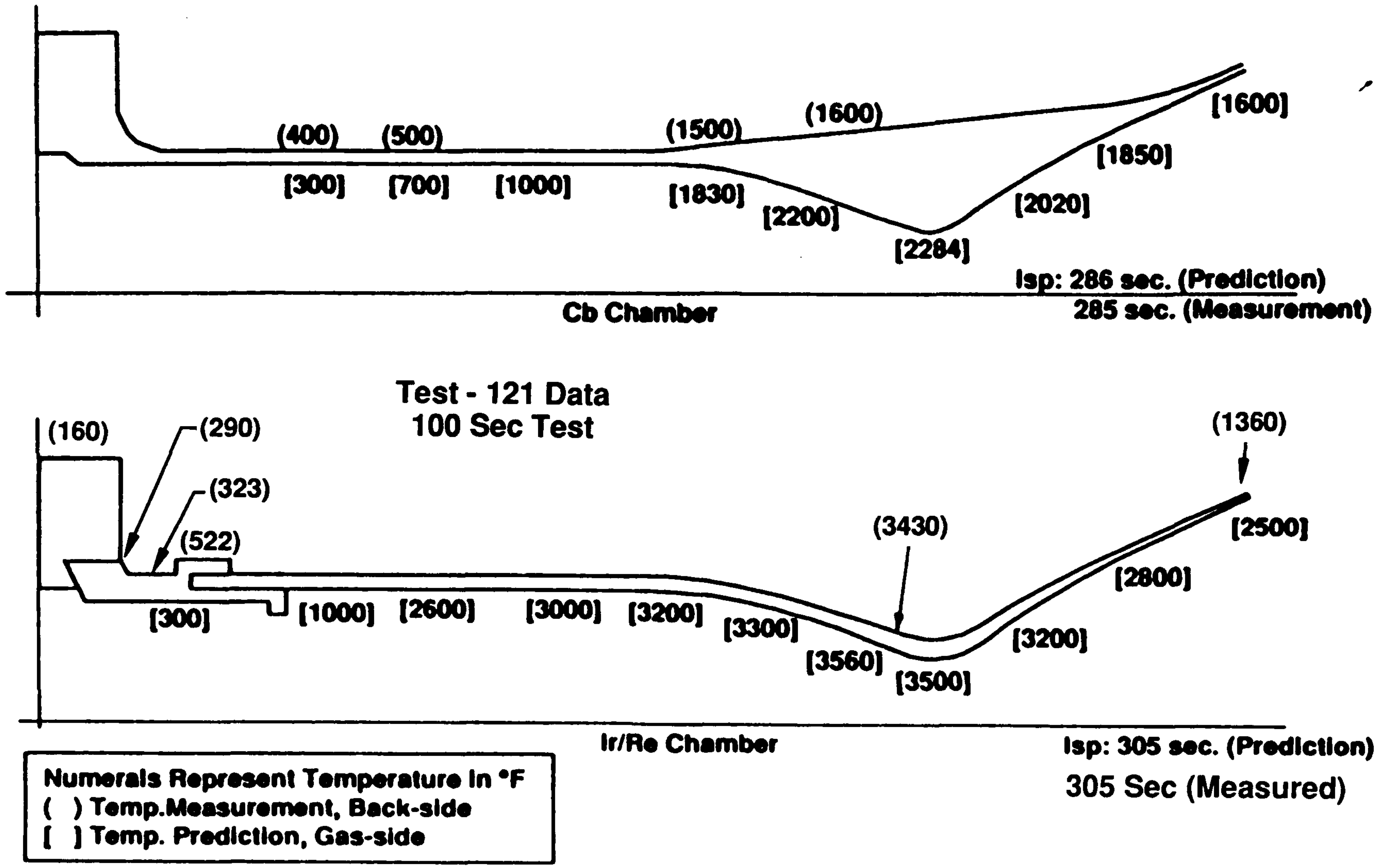


Figure 3.3-23. Thermal Comparison of RCT and Modified RCT Thrust Chambers



(C0191_0300)   5X

Figure 3.3-24.   14 lbF Ir-Re Thruster Washer Stacks After Testing

increased to 750°F and the firing was repeated as test -136. This test ran for 36 pulses. The kill computer indicated that TCF-2 had exceeded the 750°F limit; engineering unit data summaries available on line had an edit ratio of 20 (about every 40th measured data scan). This listing showed a maximum TCF-2 of 524°F; however because of the lateness of the hour it was decided to examine the data more thoroughly before pushing on with testing and possibly damaging the engine. An unedited (every other scan) listing printed the next day showed clearly that the highest temperature reached by TCF-2 was 530°F. Apparently the shutdown computer, which operates at a higher sampling rate than the data computer, had responded to a noise spike. At this point, the hot fire testing was deferred to permit vibration test of the engine.

Hot fire tests to date have demonstrated front end thermal management at steady state and 10% duty cycles (0.1 sec on, 1.0 sec off) as required by acceptance tests of the current 14-lbf engine. Since a pulse mode thermal analysis has not been conducted on the Ir-Re 14-lbf thruster and hot restart with predicted MMH decomposition as discussed in Appendix B has not been demonstrated, pulse mode thermal management at higher duty cycles remains to be demonstrated. Such tests are contained in the qualification tests, which remain to be done.

Exhaust Plume Measurements

Optical measurements were made on the exhaust plume to detect the presence of rhenium. Absorption of a 346 nm reference signal modulated at 1.1 kHz is a measure of the rhenium concentration. Figure 3.3-25 is typical of the optical measurement obtained on a normal test, Run -121. The absorption shows just noise (signal above zero level is absorption). The total radiation signal (350 nm) shows the relatively gradual hardware heat up curve. Variations which occur in the total radiation throughout the test correlate with small changes in nozzle temperature, caused by small fluctuations in MR due to changes in regulator set points. The T^4 effect on radiation makes these small changes measurable.

One test in this series, -106, showed possible indication of Re in the exhaust. In this test the PDFM's bottomed and the engine went off MR on the high side, with a gradual decay in thrust. The ESMS measurements for this test are shown in Figure 3.3-26. No evidence of damage was found in posttest inspection. No other tests showed the absorption, which is consistent with appearance of the hardware at the end of the test.

Total emission measurements at 350 nm taken during the pulse testing showed an initial rise, which was expected and can be attributed to nozzle grey body emission. However, after reaching a maximum, the emission fell throughout the pulse test. Figure 3.3-27

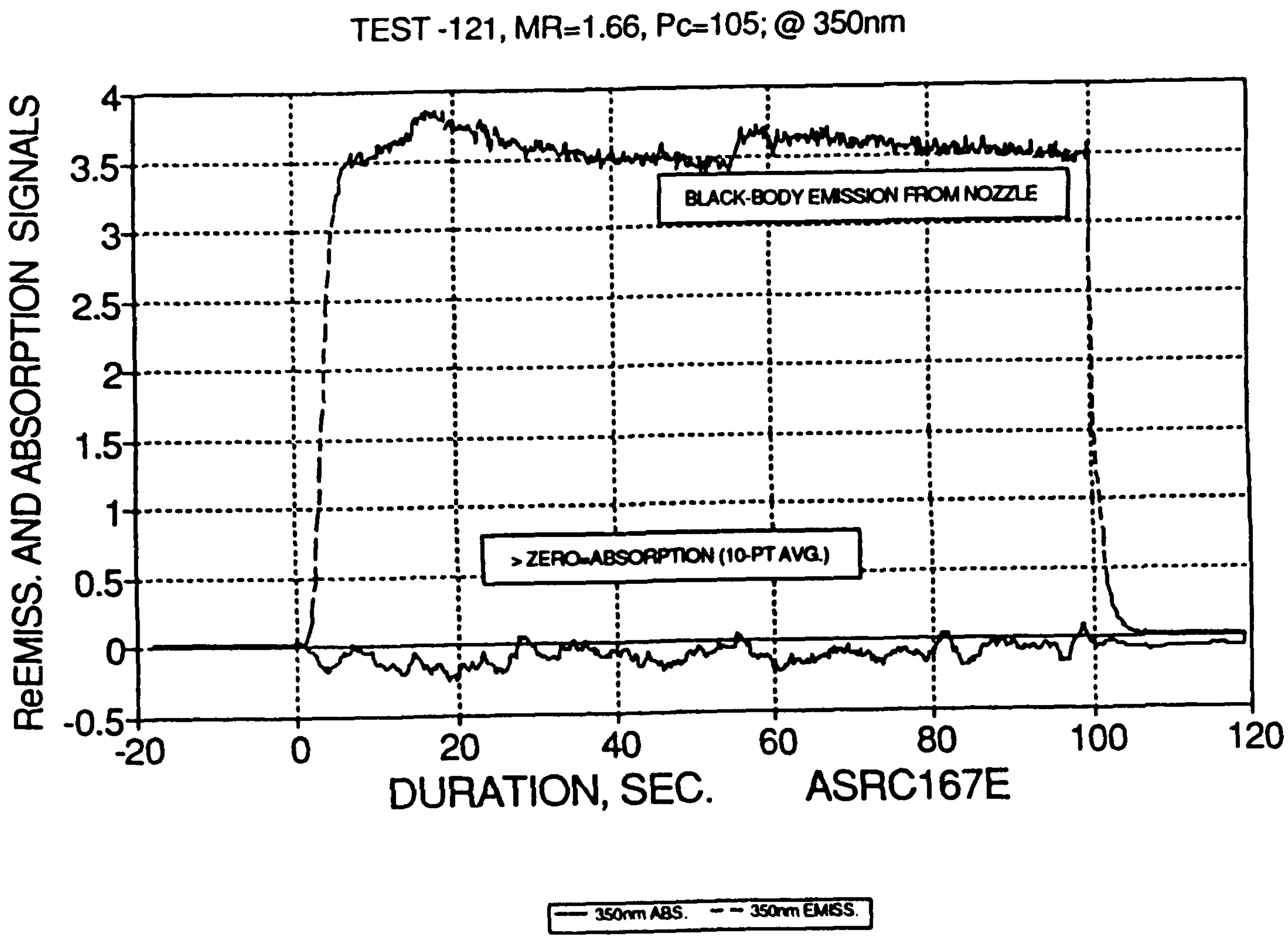


Figure 3.3-25. 14-lbF Ir-Re S/N2 Plume Optical Data

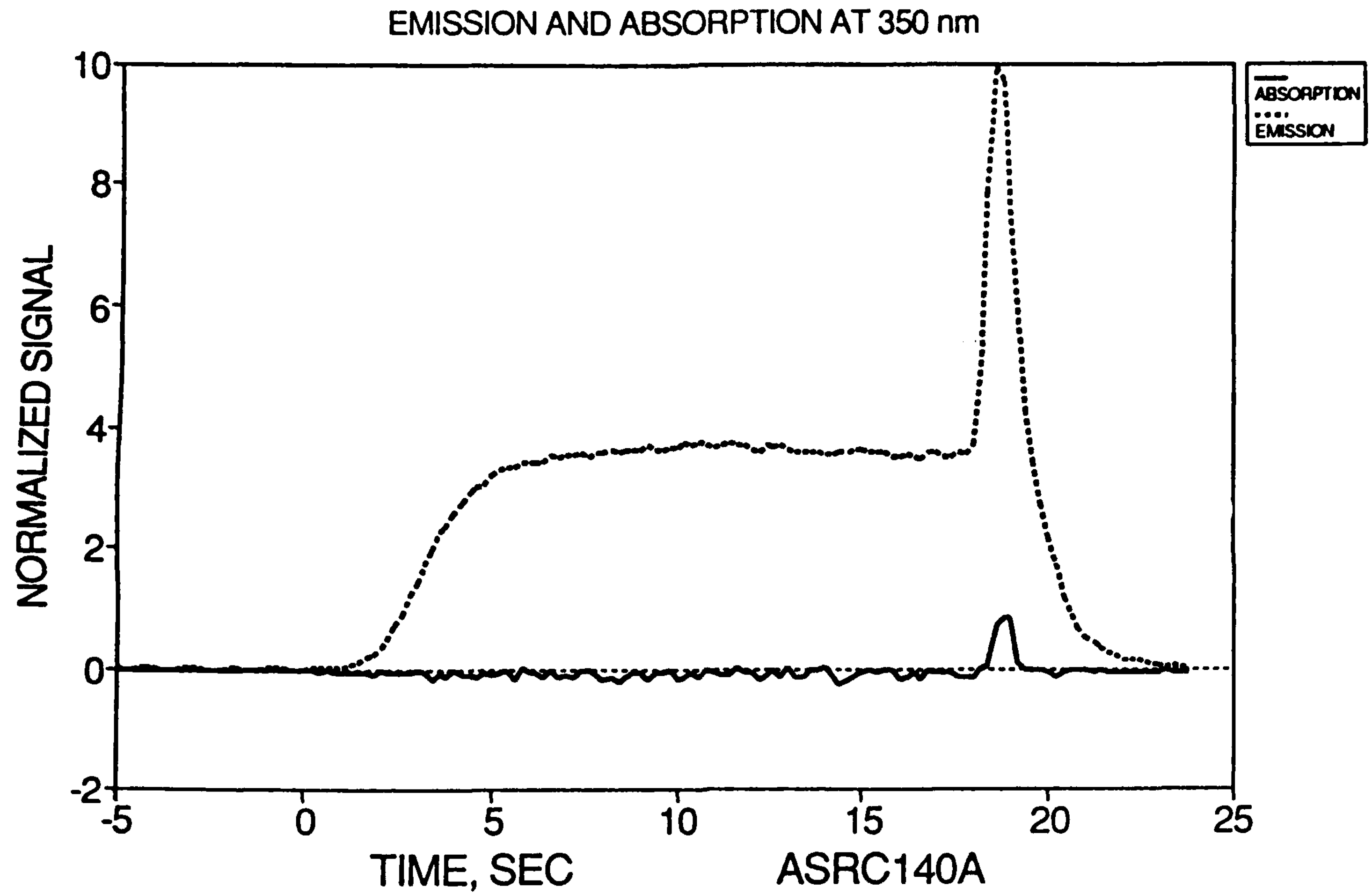


Figure 3.3-26. 14-lbF Plume Optical Measurement – Run 106

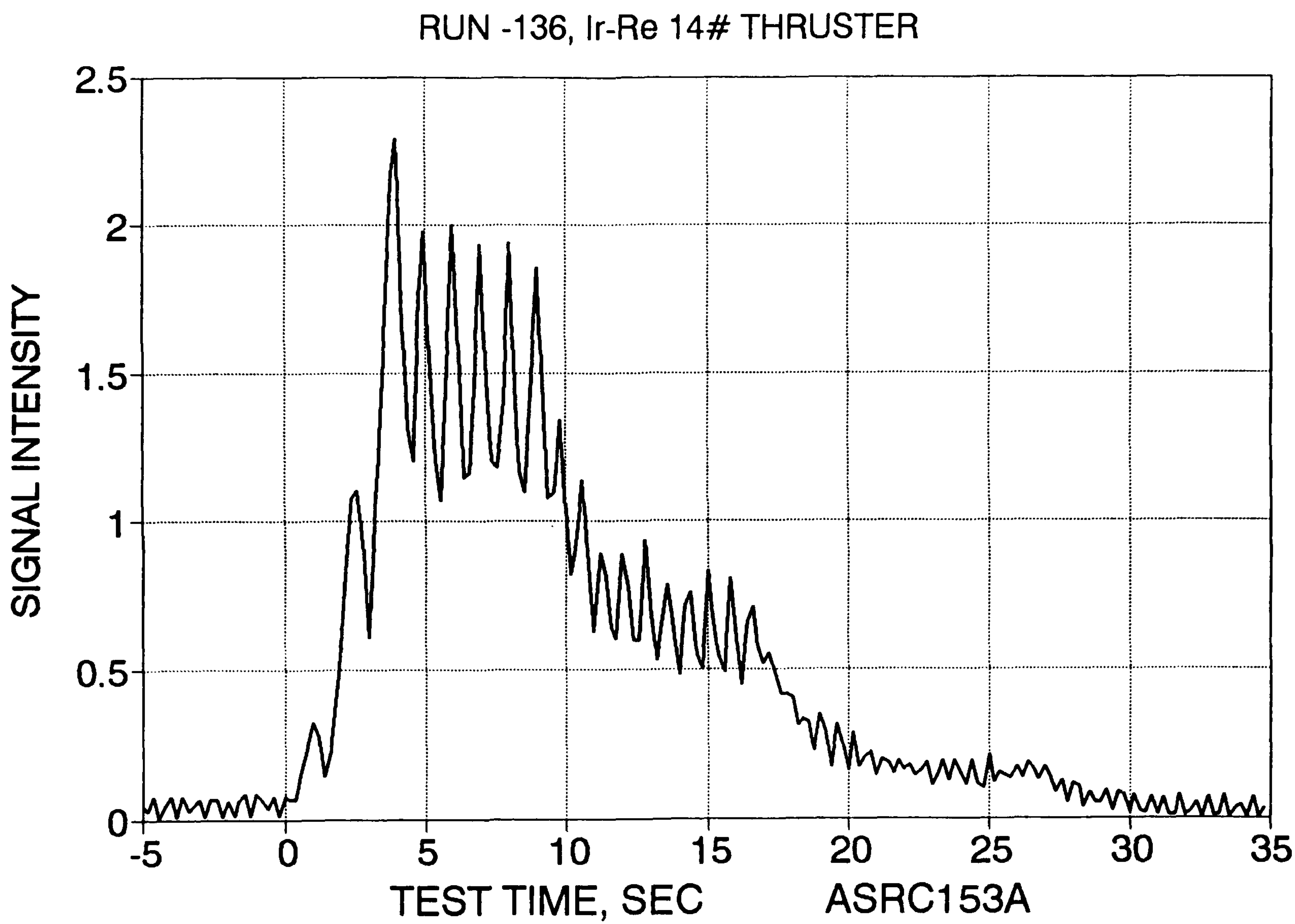


Figure 3.3-27. Total Emission at 350 nm vs Time

shows the total emission for pulse test -136; the variations in emission correspond to the individual pulses, which start out at one second duration and then reduce in steps to 0.1 sec. Nozzle temperature calculated from these data are shown in Figure 3.3-28, along with measured nozzle temperature. The agreement is good for the first 10 seconds; after this measured nozzle temperature remains constant at about 950°F while emission calculated temperature steadily drops to low values throughout. Why this occurs on the pulse test is not clear; it could represent absorption by exhaust species generated at each shutdown which is increasing as cell pressure increases throughout the test.

3.4 VIBRATION ACCEPTANCE TEST

The objective of the vibration testing was to determine if the Ir-Re chamber structure could withstand the random vibration levels to which the flight 14 lbf Cb engine is exposed for production acceptance testing. The engine successfully passed the acceptance test vibration levels without damage. Using strain measurements obtained in these tests, the margin of safety for a qualification level test (+3 db) was calculated (Appendix D). Results showed positive margins for all critical areas:

Location	Margin of Safety
Chamber Throat	0.65
Chamber Root	2.78
Trip Ring Root	2.38

Preparation

After hot fire testing the engine was disassembled and inspected. Figure 3.4-1 shows the engine prior to disassembly; Figure 3.4-2 is a detail of the chamber and valve.

After disassembly, the engine was reassembled with a new seal, and standard lock washers. The Bellville spring washers were not used since they serve no purpose on the Ir-Re chamber while increasing the thermal load into the spacecraft.

The production Cb 14# thruster is acceptance tested in the Reaction Control Thruster Module (RCTM). The RCTM consists of a pair of thrusters, instrumentation, thermal shields and their support structure, as installed in the spacecraft. The Ir-Re 14# thruster was exposed to the same vibration acceptance testing with the addition of diagnostic strain gages. The engine is shown in Figure 3.4-3 with the module structure, and a Cb engine which was used to provide proper mass distribution in the RCTM.

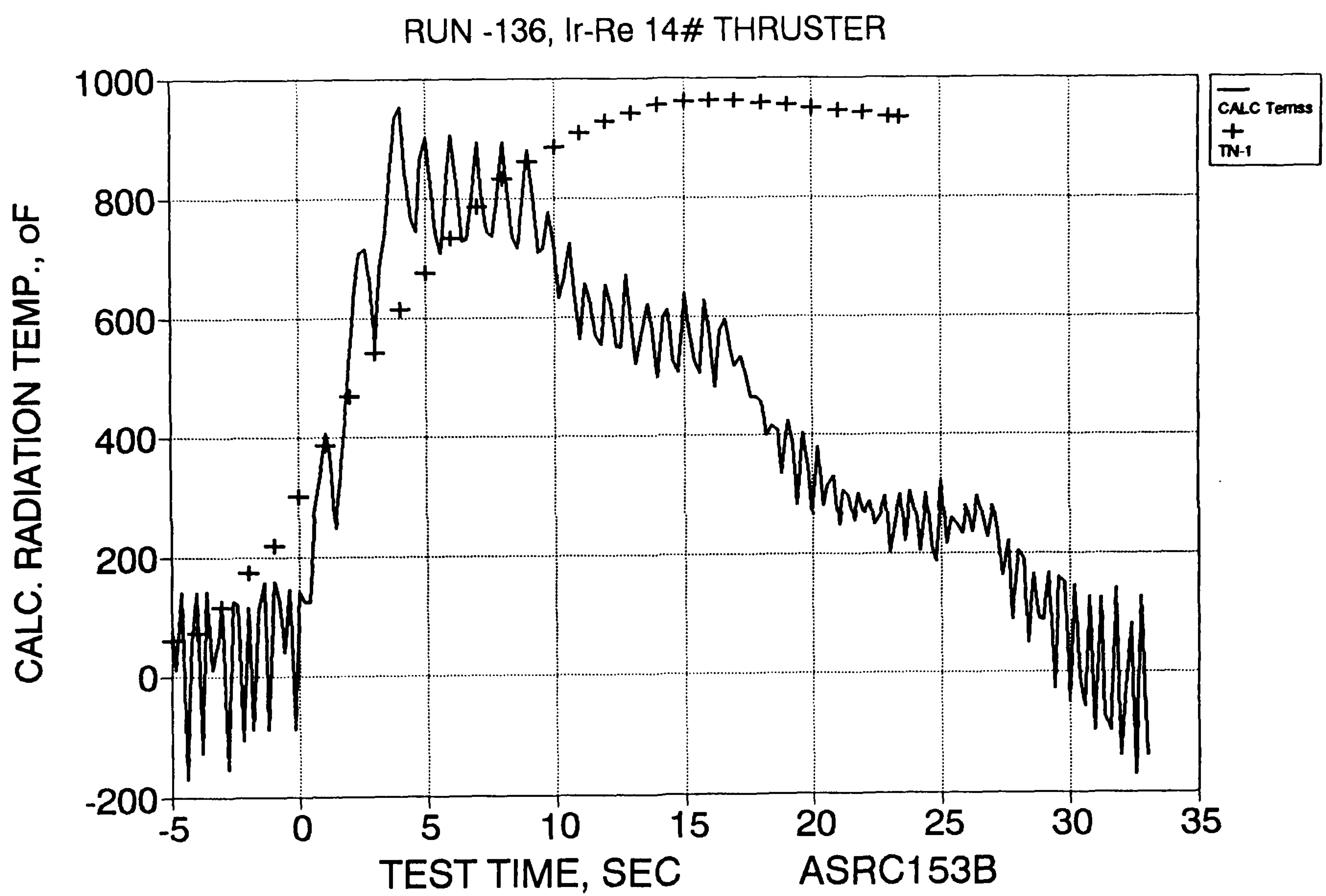


Figure 3.3-28. Calculated Temperature for 350 nm Emission



Figure 3.4-1. 14# Ir-Re Engine Prior to Posttest Inspection (C0291 749)

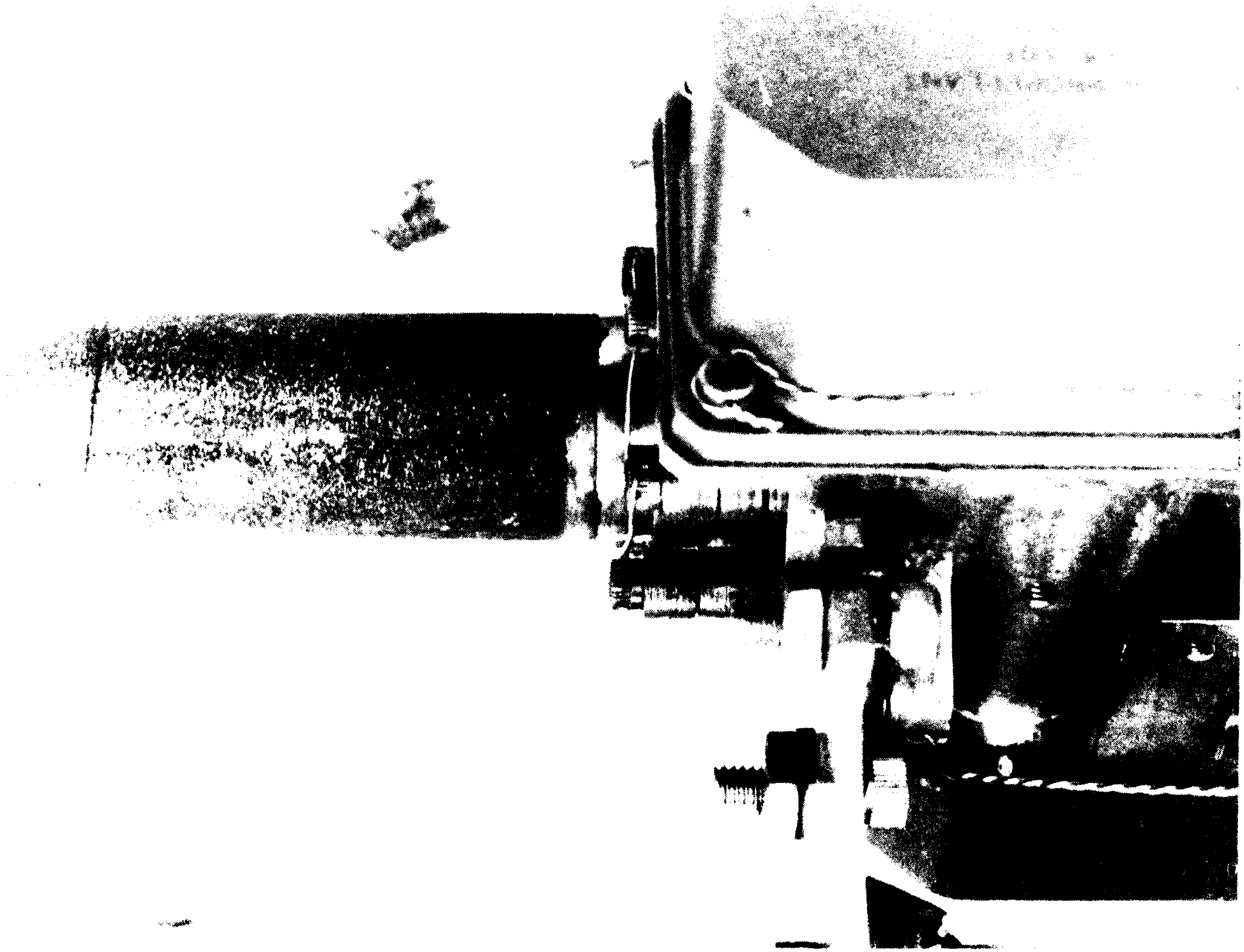


Figure 3.4-2. 14# Ir-Re Engine Posttest Chamber Appearance

(C0291 743)



Figure 3.4-3. 14 lbf Ir-Re Thruster Being Assembled Into RCTM for Vibration Acceptance Test

The planning for the vibration acceptance testing is discussed in Appendix C. The specification requirements for the vibration power levels are shown in Figure 3.4-4. The tests are conducted in three different groups, one each for the X, Y, and Z axis.

Facility and Instrumentation

The testing requires the use of two different vibration facilities, a vertical shaker for the X-axis tests and a horizontal shaker for the Y- and Z-axis tests. These are driven by a control system which monitors the acceleration levels to which the RCTM mounting fixture is exposed. For these tests, additional accelerometers were mounted on the engine. The overall setup for Z-axis vibration of the Ir-Re chamber in the RCTM is shown in Figure 3.4-5. Figure 3.4-6 is a close up which shows the RCTM mounted on the Z-axis test fixture, which is supported vertically by a slip table and coupled to the output of the acoustic driver. The lower engine in the module is the 14# Ir-Re thruster; accelerometers at the nozzle exit and strain gages at the throat are visible. Figure 3.4-7 is a closeup of the RCTM with a side panel removed showing the three accelerometers mounted on the valve. As discussed in Appendix D, strain gages were mounted on the engine at the throat to measure strain during testing. Figure 3.4-8 shows these gages. Because of the uncertainty in yield strength and fatigue life properties for Re, there was some concern that the chamber might bend at the throat at the acceptance test vibration levels. Therefore, dial indicators were set up to measure nozzle deflection, and the tests were run at progressively increasing acceleration levels, starting down 12 db and increasing in 3 db steps to the 0 db down acceptance test level (see Figure 3.4-9 for the relation between db and power).

Vibration Testing

Spectral power density curves such as shown in Figure 3.4-10 were obtained for each of the 4 nozzle strain gages for each test series. No unusual responses were noted. Deflection measurements were made after each test; no deflection was measured. Power spectral density plots were made for the control accelerometer and the 5 engine-mounted accelerometers for each axis of excitation. Figure 3.4-11 is an example of the response of the control accelerometer, for the X-axis tests. Figure 3.4-12 shows nozzle "Y" accelerometer spectral power density for the Y-axis acceleration test. A complete set of 0 db strain and accelerometer data are presented and discussed in Appendix D, where the margin of safety for the qualification (+3 db) random vibration tests is derived.

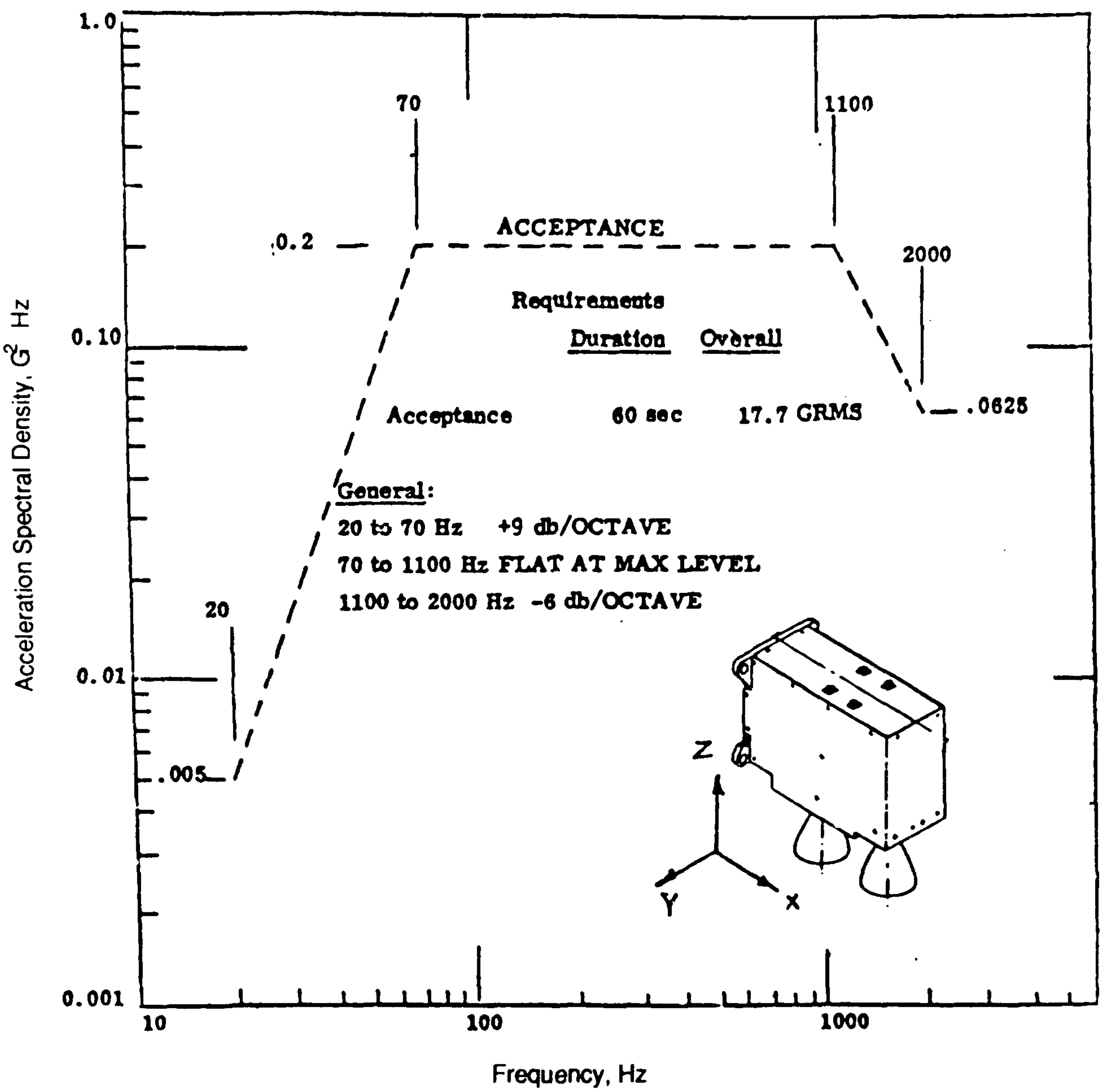


Figure 3.4-4. Production 14 lbf RCTM Acceleration Spectral Density Versus Frequency

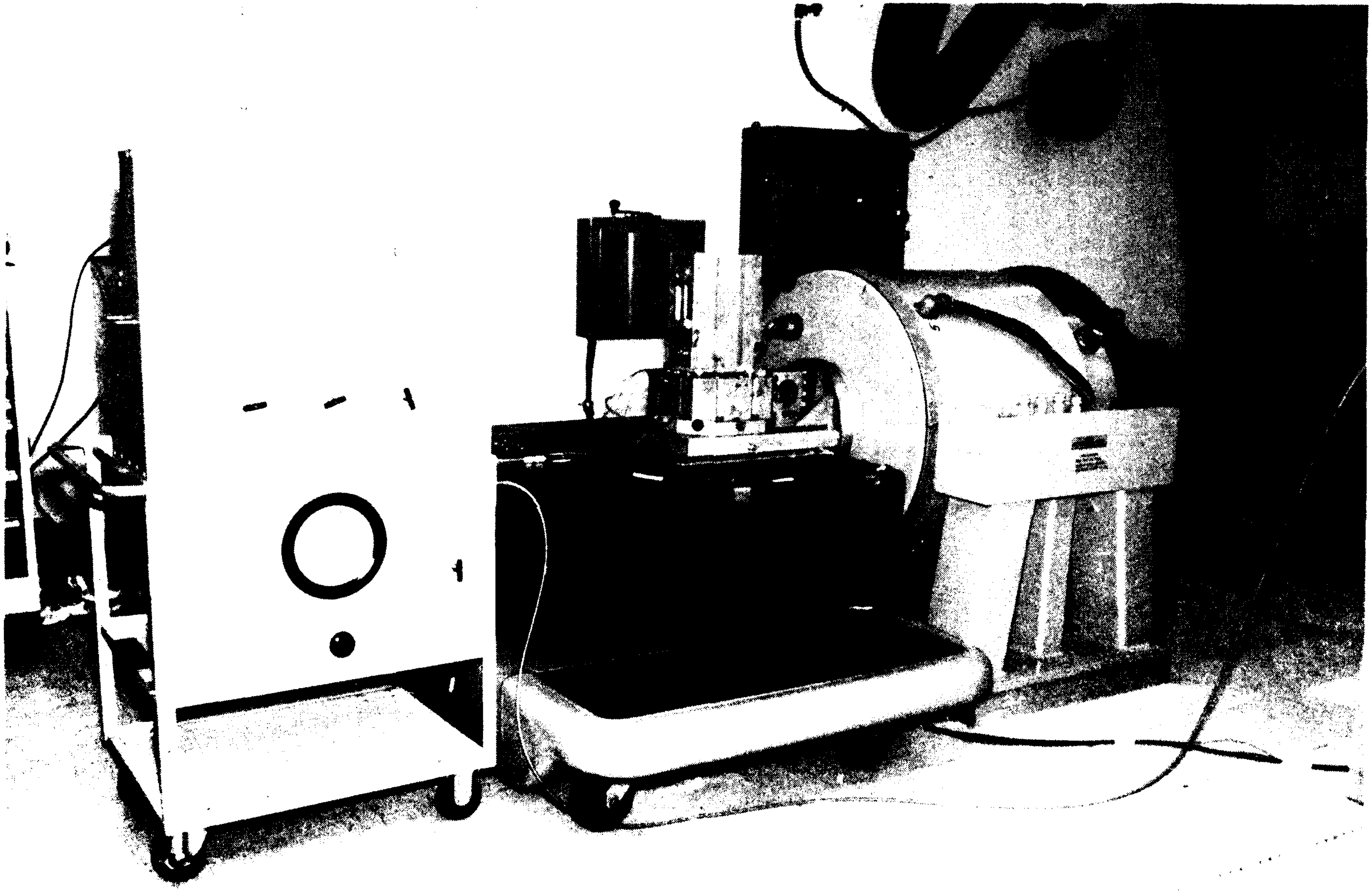


Figure 3.4-5. Z-Axis Random Vibration; Acceptance Test 14# Ir-Re Thruster

(C0291 139)

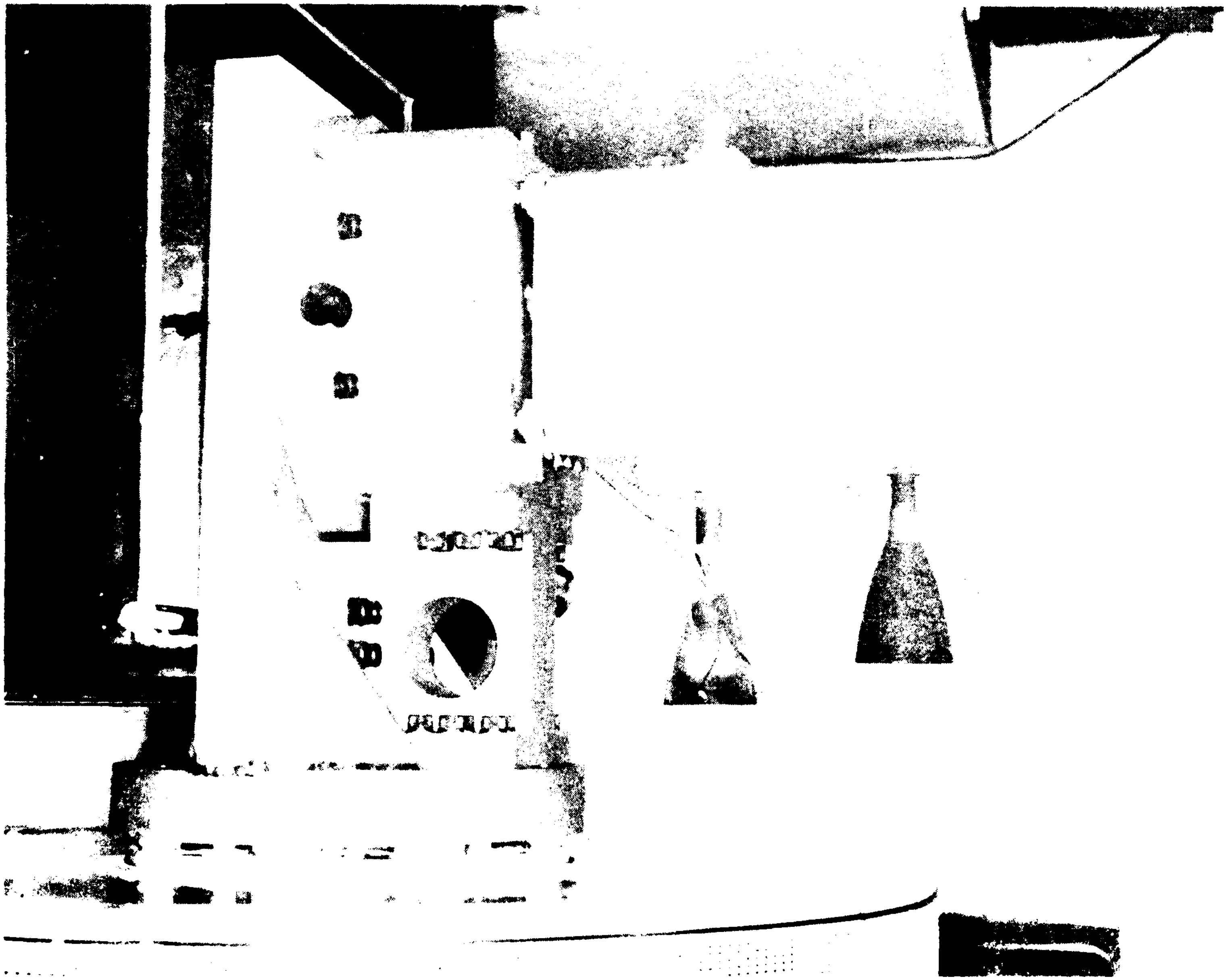


Figure 3.4-6. RCTM With 14# Ir-Re Thruster in Z-Axis Vibration Set-up

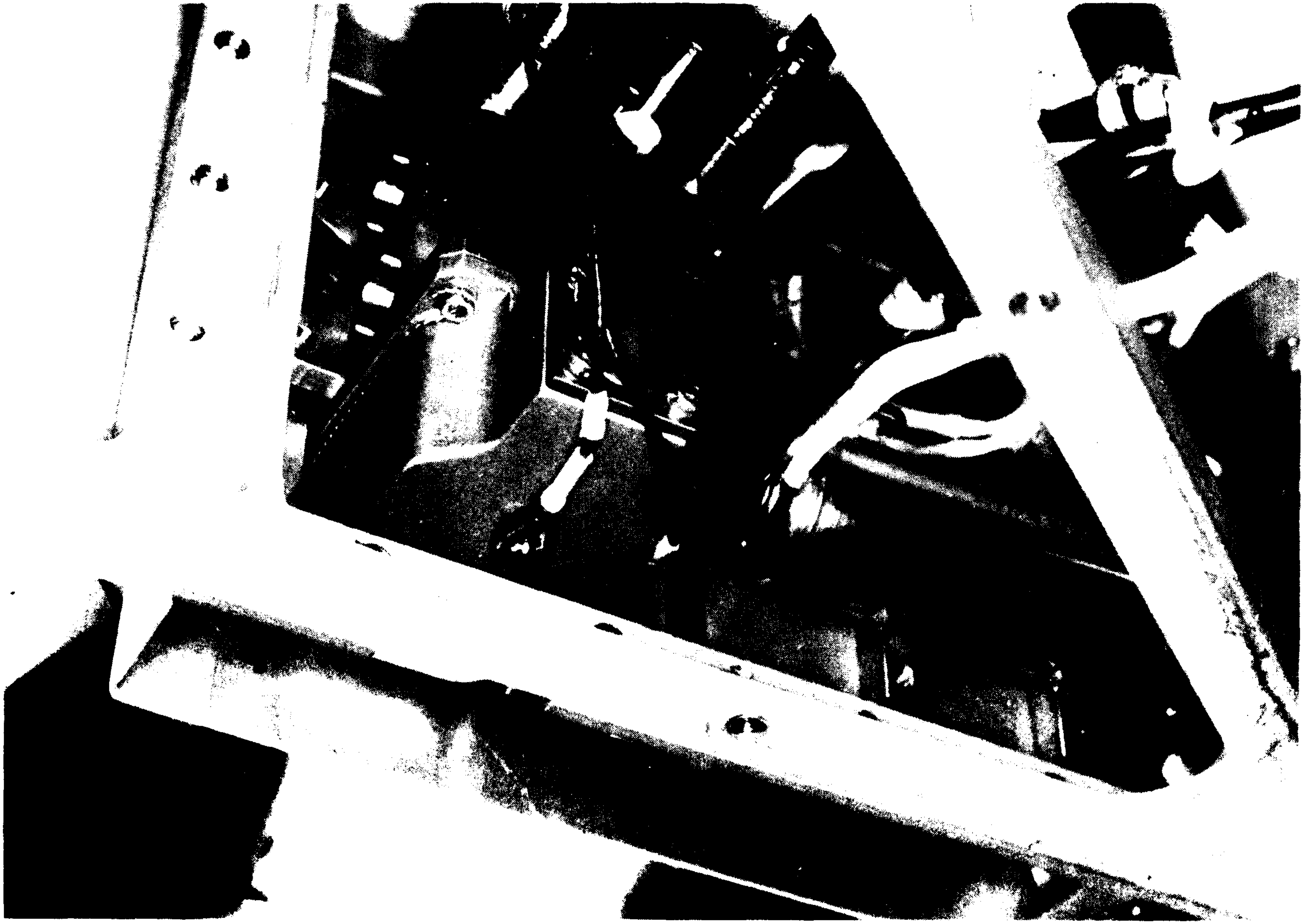


Figure 3.4-7. Accelerometers Mounted on Thruster Valve (C0291 1407)

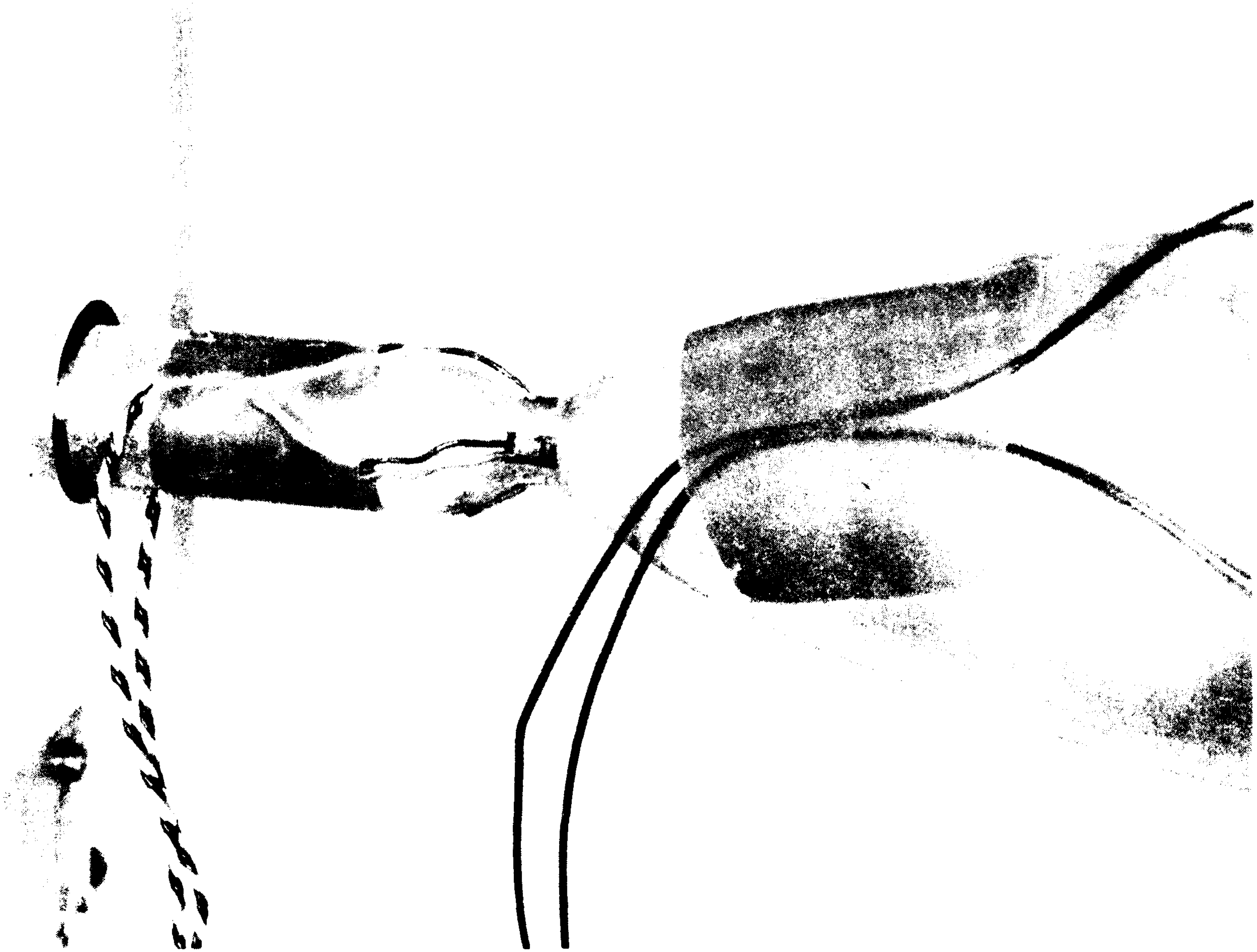


Figure 3.4-8. Strain Gages on Ir-Re Chamber Throat

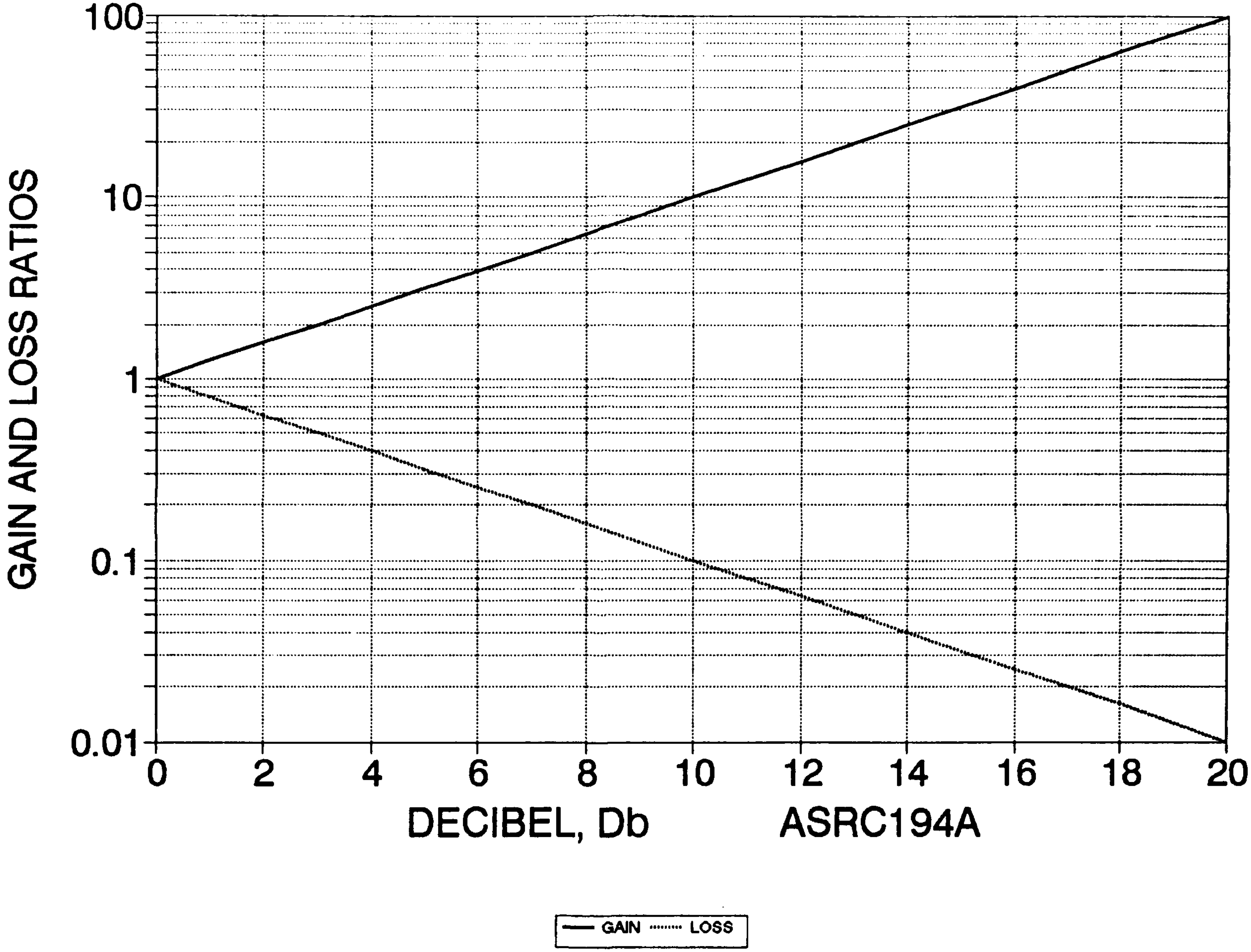


Figure 3.4.9. Power Ratio Gain and Loss vs db

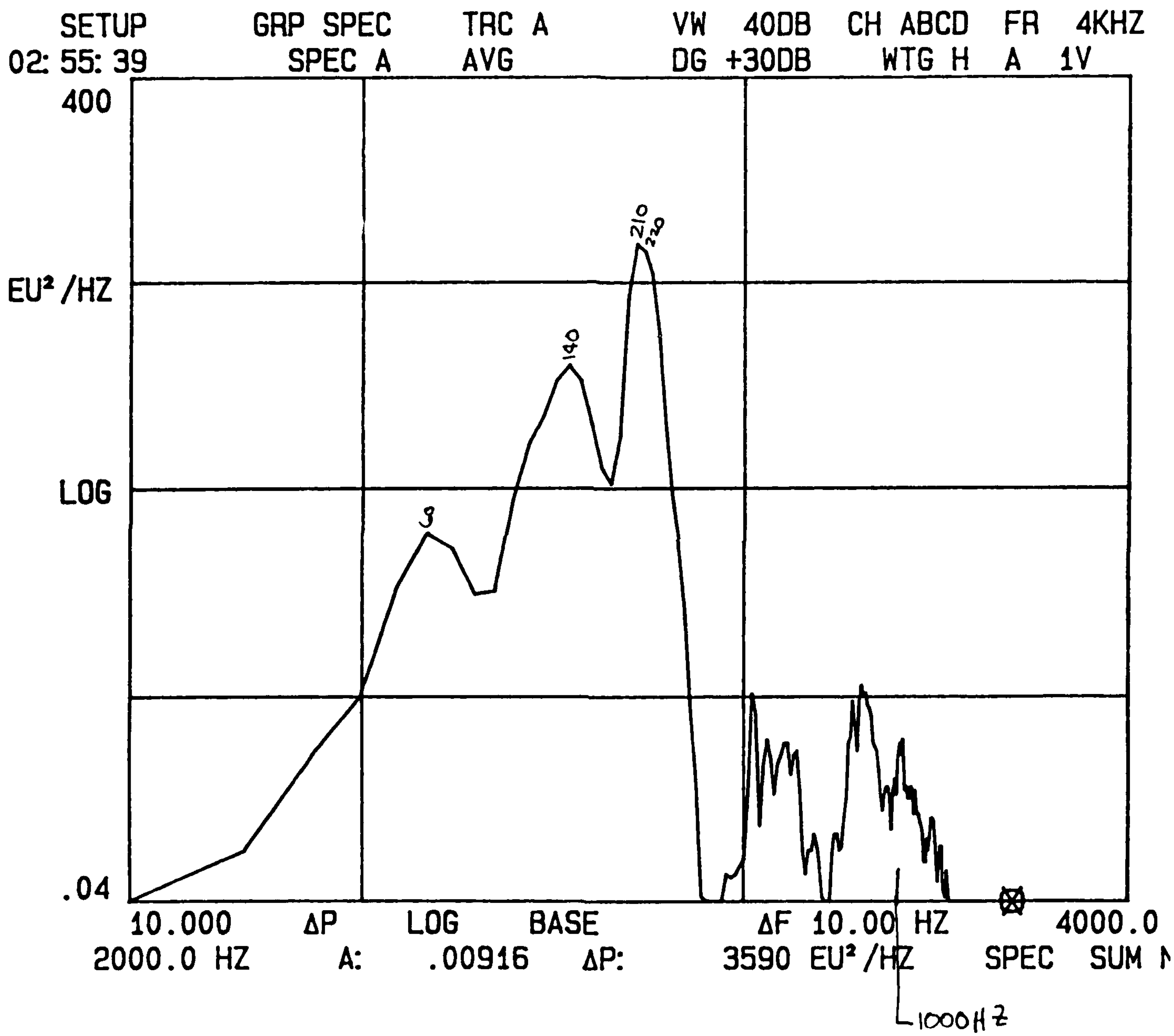


Figure 3.4-10. Advanced 14 lb X-Axis SG 1 (Micro Strain)

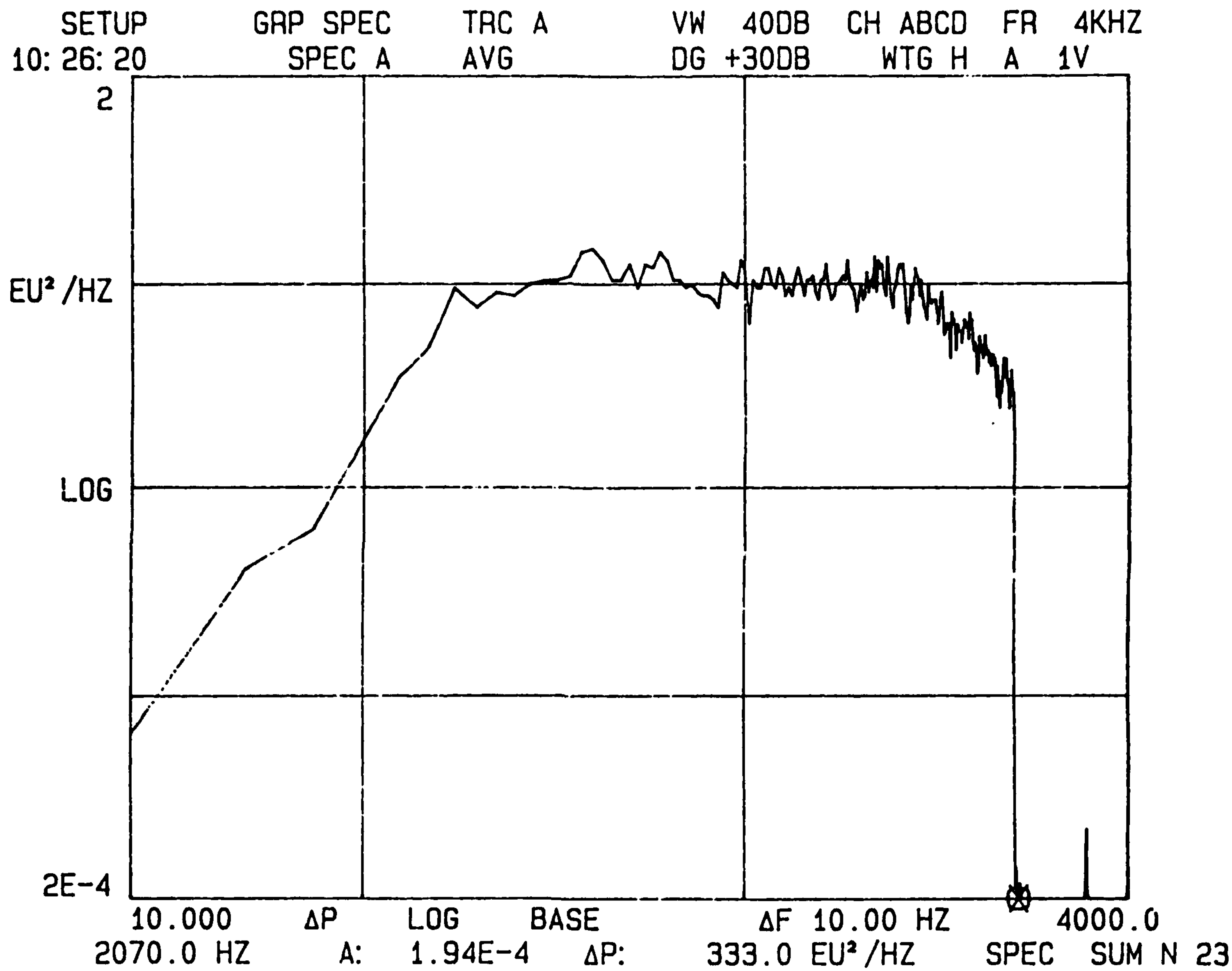


Figure 3.4-11. Advanced 14 lb X-Axis Acceleration - Control

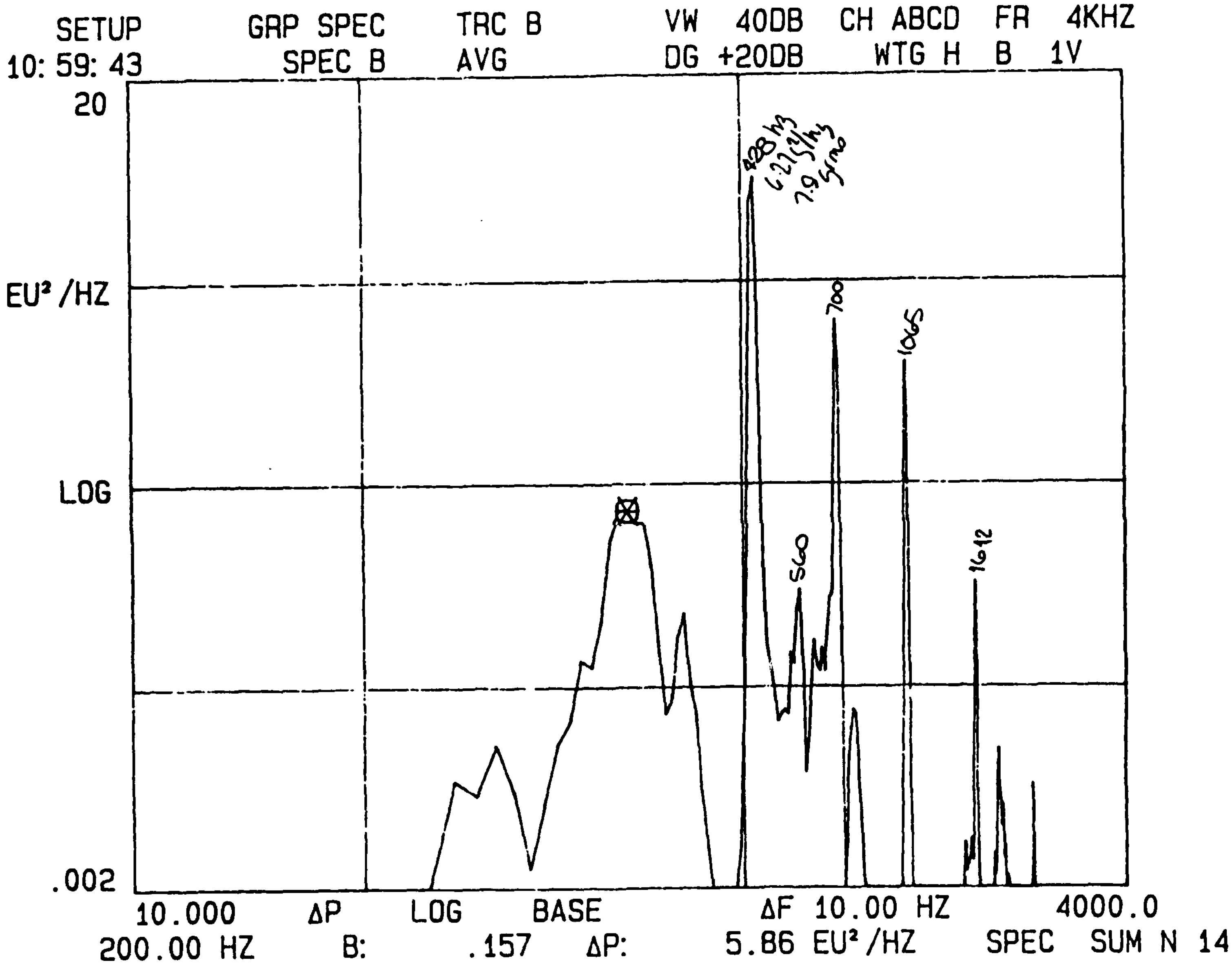


Figure 3.4-12. Advanced 14 lb X-Axis Acceleration - Nozzle Y

4.0 CONCLUSIONS AND RECOMMENDATIONS

The Ir-Re chamber technology has been demonstrated to be an advanced performance solution to high performance radiation cooled chambers in the 15 lbf class relative to conventional silicide-coated Cb chambers. This technology has been demonstrated to provide a 7% increase in Is over conventional thrusters with no other change in the engine system. It may be possible to obtain somewhat higher performance for an engine using an injector specifically designed for this application.

Because of the relatively limited test duration accumulated to date, little direct data exist for engine life or pulse testing at the 14 lbf level. However, the Ir-Re technology has demonstrated long life at 5 lbf (>14 hr) and 100 lbf (>5 hr).

Uncertainties in material properties produced dynamic analyses which predicted failure in vibration acceptance tests. However, the engine not only passed acceptance test vibration levels but has been shown to have positive margin for the qualification level.

The thermal design of the engine has been shown to be satisfactory during steady state firing. Front end temperatures are at design levels and provide ample margin for injector, valve and spacecraft. Chamber temperatures are ca. 500°F below the demonstrated long life limit of 4000°F.

The following activities should be pursued to further demonstrate this technology

- The second set of 14 lbf Ir-Re hardware should be assembled and subjected to hot fire and vibration tests. This will provide added confidence in the design approach.
- The engine should be tested for long duration (>100 sec) to provide unqualified demonstration of steady state thermal management.
- The engine should be subjected to extensive pulse tests over the full range of duty cycle to assure that no possibility of thermal pump up exists.
- The engine should be tested for thermal characteristics with a heat shield in place.
- The operation of this class of engine, with appropriate modifications, or other propellants such as O_2/MMH and O_2/H_2 should be explored.

APPENDIX A

14-lb Rhenium Nozzle Vibration Analyses

ENCORP
AEROJET
TechSystems

INTERNAL MEMO 2019/9990

TO:	M. L. Gage	17 April 1990 AJF:gg:9981:4394
FROM:	A. J. Farahyar	
SUBJECT:	14-lb Rhenium Nozzle Vibration Analyses	
COPIES TO:	L. Schoenman, S. D. Rosenberg, J.W. Salmon, 9981 File	
ENCLOSURE:	(1) 14-lb Rhenium Nozzle Vibration Analyses	

Linear analyses of the 14-lb nozzle with different throat thicknesses and lengths, and neck with and without struts, suggest that it will yield at the throat or neck if it is subjected to the vibration of the shuttle launch dispenser. These analyses assumed that the nozzle would be held cantilevered from the injector end. Using the shuttle launch dispenser environment as input to the nozzle and the fixed boundary condition probably will lead to a conservative result because it fails to account for the load transmissibility of the structure between the shuttle launch dispenser and the nozzle.

To assess the potential of the failure after the yielding, one of the following approaches is recommended:

(1) Dynamic plasticity should be performed based on the appropriate material properties for cyclic plasticity to obtain the strain state in the plastic zone. Then appropriate material properties are required to assess the stability of the above plastic zone based on strength and fatigue criteria. Also the fracture potential of the bi-material interface between the rhenium and platinum should be estimated using computational fracture mechanics. In the analysis approach, the fracture energy release rate in these regions of stress and strain singularity is calculated, then compared to the critical energy release rate. The comparison will provide the corresponding factor of safety.

(2) Random vibration testing of the nozzle should be performed after hot fire testing with appropriate fixture design which represents the appropriate mass and stiffness of the structure between the shuttle launch dispenser and the nozzle.

The enclosed report presents the analysis details and results.

A. J. Farahyar
System Design Analysis
Engineering Analysis Department

APPROVED BY:

W. E. Langhi, Manager
System Design Analysis
Engineering Analysis Department

ENCLOSURE (1)
10 April 1990

14-LB RHENIUM NOZZLE VIBRATION ANALYSIS

PREPARED BY:

A. J. Farahyar
System Design Analysis
Engineering Analysis Department

APPROVED BY:

W. E. Langhi, Manager
System Design Analysis
Engineering Analysis Department

REVIEWED BY:

D. H. Merchant
System Design Analysis
Engineering Analysis Department

INTRODUCTION

The 14-pound nozzle is subjected to two different vibration environments : 1) When the engine is being transported to outer space, and 2) When the engine is firing. Since the former environment is usually much more severe than latter, this analysis only considers the first case. The purpose of this analysis is to assess the structural integrity of the nozzle under launch dispenser random vibration environment and modify the design to reduce the stresses in the critical regions and thus ensure the survival of the nozzle.

PROCEDURE

The ANSYS finite element model of the nozzle was made using axisymmetric solid elements with antisymmetric harmonic loads. Figure 1 shows the finite element model of nozzle. To obtain the stress gradient around the throat , finer grids are used in this region. The struts were modeled using two-dimensional beam elements with an equivalent axisymmetric area for antisymmetric loading. So the total area of the struts is divided by π rather than by 2π to obtain stiffness per radian as discussed in Appendix A.

The nozzle is made of rhenium using the following room temperature material properties:

Modulus of elasticity	65,000,000 psi
Density	1.966e-3 lb-s^2/in^4
Poisson's ratio	0.26
Yield strength	55,000 psi

The neck is made of platinum using the following room temperature material properties:

Modulus of elasticity	21,000,000 psi
Density	2.006e-3 lb-s^2/in^4
Poisson's ratio	0.39
Yield strength	15,000 psi

All nodes with translation degrees-of-freedom are chosen as master-degrees- of-freedom to obtain accurate lateral bending modes. Modal analysis was performed using the Householder procedure, and modes with significant modal coefficients greater than 0.001 were expanded. The results of the modal analysis were reviewed to understand the nature and spread of modes over frequency and to help design modification if required. The first bending mode has a frequency of about 300 Hz to 420 Hz depending on the throat length and thickness, and a neck with and without struts. The second bending mode is above 1500 Hz. The modes above the first bending mode do not contribute to the dynamic response since the environment is specified only up to 1500 Hz. The accuracy of the modes depends on the finite element idealization based on the number of elements and element types and master-degrees-of-freedom that should be used to the represent the half-modal wave motion accurately. Since there is sufficient master-degrees-of-freedom and elements for the first bending mode, therefore there is sufficient modal accuracy and the model is adequate for response analysis.

Random vibration analysis was performed for lateral axis using modal analysis results. The random vibration spectrum is presented in figure 2. ANSYS modal analysis has a

shock spectrum option that was used to perform random vibration response analysis. This option was chosen since the random vibration response is dominated by the first bending mode. A viscous damping ratio of 3 percent was used. Structural damping is due to friction at the interface between elements of the structural system and internal friction within the material. The friction within the material is small in the elastic zone and is increasing with plasticity of materials due to higher energy dissipation. Since the actual damping could be from 1% to 5%, using 3% damping is reasonable.

Table 1 presents the stresses equivalent to Von Mises yield criterion at the throat and the neck sections. These stresses are calculated using 3σ level. Since the stress state exceeds yielding, the extreme value theory of probability is not used here due to limitation of this theory for the linear system. It should be mentioned that there are approximated perturbation methods applicable to non-linear random vibration system like statistical linearization technique. These methods are not used since it is beyond the scope of the budget allocation for this work.

Several modifications are considered here to reduce the stresses, which are:

(1) Increasing the throat length from 1.9 inch to 3.3 inch reduces the natural frequency and stiffness which results in stress reduction.

(2) Using the struts in the neck section reduce the effective length. This would result in increasing the natural frequency and increase the stress in the throat section slightly, but reduces stresses in neck region due to increased area. Also, using struts increase the confinement that results in undesirable reduction of fracture material properties for the bi-material interface between the rhenium and platinum. This adverse effect can be investigated.

(3) Increasing the throat thickness from 0.028 inch to 0.040 results in stress reduction in the throat section.

CONCLUSION AND RECOMMENDATION

The analyses were performed using two-dimensional axisymmetric elements with antisymmetric harmonic loads. These elements provide accurate response calculations for bending modes, but are incapable of predicting responses for the bell modes. The more accurate modeling which would use shell elements was abandoned due to lack of resources. This would probably not introduce significant errors in maximum stress calculations in the neck and the throat regions due to the high frequency content of the bell modes.

These analyses assumed that the nozzle would be held cantilevered from the injector end. Using the shuttle launch dispenser environment as input to the nozzle and using fixed boundary condition probably will lead to a conservative result because it fails to account for the load transmissibility of the structure between the shuttle launch dispenser and the nozzle.

To assess the potential of the failure after the yielding, one of the following approaches is recommended:

(1) Dynamic plasticity analysis should be performed based on the appropriate material properties for cyclic plasticity to obtain the strain state in the plastic zone. Then appropriate material properties are required to assess the stability of the above plastic zone based on strength and fatigue criteria. Also the fracture potential of the bi-material interface between the rhenium and platinum should be estimated using computational fracture mechanics. In the analysis approach, the fracture energy release rate in these regions of stress and strain singularity is calculated, then compared to the critical energy release rate. The comparison will provide the corresponding factor of safety.

(2) Random vibration testing of the nozzle should be performed after hot fire testing with appropriate fixture design which represents the appropriate mass and stiffness of the structure between the shuttle launch dispenser and the nozzle.

TABLE 1

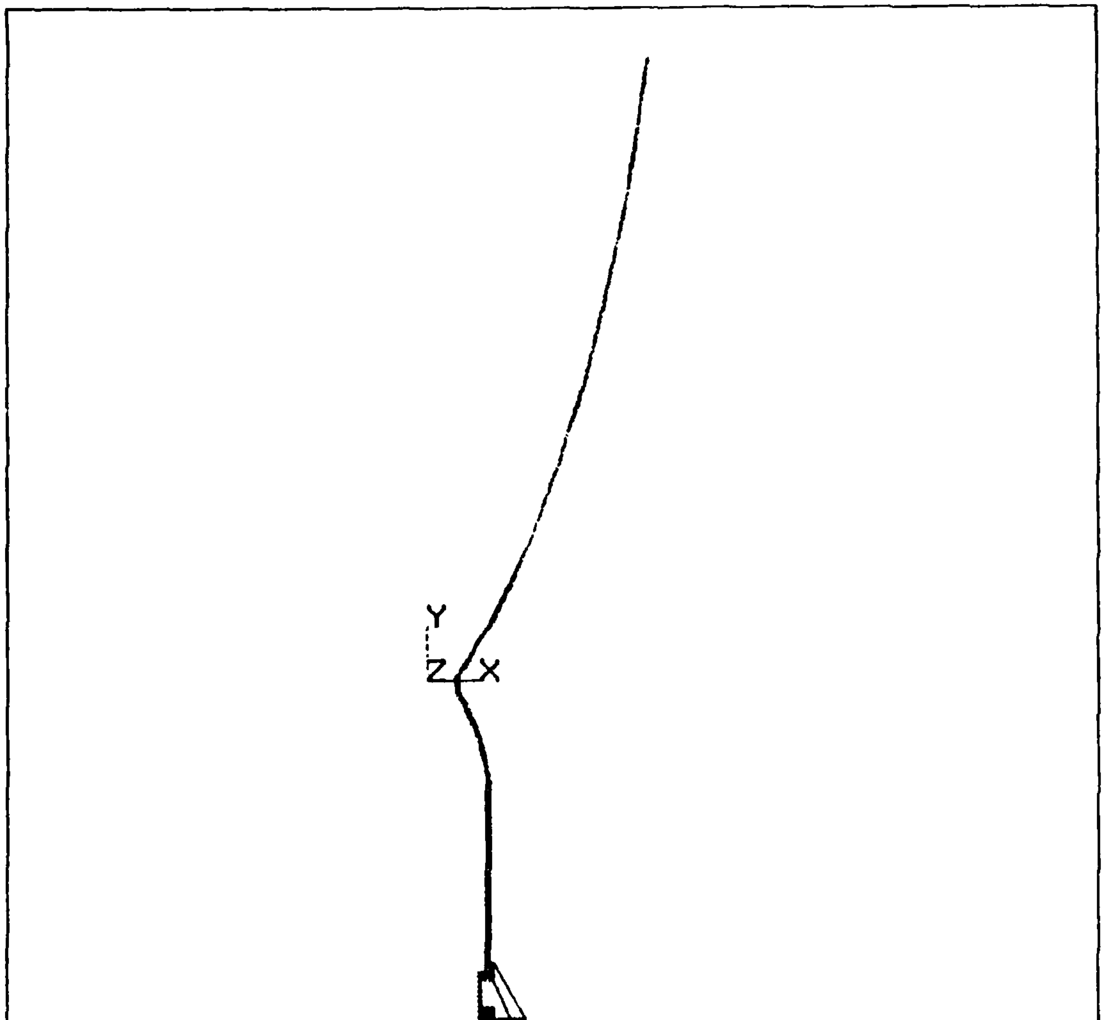
INDUCED STRESSES EQUIVALENT TO VON MISES YIELD CRITERION FOR 14-LB NOZZLE

Description	Maximum Stresses Eqivalent to Von Mises Yield Criterion at Throat Section (ksi)	Maximum Stresses Equivalent to Von Mises Yield Criterion at Front End (ksi)
1.9 inch throat length with struts and 0.028 inch throat thickness	76.8 (55.0)*	8.4 (30.0)**
1.9 inch throat length without struts and 0.028 inch throat thickness	72.9 (55.0)	24.6 (30.0)
3.3 inch throat length with struts and 0.028 inch throat thickness	74.4 (55.0)	16.5 (30.0)
3.3 inch throat length with struts and 0.04 inch throat thickness	66.0 (55.0)	16.0 (30.0)

The number in parenthesis is corresponding to yield strength.

*CVD Rhenium
**Pt-10 Rh

Maximum stresses shown in the table are 3-sigma values.



1 FIGURE 1 14-LB NOZZLE

ANSYS 4.3
APR 12 1990
15:01:01
PREP7 ELEMENTS
TDIS EC

ZV=1
DIST=3.44
XF=.783
YF=.845

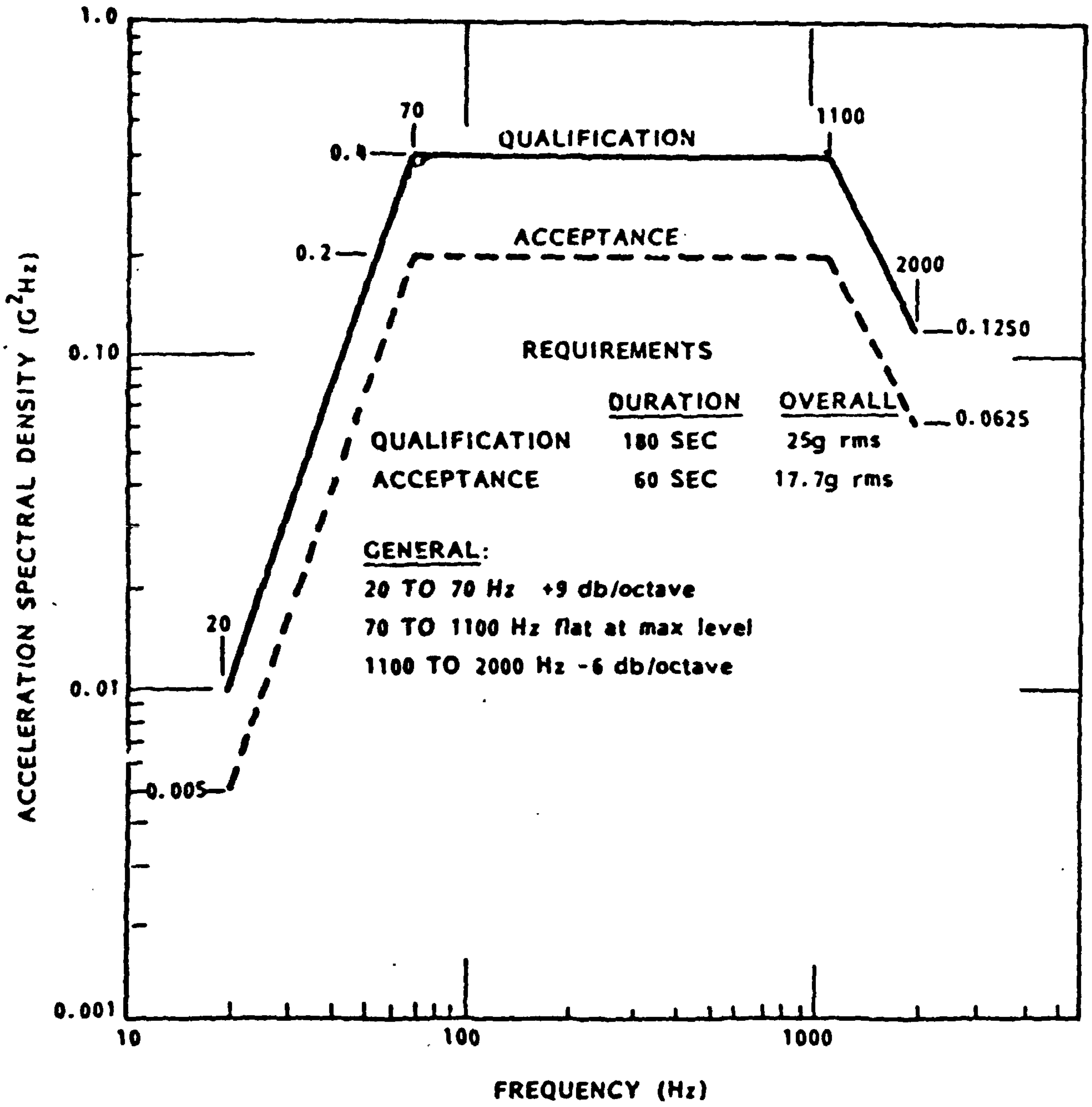


Figure 2. Random Vibration

Shuttle Launch Dispenser

wang-413

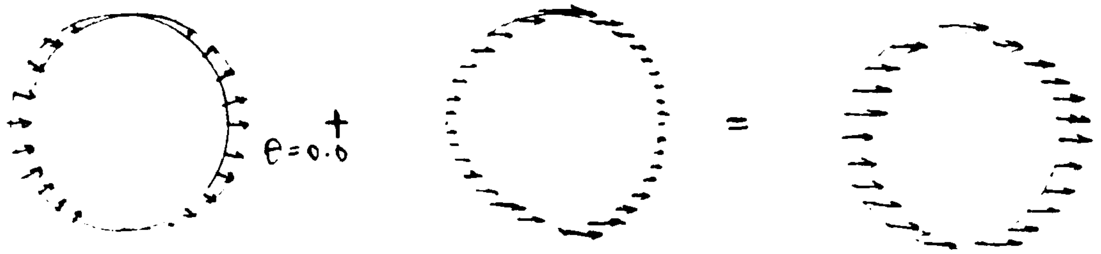
APPENDIX A

NONAXISYMMETRIC LOADS

The load applied to geometrically axisymmetric structures will not necessarily be distributed in an axisymmetric form. In dealing with base acceleration, the inertia forces arising from acceleration will comprise non-axisymmetric loading on cylindrical structures like the nozzle. In cases where the distributed load varies only with circumferential coordinate (θ) and can be represented by a number of terms of a series expansion:

$$T = \text{traction force} = \sum T_m \cos m\theta + \sum T_m \sin m\theta$$

where each term of each series is called a harmonic. In order to impose lateral acceleration on a cylindrical structure, the traction force, T, can be broken down into its radial and circumferential direction, as shown in the following figures:



$T_1 = T_r \cos\theta$ $\qquad$ $T_2 = T_\theta \sin\theta$ $\qquad$ UNIFORM ACCELERATION

$$\text{TOTAL FORCE} = \int_0^{2\pi} \frac{T_r \cos\theta}{R}(\cos\theta)(R\,\partial\theta) + \int_0^{2\pi} \frac{T_\theta \sin\theta}{R}(\sin\theta)(R\,\partial\theta)$$

$$= \pi T_r + \pi T_\theta$$

T_r and T_θ are the maximum accumulation per radian at zero and 90 degrees, respectively. For modal spectrum analysis, the R and θ direction should be analyzed for two separate runs. The results of each run should be combined using Post 27 in ANSYS.

APPENDIX B

Thermal Analysis of the 14 lbf Ir-Re Chamber

March 5, 1990

TO : Mark L. Gage

FROM : Felix. F. Chen

SUBJECT: Thermal Analysis Results of 14 lbF Rhenium Chamber

COPIES TO: S. D. Rosenberg (W/O Enclosure), L. Schoenman

ENCLOSURE:
(1) Computer output of 0.5 in. BLT, Steady State
(2) Computer output of 0.75 in. BLT, Steady State (with 760 R boundary condition)
(3) Computer output of 0.75 in BLT, Steady State (with 960 R boundary condition)
(4) Computer output of 0.75 in BLT, Transient Up to 30 Sec (with 760 R boundary condition)

SUMMARY

This report summarizes the thermal analysis results of the 14 lbF rhenium chamber design. Two different boundary layer trip (BLT) rings (one is 0.5in long and the other is 0.75in long) are used in the analysis. The predicted maximum wall temperature of the rhenium chamber is 3977 R (3517 F) at approximately 0.15 in. upstream of the throat. At the bond joint between the rhenium chamber and the platinum BLT, the maximum interface temperature with a 0.5in long BLT is 1482 R when a 760 R (300 F) constant temperature condition is applied to the surface of the BLT. The maximum interface temperature decreases to 1084 R when the length of BLT increases to 0.75 in with the same boundary conditions. During the shutdown transient heat soak back, the maximum interface temperature with a 0.75 in. BLT increases from 1084 R to 1170 R which is still well below the design temperature limit of 1460 R. At the end of 30 sec shut down transient, the average temperature increases for the platinum BLT and stainless steel flange are 270 R and 200 R, respectively.

If the platinum BLT surface temperature due to the effect of fuel film cooling increases from 300 F to 500 F, the maximum temperature at the rhenium/platinum interface temperature with a 0.75 in long BLT will be only 1256 R for steady state hot fire condition. Therefore, the 0.75 in BLT is recommended for the 14 lbF rhenium chamber testing.

BOUNDARY CONDITIONS

The results of fuel film cooling analysis for the existing 14 lbF columbium chamber design were used to calculate the gas-side boundary conditions. Since both the thrust (14 lbF) and chamber pressure (100 psia) are low, the reverse transition from turbulent flow to laminar flow in

throat region is anticipated. Table 1 lists the gas-side convective heat transfer coefficients and the flow relaminarization factor at six different axial locations. The predicted maximum heat flux location is approximately 0.15 in. upstream of the throat.

The results of fuel film cooling analysis indicate that the fuel will remain in liquid film (approximately 295 F or less) from the injection point to an axial distance of approximately 0.82 in. from the injector. Since the length of BLT in this analysis is less than 0.82 in., a 300 F constant temperature boundary condition has been applied to the surface of both BLTs (0.5 and 0.75 in. long). If the length of BLT exceeds 0.82 in., the adiabatic wall temperature increases significantly. The 300 F surface temperature boundary condition cannot be applied any more.

Beyond the tip of BLT, the flow is assumed to be fully mixed, i.e. the fuel film cooling effectiveness is assumed to be very small. The fully combusted gas temperature of 5461 R is used as the hot gas temperature for the barrel section.

Since radiation is the only cooling mechanism of the present 14 lbF rhenium chamber design, radiation loss from the outer surface to space (0 R) is incorporated in the analysis. Because the radiative power is proportionally to the fourth power of the temperature, the difference between the radiation loss from rhenium chamber wall to space with 0 R and to ambient with 530 R is negligible. This analysis results can be applied to the sea level test too. The emissivity of the rhenium surface is assumed to be 0.95, whereas the emissivity of both platinum and stainless steel is assumed to be 0.5. The surface between the steel flange and the injector body is assumed to be adiabatic which is conservative for the heat soak back evaluation of the steel flange.

A plot showing the geometry used in the analysis as well as different material regions of the model is shown in Fig. 1. In this figure, material 1 is rhenium, 2 is platinum, and 3 is stainless steel. The total chamber length (L') is 2.12 in. The operating conditions and geometric variables used in this analysis are listed in Table 2.

DISCUSSIONS OF RESULTS

The steady state temperature distributions for the 0.5 in. BLT and 0.75 in. BLT are shown in Figs. 2 and 3, respectively. The length of BLT does not have any impact on the throat temperature since the combusted gas is assumed to be fully mixed beyond the tip of BLT. The predicted maximum wall temperature is 3977 R which is very close to the desired operating temperature of 3960 R. The maximum

temperature in the barrel section of the rhenium chamber design is 3650 R for both cases.

A major benefit of using the longer BLT is the large temperature reduction at the interface of rhenium chamber and platinum BLT. The temperature at this interface is considered critical for the rhenium chamber design. The maximum interface temperature with the 0.5 in. BLT is 1482 R which is slightly higher than the design temperature limit of 1460 R. When the length of BLT increases to 0.75 in., the maximum interface temperature decreases to 1084 R which gives a significant temperature margin at the bond joint. The other benefit of using the longer BLT is the lower rhenium wall temperature at locations near the bond joint. A lower wall temperature gives a lower heat flow rate during the shut down heat soak transient and a lower temperature for both platinum BLT and stainless steel flange.

In order to investigate the effects of different platinum BLT surface temperature on the temperature distribution of the rhenium chamber design especially at the bond joint between the rhenium chamber and the platinum BLT, the 0.75 in. BLT case was re-ran with a 500 F instead of a 300 F constant temperature condition at the surface of platinum BLT. The result of steady state temperature distribution is shown in Fig. 4. The maximum interface temperature at the rhenium chamber and the platinum BLT increases from 1084 R to 1256 R which is still well below the design temperature limit of 1460 R. The average temperature increase for the barrel section of the rhenium chamber ranges from 10 R to 50 R due to the high conduction resistance associated with the thin wall of the rhenium chamber. Table 3 summarizes the results of steady state temperature at various critical locations for all three cases.

It should be noted that the effect of flow re-attachment at the rhenium chamber wall temperature due to the platinum trip ring is not included in this analysis. The gas-side convective heat transfer coefficient may increase up to 35% with the flow re-attachment. The impact on the wall temperature increase is approximately 200 R. However, as indicated earlier, an assumption of fully mixed combustion gas is used in this analysis, in reality, hot gas may not be fully mixed especially in the barrel section. Therefore, the net effect on the wall temperature increase should be small.

Since the result with a 0.75 in long BLT and a 300 F constant BLT surface temperature is the most realistic and the best representative case, the shut down transient heat soak back is performed for this case. Once the engine starts to shut down, there is no more heat addition from the hot-gas to the chamber. Therefore, the rhenium wall temperature should decrease monotonically due to the radiation loss. However, the temperature of both platinum BLT and steel

flange will increase significantly since the 300 F heat sink effect due to the fuel film cooling is gone. The heat soak back from the high temperature rhenium chamber to both platinum BLT and steel flange will be significant.

Heat soak back during the shut down transient is critical for the rhenium chamber design since the rhenium wall temperature is well above 3500 R at steady state firing. The major concerns are the bond line temperature between the rhenium chamber and the platinum BLT, the platinum BLT surface temperature, and the steel flange temperature. The bond line temperature should remain below the 1460 R design temperature limit to ensure a good bonding exists between the rhenium chamber and the platinum BLT. The platinum BLT surface temperature is critical for the engine restart. Generally, the platinum BLT surface temperature should be kept below 910 R (450 F) to prevent the auto-decomposition of MMH fuel.

Figure 5 shows the transient temperature variations of three critical locations: rhenium/platinum interface, platinum surface, and steel flange. At the rhenium/platinum interface, the temperature reaches a peak value of 1170 R at approximately 2.0 sec into the shut down transient. Then, the interface temperature starts to decrease monotonically. At the platinum BLT surface, the peak temperature will be reached approximately 4-5 sec into the shut down transient. The maximum temperature of the platinum BLT surface is 1030 R which is approximately 120 R higher than the auto-decomposition temperature of the MMH fuel. At the end of 30 sec shut down transient, the temperature of platinum BLT surface is 983 R which is still higher than 910 R. Therefore, the engine must wait at least 30 to 60 sec before it can be re-started to avoid the auto-decompostion of the MMH fuel.

The steel flange temperature increases monotonically during the 30 sec shut down transient. At the end of 30 sec, the flange temperature is 956 R which is a 200 R increase over the 30 sec shut down transient. Since the flange wall is assumed to adiabatic, the actual flange temperature should be lower due to the conduction to the injector body.

The transient temperature variations at three different locations of the rhenium chamber (maximum temperature location, mid-point of the barrel, and forward end of the barrel without the cover of platinum BLT) are shown in Fig. 6. The temperature variation at the rhenium/platinum interface is also shown in this figure for comparison. The rhenium wall temperature drops significantly during the initial 10 sec of the shut down transient. After 10 sec into the shut down transient, the maximum rhenium wall temperature decreases from 3977 R to 1800 R. A temperature reduction of 2200 R in 10 sec!

Figure 7 illustrates the transient temperature variations at different locations of the rhenium/platinum interface, the maximum temperature variation of the platinum surface, and the steel flange temperature. At the end of 30 sec shut down transient, the maximum temperature difference is 250 R.

A snap shot of temperature distribution in color at five different time intervals during the shut down transient is not included in this memo. Those figures are available for viewing or reproduction.

CONCLUSIONS AND RECOMMENDATIONS

Thermal analysis results of the 14 lbF rhenium chamber indicate that the predicted maximum rhenium wall temperature is 3977 R and the average barrel temperature is 3650 R. The predicted maximum interface temperature of the rhenium chamber and the platinum BLT is only 1084 R with a 0.75 in. long BLT and a 300 F constant BLT surface temperature condition. If the length of BLT decrease, the interface temperature increases, the operational margin for the bond joint becomes smaller. However, if the length of BLT exceeds 0.82 in., the effectiveness of fuel film cooling at the end of BLT is small, the tip of BLT has a high possibility of melting. Therefore the 0.75 in. long BLT is recommended for the future tests.

The results of a 30 sec shut down transient indicate that the rhenium/platinum interface has plenty of temperature margin with the 0.75 in. long BLT. However, the platinum BLT surface temperature will exceed the auto-decomposition temperature of MMH fuel. The BLT surface temperature and the steel flange temperature are recommended to closely monitored during the shut down transient.

Felix F. Chen
Research and Technology

TABLE 1

Gas-Side Heat Transfer Coefficients and Flow Relaminarization Factor at Different Axial Locations

	Barrel →			← Convergent Section →		Throat
Axial Distance from Injector (In.)	0.0	0.82	1.436	1.625	1.983	2.12
Convective Heat Transfer Coefficients (Btu/in²-s-°F)	0.000315	0.000315	0.000315	0.000368	0.000944	0.000612
Flow Relaminarization Factor	1.0	1.0	1.0	0.93	0.73	0.46

TABLE 2

Operating Conditions and Geometric Variables of 14 lbF Rhenium Chamber

Thrust (lbF)	14
Chamber Pressure (psia)	100
Mixture Ratio	1.65
Propellants	NTO/MMH
Chamber Diameter (IN.)	0.728
Throat Diameter (IN.)	0.326
Length of Chamber (L′)	2.12
Length of BLT	0.5 and 0.75
Wall Thickness (in.)	
Rhenium Chamber	0.028
Platinum BLT	0.032

TABLE 3

STEADY STATE TEMPERATURE AT VARIOUS CRITICAL LOCATIONS

Length of BLT (in.)	0.75	0.75	0.5
Pt. BLT Surface Temp (R)	960	760	760
Throat Wall Temp (R)	3944	3944	3944
Max Wall Temp (R)	3977	3977	3977
Max Barrel Temp (R)	3650	3650	3650
Mid-Point Barrel Temp (R)	3608	3560	3565
Max Temp at Re/Pt Interface (R)	1256	1084	1482
Forward End of Re/Pt Interface Temp (R)	1034	841	940
Mid-Point of Pt BLT (R)	970	771	785
Steel Flange Temp (R)	956	758	758

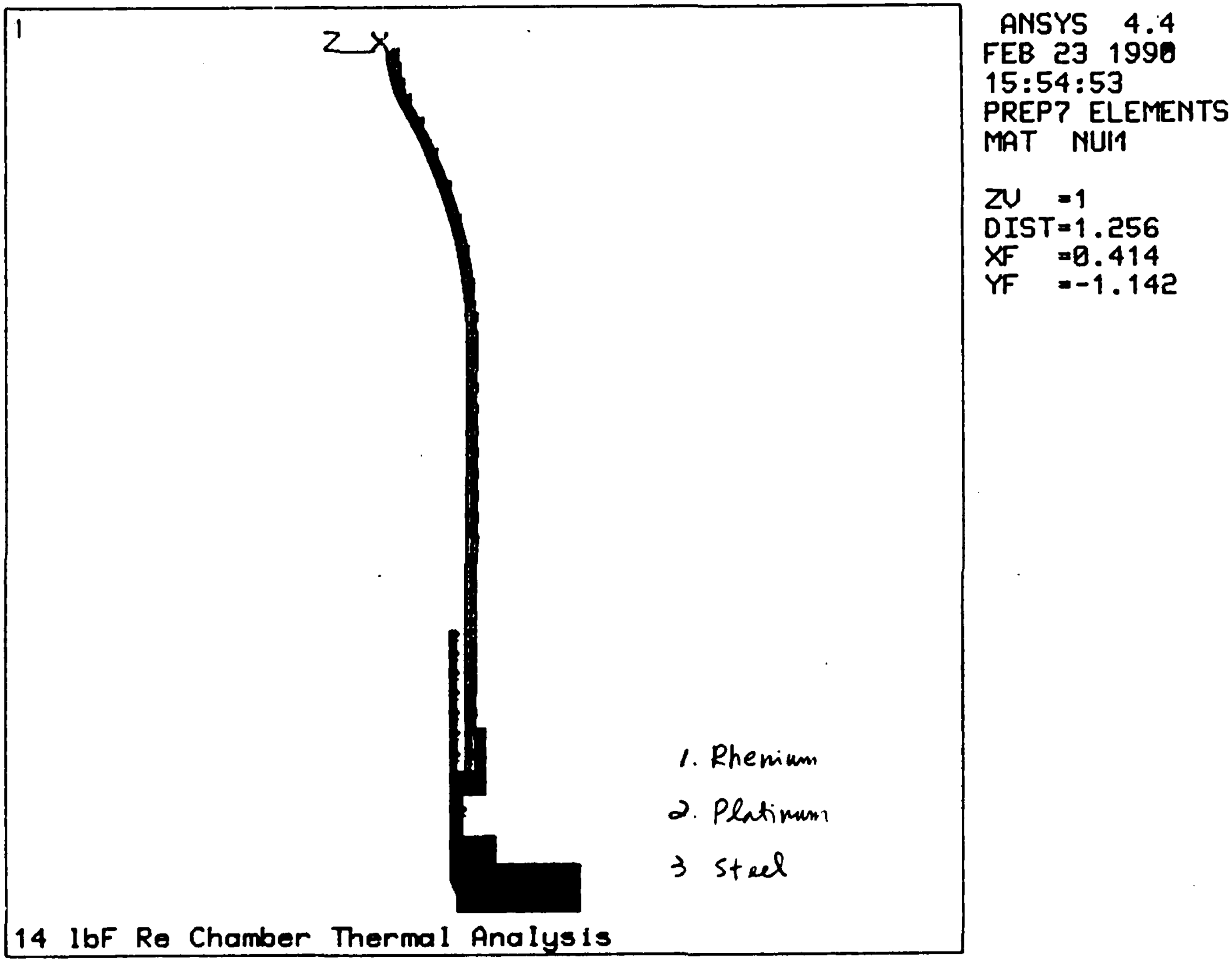


Figure 1 Model Geometry and Materials used in 14lbF Chamber

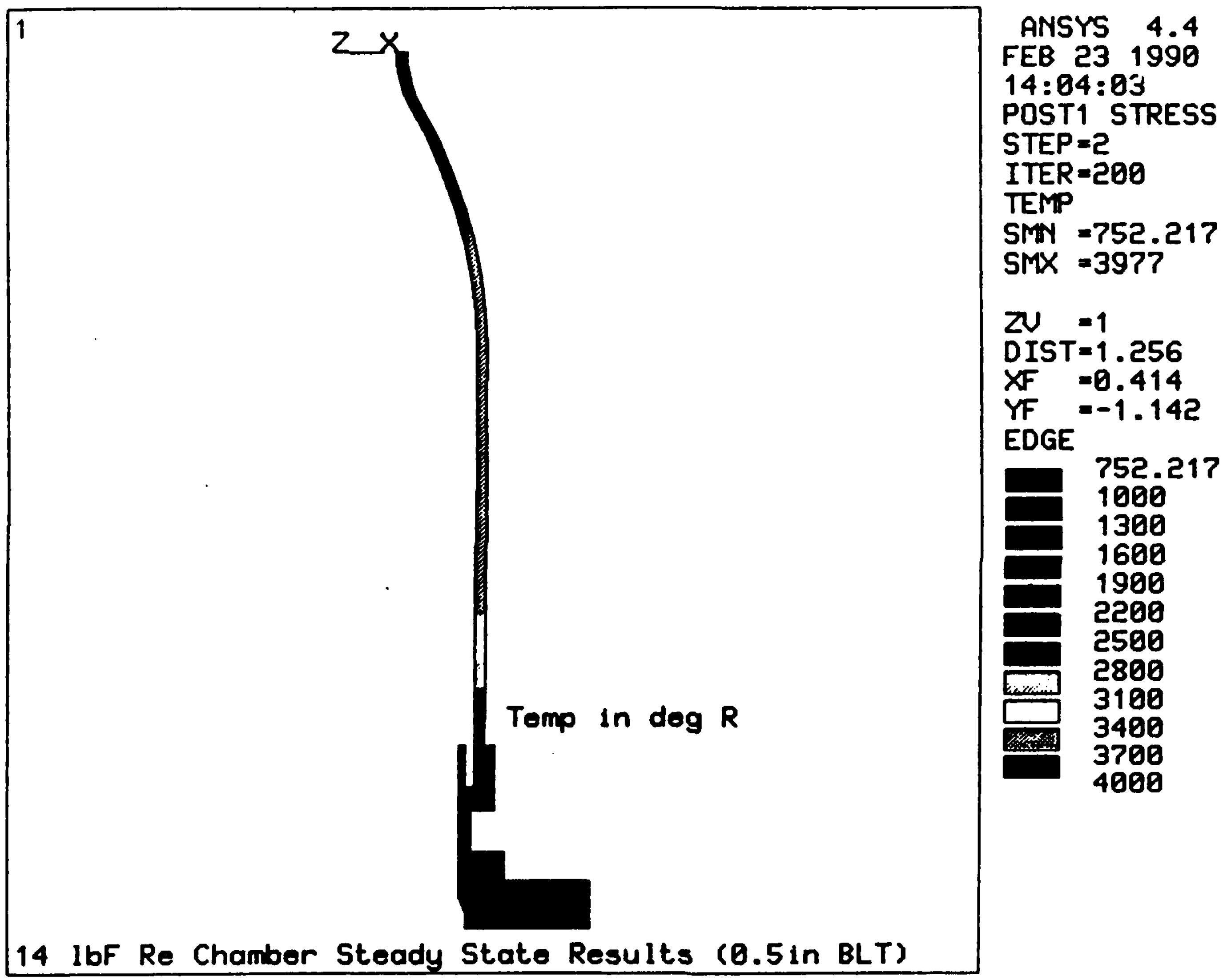


Figure 2 Steady state Temperature Distribution with a 0.5 in BLT

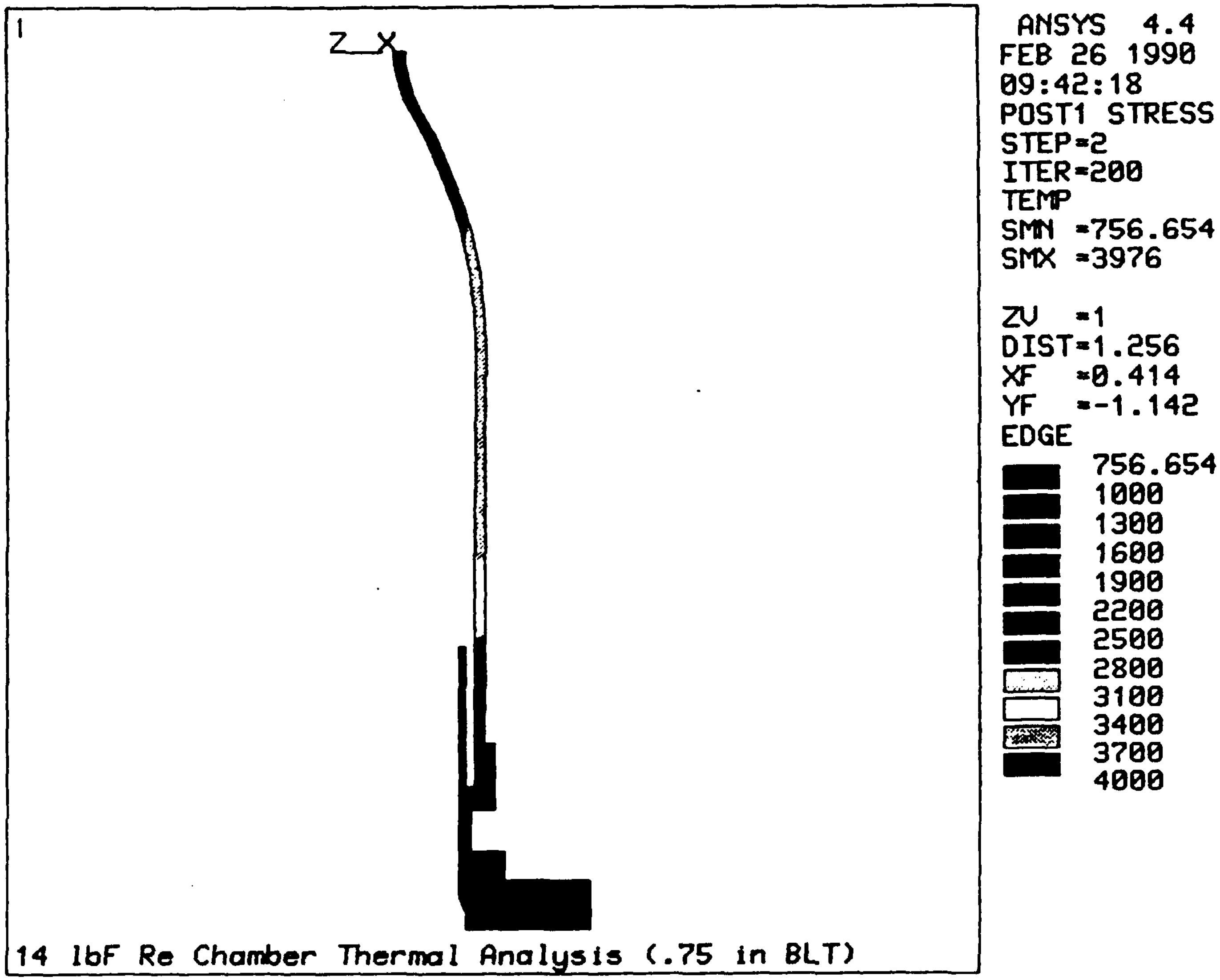


Figure 3 Steady state Temperature Distribution with a 0.75 in BLT and 760R Constant Temperature at Platinum BLT Surface

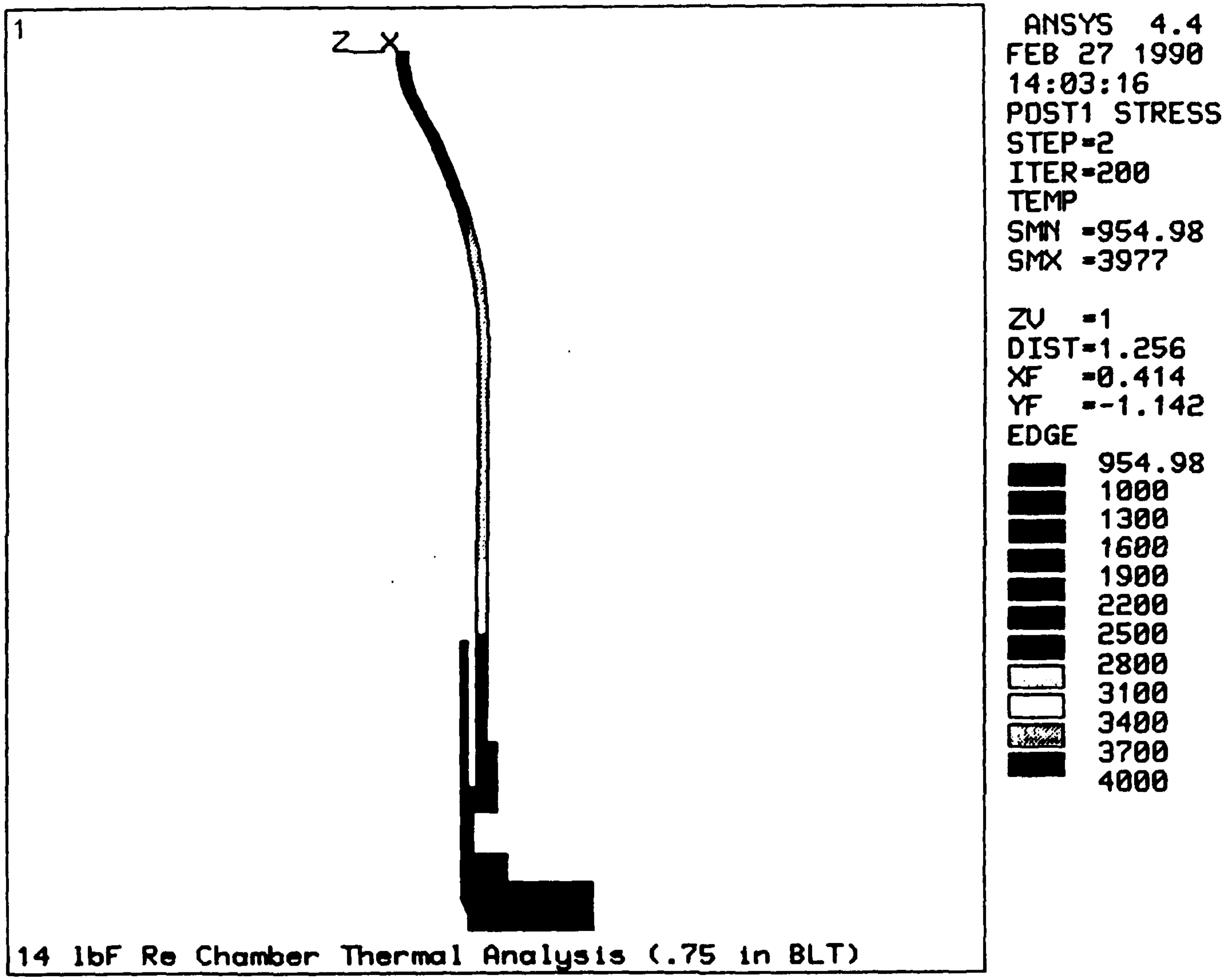
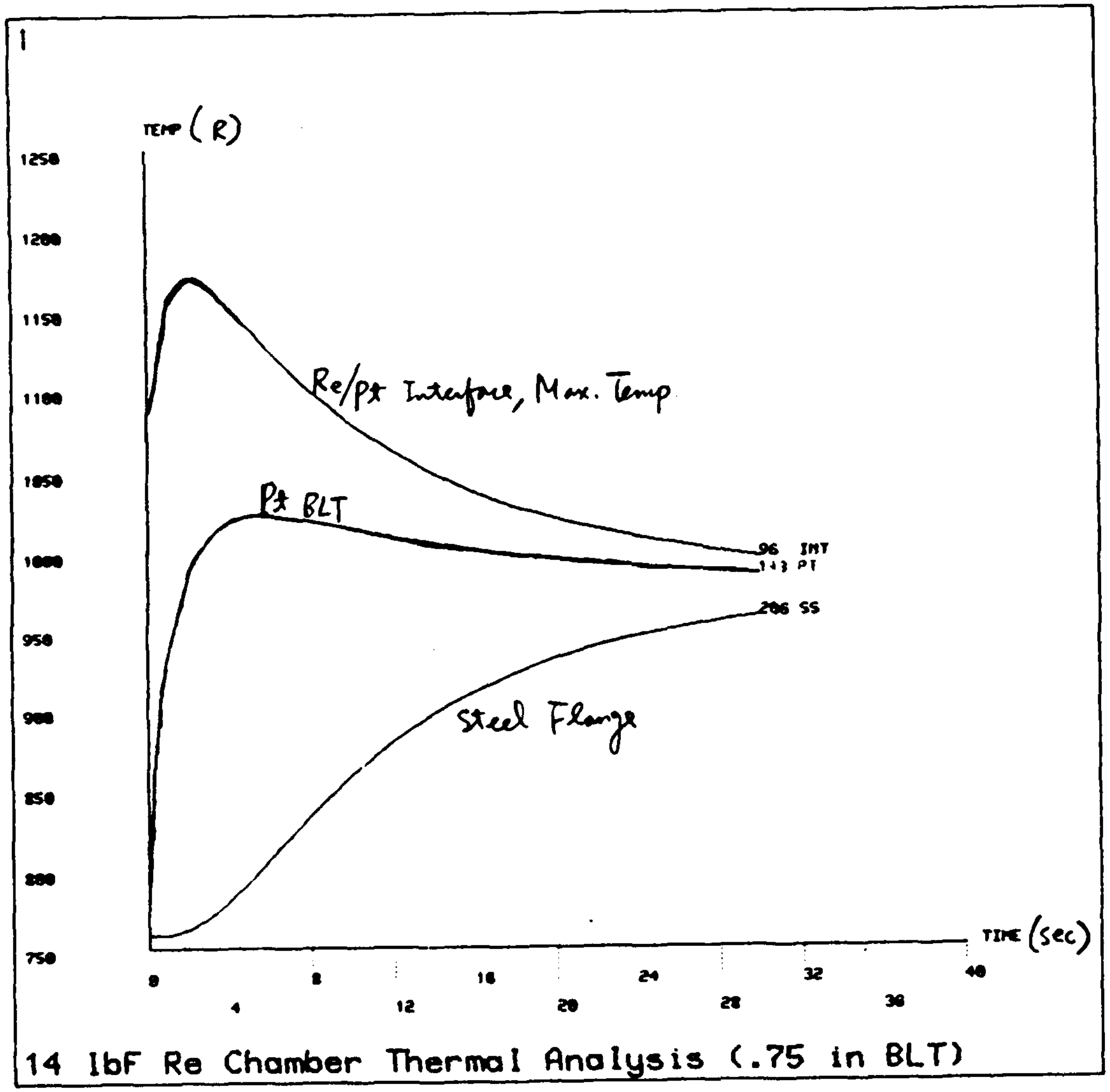


Figure 4 Steady state Temperature Distribution With a 0.75 in BLT and 960 R Constant Temperature at Platinum BLT Surface



ANSYS 4.4
FEB 28 1990
08:08:56
POST26

ZV =1
DIST=0.6666
XF =0.5
YF =0.5
ZF =0.5

Figure 5 Transient Temperature Variation for Rhenium/Platinum Interface, Platinum BLT, and Steel Flange

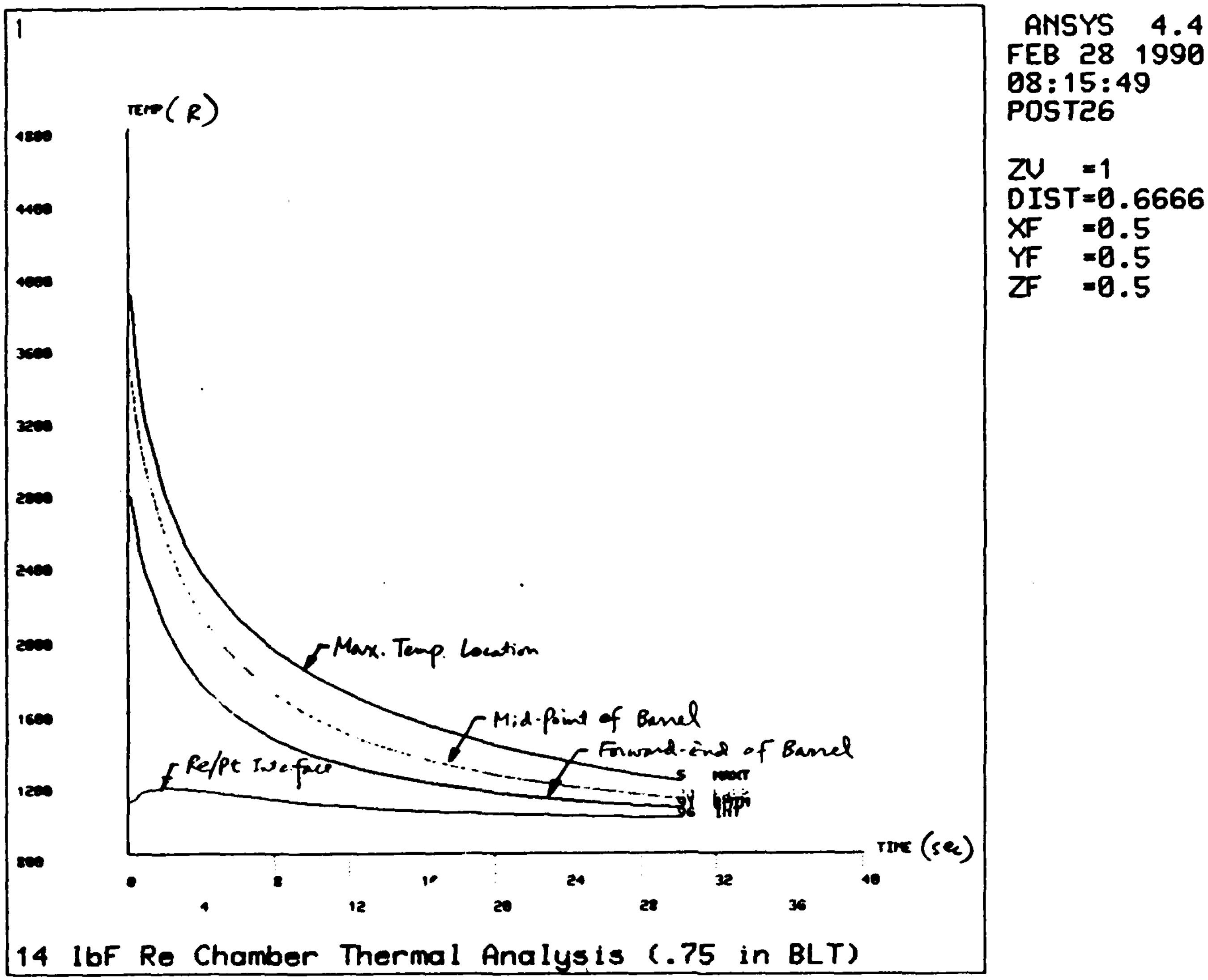


Figure 6 Transient Temperature Variation of Rhenium Chamber Wall

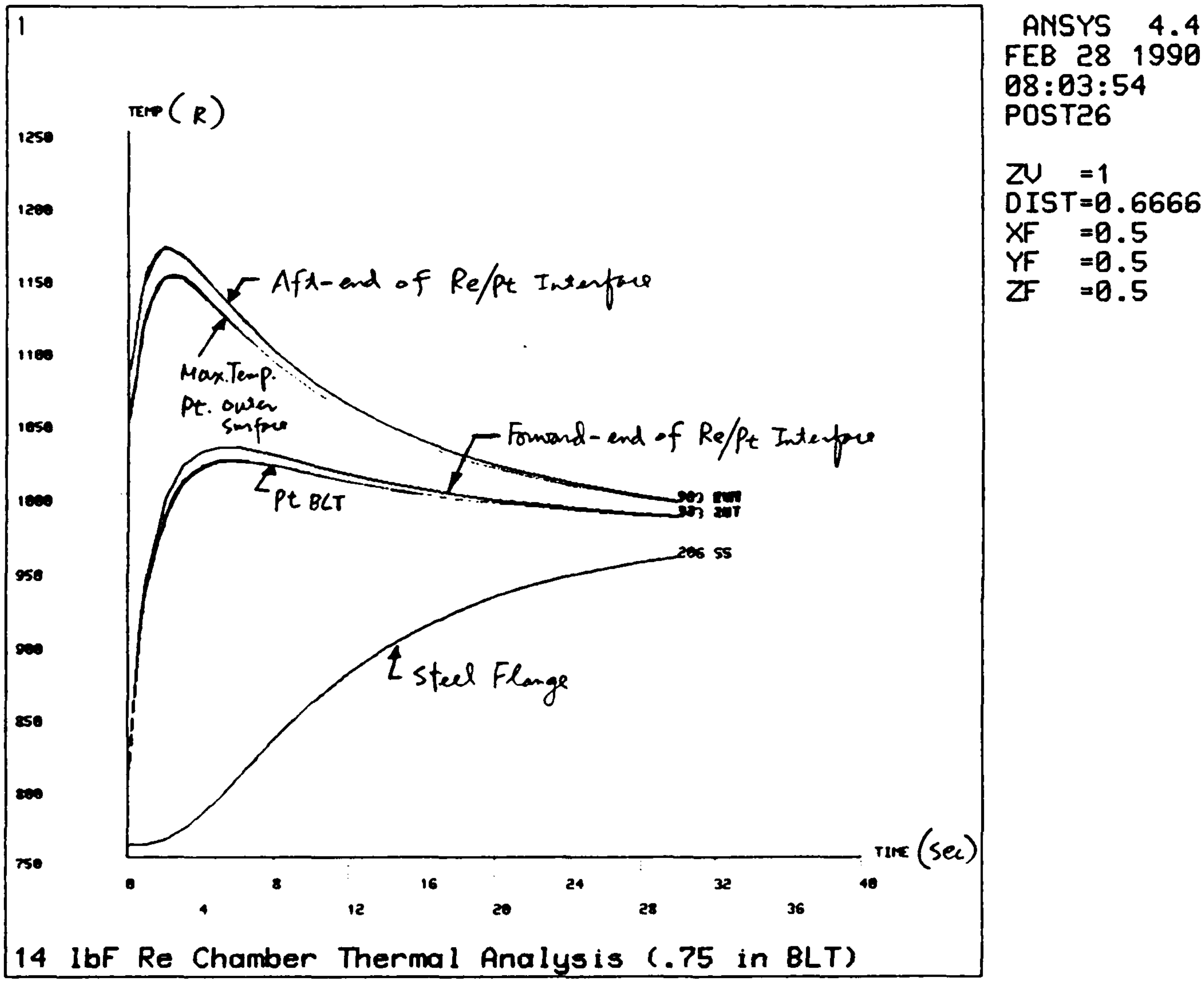


Figure 7 Transient Temperature Variations at Different Locations of Rhenium and Platinum interface

TO : Mark L. Gage March 20, 1990

FROM : Felix. F. Chen

SUBJECT: Thermal Stress Analysis Results of 14 lbF Rhenium Chamber

COPIES TO: S. D. Rosenberg (W/O Enclosure), L. Schoenman

REFERENCE: (1) Memo to M. L. Gage from F. F. Chen, Dated March 5, 1990

ENCLOSURE: (1) Computer output of 0.75 in. BLT steady state thermal stress analysis results

SUMMARY

This memo summarizes the continuation effort of Ref. (1) to include the recent design changes of the 14 lbF rhenium chamber in the throat section and the thermal stress results. The rhenium chamber wall thickness in the throat section has been increased from 0.028 in. to 0.040 in. In addition, the downstream radius of curvature (DRAD) increases from 0.2125 to 1.875 to ease the fabrication problem. The impact on the maximum throat wall temperature is very small (the maximum temperature increases from 3977 R to 4022 R). The temperature at rhenium chamber and platinum BLT interface remains the same, 1084 R. The maximum thermal stress occurs at the forward end of the rhenium chamber near platinum BLT. The maximum nodal stress for the rhenium chamber is 44.6 ksi which is about 10 ksi lower than the yield stress of the rhenium. The average thermal stress for the platinum BLT is approximately 20 ksi.

THERMAL ANALYSIS RESULTS

The temperature distribution for the 14 lbF rhenium chamber with a 15:1 nozzle is shown in Fig. 1. The maximum wall temperature is 4022 R occurring at approximately 0.15 in. upstream of the throat. This temperature represents an increase of 45 R which is considered negligible. The temperature distributions in the platinum BLT and steel flange are the same as Ref. (1). Therefore, the results of transient temperature variations presented in Ref. (1) are applicable for this design. The shutdown heat soak back analysis is not conducted for this design. At the exit of the nozzle (15:1), the predicted wall temperature is 2960 R (2500 F) which is the current maximum operating temperature of the 14 lbF columbium skirt. At an expansion area ratio of 9:1, the predicted wall temperature is 3110 R (2650 F). However, the results is considered conservative since the combustion gas is assumed fully mixed. The actual wall temperature could be slightly lower.

THERMAL STRESS ANALYSIS RESULTS

Figure 2 shows the thermal stress distribution for the 14 lbF rhenium chamber. The maximum nodal stress is 44.6 ksi occurring at the forward end of the rhenium chamber near platinum BLT. In the throat region, the thermal stress is only 10 to 15 ksi.

A blowup illustration of the thermal stress distribution for the vicinity of platinum BLT is shown in Fig. 3. It is clear that most of the high thermal stress concentration occur near the interface of rhenium chamber and platinum BLT. A radius corner at the interface may reduce thermal stress. For the platinum BLT, the thermal stress ranges from less than 5 ksi for BLT itself to approximately 25 ksi at the interface of platinum BLT and steel flange.

A deformation plot of the 14 lbF rhenium chamber at the steady state hot fire conditions is shown in Fig. 4. For the regions before the throat, rhenium chamber will be pushed outward radially due to the tension. The maximum radial displacement is approximately 0.005 in. However, in the divergent section (nozzle), the nozzle will be pulled inward radially. The dotted line represents the original chamber geometry, whereas the solid portion represents the predicted chamber contour during hot fire.

The effective strain plot for the 14 lbF rhenium chamber is shown in Fig. 5. The predicted maximum thermal strain is 1.32%. Since the low cycle fatigue (LCF) curve is not available, cycle life prediction was not conducted.

Felix F. Chen
Research and Technology

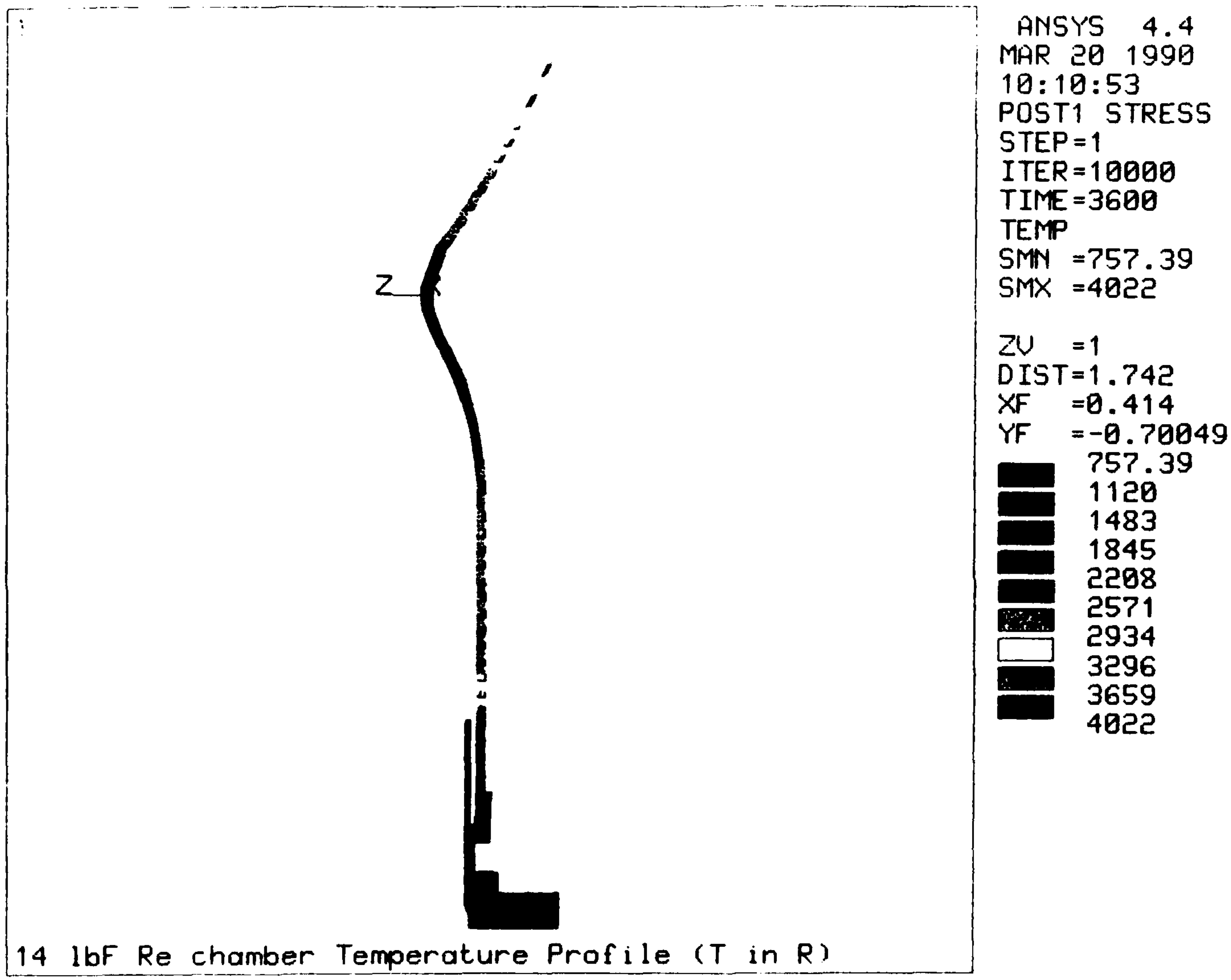


Figure 1. Steady State Temperature Distribution with a 0.75 in. Long BLT (Temperature in °R)

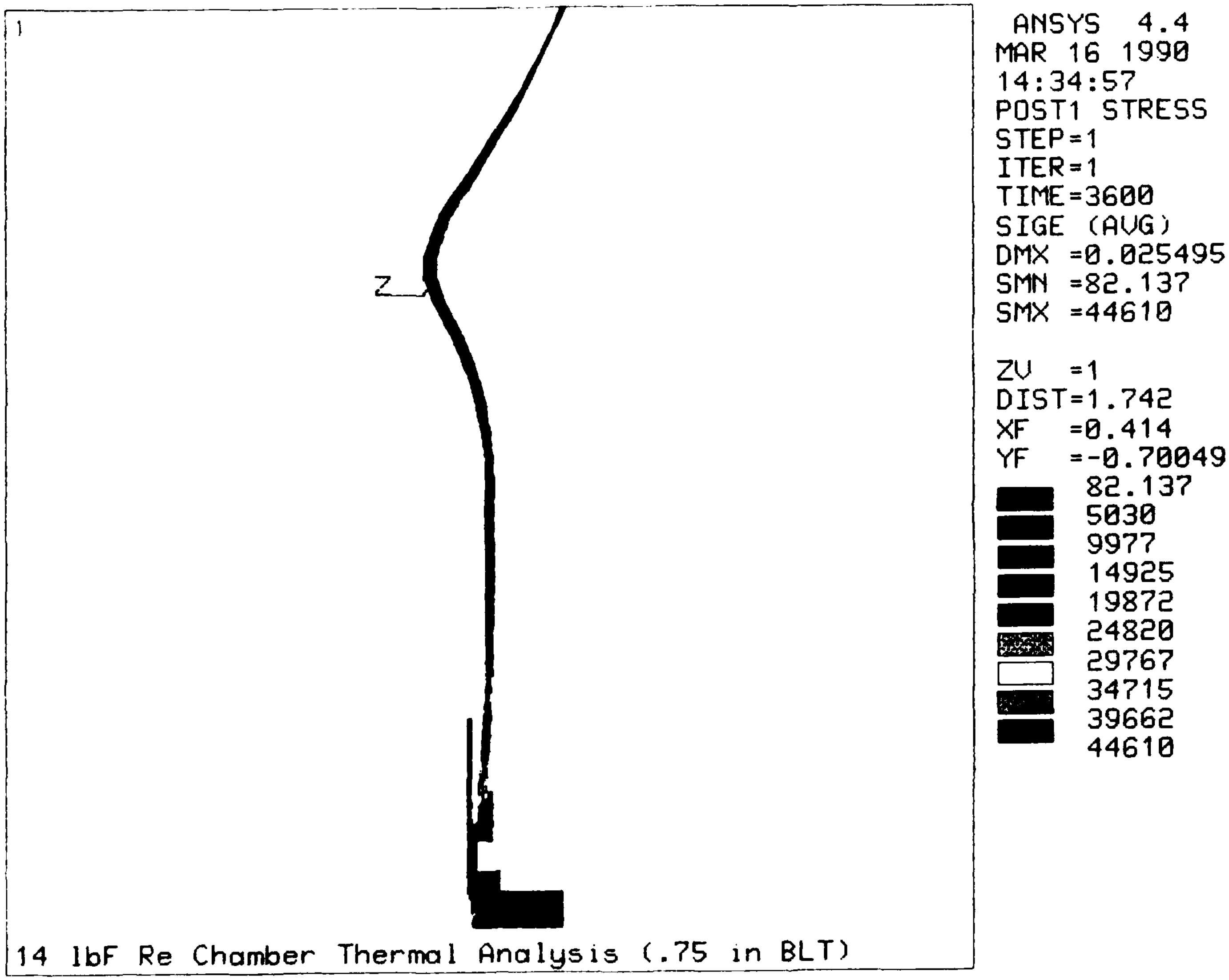


Figure 2. Thermal Stress Distribution at Steady State Conditions

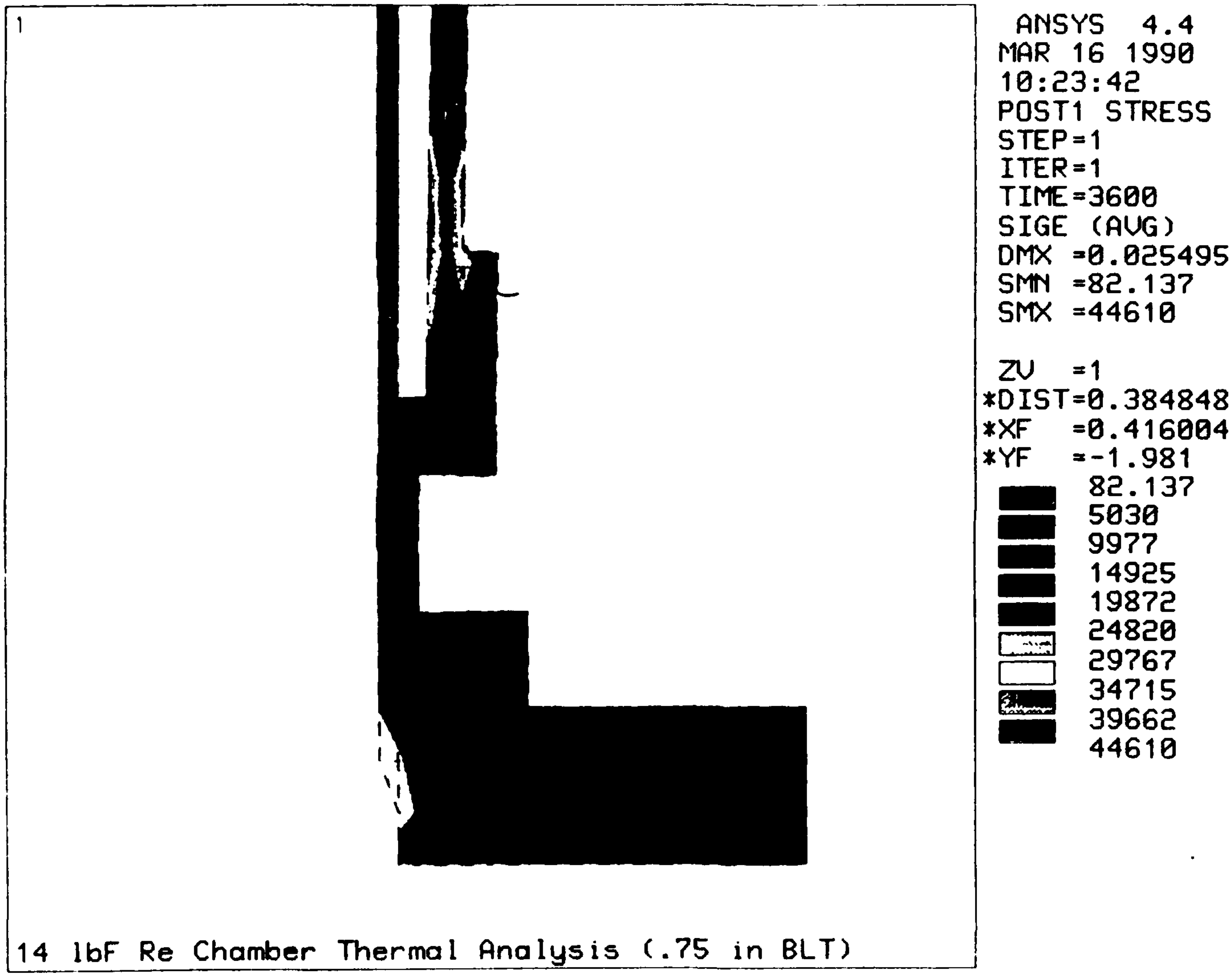


Figure 3. Blowup Illustration of Thermal Stress Distribution for Vicinity of Platinum BLT

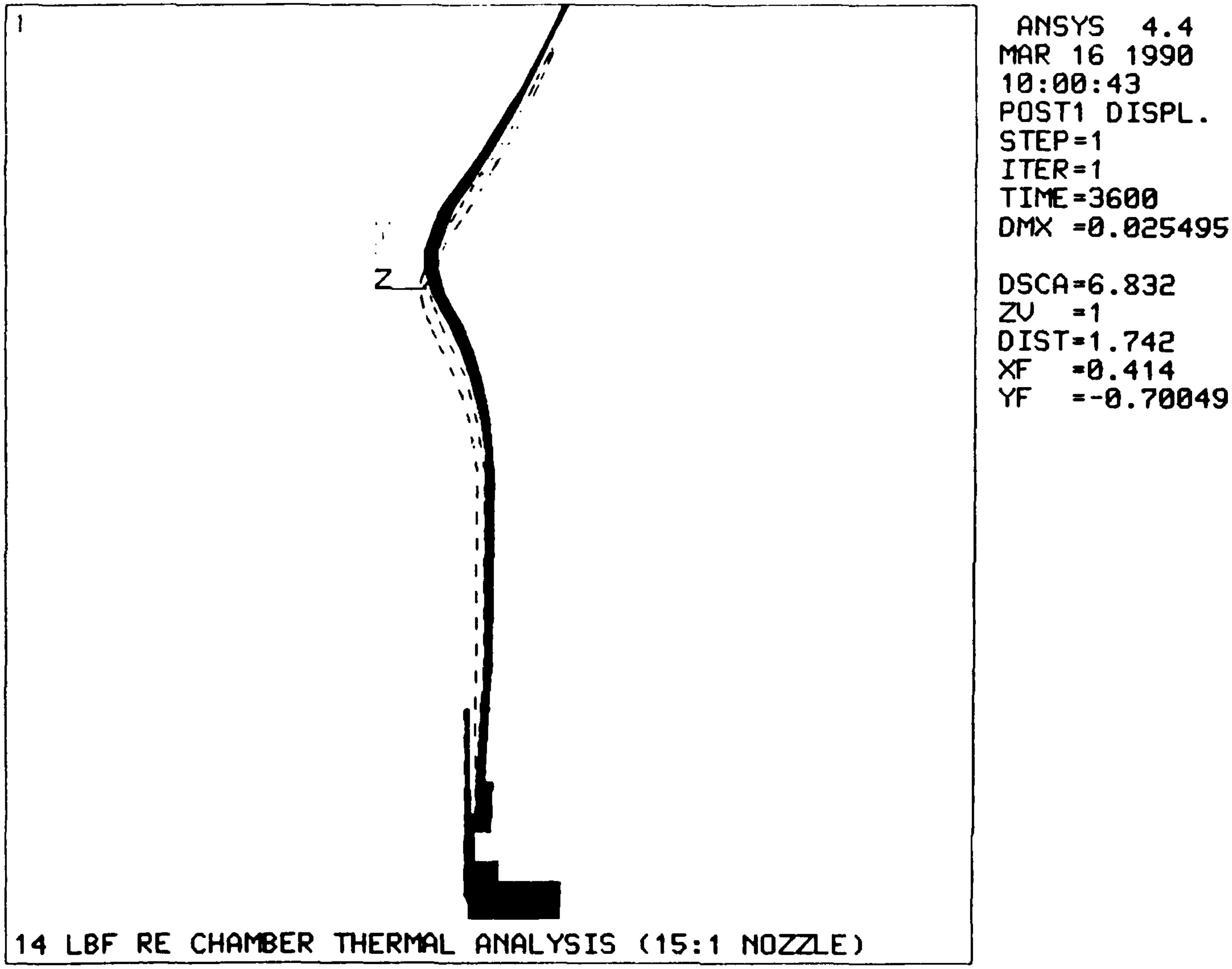


Figure 4. Illustration of Chamber Deformation at Steady State Hot Fire

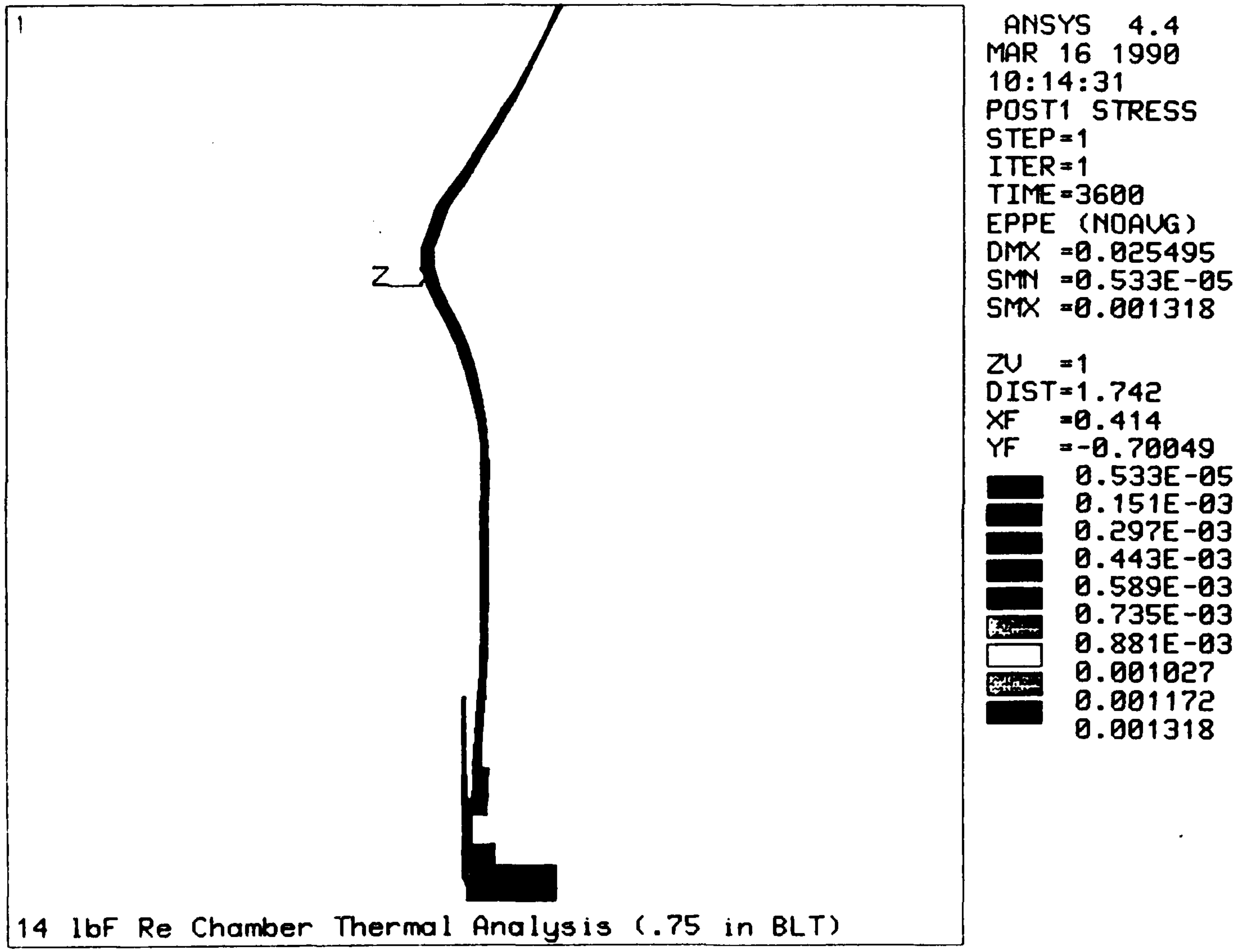


Figure 5. Maximum Effective Thermal Strain is only 1.32% at Steady State Hot Fire

APPENDIX C

High Performance 14 lb Thruster
Random Vibration Test

Test Readiness Review
21 February 1991

ASRC185 Vibration Test Requirements For 14# Ir-Re Thruster S/N 002 (Don Jassowski)

Test Procedure: Per 14# RCTM Production Vibration as Defined in Specification ATC-47145 With the Following Changes:

- No QC/Inspection Required
- Install and Monitor Accelerometers on Valve to Match Locations in Previous 14# Tests
- Install and Monitor Accelerometers on Nozzle Exit to Match Locations in Previous 14# Testing
- Install and Monitor Four Strain Gages at Nozzle Throat
- Measure Pre- and Post-Position of Nozzle Exit Plane With Dial Indicators

Special Considerations:

- Monitor Nozzle For Permanent Deflection and Terminate Testing if Values in Excess of .001 inch Are Detected
- Provide Photos of Accelerometer and Strain Gage Installation and Overall Test Set Up, Including Test Personnel

Instrumentation
(Russ Miller)

Accelerometers

(1)	Control		UDC 10B10
(1)	Control Monitor		UDC 10B10
(2)	Cross Axis		UDC 10B10
(3)	Biprop Valve	(x,y,z)	END 2222
(2)	Nozzle	(x,y)	B&K

Accelerometer Signals Conditioned by UDC D22PM Charge Amplifiers, and Recorded on FM Tape.

Strain Gages

(4)	Throat	(x,y)	MM CEA Type

Strain Gage Signals Conditioned by Validyne Amplifiers, Recorded on FM Tape. Strain Gage Output and Bond Type May Not Have Adequate High Frequency Response. Dead-Weight Calibration Will be Performed Prior to Test.

RPT/D0201 39-Presentation

Instrumentation (cont.)
(Russ Miller)

Data Output

- **PSD Plots of Accelerometers**
- **PSD Plots of Strain Gages If Requested**
- **Pre and Post Test Nozzle Position**
- **Oscillographs of Selected Transducers on Request**

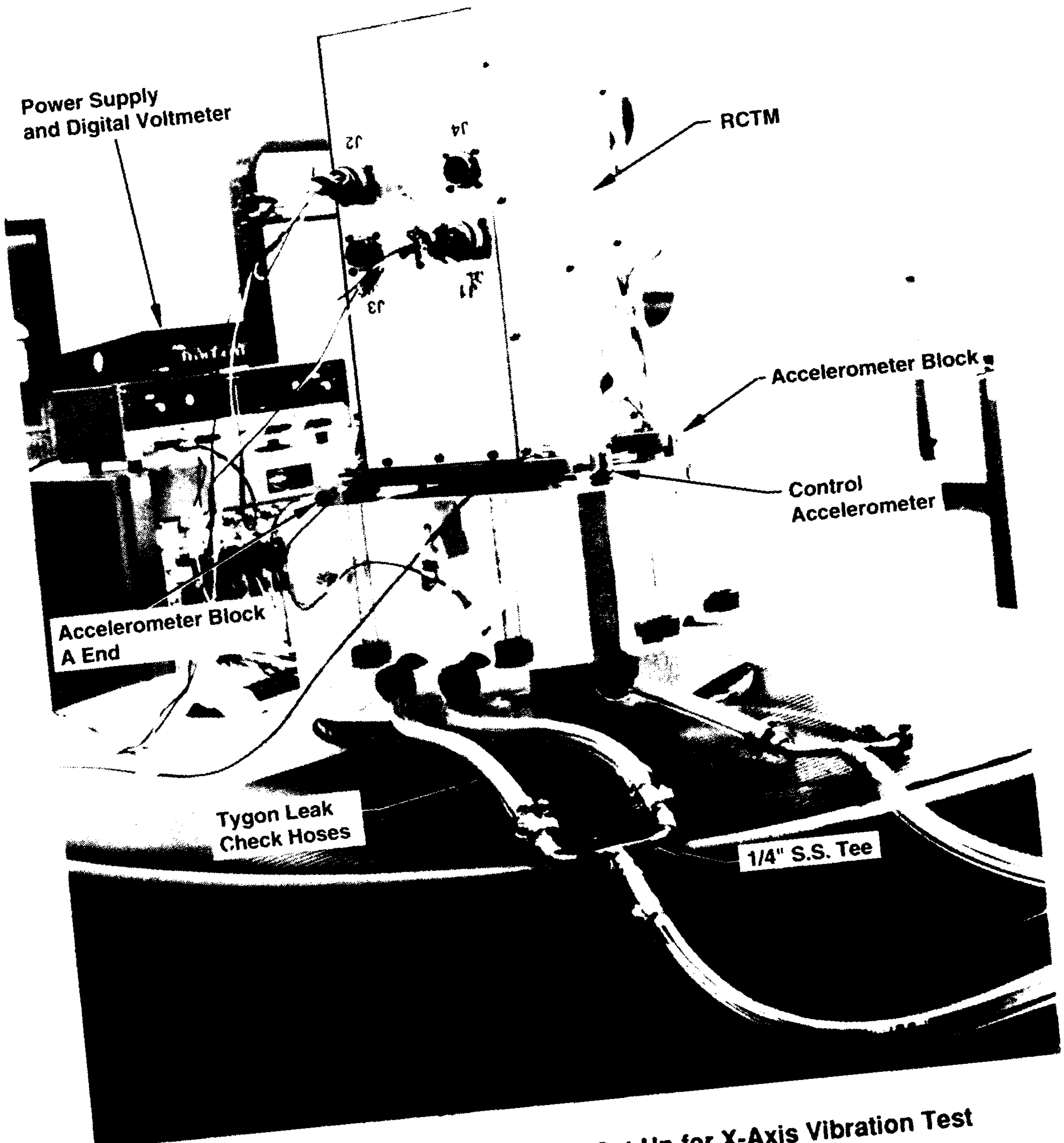


Figure C-1. Production 14# RCTM Set Up for X-Axis Vibration Test
Aerojet "A" Area Vibration Test Laboratory

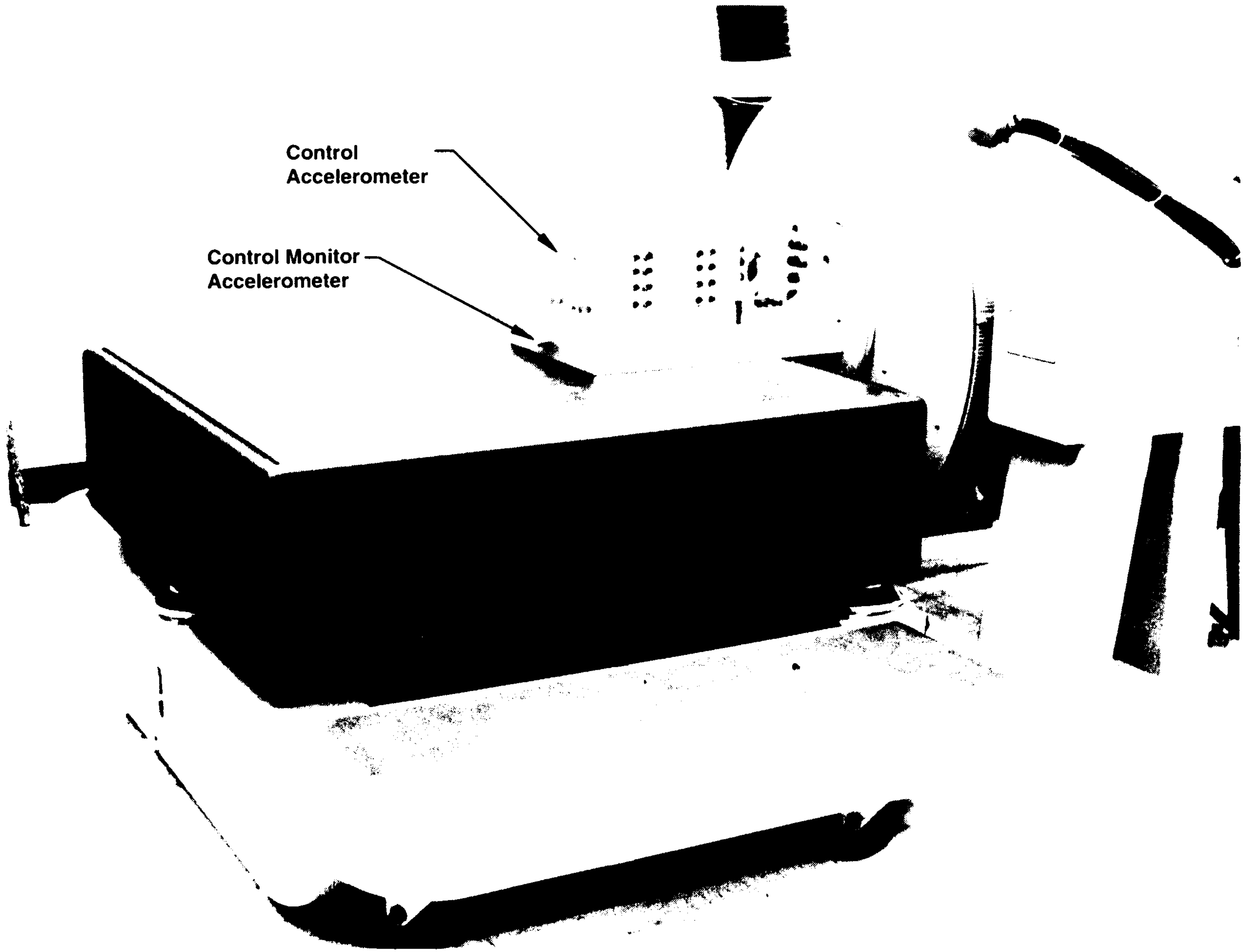


Figure C-2. Vibration Fixture for Y- and Z- Axis Vibration Test

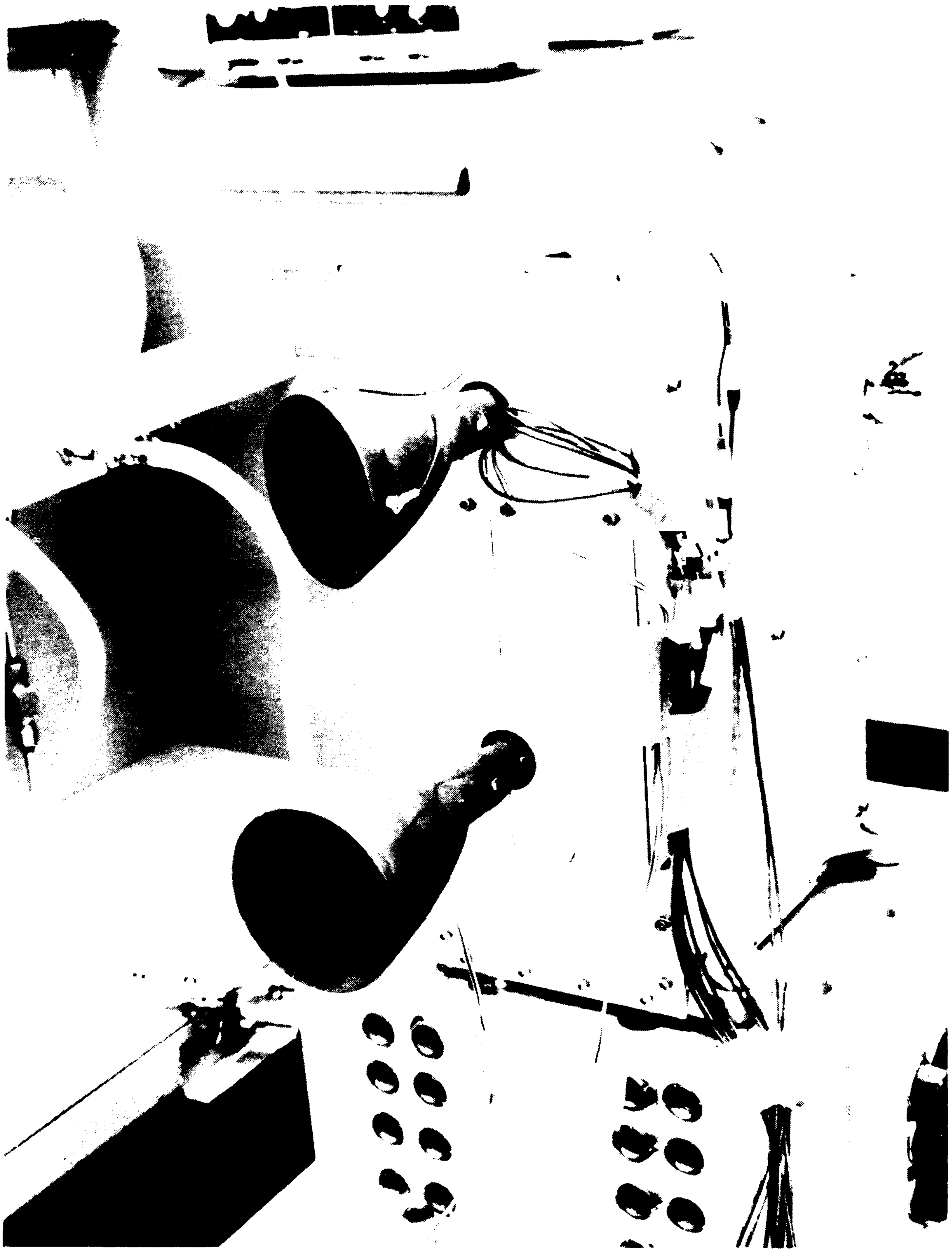


Figure C-3. Production 14# RCTM Setup for Y-Axis Vibration

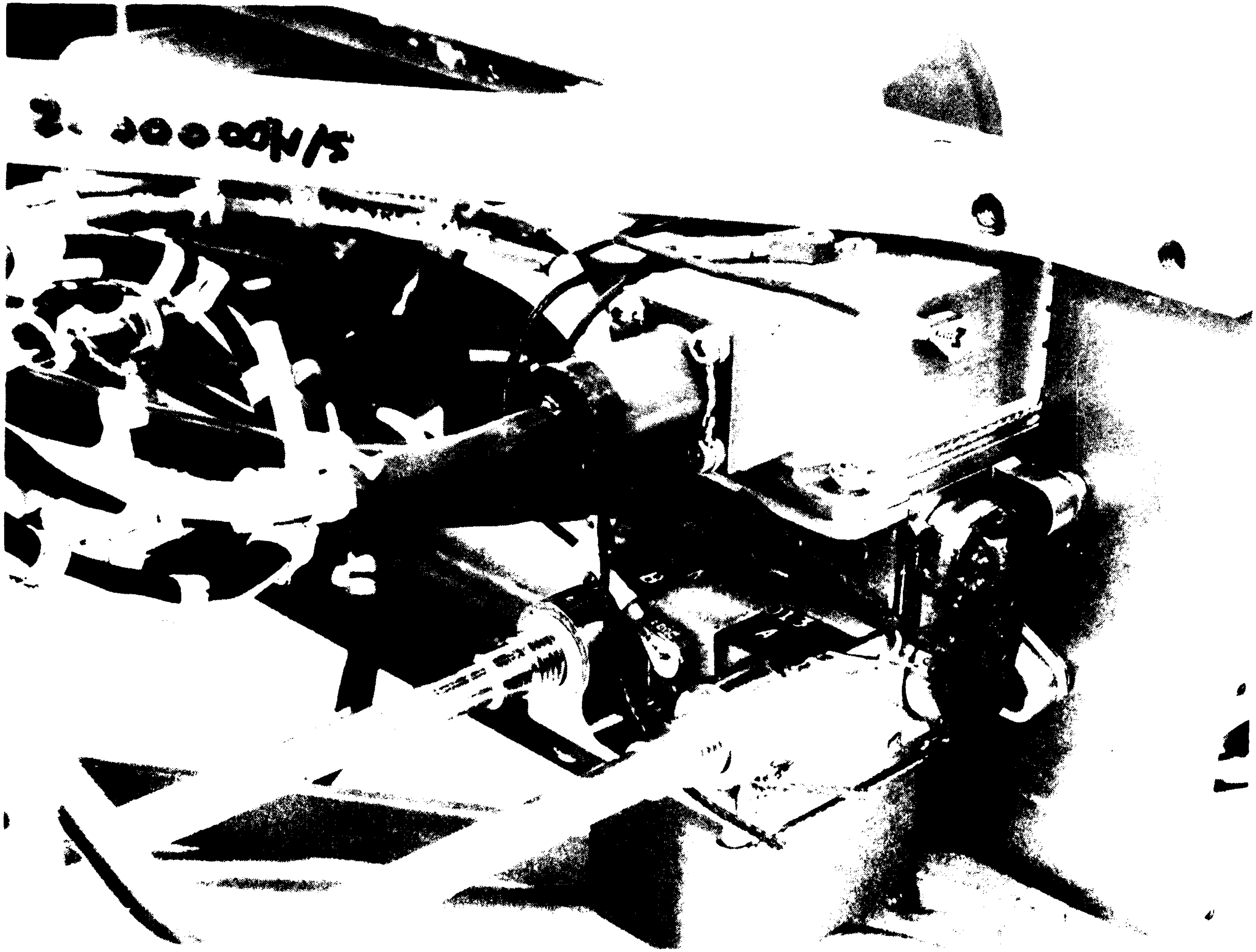
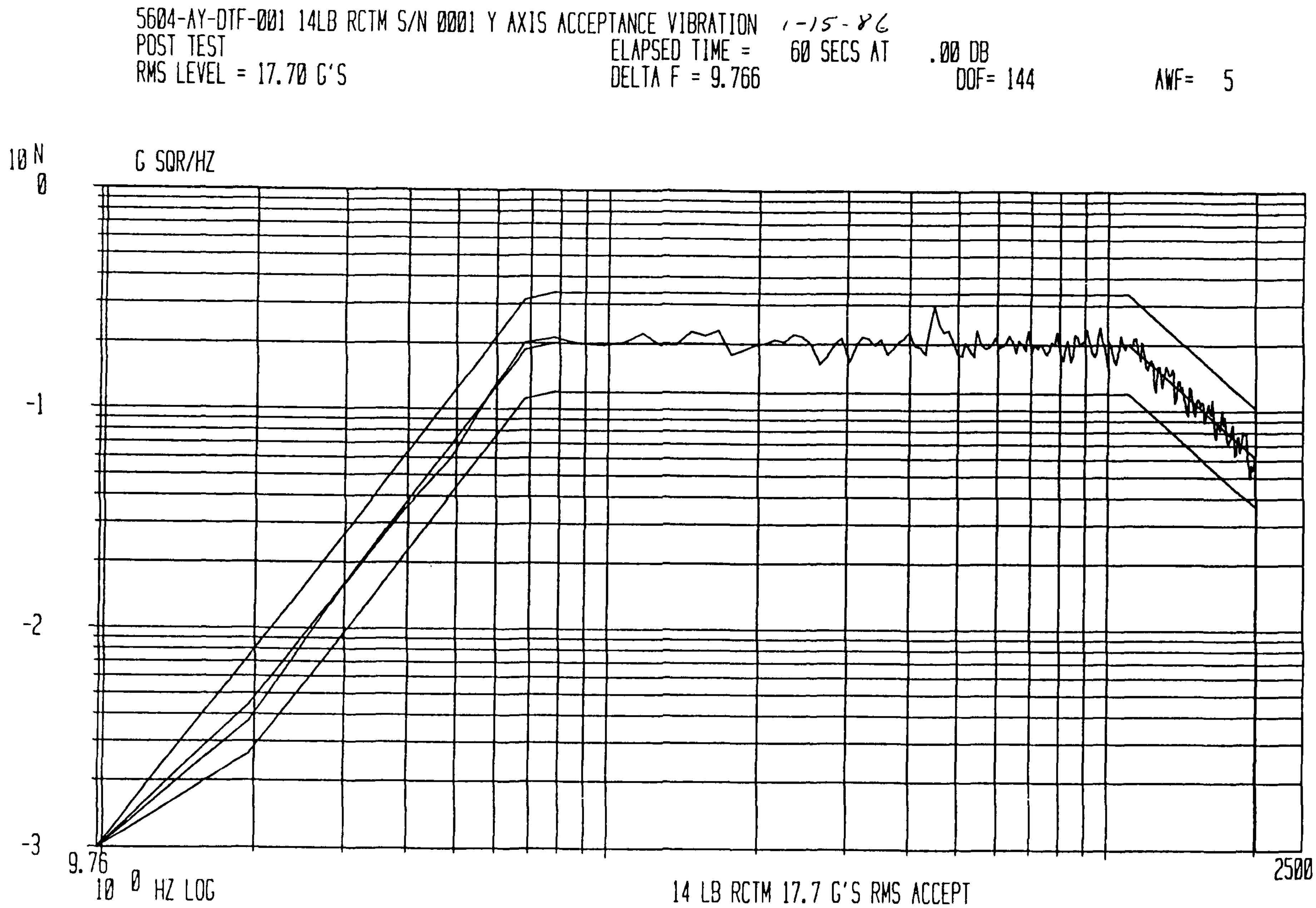


Figure C-4. Accelerometer Installation on Production Type 14# Thruster During Engineering Evaluation Testing



5604-AY-DTF-001 14LB RCTM S/N 0001 Y AXIS ACCEPTANCE VIBRATION 1-15-86
POST TEST
RMS LEVEL = 17.70 G'S
ELAPSED TIME = 60 SECS AT .00 DB
DELTA F = 9.766
DOF= 144
AWF= 5
10 N
G SQR/HZ
0
-1
-2
-3
9.76
10 0 HZ LOG
2500
14 LB RCTM 17.7 G'S RMS ACCEPT

Figure C-5.

14# RCTM

PRODUCTION ACCEPTANCE VIBRATION

1.0 PURPOSE

To demonstrate that the RCTM is capable of withstanding the random vibration environments as defined in Specification ATC-47145.

2.0 REQUIREMENTS

Requirements shall be in accordance with ATC-47145, Paragraph 4.2.14 and Paragraph 3.5 Instrumentation.

3.0 APPLICABLE DOCUMENTS

ATC 47145	Acceptance Test Specification, Reaction Control Thruster Module AJ10-220
Q & RA Standard 8151070	Supplier Quality Assurance System Requirements for Aerospace Systems and Critical Aerospace Components

4.0 TEST FACILITY

RCTM Random vibration testing shall be performed in the Dynamics Test Facility located in ATC Test Operations building 30003 DTF.

5.0 SPECIAL INSTRUCTIONS

The RCTM propellant inlet lines as received from manufacturing will have installed 2 micron nominal filters to prevent contamination of the internal surfaces.

The RCTM propellant inlet lines shall be capped or plugged at all times except as required for buildup or test.

6.0 Test Equipment

6.1 FACILITY:

Equipment	Description
Unholtz-Dickie TA-130-70 (includes AM-123)	Vibration testing system
HP5427A	Digital vibration controller
Wyle WM-450	Slip table
Facility sketch A-14A-1008	Pressure decay leak test system

6.2 AT AND SE

T-1072424	Vibration fixture

6.3 INSTRUMENTATION:

Make/Model	Description
Endevco 2222 series	acceleromenter
Endevco 2272	accelerometer
Unholtz-Dickie D22PM series	charge amplifier
Ballantine 320	true RMS meter
HP1222A	oscilloscope
Ampex FR1300	tape recorder
VIZ WP-707	0-25 volt D.C. power supply
Fluke 8000A	digital multimeter

NOTE: It is permissible to use replacement instrumentation if its accuracy is equal or better. Any instrument change shall be noted on the procedure and approved by Quality Control.

6.4 DATA PROCESSING:

Make/Model	Description
HP5427A	Digital vibration controller/ plotter
Nicolet 660	FFT Analyzer/plotter.

7.0 ACCEPTANCE VIBRATION PROCEDURE SEQUENCE

A-14A-8000 14LB RCTM Non-Hardware Acceptance Vibration Pretest Procedures Index

A-14A-1000 Non-Hardware Pretest Setup 14LB RCTM Acceptance Vibration

A-14A-1002 Verification of Overtest Control Monitor Performance Acceptance Vibration 14LB RCTM

NOTE: The P.C. and/or Q.A. reserves the right to audit or request demonstration of compliance of A-14A-1002 at any time during the program.

COMMENT - POTENTIAL COST IMPACT: Demonstration may require removal of hardware and a complete system setup.

<u>A-14A-8001</u> 14LB RCTM Acceptance Vibration Hardware Pretest Procedures Index

A-14A-1003 14LB RCTM Acceptance Vibration Hardware Receiving and Inspection

A-14A-1004 14LB RCTM Leak Test Tygon Hose Installation

A-14A-1016 Facility GN_2 Pressurant Certification 14LB RCTM

<u>A-14A-8002</u> 14LB RCTM X Axis Vibration Setup Procedure Index

A-14A-1005 14LB RCTM X Axis Vibration Fixture Installation Procedure

A-14A-1006 14LB RCTM X Axis Vibration RCTM Installation

<u>A-14A-8005</u> 14LB RCTM Acceptance X Axis Vibration Test Index

A-14A-1007 Acceptance Vibration Pretest Instrumentation and HP Controller Setup 14LB RCTM

A-14A-1008 Pretest Leak Check Cart Setup Acceptance Vibration 14LB RCTM

A-14A-1009 Vibration Pressure Decay Leak Check Measurement and Acceptance Test 14LB RCTM

A-14A-1010 Posttest Leak Check Cart Procedure 14LB RCTM

A-14A-1011 Leak Rate Calculation Acceptance Vibration Test 14LB RCTM

<u>A-14A-8006</u> 14LB RCTM Z Axis Vibration Setup Procedure Index

A-14A-1012 14LB RCTM Z Axis Vibration Fixture Installation Procedure

A-14A-1013 14LB RCTM Z Axis Vibration RCTM Installation

<u>A-14A-8007</u> 14LB RCTM Acceptance Z Axis Vibration Test Index

A-14A-1007	Acceptance Vibration Pretest Instrumentation and HP Controller Setup 14LB RCTM
A-14A-1008	Pretest Leak Check Cart Setup Acceptance Vibration 14LB RCTM
A-14A-1009	Vibration Pressure Decay Leak Check Measurement and Acceptance Test 14LB RCTM
A-14A-1010	Posttest Leak Check Cart Procedure 14LB RCTM
A-14A-1011	Leak Rate Calculation Acceptance Vibration Test 14LB RCTM

<u>A-14A-8008</u> 14LB RCTM Y Axis Vibration Setup Procedure Index

A-14A-1014	14LB RCTM Y Axis Vibration Fixture Installation Procedure
A-14A-1015	14LB RCTM Y Axis Vibration RCTM Installation

<u>A-14A-8009</u> 14LB RCTM Acceptance Y Axis Vibration Test Index

A-14A-1007	Acceptance Vibration Pretest Instrumentation and HP Controller Setup 14LB RCTM
A-14A-1008	Pretest Leak Check Cart Setup Acceptance Vibration 14LB RCTM
A-14A-1009	Vibration Pressure Decay Leak Check Measurement and Acceptance Test 14LB RCTM
A-14A-1010	Posttest Leak Check Cart Procedure 14LB RCTM
A-14A-1011	Leak Rate Calculation Acceptance Vibration Test 14LB RCTM

APPENDIX D

Vibtration Test Data Analysis

GenCorp
Aerojet

Propulsion Division

Memo

11 April 1991
CSV:gg:5242:4634

TO: M. L. Gage

FROM: C. S. Vallance

SUBJECT: Transmittal for Vibration Testing of the Advanced 14 LBF Chamber for RCTM

DISTRIBUTION: D.M. Jassowski, R.J. Miller, L. Schoenman, N.R. Shimp, 5242 File

ENCLOSURES: (1) Vallance, C.S., **Vibration Testing of the Advanced 14 LBF Chamber for the RCTM**

Enclosure (1) contains predictions regarding the survivability of the Advanced 14 LBF Chamber for the RCTM to qualification level Reaction Control Thrust Module vibration levels.

The predictions are based on a limited number of test measurements made at acceptance level vibration levels.

C. S. Vallance
Metallic Structures & Dynamics
Engineering Analysis Department

APPROVED BY:

E. Lueders, Manager
Metallic Structures & Dynamics
Engineering Analysis Department

ENCLOSURE (1)

5242:4634

VIBRATION TESTING

OF THE

ADVANCED 14 LBF CHAMBER

FOR THE

REACTION CONTROL THRUST MODULE

PREPARED BY:

C. S. Vallance
Metallic Structures & Dynamics
Engineering Analysis Department

APPROVED BY:

E. Lueders, Manager
Metallic Structures & Dynamics
Engineering Analysis Department

REVIEWED BY:

J. E. Jellison
Metallic Structures & Dynamics
Engineering Analysis Department

1.0 INTRODUCTION

Recent low level testing of the Advanced 14 LBF Chamber mounted on a Reaction Control Thrust Module (RCTM) has proven the ability of the iridium/rhenium chamber to meet max-expected vibration levels expected during launch vehicle ascent.

The chamber's ability to withstand a 3 dB margin test is addressed. Predicated on limited test data, predicted stress levels of the throat and chamber root are explored.

Brevity is employed in the documentation of the calculations to conserve resources.

2.0 SUMMARY OF RESULTS

Calculations for the rhenium chamber show positive margins as indicated in Table I.

Table I: Predicted Margins of Safety

Location	M.S.
Chamber Throat	0.65
Chamber Root	2.78
Trip Ring Root	2.38

Analysis of the measurement test functions indicate the highest throat strain to be 93 $\mu in/in_{rms}$. A crest factor of 3.9 was seen in the time histories and is used for the strength calculations.

Bi-propellant valve accelerometers show frequency response and level to be closely identical to measurements made during RCTM engineering unit evaluations.

Although the limited number of test functions hinders mode identification, chamber bending modes are surmised to be below 450 Hz. Higher frequency modes are presumed to be flexural in nature.

3.0 CONCLUSIONS

1) The Advanced 14 LBF Chamber will survive an increase in vibration levels of 3 dB.

2) Positive margins of safety are predicted at all critical locations for a vibration load increased by 3 dB.

3) The most critically stressed area is the chamber throat.

4) Cantilevered bending modes of the chamber occur below 450 Hz.

5) More instrumentation is required to accurately predict chamber flexural modes and to better understand the stress state of the chamber.

4.0 RECOMMENDATIONS

1) Perform a vibration test of the Advanced 14 LBF Chamber at vibration levels increased by 3 dB to simulate qualification level ascent loading.

5.0 DETAILED ANALYSIS

5.1 Strain Gage Data Reduction

Four strain gages located at the chamber throat were measured. They were evenly spaced around the circumference and oriented in the axial direction. See Figures 1 and 2. All strain gage data is presented in Appendix B. Table II shows the rms micro-strain levels for each gage and test.

Table II: Strain Gage Measurements			
	TEST AXIS		
Strain Gage	X $\mu\epsilon_{rms}$	Y $\mu\epsilon_{rms}$	Z $\mu\epsilon_{rms}$
1	60	16	86
2	13	35	15
3	64	11	93
4	14	29	11

Examination of time histories (e.g. Z axis, strain gage #3) show peak strain levels of -363 $\mu\epsilon_{0-p}$ with rms levels of 93 $\mu\epsilon_{rms}$. This yields an observed crest factor of

$$CF = 363 / 93$$
$$CF = 3.9$$

This crest factor will be used for all strength calculations to follow.

The largest modes are all below 450 Hz. Due to the orientation of the strain gages these modes are likely to be chamber bending modes.

5.2 Material Properties

These material properties are approximate and reported in IOM 9990:R&T:2797 with revisions by M.L. Gage. See Appendix A.

5.2.1 Rhenium

Young's Modulus, E	65×10^6	psi
Density, τ	1.966×10^{-3}	$lb\text{-}s^2/in^4$
Yield Strength, σ_y	55×10^3	psi
Ultimate Strength, σ_u	170×10^3	psi

5.2.2 Platinum

Young's Modulus, E	21×10^6	psi
Density, τ	2.006×10^{-3}	$lb\text{-}s^2/in^4$
Yield Strength, σ_y	30×10^3	psi
Ultimate Strength, σ_u	60×10^3	psi

5.3 Calculated Stress in the Rhenium Throat Due to Test

Only strength calculations to follow, no fatigue calculations.

$$\sigma = E \times \epsilon_{meas}$$

and,

$$\sigma = (65 \times 10^6 \text{ psi})(363 \ \mu\text{in/in})$$

$$\sigma = 23.6 \times 10^3 \text{ psi}_{0-p}$$

Therefore the measured stress in the throat region is well below the yield limit. Projected stress, linearly scaled for a vibration test 3 dB higher would be

$$\sigma_{3dB} = (23.6 \times 10^3)(\sqrt{2})$$

$$\sigma_{3dB} = 33.3 \times 10^3 \text{ psi}_{0-p}$$

The margin of safety with no safety factor is

$$M.S. = (\sigma_y / \sigma_{3dB}) - 1$$

$$M.S. = (55 / 33.3) - 1$$

$$\underline{\underline{M.S. = 0.65}}$$

No safety factor has been used because this is non-flight hardware. It should be noted however that the material properties are not accurately known.

5.4 Stress at the Chamber and Trip Ring Roots due to Test

In order to approximate stress at the roots assume cantilevered beam model with applied moment. The applied moment will be developed with two techniques for comparison purposes. In the first technique, the applied moment is determined by backing out the moment required to produce the stresses in Section 5.3. In the second technique, the load is approximated by inertial loading of chamber, WG, and moment arm determined by the c.g. of the chamber.

5.4.1 Chamber Mass Properties

Determine chamber mass properties roughly in three sections; 1) straight hollow cylinder from root to convergent section of throat, 2) convergent section of throat, and 3) divergent nozzle section. All section properties are taken from hardware drawings as listed below and Appendix D which contains the as-built wall thicknesses.

Name	Drawing No.
Nozzle, 14 lbs	1204474
Chamber, 14 lb	1204490
Ring, Trip	1204495

5.4.1.1 First section

$\tau = 1.966 \times 10^{-3}$ lb-s^2/in^4 $\qquad r_o \approx 0.389$ in

$l \approx 1.650$ in $\qquad r_i \approx 0.364$ in

$$m_1 = \tau \; l \; \pi \; (r_o^2 - r_i^2)$$

$$m_1 = 192 \times 10^{-6} \text{ lb-s}^2\text{/in}$$

Center of gravity is located at the centroid, thus $x_{bar1} \approx 0.825$ in.

5.4.1.2 Second section

Use hollow frustum of cone formula for volume.

$\tau = 1.966 \times 10^{-3}$ lb-s^2/in^4 $\qquad r_{1i} \approx 0.364$ in

$h \approx 0.61$ in $\qquad r_{2o} \approx 0.209$ in

$r_{1o} \approx 0.389$ in $\qquad r_{2i} \approx 0.160$ in

$$m_2 = 1/3 \; \tau \; \pi \; h \; [r_{1o}^2 + (r_{1o})(r_{2o}) + r_{2o}^2 - r_{1i}^2 - (r_{1i})(r_{2i}) - r_{2i}^2]$$

$$m_2 = 75.3 \times 10^{-6} \text{ lb-s}^2\text{/in}$$

Center of gravity is located 1/3 of the distance from the largest end towards the small end of the frustum, thus $x_{bar2} \approx 1.853$ in.

5.4.1.3 Third section

Use hollow frustum of cone formula for volume.

$\gamma = 1.966 \times 10^{-3}$ lb-s^2/in^4 $\quad r_{1i} \approx 0.160$ in

$h \approx 3.974$ in $\quad r_{2o} \approx 1.403$ in

$r_{1o} \approx 0.209$ in $\quad r_{2i} \approx 1.389$ in

$$m_3 = 1/3 \times \gamma \times \pi \times h \times [r_{1o}^2 + (r_{1o})(r_{2o}) + r_{2o}^2 - r_{1i}^2 - (r_{1i})(r_{2i}) - r_{2i}^2]$$

$$m_3 = 1.049 \times 10^{-3} \text{ lb-s}^2\text{/in}$$

Center of gravity is located 1/3 of the distance from the largest end towards the small end of the frustum, thus $x_{bar3} \approx 4.923$ in.

5.4.1.4 Determine center of gravity of test section

5.4.1.4.1 Total Mass

$$M_{tot} = \Sigma_i \, m_i$$

$$M_{tot} = 1.316 \times 10^{-3} \text{ lb-s}^2\text{/in}$$

5.4.1.4.2 Center of gravity

$$X_{bar} = \Sigma_i \, (m_i \times x_{bari}) \, / \, M_{tot}$$

$$X_{bar} = 9.987 \times 10^{-3} \, / \, M_{tot}$$

$$X_{bar} = 4.151 \text{ in}$$

5.4.2 Loads

Use two methods to estimate loads to be used for calculating chamber root stresses.

5.4.2.1 Method 1: Load Based on Measured Strain

Assume all stress in chamber throat is produced by moment application. Back calculate required moment to produce this stress. Use bending stress formula

$$\sigma = M c / I$$

Rearranging for M yields

$$M = \sigma I / c$$

and σ = 23600 psi (para 5.3), I = 984 x 10^{-6} in^4 (para 5.4.2.1.1), c ≈ 0.209 in. Thus

$$M = 111 \text{ in-lbs}$$

5.4.2.1.1 Area Moment of Inertia of Throat

r_o = 0.209 in
r_i = 0.160 in

$$I = \pi (r_o^4 - r_i^4) / 4$$

$$I = 984 \times 10^{-6} \text{ in}^4$$

5.4.2.2 Method 2: Load Based on Acceleration Measurements

Develop load using F = W G. Where W = mg and G is measured from test. This load applied at the moment arm determined by the c.g. will yield another estimate of applied moment. In comparison to Method 1 (Sect 5.4.2.1), this load should be considered conservative. It is calculated as follows

$$M = M_{tot}\, g\, G\, l$$

where M_{tot} = 1.316 x 10^{-3} lb-s^2/in (para 5.4.1.4.1), g = 386 in/s^2, G = 74.1 G's (para 5.4.2.2.1) and l = 4.151 in (para 5.4.1.4.2). Therefore

$$M = 156.2 \text{ in-lbs}$$

instead of actual modal mass, accounting for the higher value in comparison to the moment developed in Method 1 (para 5.2.4.1). The numbers appear to be a relatively good check. The smaller number based on actual strain will be used for further analysis.

5.4.2.2.1 Nozzle Accelerometer Data Reduction

All accelerometer data reduction is presented in Appendix C as power spectral density plots. The orientation of the accelerometers is seen in Figures 1 and 3. This orientation allows the accels to respond to all modes of the chamber; bending, breathing and flexural. There are not enough accels to determine the modes accurately. However, in conjunction with the strain gages, the bending modes are expected below 450 Hz.

The responses from these lower modes only are used in determining the chamber root stresses and are presented in Table III. Use maximum rms value encountered during any of three axes of testing. See Appendix C for particular peaks used. RMS is determined using

$$G_{rms} \approx [\Sigma_i \ (PSD_i * \delta f_i)]^{\frac{1}{2}}$$

Table III: Accelerometer Measurements

Accelerometer	TEST AXIS X G_{rms}	Y G_{rms}	Z G_{rms}
Nozzle X	**19**	4	4
Nozzle Y	7.9	6	5.6

A crest factor of 3.9 on 19 G_{rms} should be used in accordance with section 5.1. Therefore, G_{0-p} = 74.1.

Matching accelerometers located on the bi-propellant valve with the engineering unit RCTM (Reference (1)) shows a good match in frequency and magnitude. No other accels for which matches can be made exist. The nozzle accels are very different because of geometry changes.

5.4.3 Calculated Stress in the Chamber and Trip Ring Roots

Calculate stresses using bending formulation. No shear included.

5.4.3.1 Area moment of Inertia

Determine area moments of inertia for bending calculations in paragraph 5.4.3.2 and 5.4.3.3.

5.4.3.1.1 Chamber

$$I = \pi \times (r_o^4 - r_i^4) / 4$$

$$I = \pi \times (0.389^4 - 0.364^4) / 4$$

$$I = 0.0042 \text{ in}^4$$

5.4.3.1.2 Trip Ring

$$I = \pi \times (0.374^4 - 0.325^4) / 4$$

$$I = 0.0066$$

5.4.3.2 Stress in the Chamber Root

Use bending loads only, ignore shear.

$$\sigma = M c / I$$

where c is distance to outer fiber from neutral axis. So,

$$\sigma = 111 \times 0.389 / 0.0042$$

$$\sigma = 10280 \text{ psi}$$

Linearly scale for 3 dB amplification

$$\sigma_{3dB} = 10280 \times \sqrt{2}$$

$$\sigma_{3dB} = 14540 \text{ psi}$$

The margin of safety with no safety or stress concentration factors is

$$M.S. = (\sigma_y / \sigma_{3dB}) - 1$$

$$M.S. = (55 / 14.54) - 1$$

$$\underline{M.S. = 2.78}$$

5.4.3.3 Stress at Trip Ring

Use bending loads only, ignore shear.

$$\sigma = M \times c / I$$

where c is distance to outer fiber from neutral axis. So,

$$\sigma = 111 \times 0.374 / 0.0066$$

$$\sigma = 6290 \text{ psi}$$

Linearly scale for 3 dB amplification

$$\sigma_{3dB} = 6290 \times \sqrt{2}$$

$$\sigma_{3dB} = 8895 \text{ psi}$$

The margin of safety with no safety or stress concentration factors is

$$M.S. = (\sigma_y / \sigma_{3dB}) - 1$$

$$M.S. = (30 / 8.9) - 1$$

$$\underline{M.S. = 2.37}$$

6.0 REFERENCES

1. Vallance, C.S., **Reaction Control Thrust Module, P/N 1197360, S/N's 001, 002 Engineering Evaluation Test - June 1985**, IOM 9950:2182, dtd 26 June 1985.

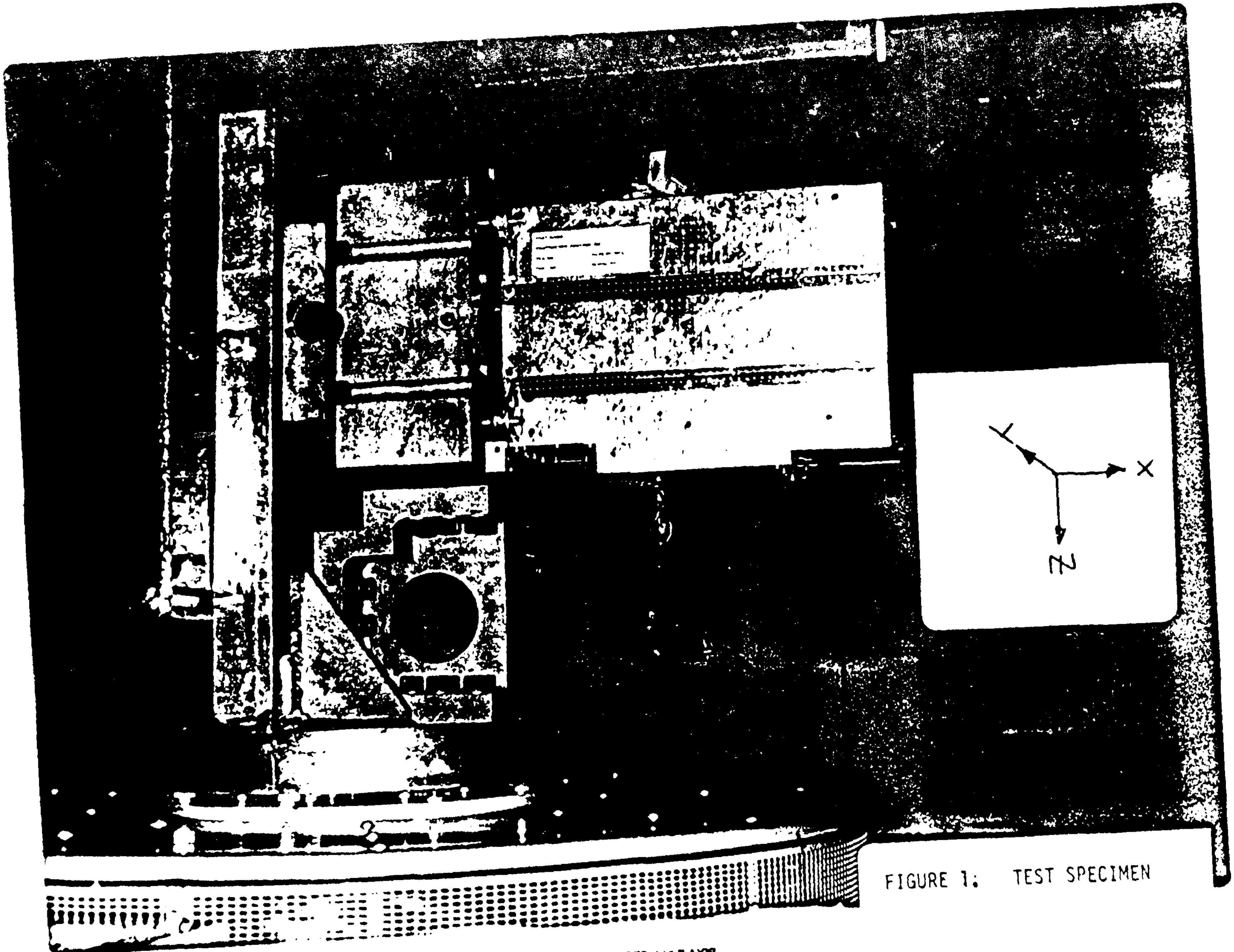


FIGURE 1: TEST SPECIMEN

ADVANCED 148 Z AXIS
VIBRATION 2/27/91

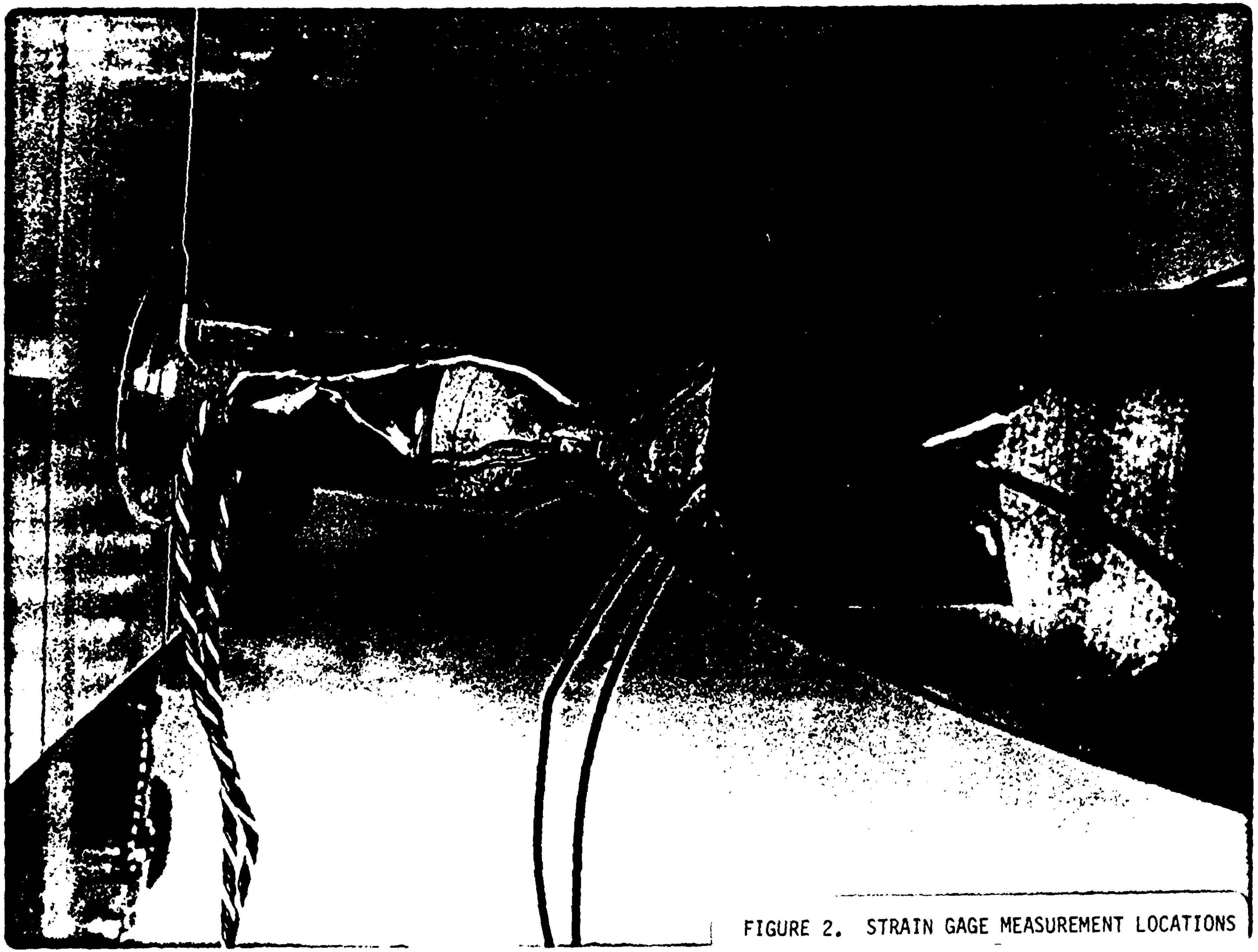


FIGURE 2. STRAIN GAGE MEASUREMENT LOCATIONS

ADVANCED 148 Z AXIS
VIBRATION 2/27/91

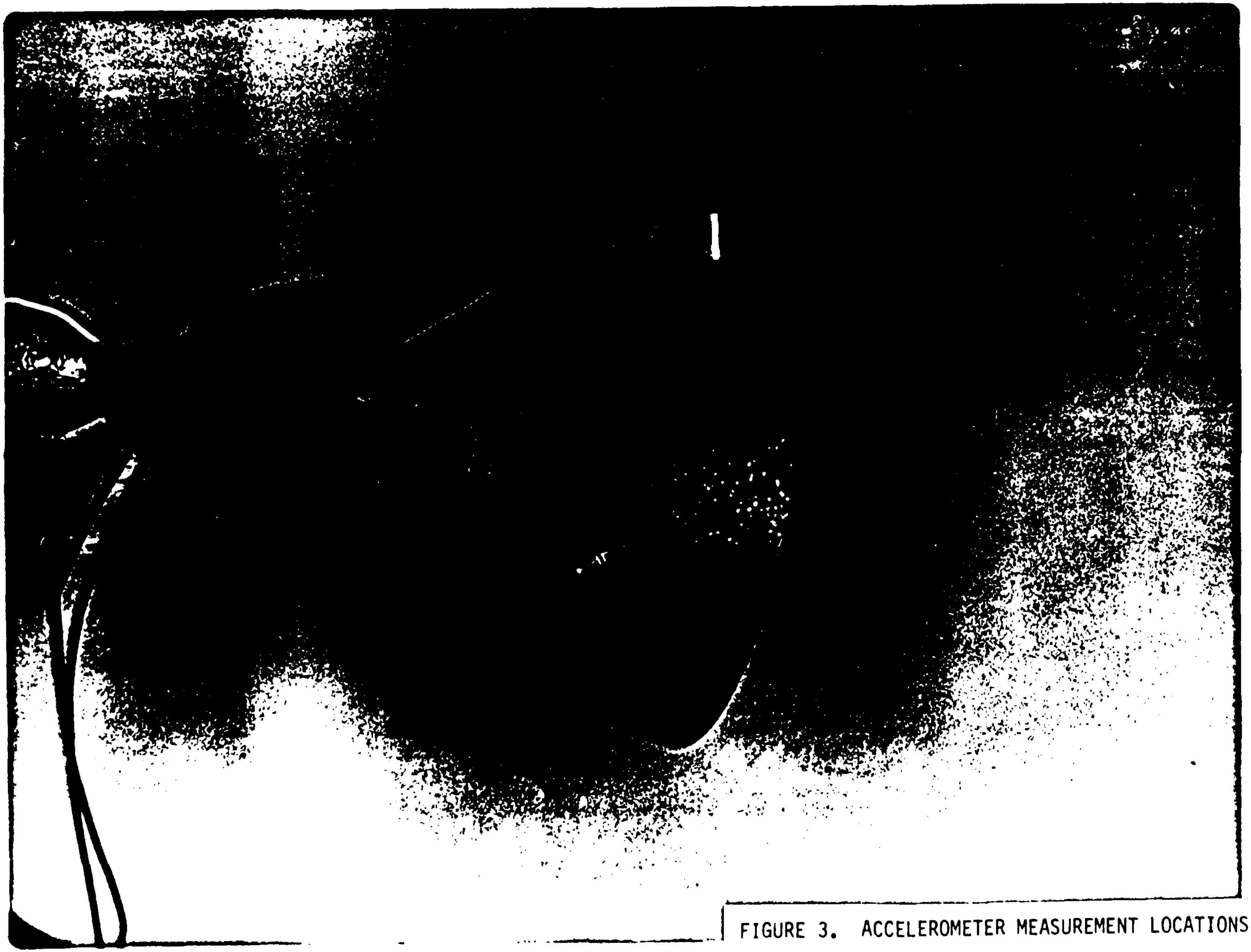


FIGURE 3. ACCELEROMETER MEASUREMENT LOCATIONS

ADVANCED 14# Z AXIS
VIBRATION 2/27/81

APPENDIX A:

MATERIAL PROPERTIES

Aerojet
TechSystems
Company

Internal Memo

24 January 1990
9990:R&T:2797

To: A. J. Farahyar

From: M. L. Gage

Subject: Vibration Analysis of 14 lbF Chamber

Copies to: Len Schoenman, Sandy Rosenberg, Walt Langhi

At our introduction yesterday we discussed the objectives of the 14 lbF Ir/Re chamber program. We are undertaking the vibration analysis of this chamber to determine important design parameters for a chamber which will pass current qualification vibration requirements, namely, (1) skirt thickness and material selection and (2) front end external support requirements. To establish answers to these design issues, I anticipate that three iterations of modeling and dynamic analysis will be required. This memorandum presents the ground rules to be used for the first case of the vibration analysis.

1. Chamber Geometry

The chamber geometry to be used for the first case is shown on attached drawing 1204474, with two changes:
(1) the length from the front of the chamber to the chamber throat will be 1.912" and (2) the wall thickness of the chamber will be 0.014" in the region from x = 0.769" to the end of the nozzle.

The conceptual layout of the front end of the chamber is as shown in Figure 1. I anticipate that additional structural support will be required in the front to take the stress off the platinum. I anticipate that this first analysis will estimate the loads which must be accomodated. Subsequent interations of the analysis will establish the effectiveness of front end support solutions.

2. Material Properties

Assume the following room temperature material properties:

(1) Rhenium

Modulus of Elasticity	65,000,000 psi
Density	1.966e-3 lb-s^2/in^4
Ultimate Strength	170,000 psi
Yield Strength	55,000 psi

(2) Platinum

Modulus of Elasticity	21,000,000 psi

APPENDIX B:

STRAIN GAGE DATA REDUCTION

2/28/91

Don -

A few Notes:

S.G. 1 and 2 ~~too~~ Looked like 3 and 4 (1=3,
but they were noisier due to lower
signal level (gain onto the tape) - so I
only plotted 3 and 4.

The analyser apparently couldn't do the
~~convers~~ scaling to ~~με~~ %ε so I did με instead
Be sure to look at the scale (Y) for
each plot since they might differ.

Each plot is marked with ~~the~~ the vibration
axis and plot parameter



There is a blip @ about 3 kHz —
I don't know if it is real or an
artifact of running the tape @ 15 ips.
You might ask Konrad if you want to know -
SATPROP never looks beyond 2500 Hz so that
won't shed any light on the subject.

Russ

mV/με settings

Z axis

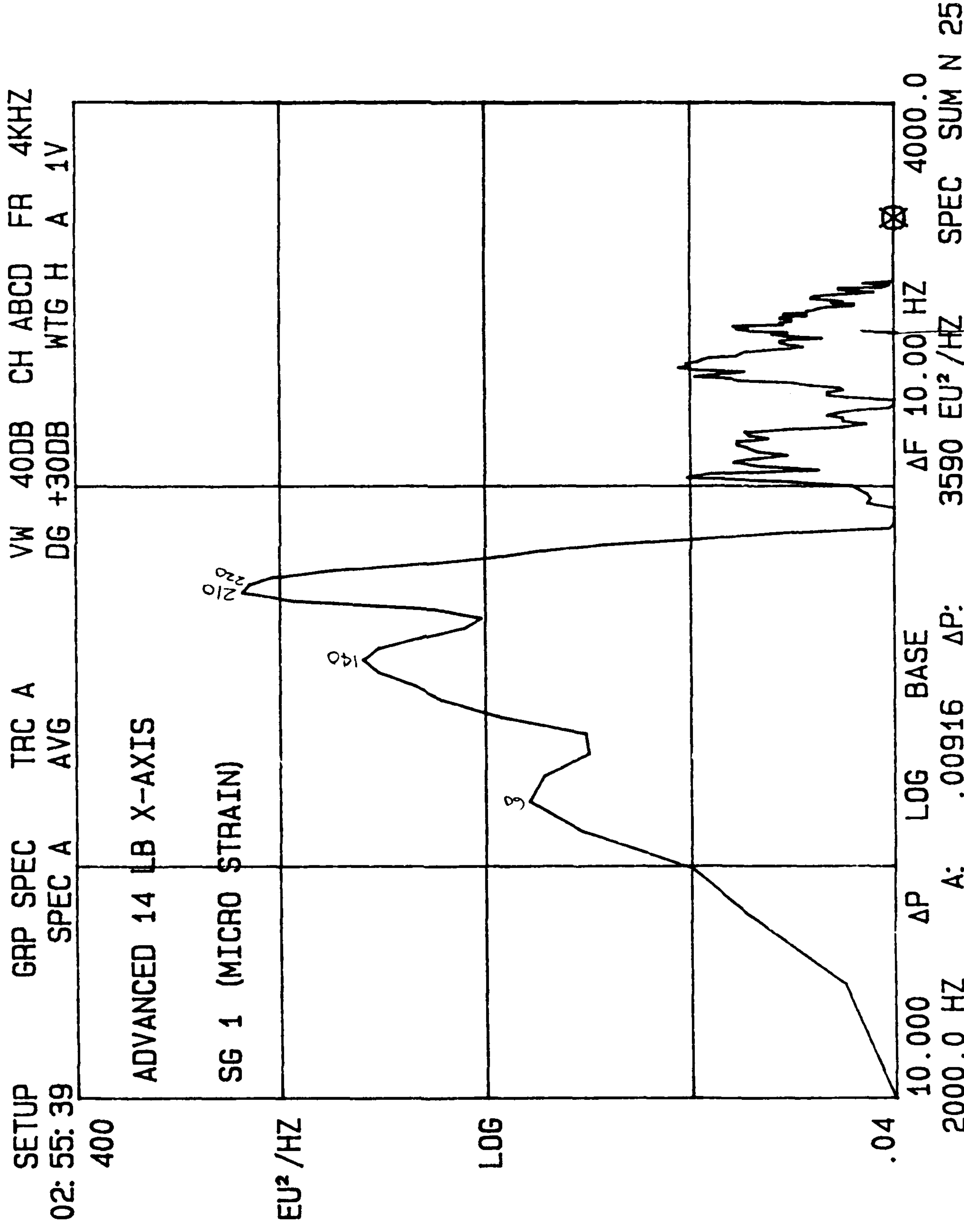
SG	1	.1053
	2	.1053
	3	1.053
	4	1.053

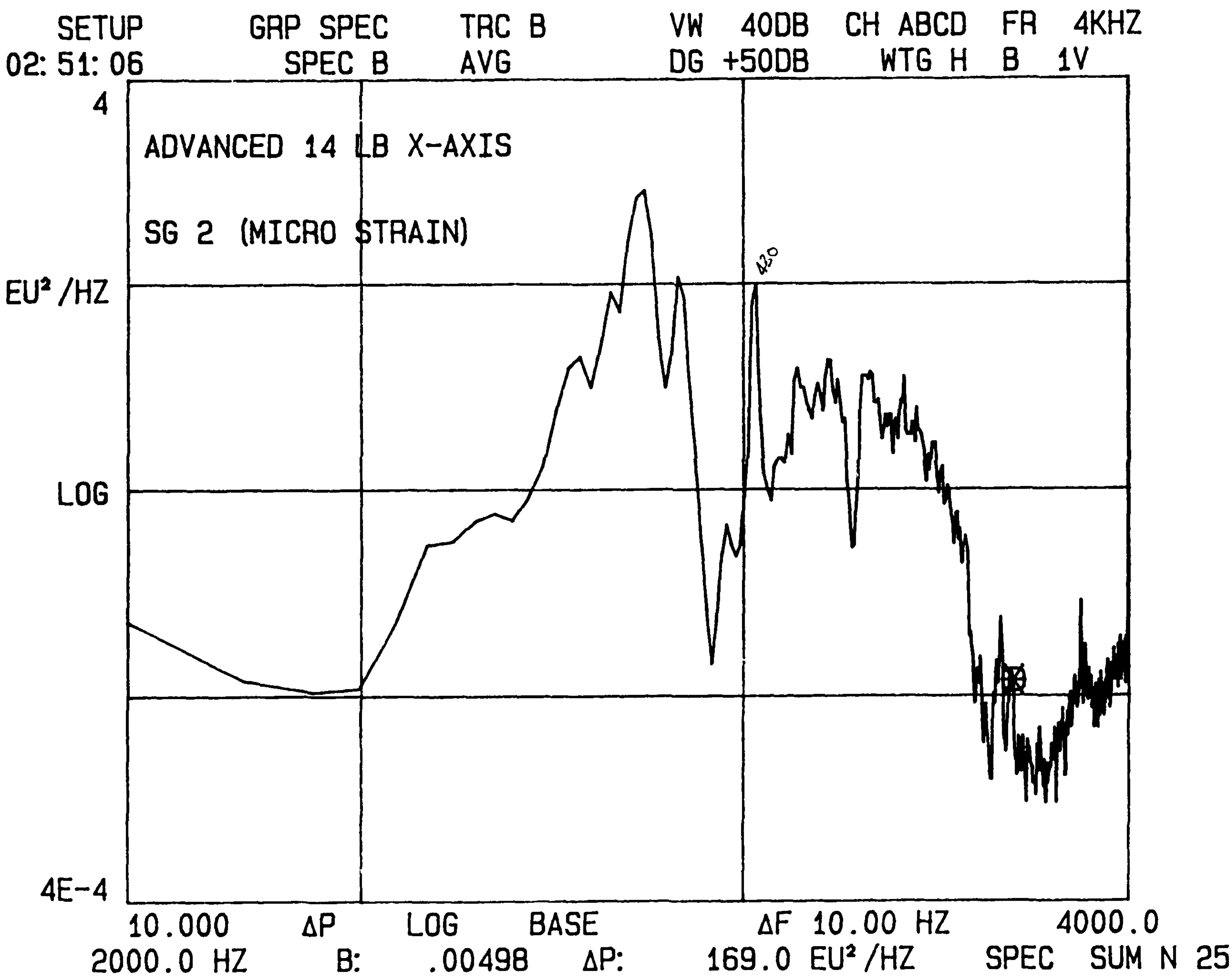
Y-axis

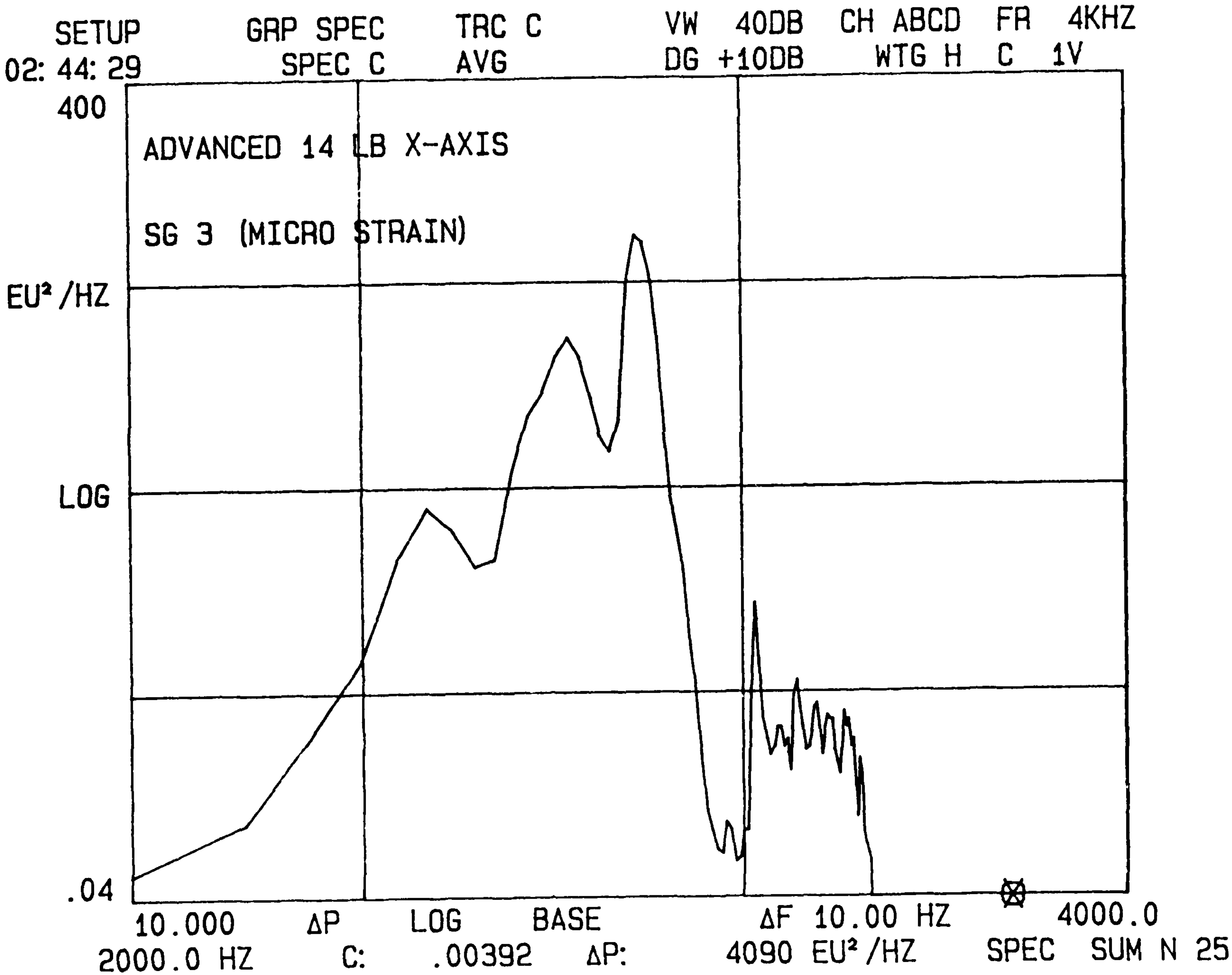
S.G.	1	.1053
	2	.1053
	3	1.053
	4	1.053

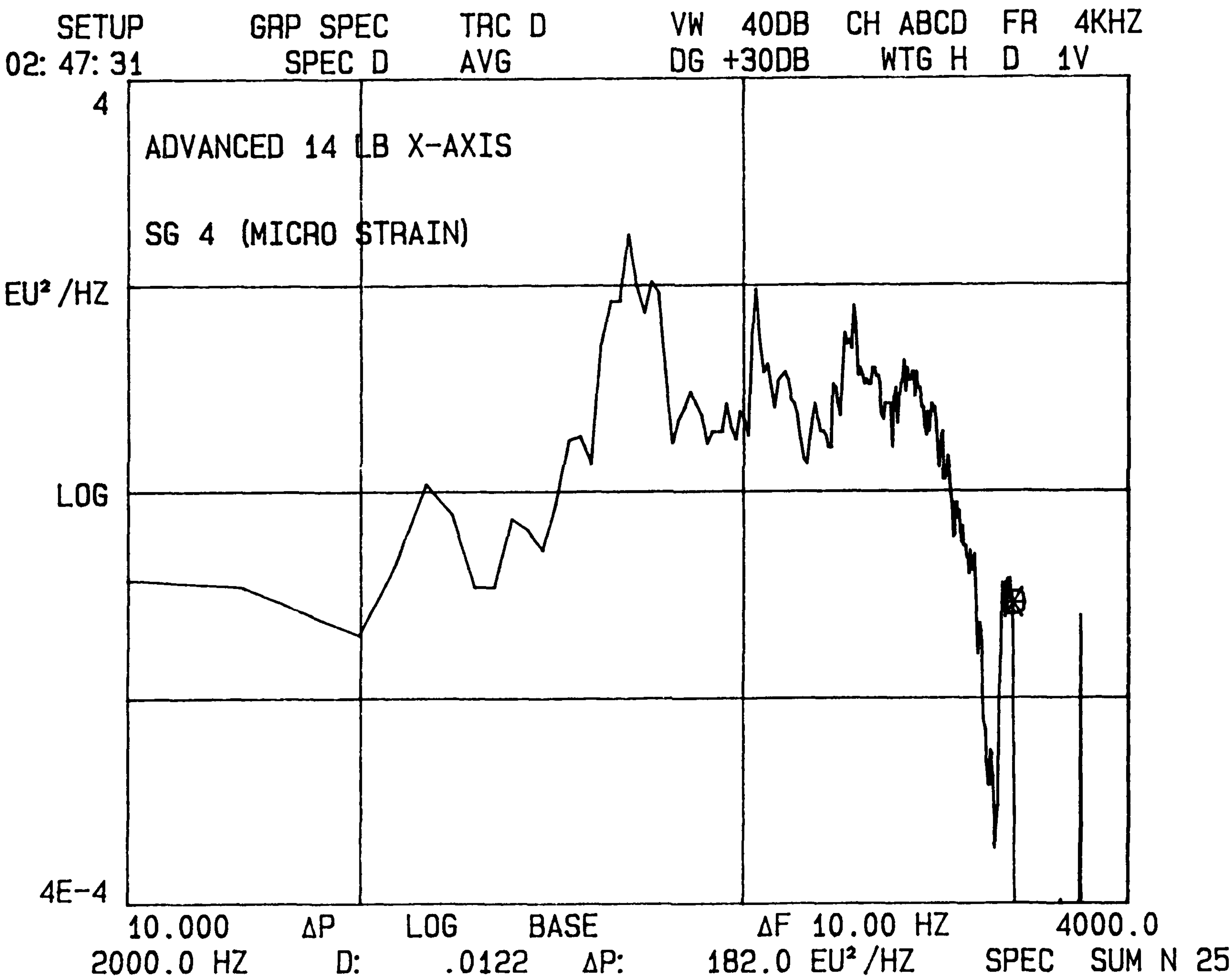
X-axis

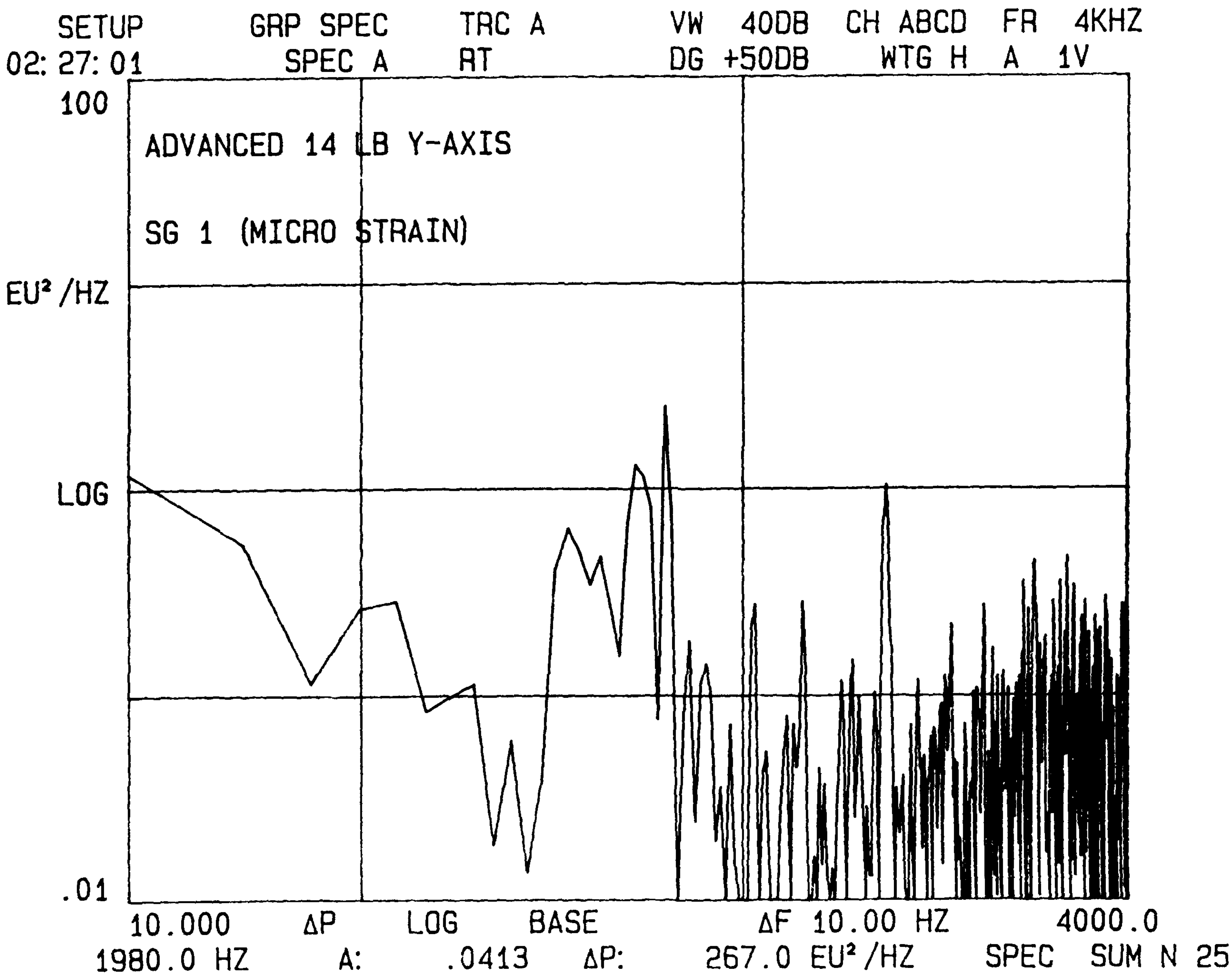
S.G	1	.5265
	2	.5265
	3	5.265
	4	5.265

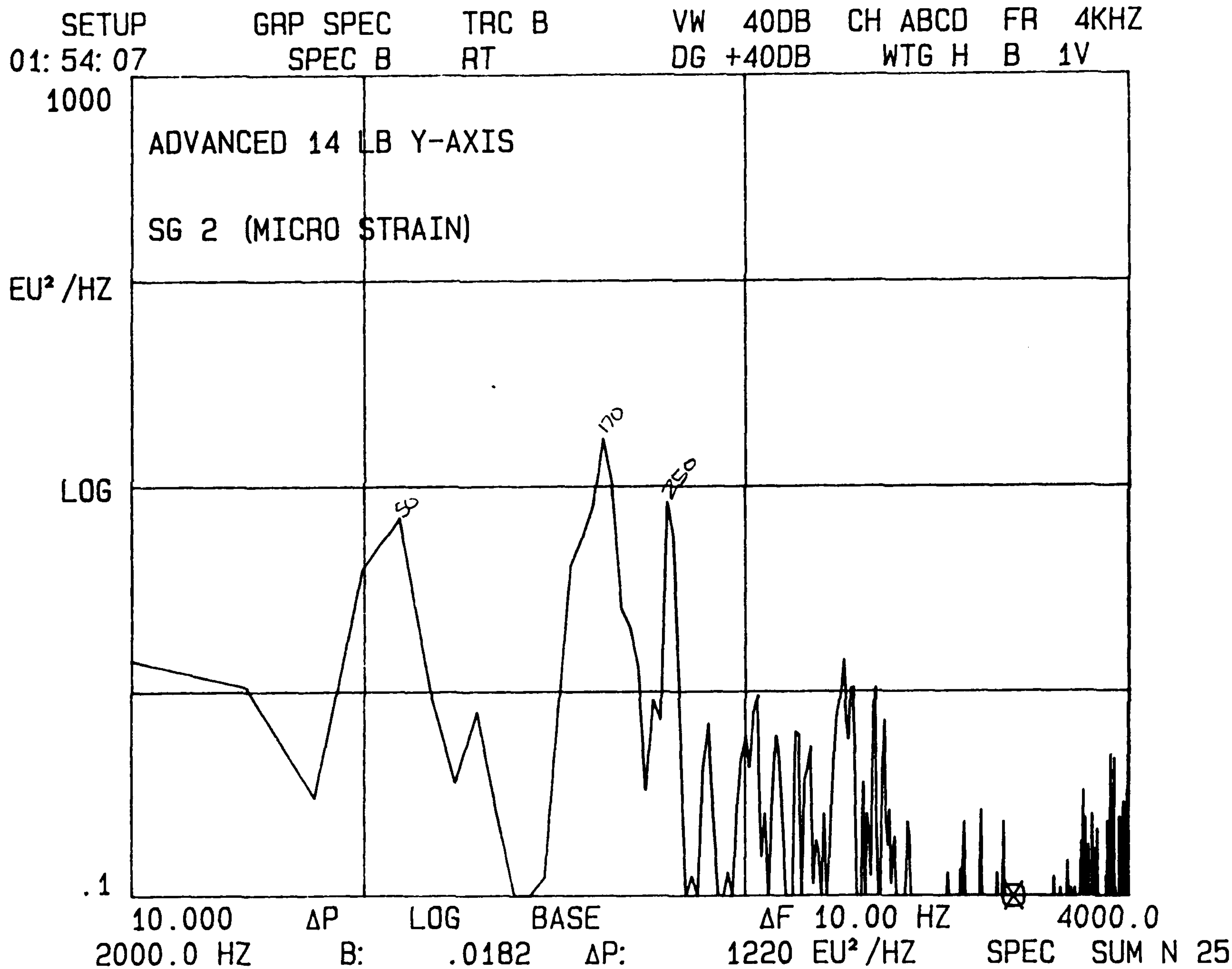

SETUP GRP SPEC TRC A VW 40DB CH ABCD FR 4KHZ
02:55:39 SPEC A AVG DG +30DB WTG H A 1V
ADVANCED 14 LB X-AXIS
SG 1 (MICRO STRAIN)
400
EU²/HZ
LOG
.04
210
220
140
10.000 ΔP LOG BASE ΔF 10.00 HZ 4000.0
2000.0 HZ A: .00916 ΔP: 3590 EU²/HZ SPEC SUM N 25

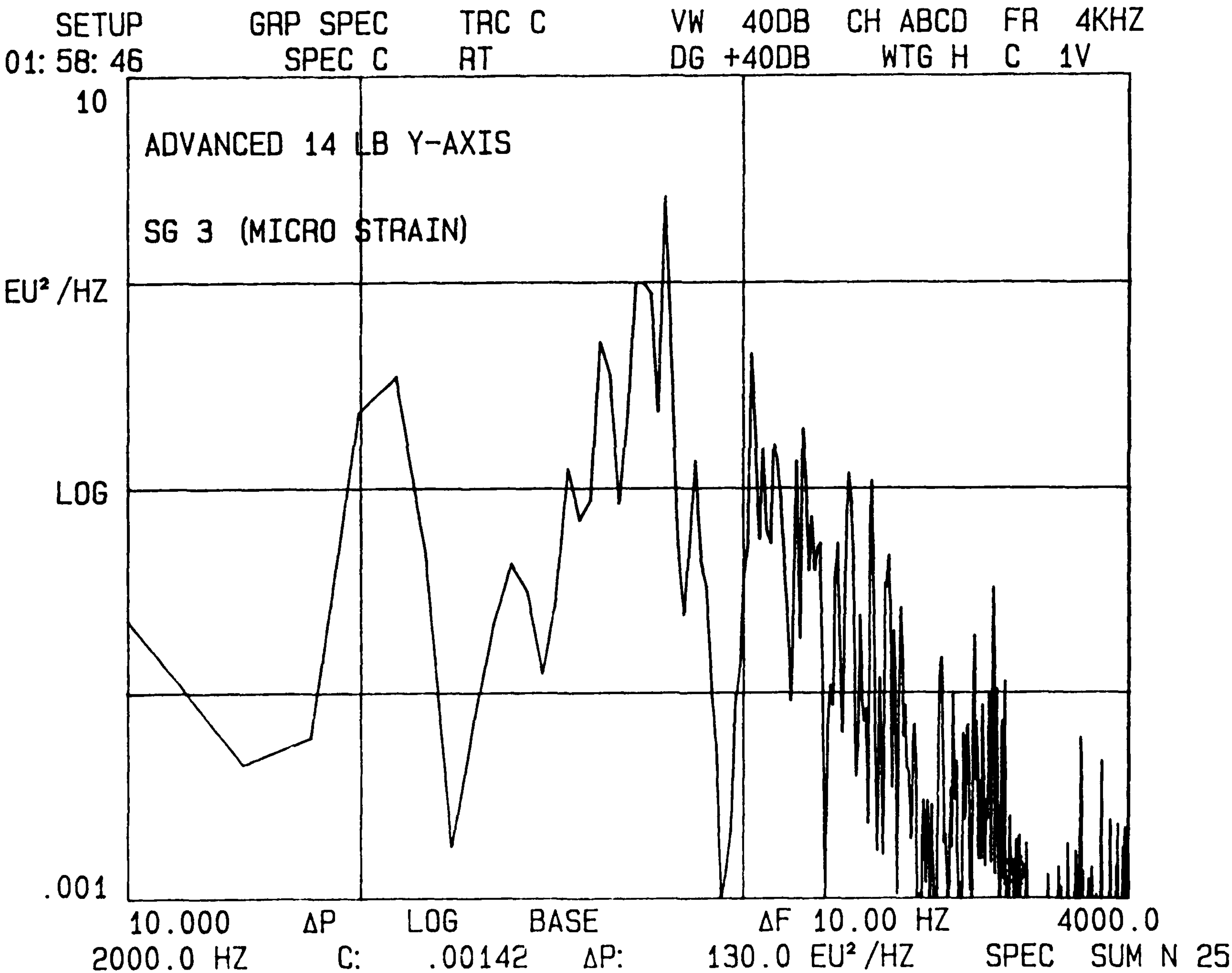

SETUP
02: 51: 06
GRP SPEC
SPEC B
TRC B
AVG
VW 40DB
DG +50DB
CH ABCD
WTG H
FR 4KHZ
B 1V
4
EU²/HZ
LOG
4E-4
ADVANCED 14 LB X-AXIS
SG 2 (MICRO STRAIN)
420
10.000
2000.0 HZ
ΔP
B:
LOG
.00498
BASE
ΔP:
ΔF 10.00 HZ
169.0 EU²/HZ
4000.0
SPEC
SUM N 25

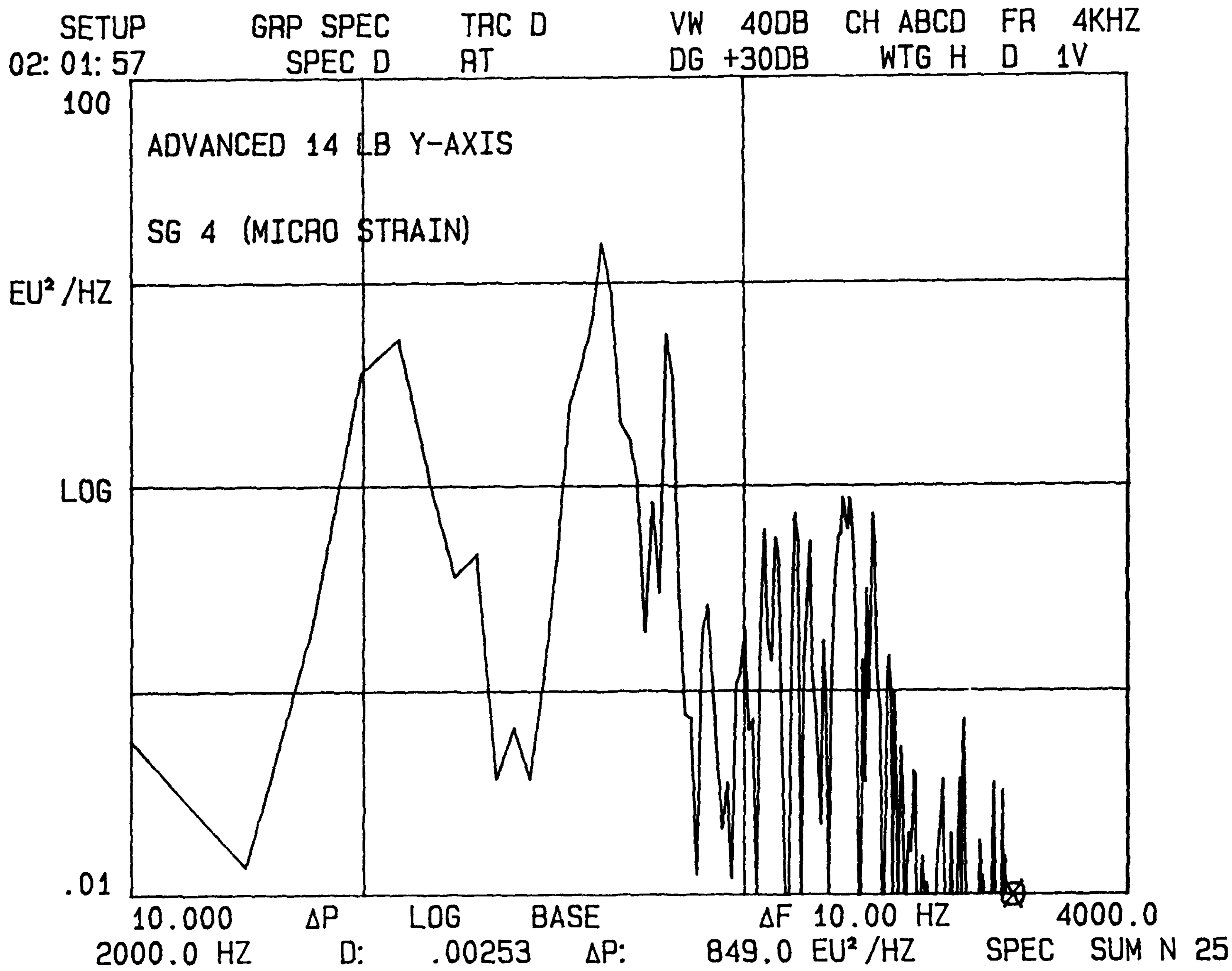

SETUP
02: 44: 29
GRP SPEC
SPEC C
TRC C
AVG
VW 40DB
DG +10DB
CH ABCD
WTG H
FR 4KHZ
C 1V
400
ADVANCED 14 LB X-AXIS
SG 3 (MICRO STRAIN)
EU²/HZ
LOG
.04
10.000
2000.0 HZ
ΔP
C:
LOG
.00392
BASE
ΔP:
ΔF 10.00 HZ
4090 EU²/HZ
4000.0
SPEC SUM N 25


SETUP
02: 47: 31
GRP SPEC
SPEC D
TRC D
AVG
VW 40DB
DG +30DB
CH ABCD
WTG H
FR 4KHZ
D 1V
4
EU² /HZ
LOG
4E-4
ADVANCED 14 LB X-AXIS
SG 4 (MICRO STRAIN)
10.000
2000.0 HZ
ΔP
D:
LOG
.0122
BASE
ΔP:
ΔF 10.00 HZ
182.0 EU² /HZ
4000.0
SPEC SUM N 25

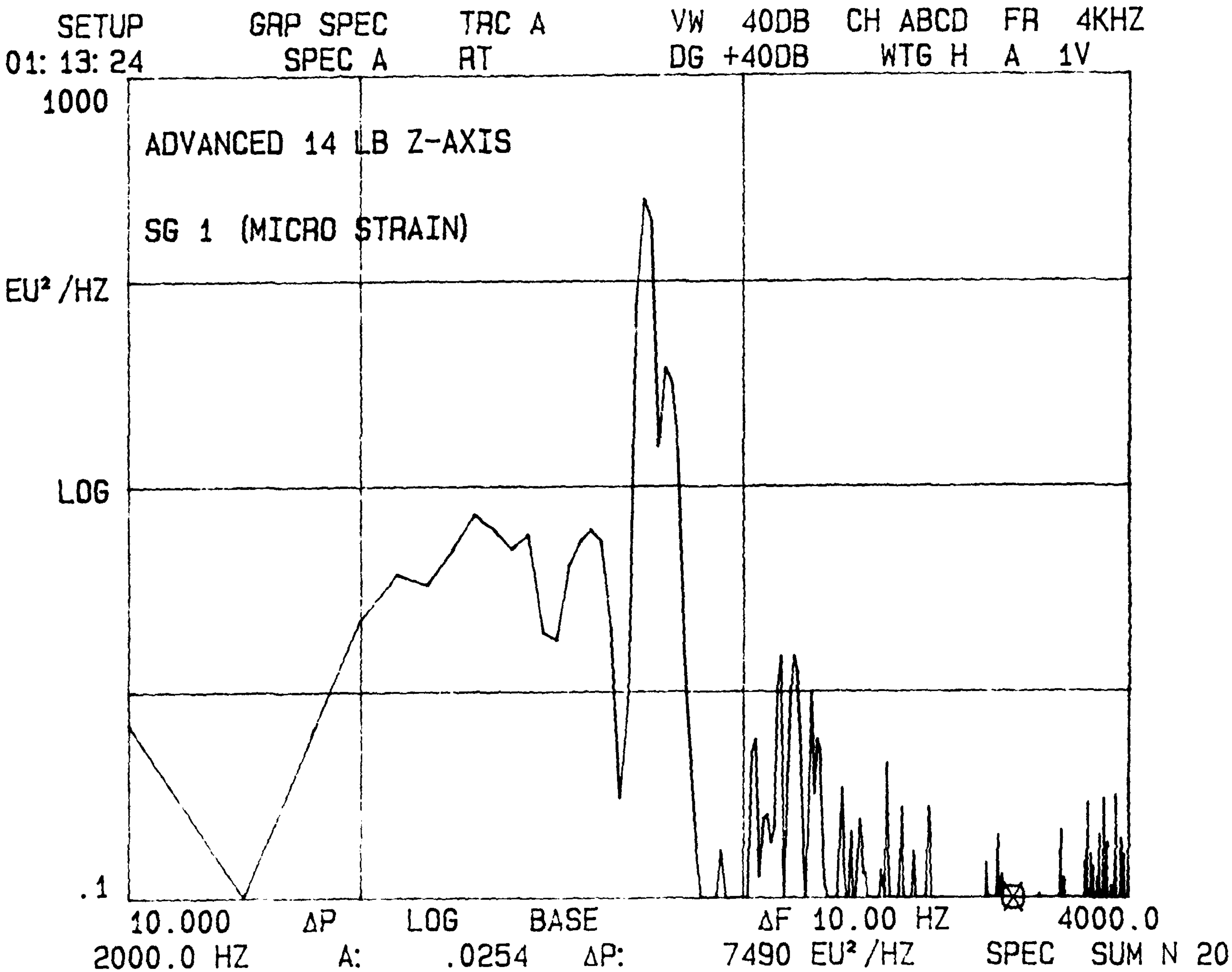

SETUP
02: 27: 01
GRP SPEC
SPEC A
TRC A
RT
VW 40DB
DG +50DB
CH ABCD
WTG H
FR 4KHZ
A 1V
100
ADVANCED 14 LB Y-AXIS
SG 1 (MICRO STRAIN)
EU² /HZ
LOG
.01
10.000
ΔP
LOG
BASE
ΔF 10.00 HZ
4000.0
1980.0 HZ
A:
.0413
ΔP:
267.0 EU² /HZ
SPEC
SUM N 25

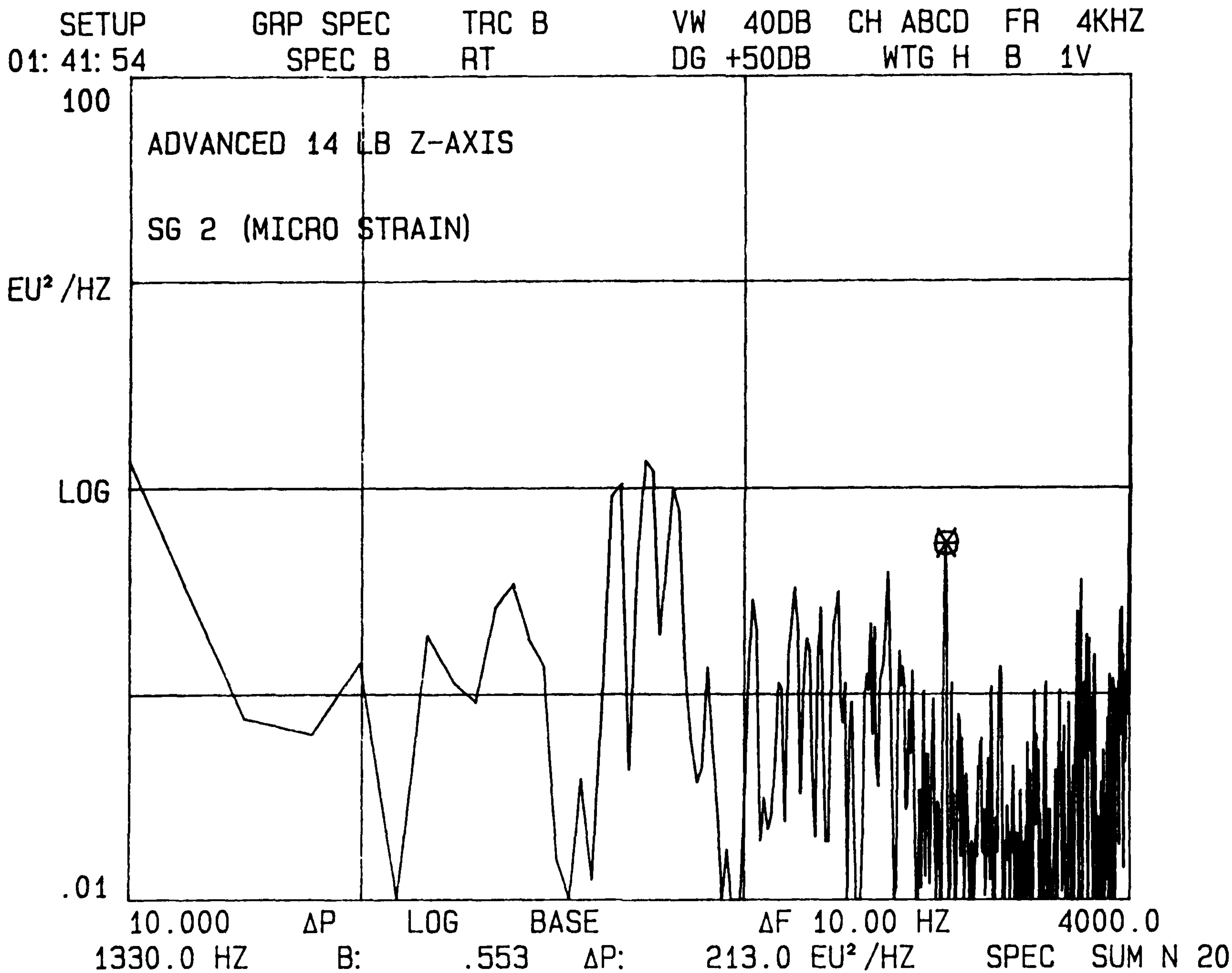

SETUP GRP SPEC TRC B VW 40DB CH ABCD FR 4KHZ
01:54:07 SPEC B RT DG +40DB WTG H B 1V
1000
ADVANCED 14 LB Y-AXIS
SG 2 (MICRO STRAIN)
EU²/HZ
LOG
.1
50
170
250
10.000 ΔP LOG BASE ΔF 10.00 HZ 4000.0
2000.0 HZ B: .0182 ΔP: 1220 EU²/HZ SPEC SUM N 25

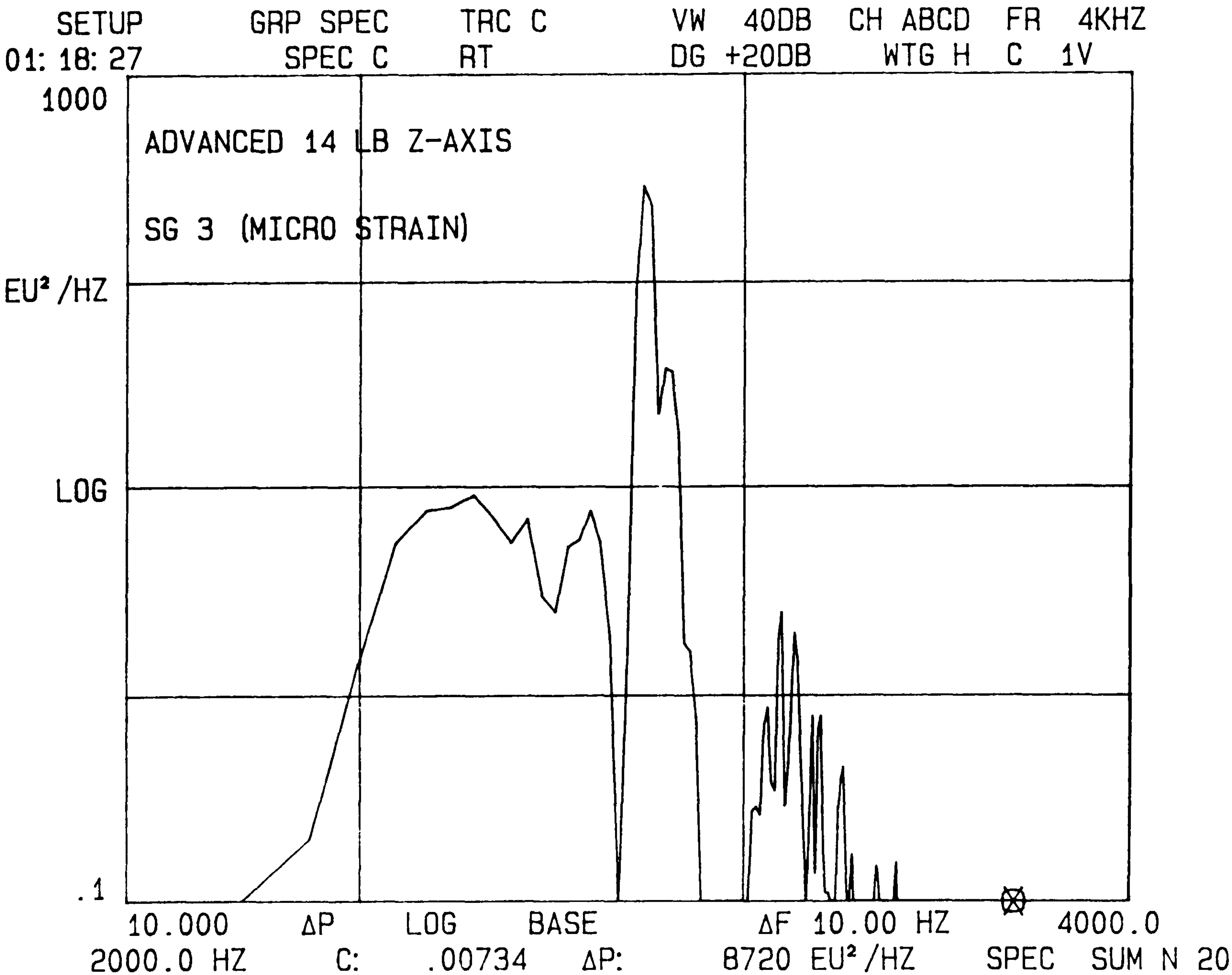

SETUP
01: 58: 46
GRP SPEC
SPEC C
TRC C
RT
VW 40DB
DG +40DB
CH ABCD
WTG H
FR 4KHZ
C 1V
10
ADVANCED 14 LB Y-AXIS
SG 3 (MICRO STRAIN)
EU² /HZ
LOG
.001
10.000
2000.0 HZ
ΔP
C:
LOG
.00142
BASE
ΔP:
ΔF 10.00 HZ
130.0 EU² /HZ
4000.0
SPEC SUM N 25



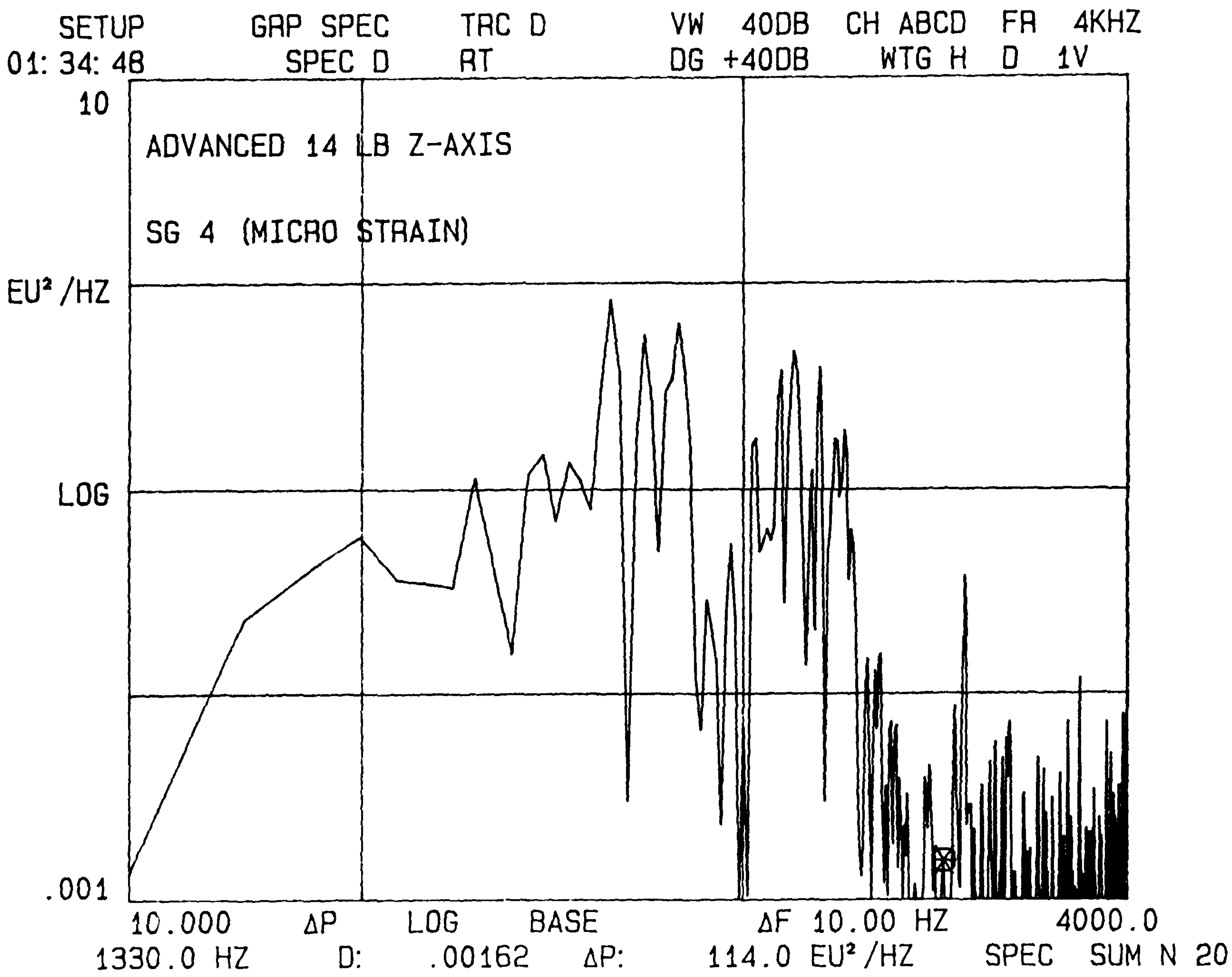
SETUP GRP SPEC TRC D VW 40DB CH ABCD FR 4KHZ
02: 01: 57 SPEC D RT DG +30DB WTG H D 1V
100
ADVANCED 14 LB Y-AXIS
SG 4 (MICRO STRAIN)
EU²/HZ
LOG
.01
10.000 ΔP LOG BASE ΔF 10.00 HZ 4000.0
2000.0 HZ D: .00253 ΔP: 849.0 EU²/HZ SPEC SUM N 25

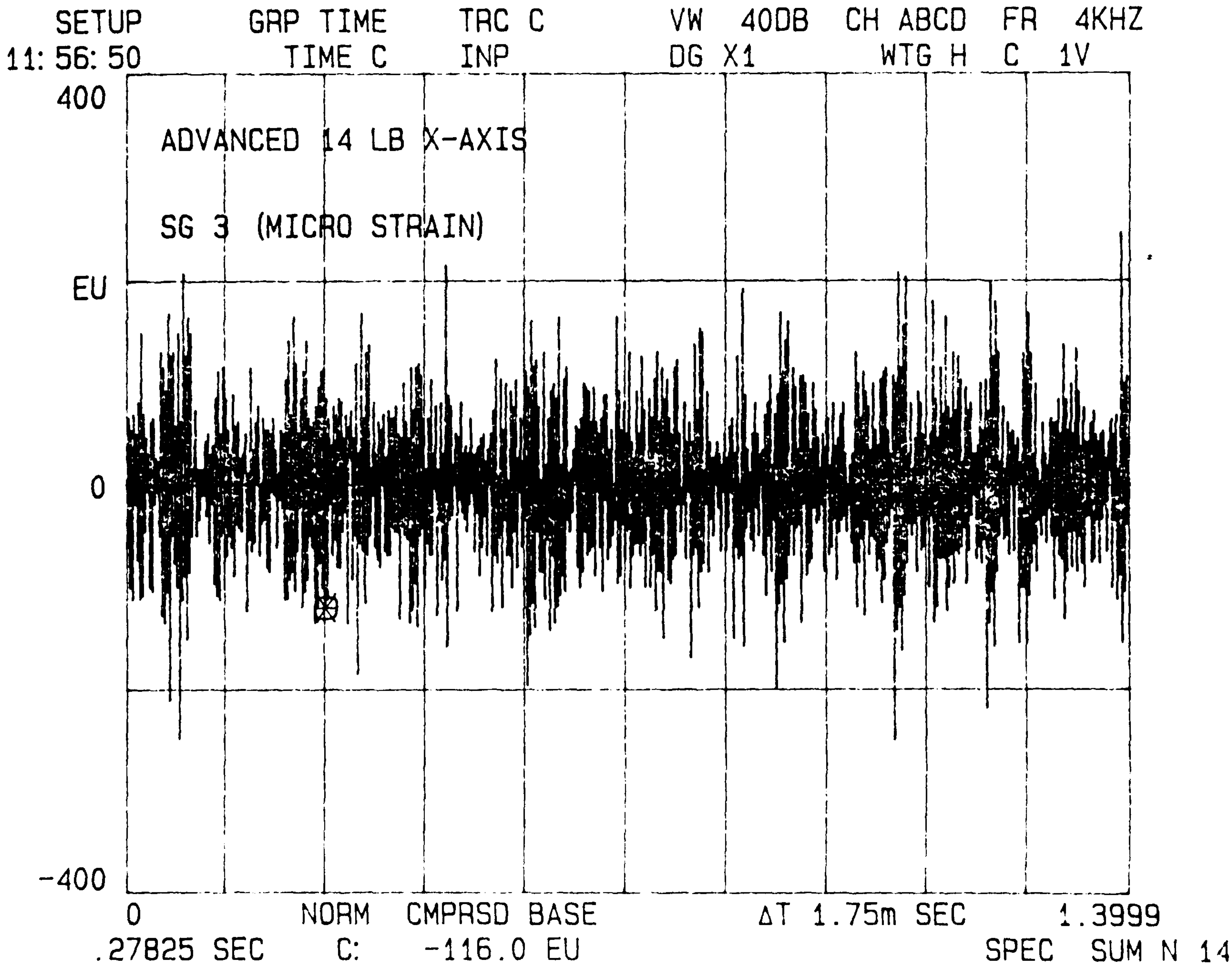

SETUP
01: 13: 24
GRP SPEC
SPEC A
TRC A
RT
VW 40DB
DG +40DB
CH ABCD
WTG H
FR 4KHZ
A 1V
1000
ADVANCED 14 LB Z-AXIS
SG 1 (MICRO STRAIN)
EU²/HZ
LOG
.1
10.000
2000.0 HZ
ΔP
A:
LOG
.0254
BASE
ΔP:
ΔF 10.00 HZ
7490 EU²/HZ
4000.0
SPEC
SUM N 20


SETUP
01: 41: 54
GRP SPEC
SPEC B
TRC B
RT
VW 40DB
DG +50DB
CH ABCD
WTG H
FR 4KHZ
B 1V
100
EU² /HZ
LOG
.01
ADVANCED 14 LB Z-AXIS
SG 2 (MICRO STRAIN)
10.000
1330.0 HZ
ΔP
B:
LOG
.553
BASE
ΔP:
ΔF 10.00 HZ
213.0 EU² /HZ
4000.0
SPEC SUM N 20

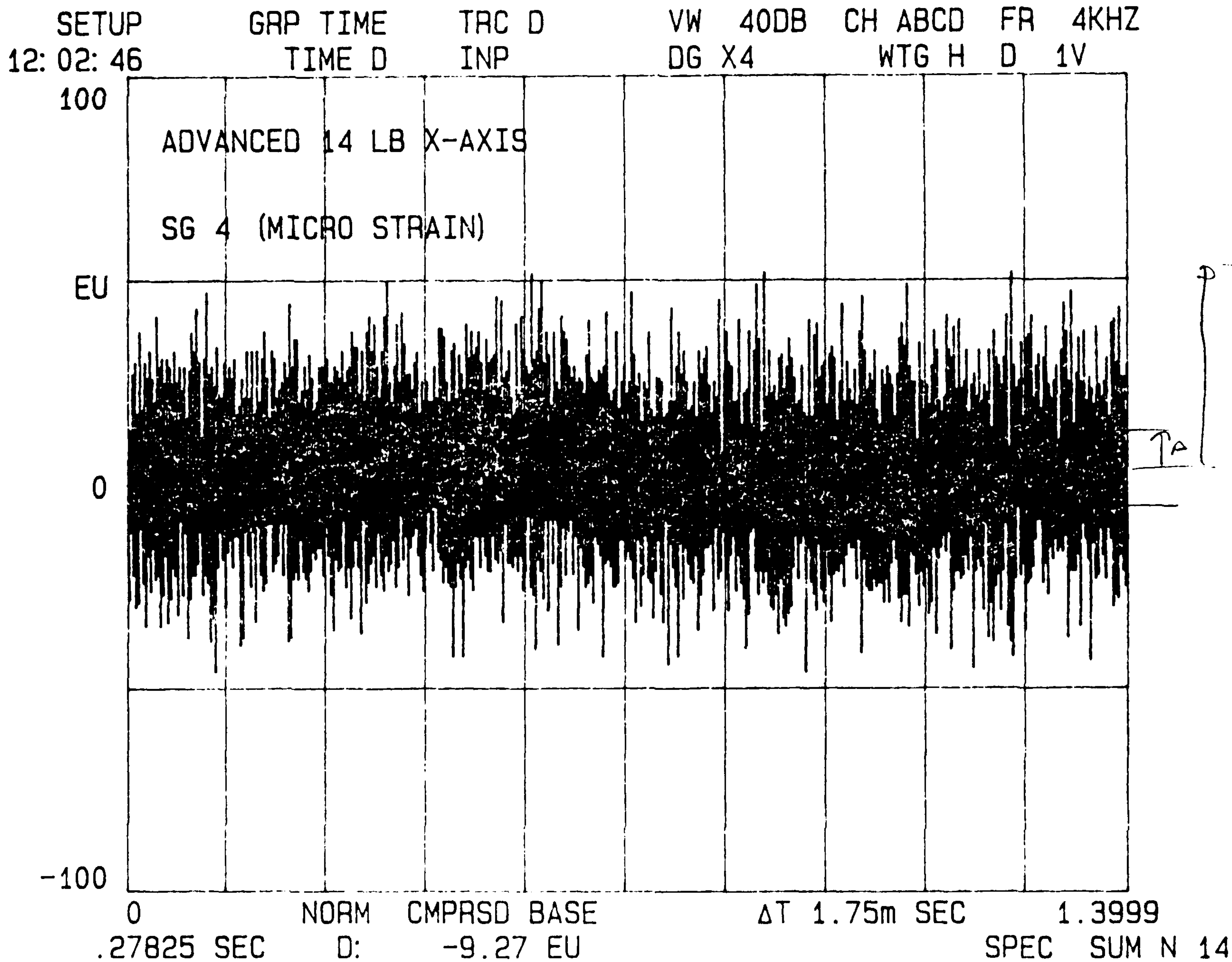


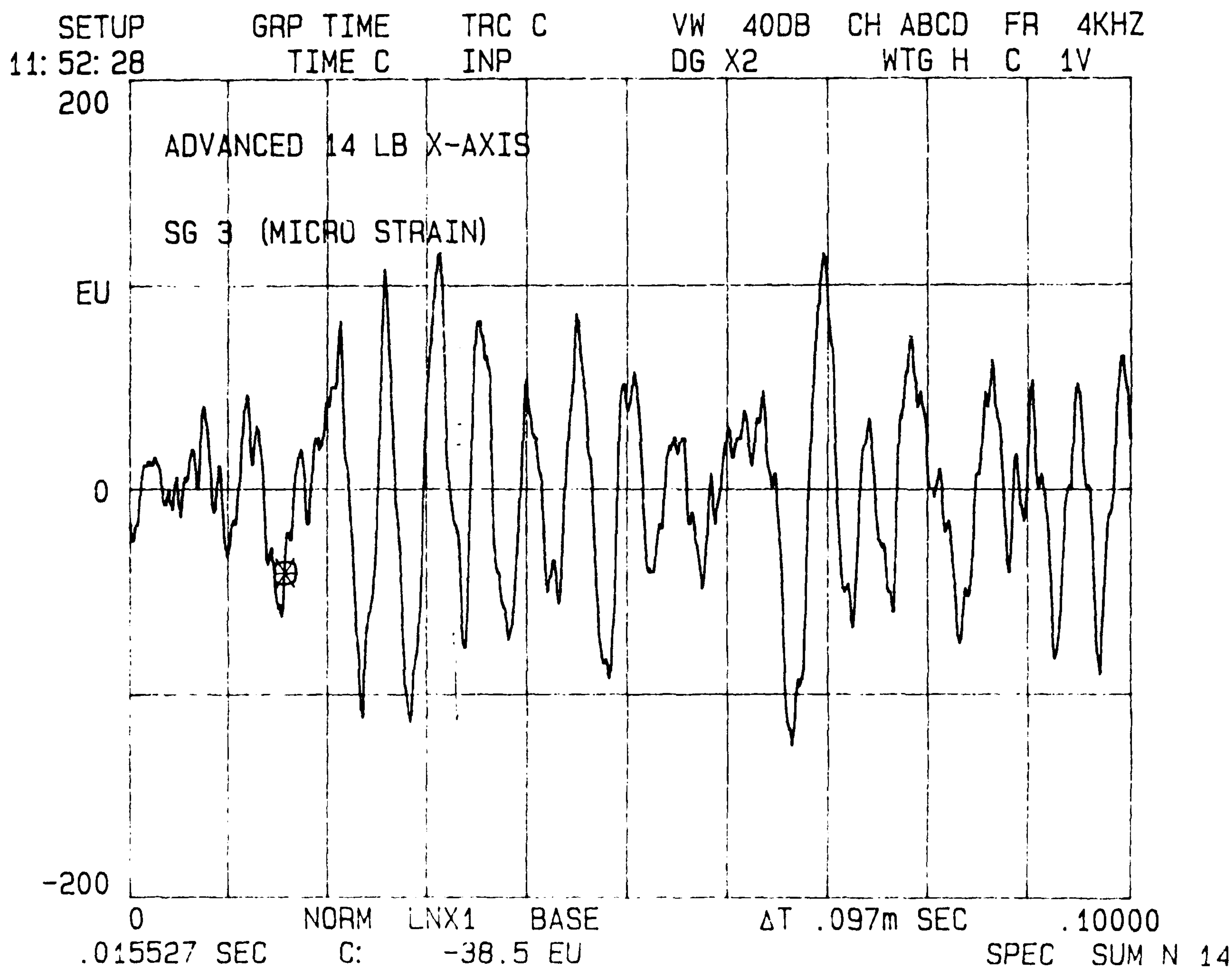
SETUP
01: 18: 27
GRP SPEC
SPEC C
TRC C
RT
VW 40DB
DG +20DB
CH ABCD
WTG H
FR 4KHZ
C 1V
1000
EU²/HZ
LOG
.1
ADVANCED 14 LB Z-AXIS
SG 3 (MICRO STRAIN)
10.000
ΔP
LOG
BASE
ΔF 10.00 HZ
4000.0
2000.0 HZ
C:
.00734
ΔP:
8720 EU²/HZ
SPEC
SUM N 20

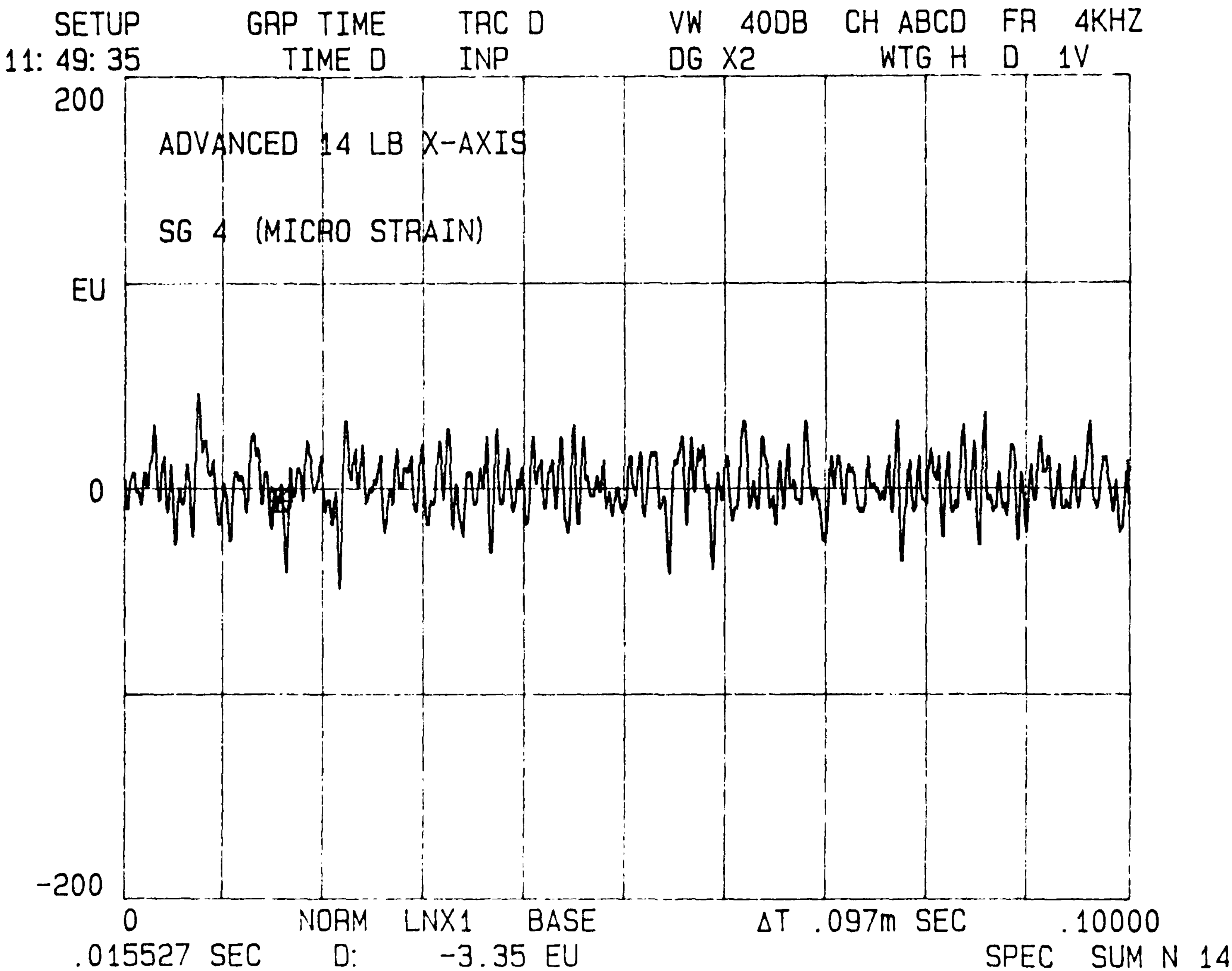

SETUP
01: 34: 48
GRP SPEC
SPEC D
TRC D
RT
VW 40DB
DG +40DB
CH ABCD
WTG H
FR 4KHZ
D 1V
10
ADVANCED 14 LB Z-AXIS
SG 4 (MICRO STRAIN)
EU² /HZ
LOG
.001
10.000
ΔP
LOG
BASE
ΔF 10.00 HZ
4000.0
1330.0 HZ
D:
.00162
ΔP:
114.0 EU² /HZ
SPEC
SUM N 20

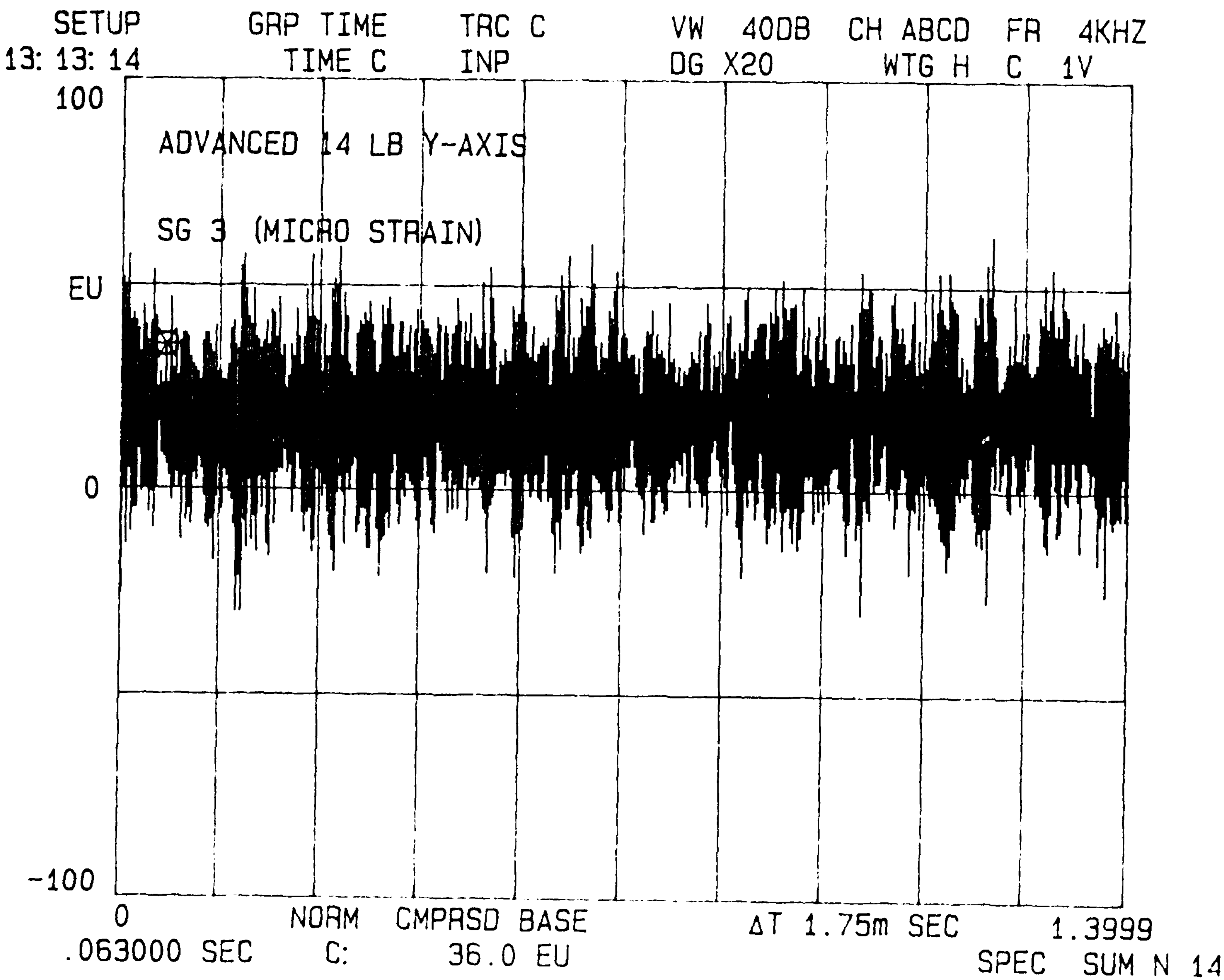


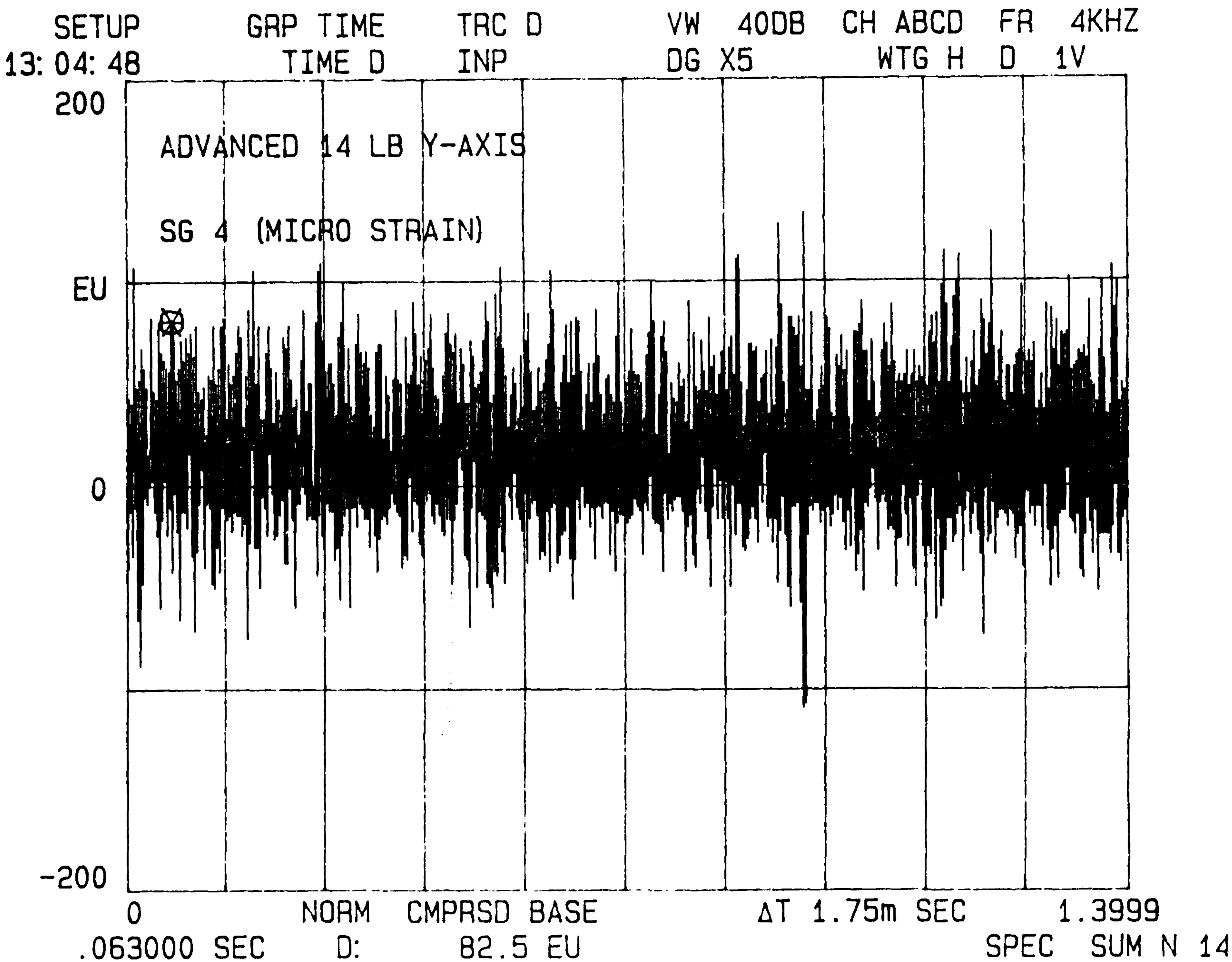
SETUP
11: 56: 50
GRP TIME
TIME C
TRC C
INP
VW 40DB
DG X1
CH ABCD
WTG H
FR 4KHZ
C 1V
400
ADVANCED 14 LB X-AXIS
SG 3 (MICRO STRAIN)
EU
0
-400
0
NORM CMPRSD BASE
ΔT 1.75m SEC
1.3999
.27825 SEC
C: -116.0 EU
SPEC SUM N 14


SETUP
12: 02: 46
GRP TIME
TIME D
TRC D
INP
VW 40DB
DG X4
CH ABCD
WTG H
FR 4KHZ
D 1V
100
EU
0
-100
ADVANCED 14 LB X-AXIS
SG 4 (MICRO STRAIN)
0
.27825 SEC
NORM
D:
CMPRSD BASE
-9.27 EU
ΔT 1.75m SEC
1.3999
SPEC SUM N 14

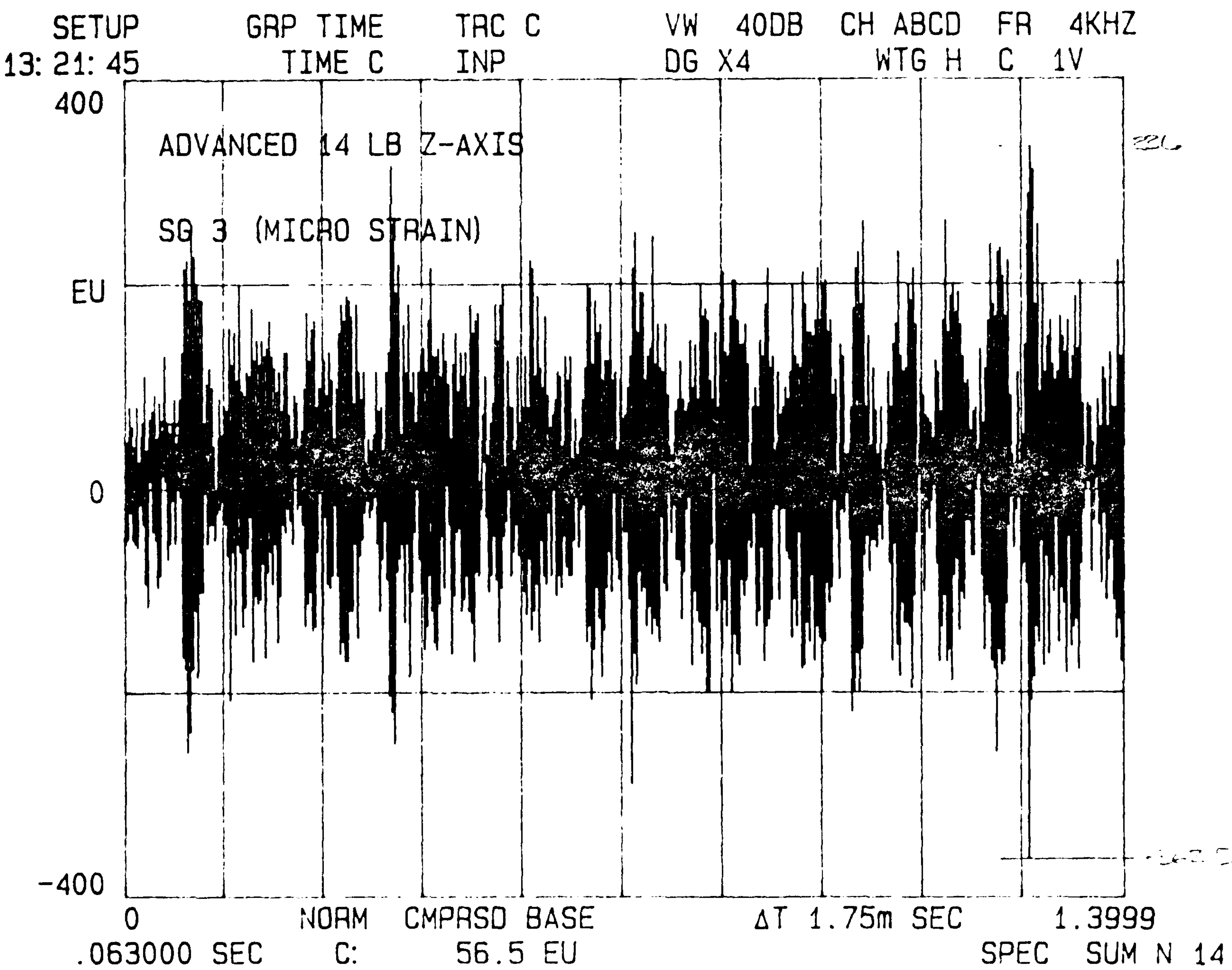

SETUP
11: 52: 28
GRP TIME
TIME C
TRC C
INP
VW 40DB
DG X2
CH ABCD
WTG H
FR 4KHZ
C 1V
200
EU
0
-200
ADVANCED 14 LB X-AXIS
SG 3 (MICRO STRAIN)
0
.015527 SEC
NORM
C:
LNX1
-38.5 EU
BASE
ΔT .097m SEC
.10000
SPEC SUM N 14

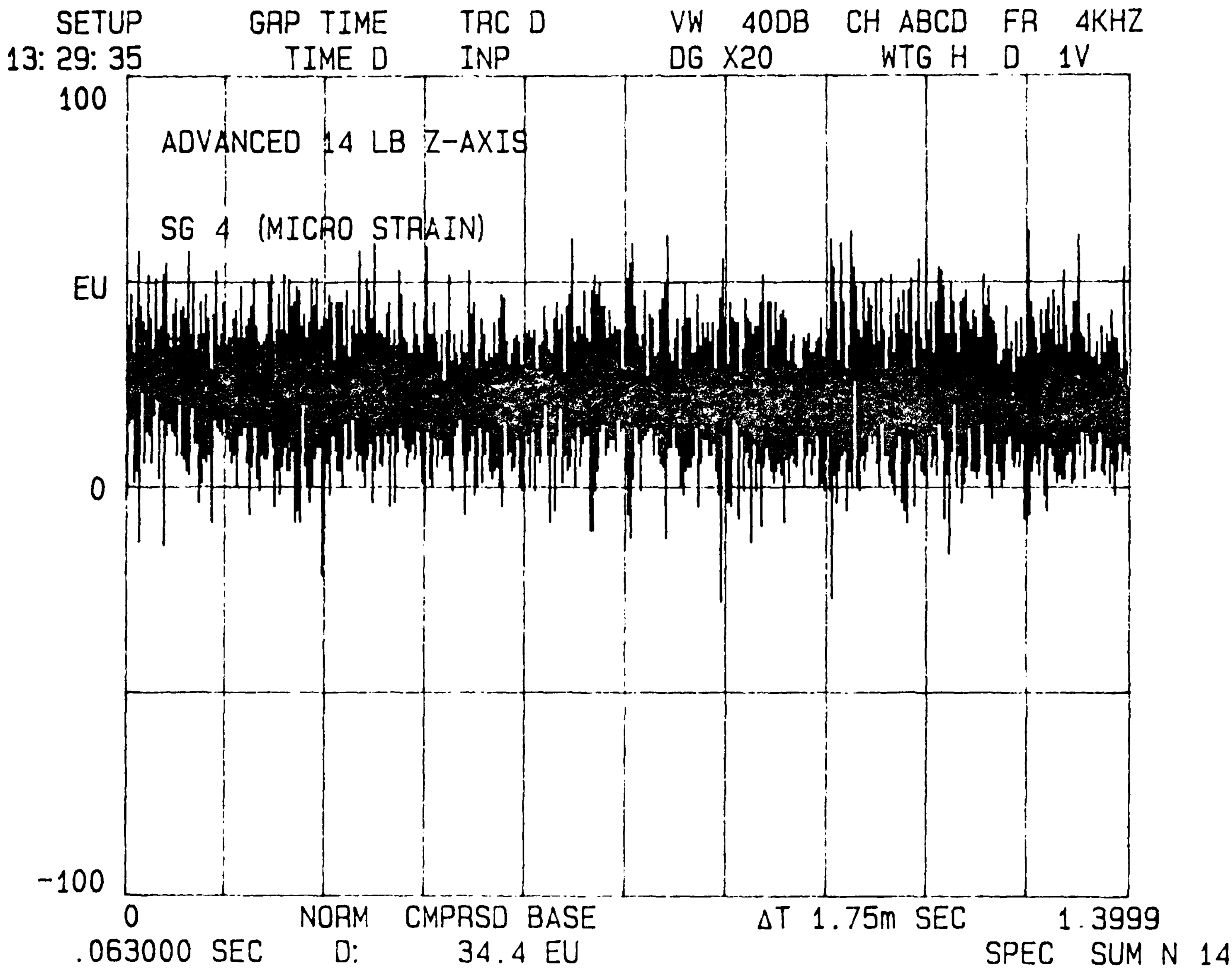

SETUP
11: 49: 35
GRP TIME
TIME D
TRC D
INP
VW 40DB
DG X2
CH ABCD
WTG H
FR 4KHZ
D 1V
200
ADVANCED 14 LB X-AXIS
SG 4 (MICRO STRAIN)
EU
0
-200
0
.015527 SEC
NORM LNX1 BASE
D: -3.35 EU
ΔT .097m SEC
.10000
SPEC SUM N 14


SETUP
13: 13: 14
GRP TIME
TIME C
TRC C
INP
VW 40DB
DG X20
CH ABCD
WTG H
FR 4KHZ
C 1V
ADVANCED 14 LB Y-AXIS
SG 3 (MICRO STRAIN)
100
EU
0
-100
0
.063000 SEC
NORM
C:
CMPRSD BASE
36.0 EU
ΔT 1.75m SEC
1.3999
SPEC SUM N 14



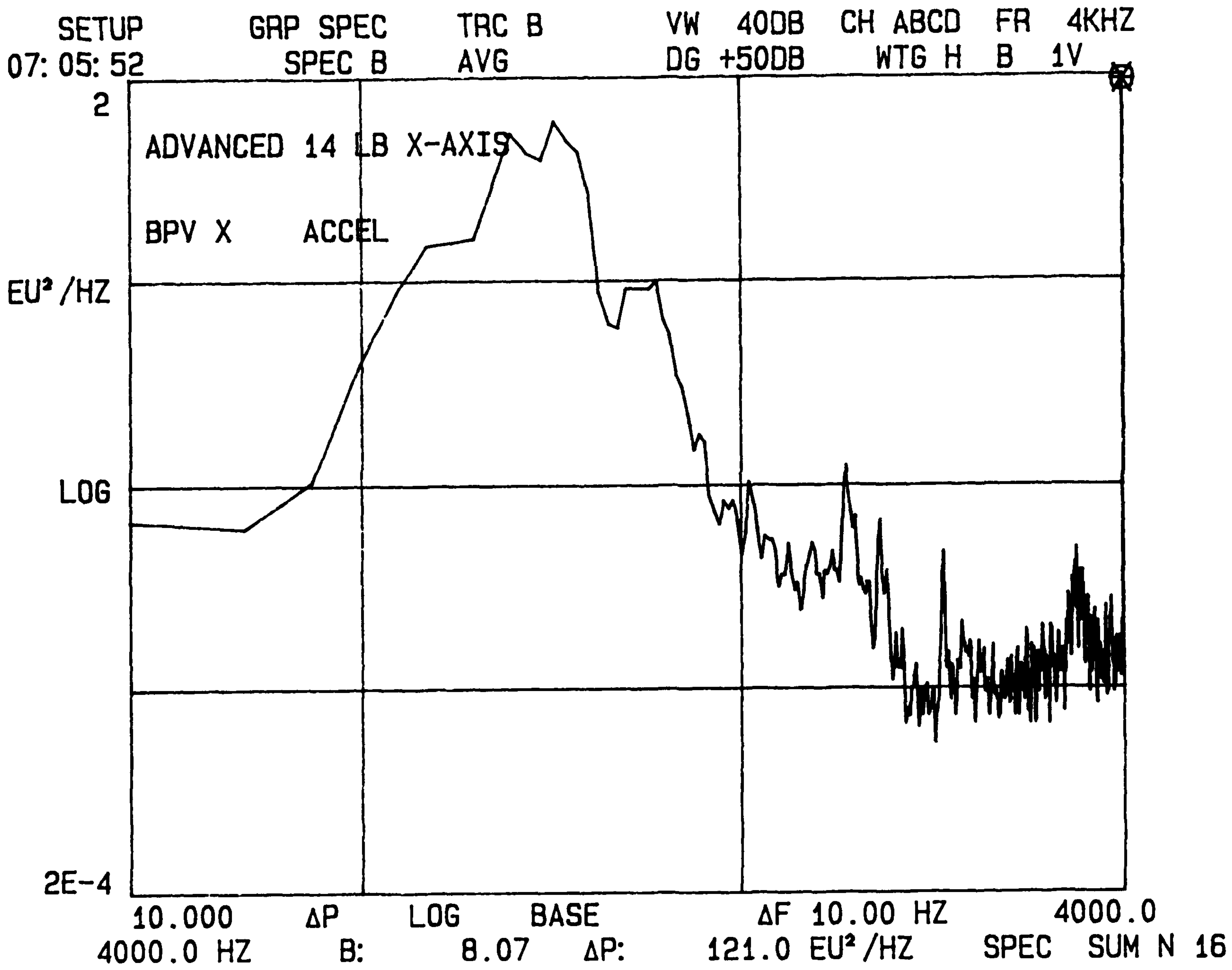
SETUP
13: 04: 48
GRP TIME
TIME D
TRC D
INP
VW 40DB
DG X5
CH ABCD
WTG H
FR 4KHZ
D 1V
200
ADVANCED 14 LB Y-AXIS
SG 4 (MICRO STRAIN)
EU
0
-200
0
.063000 SEC
NORM
D:
CMPRSD BASE
82.5 EU
ΔT 1.75m SEC
1.3999
SPEC SUM N 14

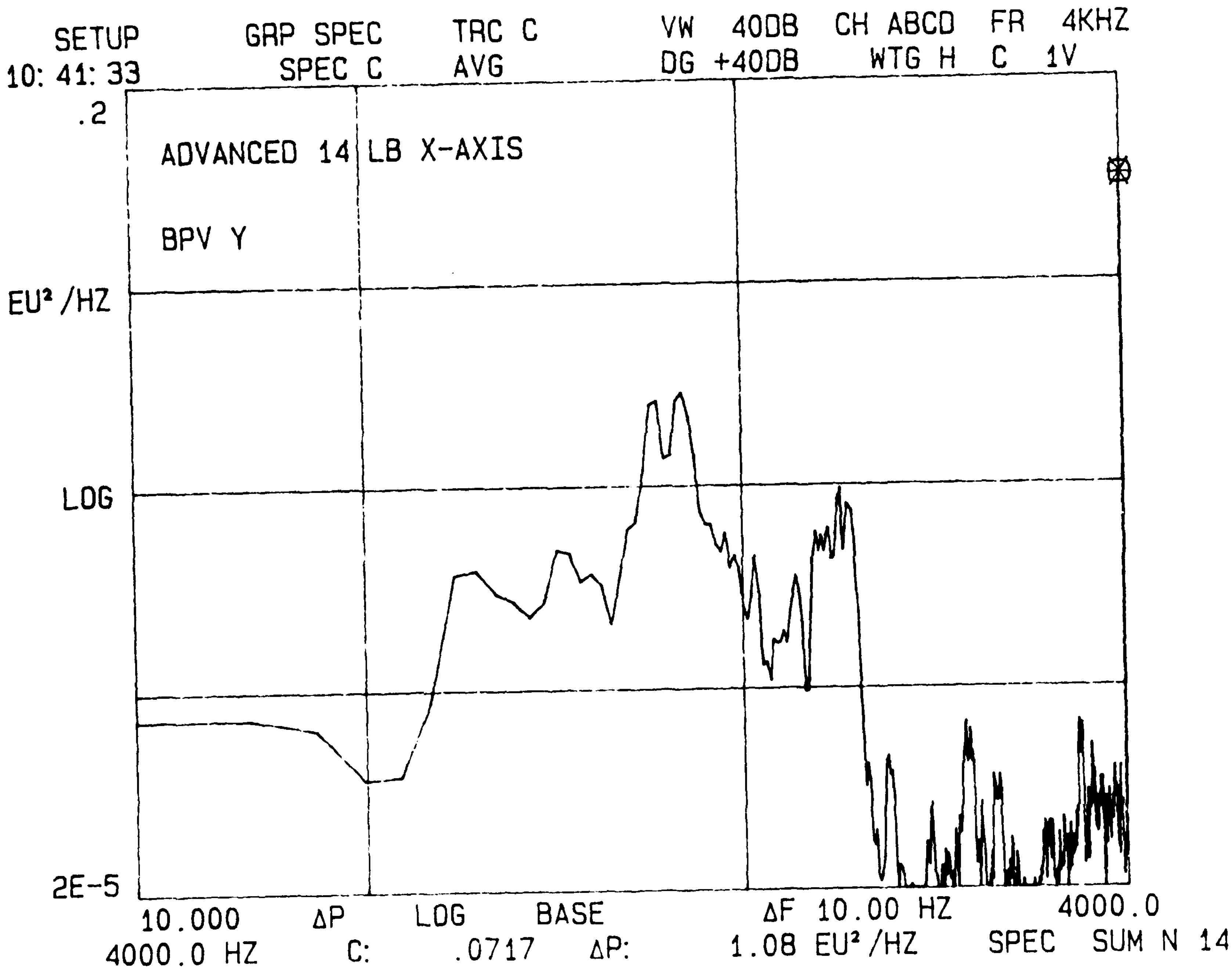

SETUP GRP TIME TRC C VW 40DB CH ABCD FR 4KHZ
13: 21: 45 TIME C INP DG X4 WTG H C 1V
400
ADVANCED 14 LB Z-AXIS
SG 3 (MICRO STRAIN)
EU
0
-400
0 NORM CMPRSD BASE ΔT 1.75m SEC 1.3999
.063000 SEC C: 56.5 EU SPEC SUM N 14

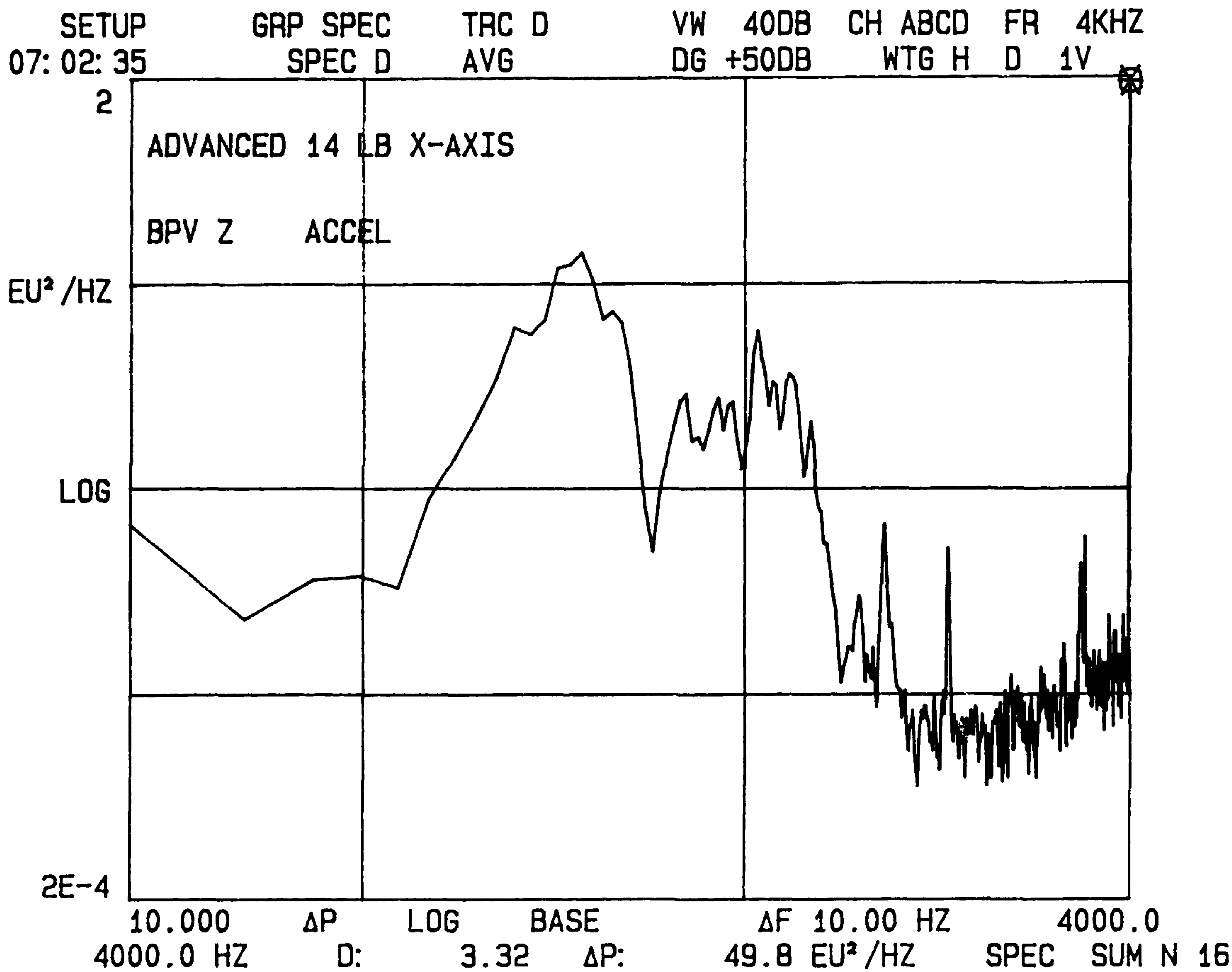

SETUP
13: 29: 35
GRP TIME
TIME D
TRC D
INP
VW 40DB
DG X20
CH ABCD
WTG H
FR 4KHZ
D 1V
100
EU
0
-100
ADVANCED 14 LB Z-AXIS
SG 4 (MICRO STRAIN)
0
.063000 SEC
NORM
D:
CMPRSD BASE
34.4 EU
ΔT 1.75m SEC
1.3999
SPEC SUM N 14

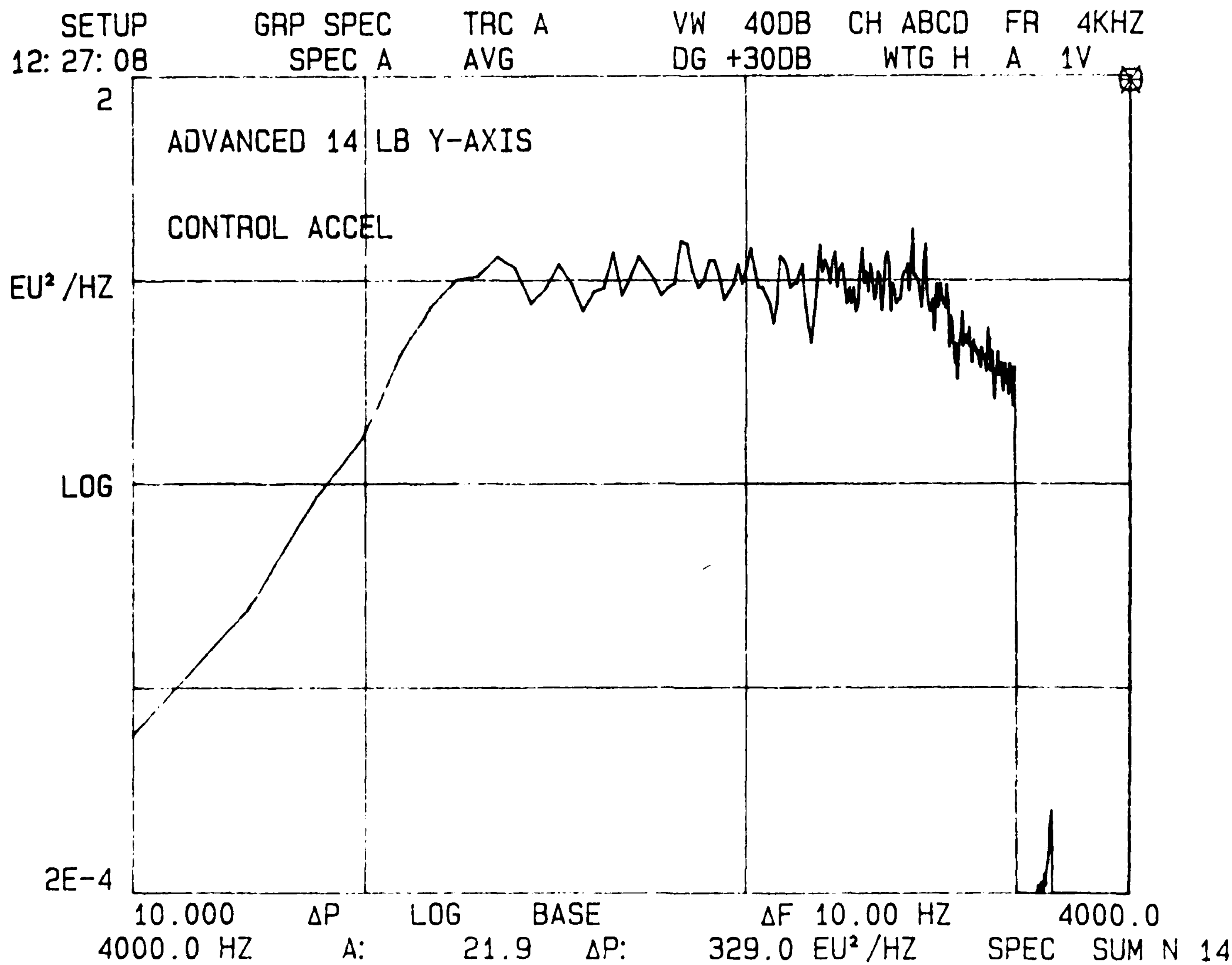
APPENDIX C:

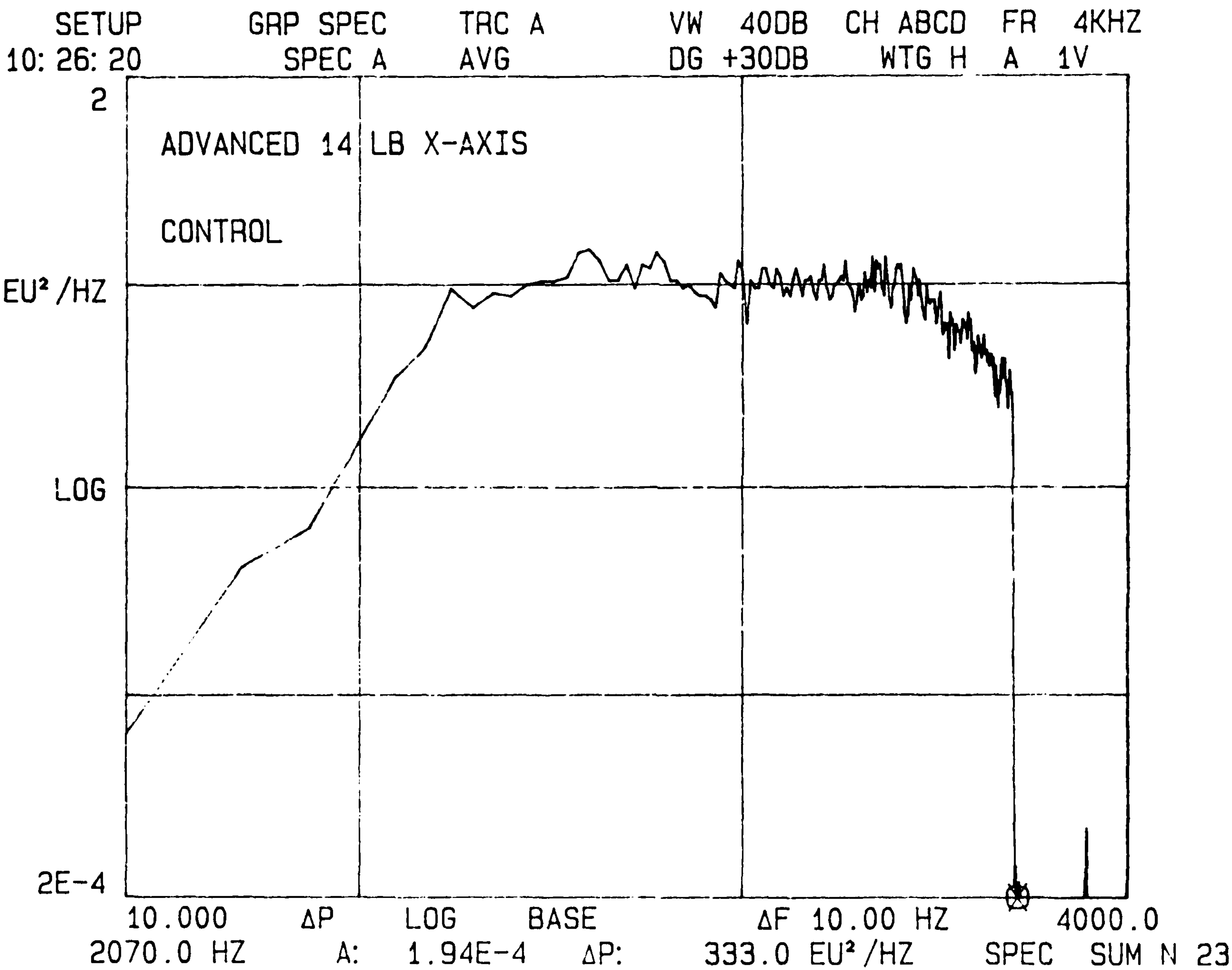
ACCELEROMETER DATA REDUCTION

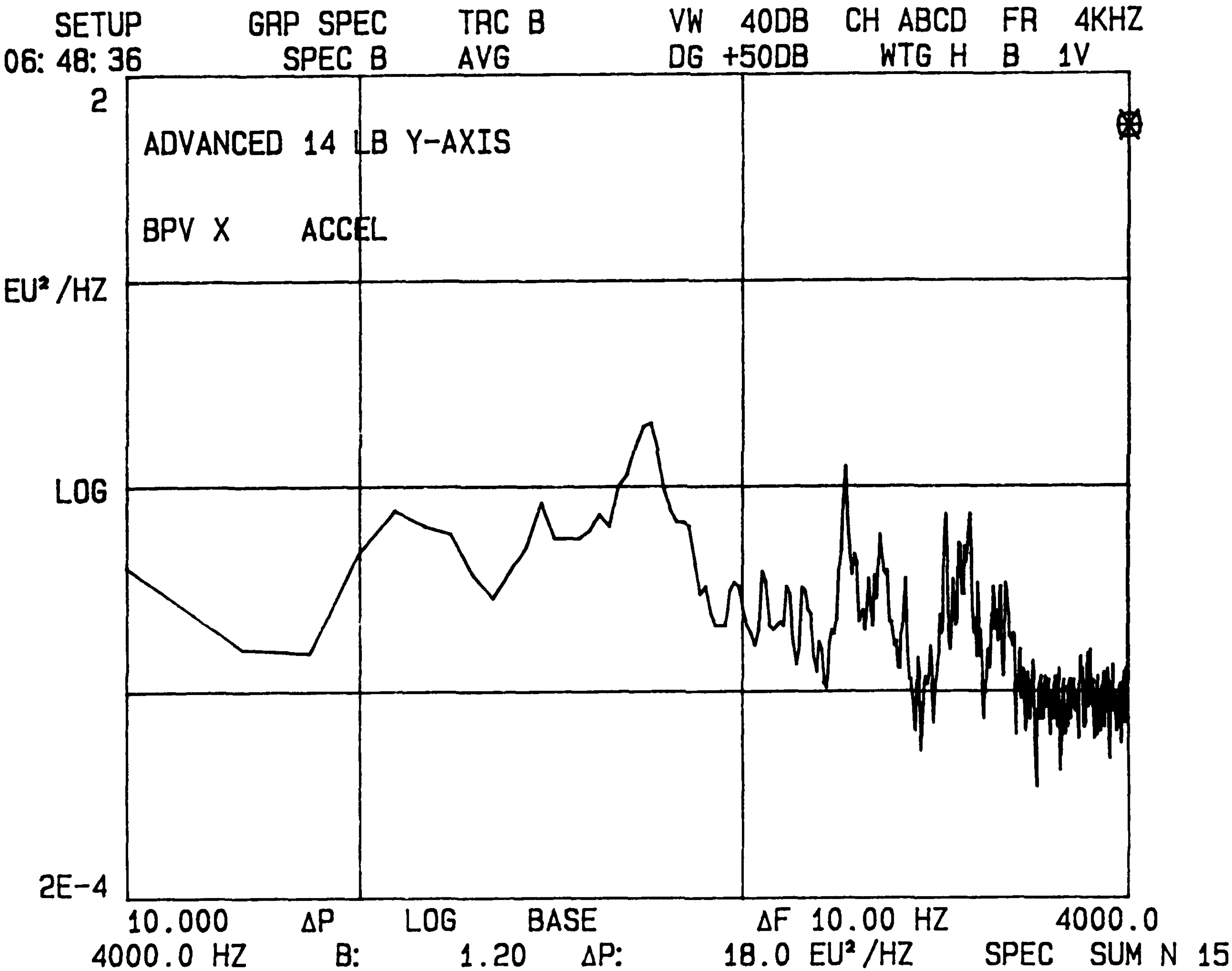

SETUP GRP SPEC TRC B VW 40DB CH ABCD FR 4KHZ
07: 05: 52 SPEC B AVG DG +50DB WTG H B 1V
2
ADVANCED 14 LB X-AXIS
BPV X ACCEL
EU²/HZ
LOG
2E-4
10.000 ΔP LOG BASE ΔF 10.00 HZ 4000.0
4000.0 HZ B: 8.07 ΔP: 121.0 EU²/HZ SPEC SUM N 16

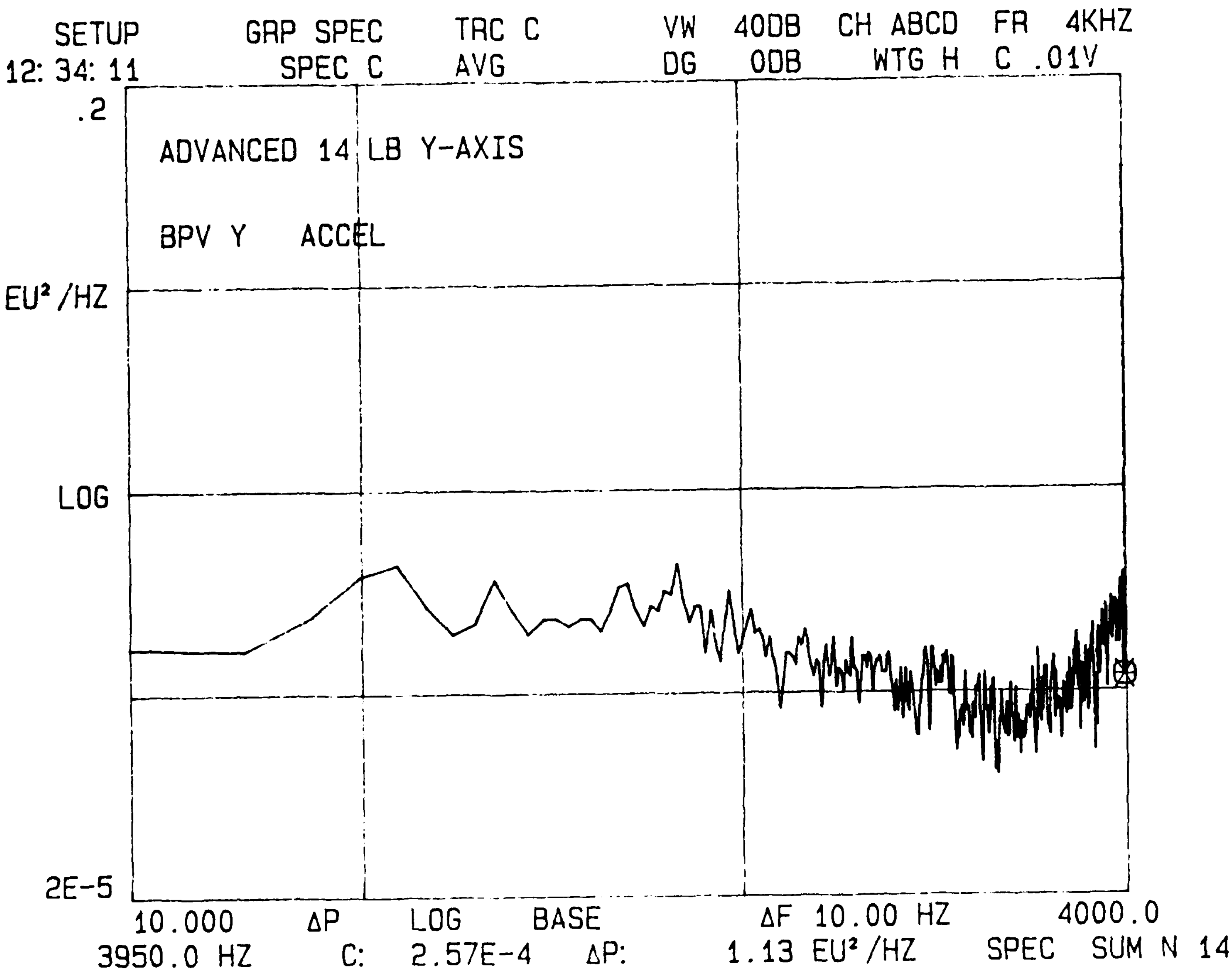

SETUP
10: 41: 33
GRP SPEC
SPEC C
TRC C
AVG
VW 40DB
DG +40DB
CH ABCD
WTG H
FR 4KHZ
C 1V
.2
ADVANCED 14 LB X-AXIS
BPV Y
EU² /HZ
LOG
2E-5
10.000
4000.0 HZ
ΔP
C:
LOG
.0717
BASE
ΔP:
ΔF 10.00 HZ
1.08 EU² /HZ
4000.0
SPEC
SUM N 14

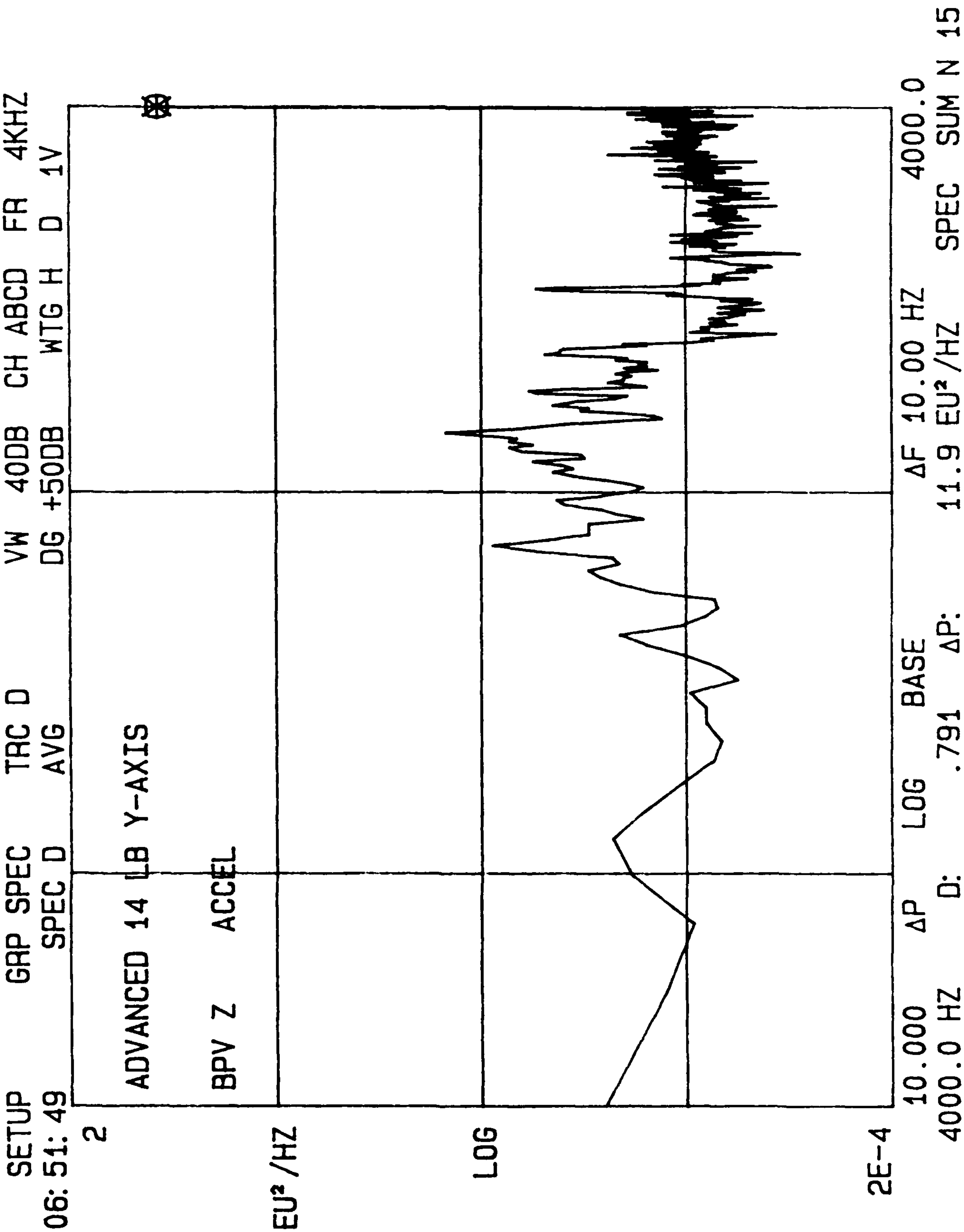

SETUP GRP SPEC TRC D VW 40DB CH ABCD FR 4KHZ
07: 02: 35 SPEC D AVG DG +50DB WTG H D 1V
2
ADVANCED 14 LB X-AXIS
BPV Z ACCEL
EU²/HZ
LOG
2E-4
10.000 ΔP LOG BASE ΔF 10.00 HZ 4000.0
4000.0 HZ D: 3.32 ΔP: 49.8 EU²/HZ SPEC SUM N 16

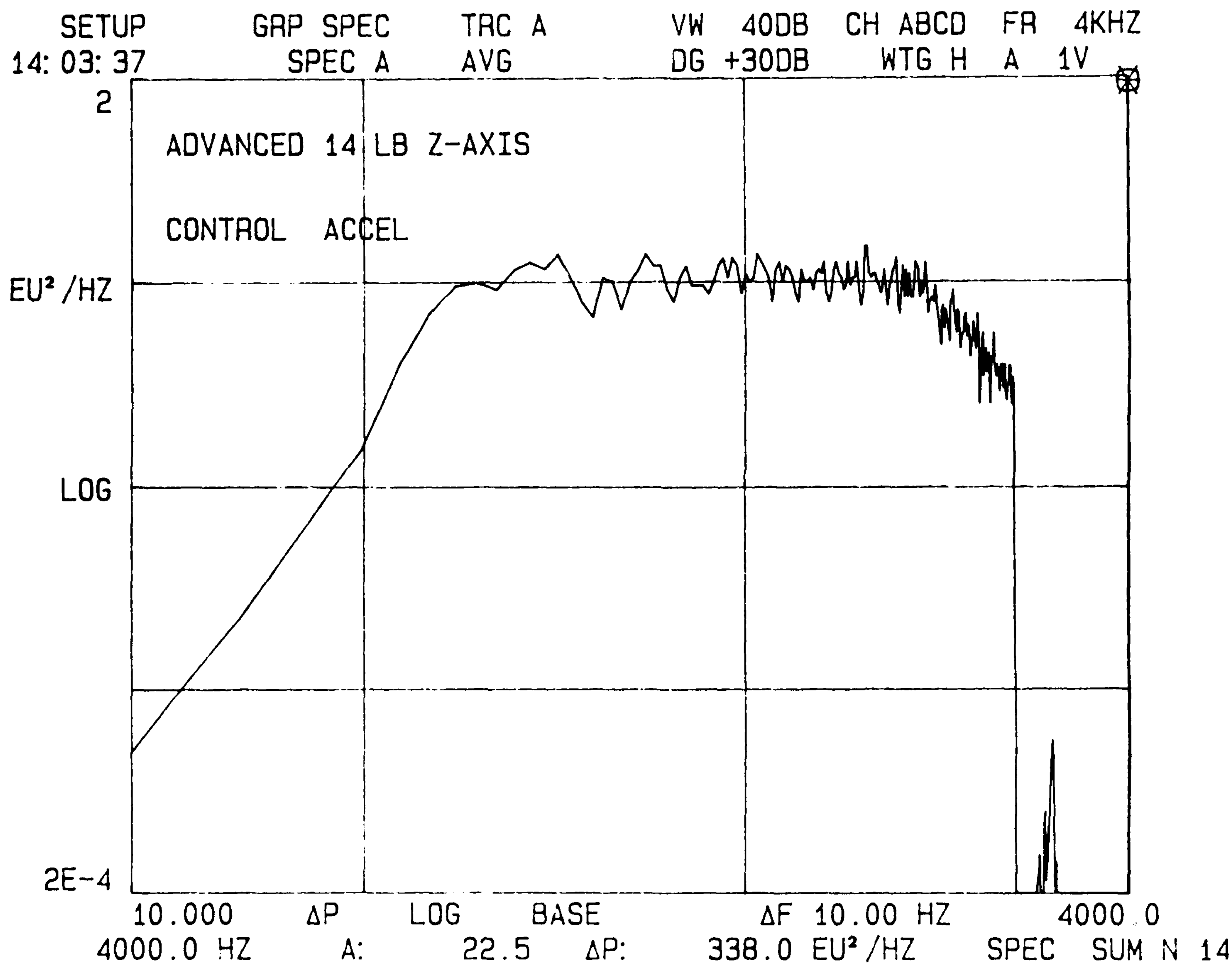

SETUP
12: 27: 08
GRP SPEC
SPEC A
TRC A
AVG
VW 40DB
DG +30DB
CH ABCD
WTG H
FR 4KHZ
A 1V
2
EU² /HZ
LOG
2E-4
ADVANCED 14 LB Y-AXIS
CONTROL ACCEL
10.000
4000.0 HZ
ΔP
A:
LOG
21.9
BASE
ΔP:
ΔF 10.00 HZ
329.0 EU² /HZ
4000.0
SPEC
SUM N 14

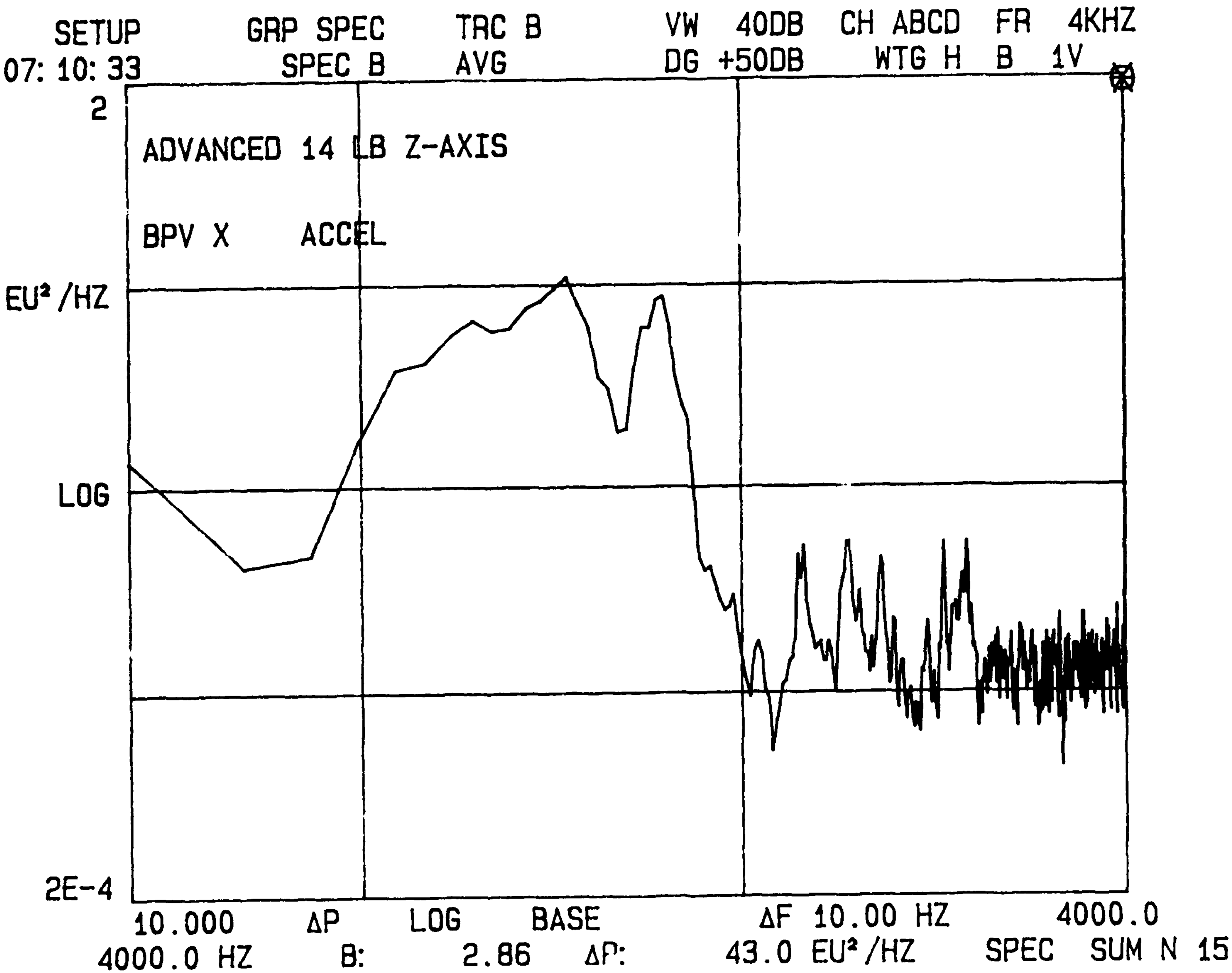

SETUP
10: 26: 20
GRP SPEC
SPEC A
TRC A
AVG
VW 40DB
DG +30DB
CH ABCD
WTG H
FR 4KHZ
A 1V
2
EU²/HZ
LOG
2E-4
ADVANCED 14 LB X-AXIS
CONTROL
10.000
ΔP
LOG
BASE
ΔF 10.00 HZ
4000.0
2070.0 HZ
A: 1.94E-4
ΔP:
333.0 EU²/HZ
SPEC
SUM N 23


SETUP
06: 48: 36
GRP SPEC
SPEC B
TRC B
AVG
VW 40DB
DG +50DB
CH ABCD
WTG H
FR 4KHZ
B 1V
2
ADVANCED 14 LB Y-AXIS
BPV X ACCEL
EU² /HZ
LOG
2E-4
10.000
4000.0 HZ
ΔP LOG BASE
B: 1.20 ΔP:
ΔF 10.00 HZ
18.0 EU² /HZ
4000.0
SPEC SUM N 15

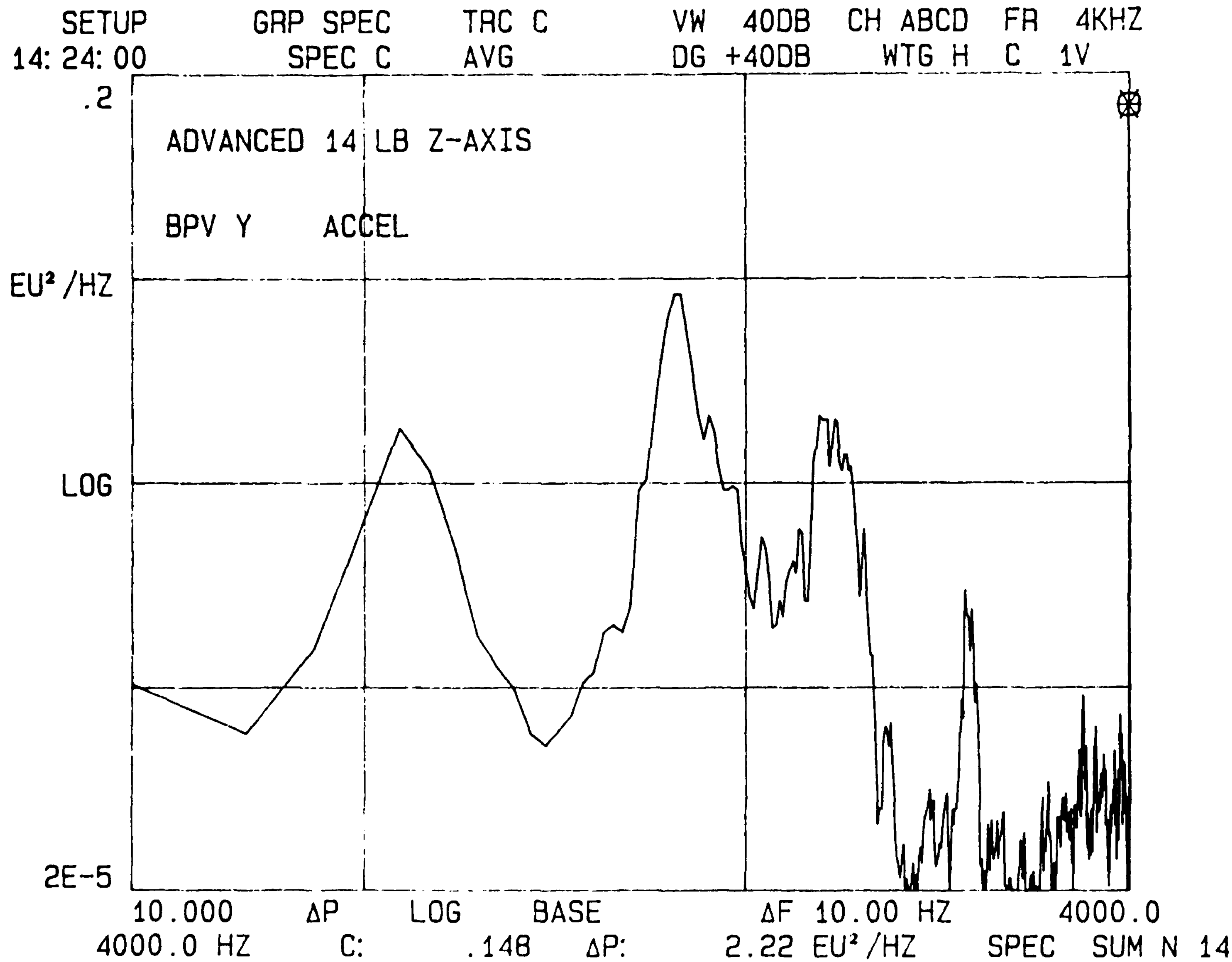

SETUP
12: 34: 11
GRP SPEC
SPEC C
TRC C
AVG
VW
DG
40DB
0DB
CH ABCD
WTG H
FR 4KHZ
C .01V
.2
ADVANCED 14 LB Y-AXIS
BPV Y ACCEL
EU²/HZ
LOG
2E-5
10.000
ΔP
LOG
BASE
ΔF 10.00 HZ
4000.0
3950.0 HZ
C: 2.57E-4
ΔP:
1.13 EU²/HZ
SPEC SUM N 14

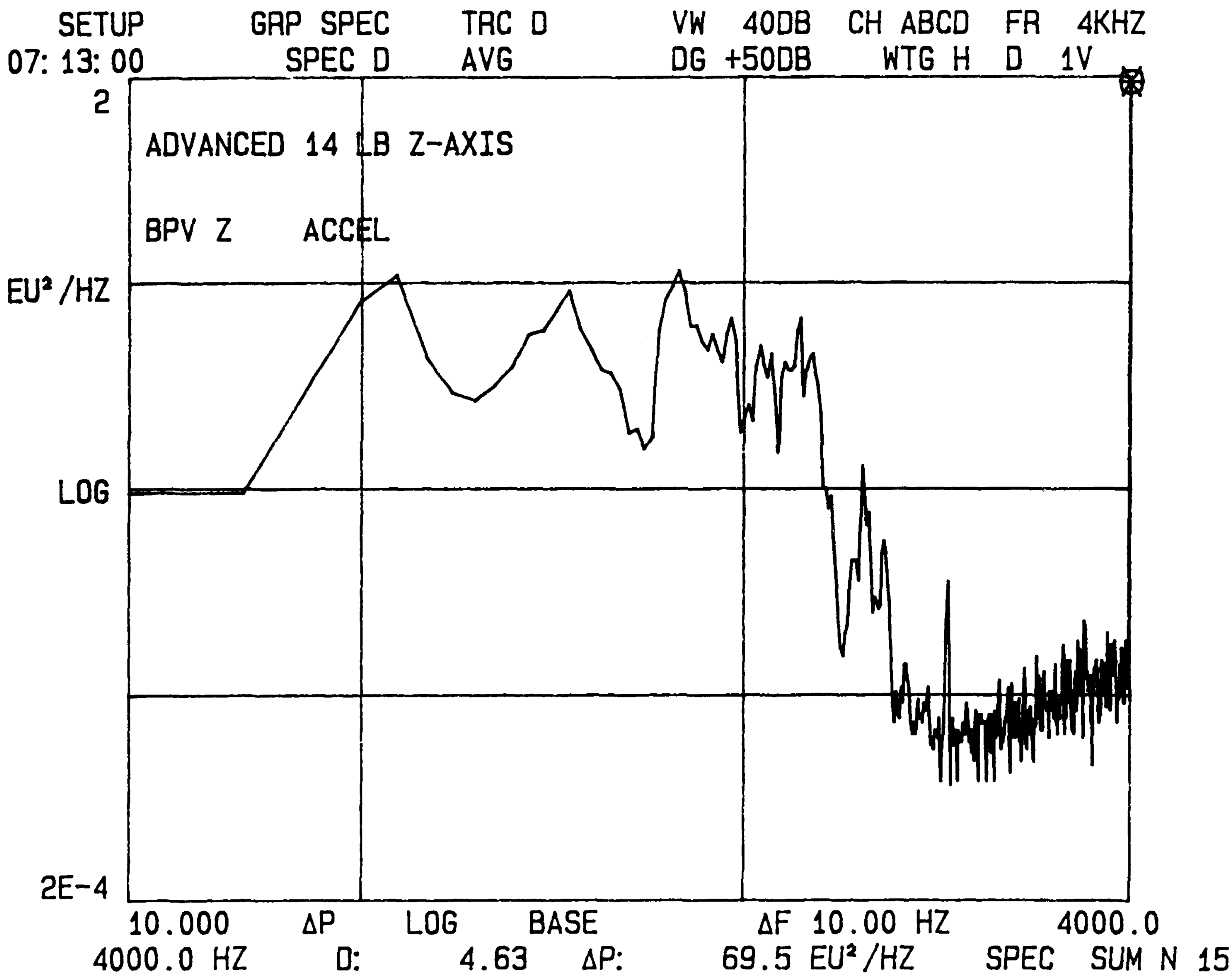

SETUP 06:51:49
GRP SPEC SPEC D
TRC D AVG
VW DG
40DB +50DB
CH ABCD WTG H
FR D
4KHZ 1V
ADVANCED 14 LB Y-AXIS
BPV Z ACCEL
2
EU²/HZ
LOG
2E-4
10.000 4000.0 HZ
ΔP D:
LOG .791
BASE ΔP:
ΔF 10.00 HZ 11.9 EU²/HZ
4000.0
SPEC SUM N 15

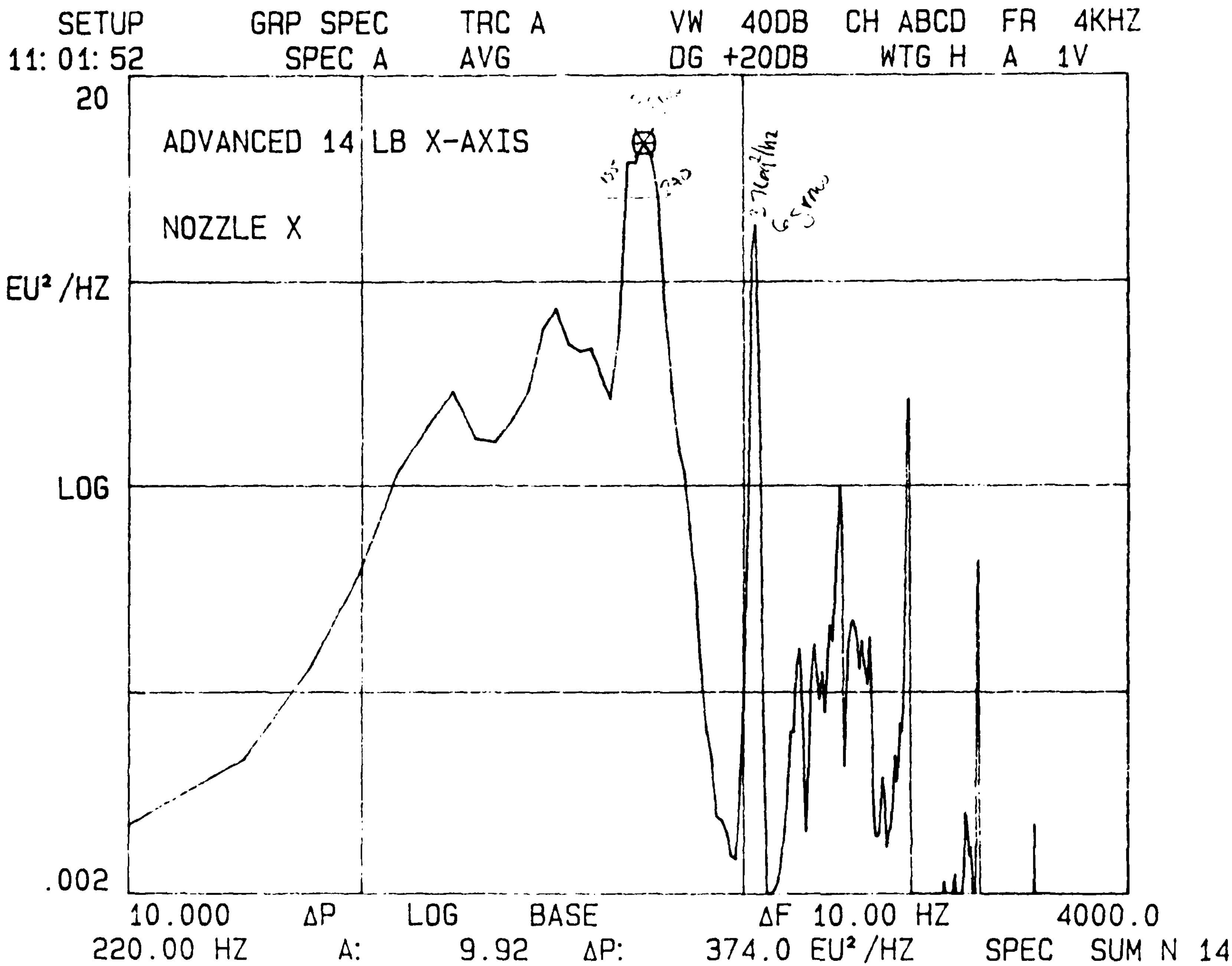

SETUP GRP SPEC TRC A VW 40DB CH ABCD FR 4KHZ
14: 03: 37 SPEC A AVG DG +30DB WTG H A 1V
2
ADVANCED 14 LB Z-AXIS
CONTROL ACCEL
EU²/HZ
LOG
2E-4
10.000 ΔP LOG BASE ΔF 10.00 HZ 4000.0
4000.0 HZ A: 22.5 ΔP: 338.0 EU²/HZ SPEC SUM N 14

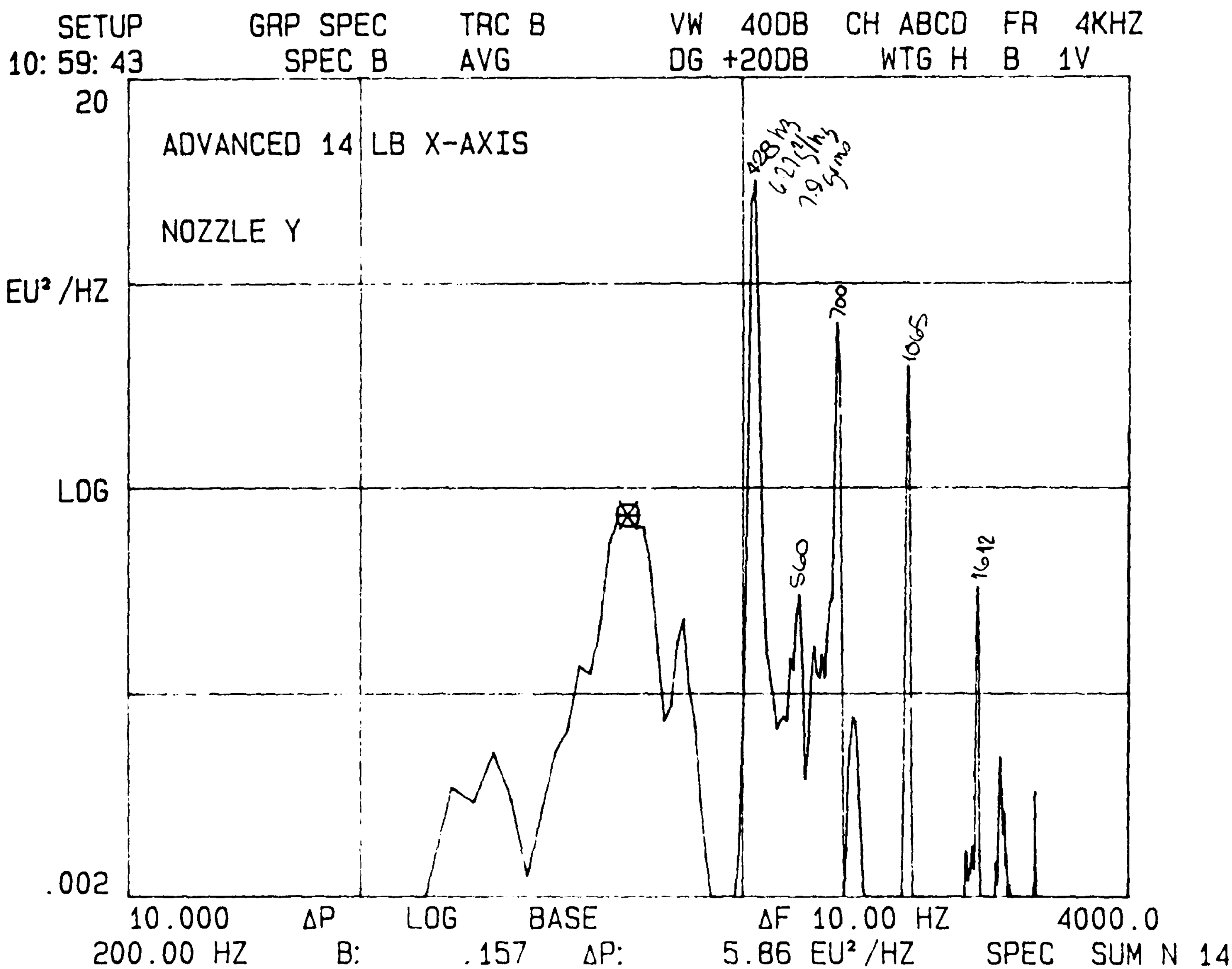


SETUP
07: 10: 33
GRP SPEC
SPEC B
TRC B
AVG
VW 40DB
DG +50DB
CH ABCD
WTG H
FR 4KHZ
B 1V
2
ADVANCED 14 LB Z-AXIS
BPV X ACCEL
EU²/HZ
LOG
2E-4
10.000
4000.0 HZ
ΔP
B:
LOG
2.86
BASE
ΔP:
ΔF 10.00 HZ
43.0 EU²/HZ
4000.0
SPEC SUM N 15

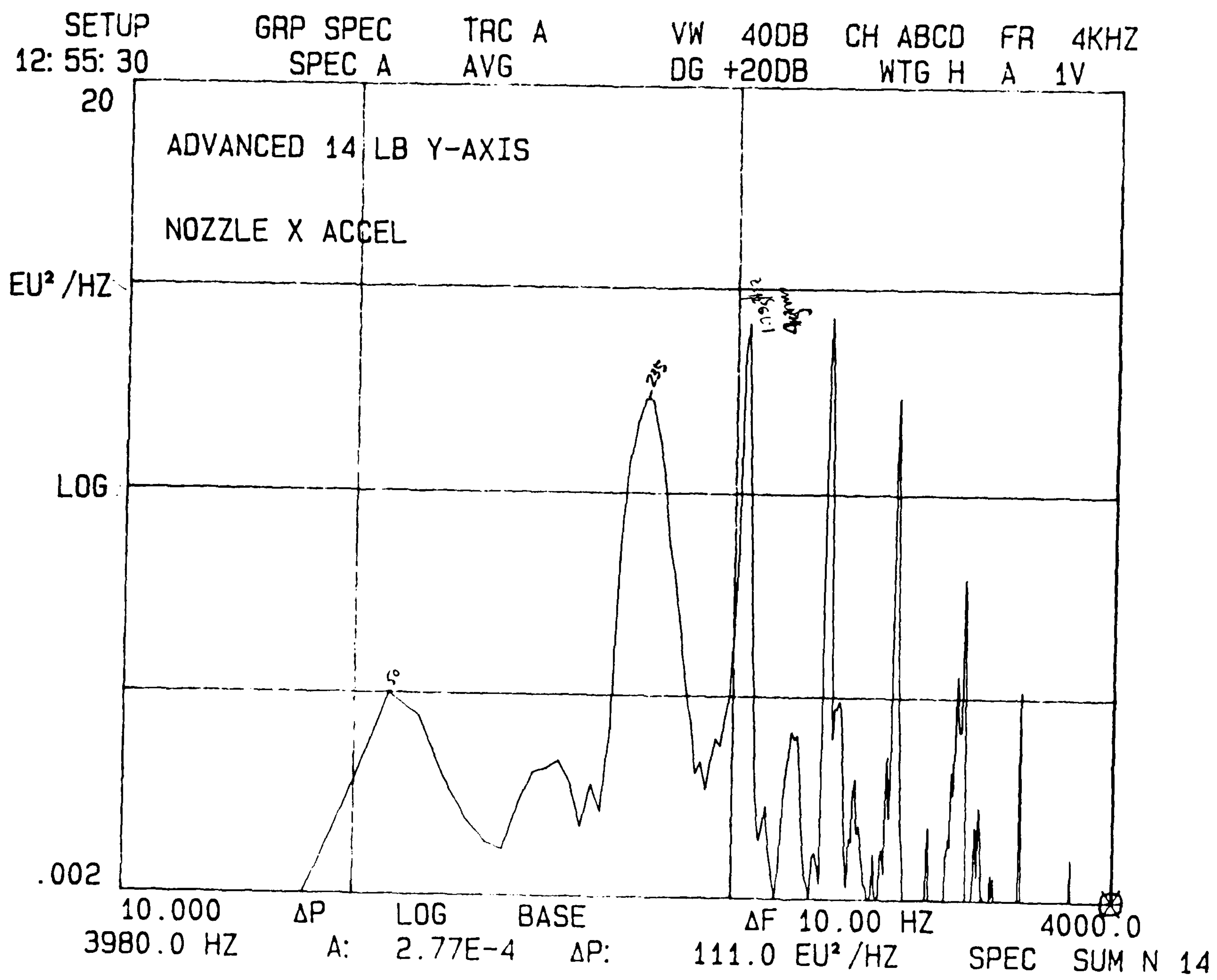

SETUP
14: 24: 00
GRP SPEC
SPEC C
TRC C
AVG
VW 40DB
DG +40DB
CH ABCD
WTG H
FR 4KHZ
C 1V
.2
ADVANCED 14 LB Z-AXIS
BPV Y ACCEL
EU²/HZ
LOG
2E-5
10.000
4000.0 HZ
ΔP
C:
LOG
.148
BASE
ΔP:
ΔF 10.00 HZ
2.22 EU²/HZ
4000.0
SPEC SUM N 14


SETUP
07: 13: 00
GRP SPEC
SPEC D
TRC D
AVG
VW 40DB
DG +50DB
CH ABCD
WTG H
FR 4KHZ
D 1V
2
ADVANCED 14 LB Z-AXIS
BPV Z ACCEL
EU²/HZ
LOG
2E-4
10.000
4000.0 HZ
ΔP
D:
LOG
4.63
BASE
ΔP:
ΔF 10.00 HZ
69.5 EU²/HZ
4000.0
SPEC SUM N 15

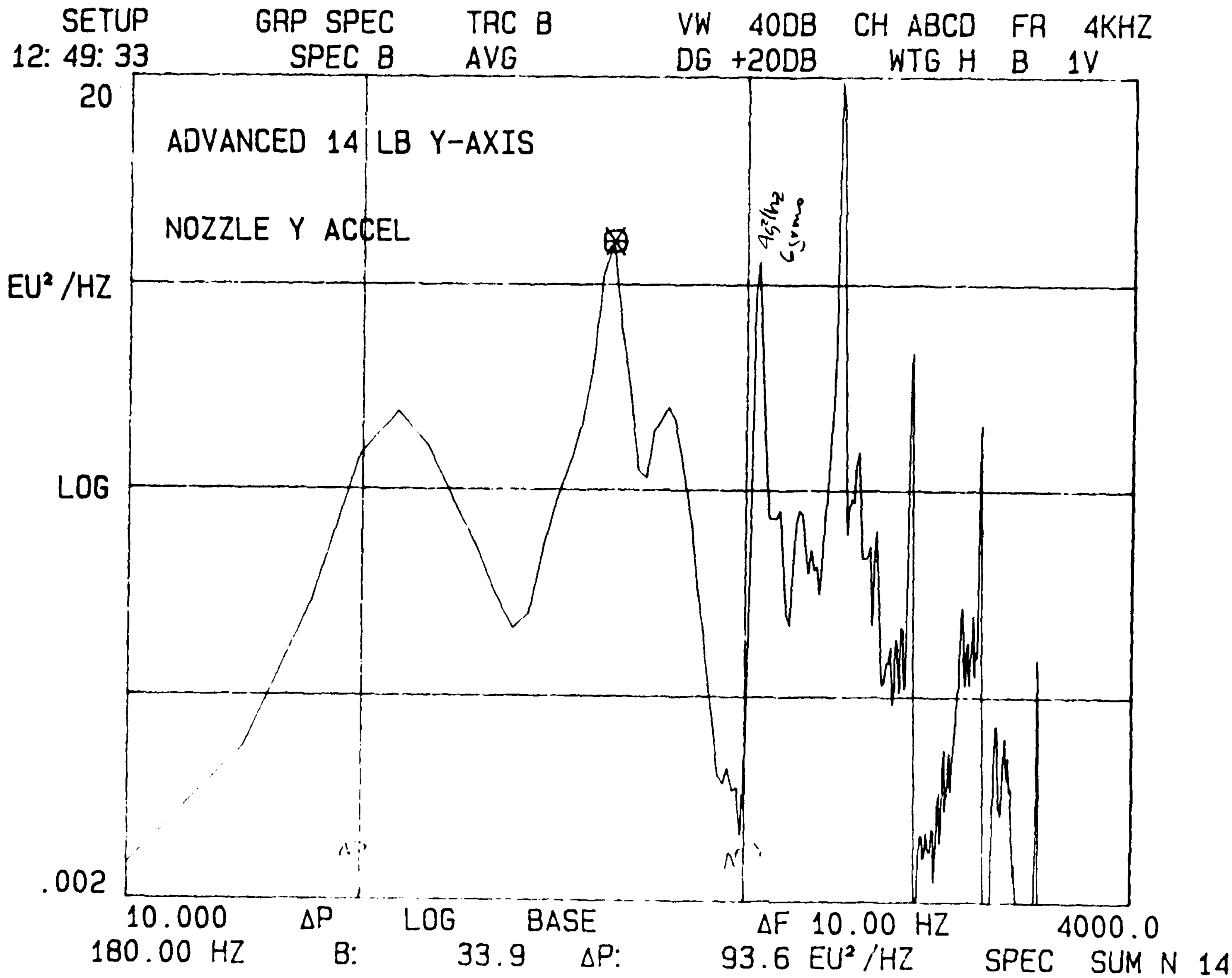

SETUP
11: 01: 52
GRP SPEC
SPEC A
TRC A
AVG
VW 40DB
DG +20DB
CH ABCD
WTG H
FR 4KHZ
A 1V
20
ADVANCED 14 LB X-AXIS
NOZZLE X
EU² /HZ
LOG
.002
10.000
ΔP
LOG
BASE
ΔF 10.00 HZ
4000.0
220.00 HZ
A:
9.92
ΔP:
374.0 EU² /HZ
SPEC
SUM N 14

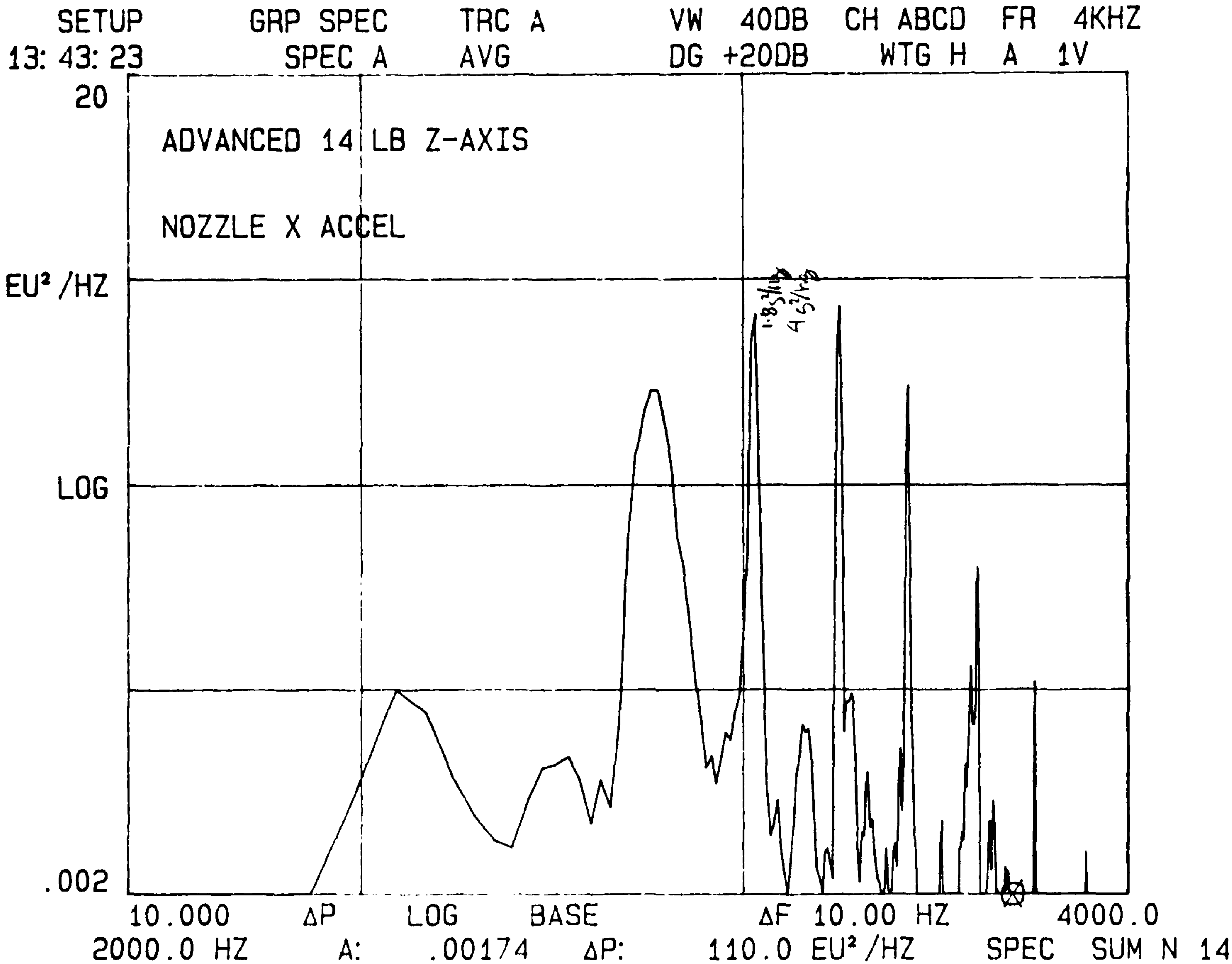


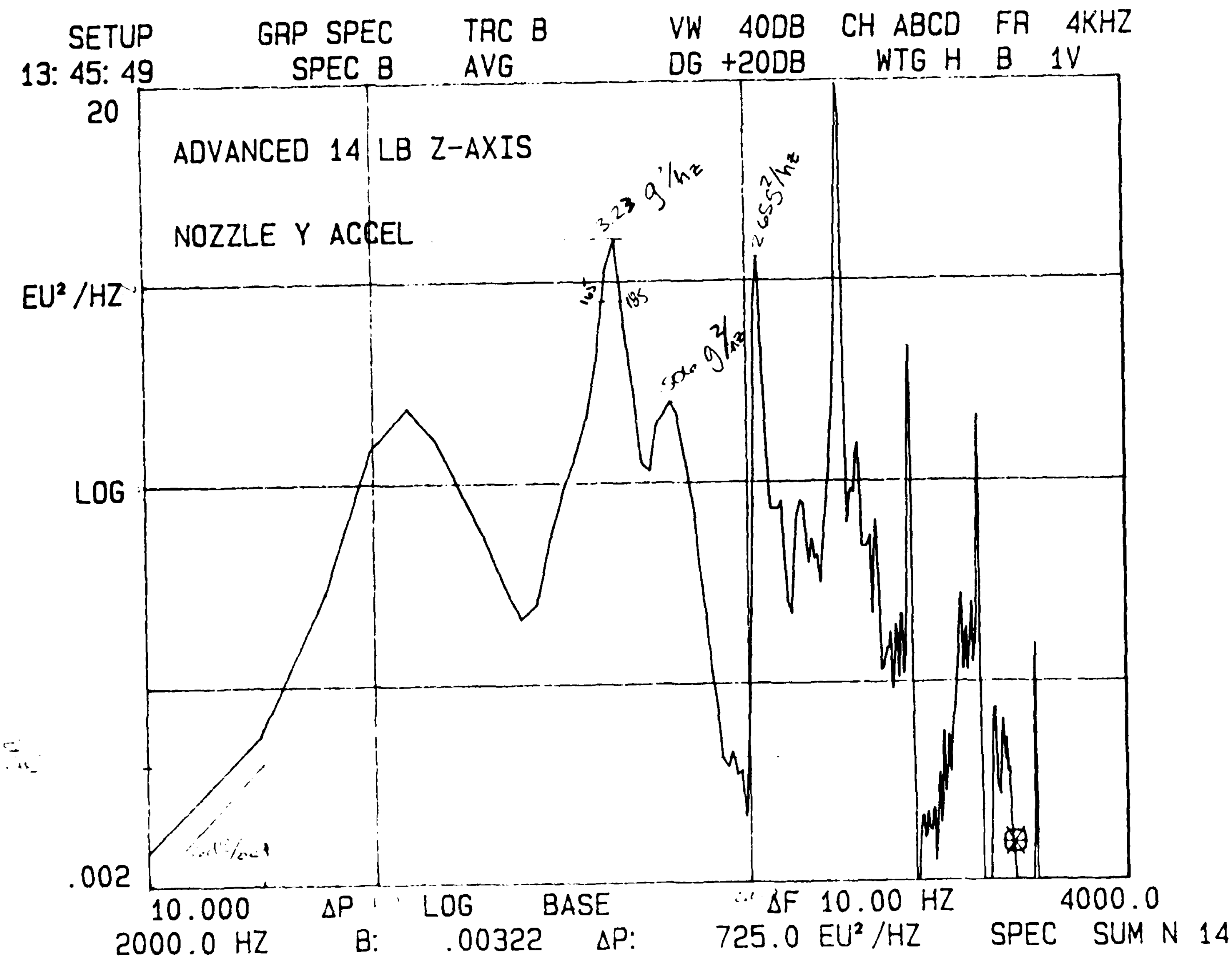
SETUP
10: 59: 43
GRP SPEC
SPEC B
TRC B
AVG
VW 40DB
DG +20DB
CH ABCD
WTG H
FR 4KHZ
B 1V
20
EU² /HZ
LOG
.002
ADVANCED 14 LB X-AXIS
NOZZLE Y
708
1065
560
1642
10.000 ΔP LOG BASE ΔF 10.00 HZ 4000.0
200.00 HZ B: .157 ΔP: 5.86 EU² /HZ SPEC SUM N 14



SETUP
12: 55: 30
GRP SPEC
SPEC A
TRC A
AVG
VW 40DB
DG +20DB
CH ABCD
WTG H
FR 4KHZ
A 1V
20
ADVANCED 14 LB Y-AXIS
NOZZLE X ACCEL
EU² /HZ
LOG
.002
10.000
3980.0 HZ
ΔP
A:
LOG
2.77E-4
BASE
ΔP:
ΔF 10.00 HZ
111.0 EU² /HZ
4000.0
SPEC
SUM N 14

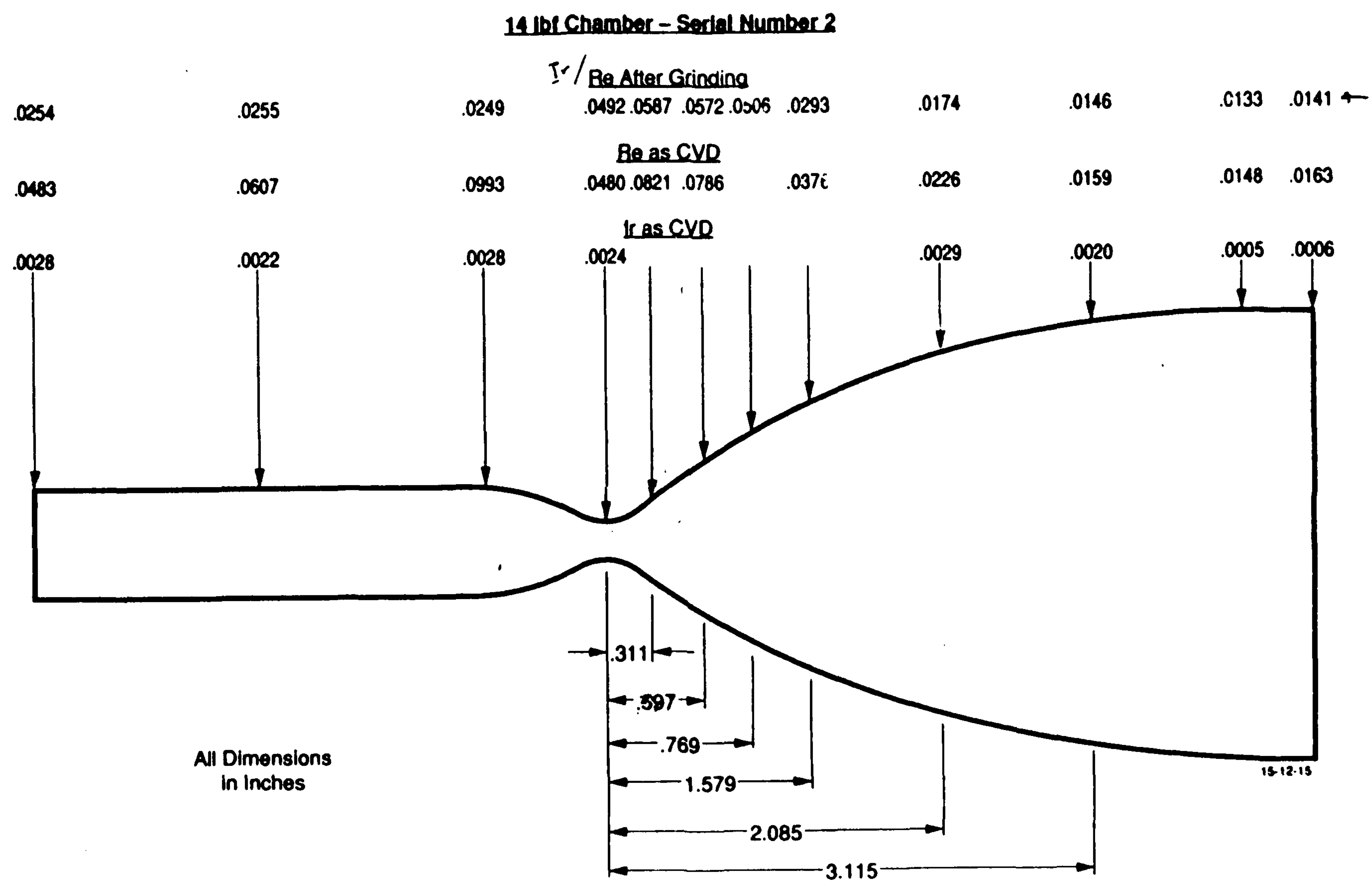

SETUP
12: 49: 33
GRP SPEC
SPEC B
TRC B
AVG
VW 40DB
DG +20DB
CH ABCD
WTG H
FR 4KHZ
B 1V
20
EU² /HZ
LOG
.002
ADVANCED 14 LB Y-AXIS
NOZZLE Y ACCEL
10.000
180.00 HZ
ΔP
B:
LOG
33.9
BASE
ΔP:
ΔF 10.00 HZ
93.6 EU² /HZ
4000.0
SPEC
SUM N 14


SETUP GRP SPEC TRC A VW 40DB CH ABCD FR 4KHZ
13: 43: 23 SPEC A AVG DG +20DB WTG H A 1V
20
ADVANCED 14 LB Z-AXIS
NOZZLE X ACCEL
EU² /HZ
LOG
.002
10.000 ΔP LOG BASE ΔF 10.00 HZ 4000.0
2000.0 HZ A: .00174 ΔP: 110.0 EU² /HZ SPEC SUM N 14


SETUP
13: 45: 49
GRP SPEC
SPEC B
TRC B
AVG
VW 40DB
DG +20DB
CH ABCD
WTG H
FR 4KHZ
B 1V
20
ADVANCED 14 LB Z-AXIS
NOZZLE Y ACCEL
EU² /HZ
LOG
.002
3.23 g²/hz
10.000
2000.0 HZ
ΔP
LOG
BASE
B: .00322
ΔP:
ΔF 10.00 HZ
725.0 EU² /HZ
4000.0
SPEC SUM N 14

APPENDIX D:

AS-BUILT CHAMBER WALL THICKNESSES



Ir-Re Chamber S/N 2 Demonstrated Good Control of the CVD Wall Thickness. Subsequent Grinding Operation Further Shaped Wall Thickness.